Space-Based Observations for Understanding Changes in the Arctic-Boreal Zone

Duncan, Bryan N.; Ott , Lesley E.; Abshire , James B. ; Brucker , Ludovic ; Carroll , Mark L. ; Carton , James ; Comiso, Josefino C.; Dinnat , Emmanuel P. ; Forbes, Bruce C.; Gonsamo, Alemu; Gregg , Watson W. ; Hall , Dorothy K. ; Ialongo, Iolanda ; Jandt, Randi; Kahn, Ralph A. ; Karpechko , Alexey ; Kawa, Stephan R. ; Kato, Seiji ; Kumpula, Timo; Kyrölä, Erkki; Loboda , Tatiana V. ; McDonald, Kyle C.; Montesano, Paul M. ; Nassar, Ray; Neigh, Christopher S.R. ; Parkinson, Claire L. ; Poulter , Benjamin; Pulliainen, Jouni; Rautiainen, Kimmo; Rogers, Brendan M; Rousseaux , Cecile S. ; Soja, Amber J. ; Steiner , Nicholas ; Tamminen, Johanna; Taylor, Patrick C. ; Tzortziou, Maria A. ; Virta, Henrik ; Wang, James S.; Watts , Jennifer D. ; Winker , David M. ; Wu, Dong L.

Published in:
Reviews of Geophysics

DOI:
10.1029/2019RG000652

E-pub ahead of print: 01.01.2019

Document Version
Publisher's PDF, also known as Version of record

Citation for pulished version (APA):
Duncan, B. N., Ott , L. E., Abshire , J. B., Brucker , L., Carroll , M. L., Carton , J., Comiso, J. C., Dinnat , E. P., Forbes, B. C., Gonsamo, A., Gregg , W. W., Hall , D. K., Ialongo, I., Jandt, R., Kahn, R. A., Karpechko , A., Kawa, S. R., Kato, S., Kumpula, T., ... Wu, D. L. (2019). Space-Based Observations for Understanding Changes in the Arctic-Boreal Zone. *Reviews of Geophysics*, 1-94. Advance online publication. https://doi.org/10.1029/2019RG000652

Reviews of Geophysics

REVIEW ARTICLE
10.1029/2019RG000652

Space-Based Observations for Understanding Changes in the Arctic-Boreal Zone

Bryan N. Duncan[1], Lesley E. Ott[1], James B. Abshire[1], Ludovic Brucker[1,2], Mark L. Carroll[1], James Carton[3], Josefino C. Comiso[1], Emmanuel P. Dinnat[1,4], Bruce C. Forbes[5], Alemu Gonsamo[6], Watson W. Gregg[1], Dorothy K. Hall[7], Iolanda Ialongo[8], Randi Jandt[9], Ralph A. Kahn[1], Alexey Karpechko[8], Stephan R. Kawa[1], Seiji Kato[10], Timo Kumpula[11], Erkki Kyrölä[8], Tatiana V. Loboda[12], Kyle C. McDonald[13], Paul M. Montesano[1,14], Ray Nassar[15], Christopher S.R. Neigh[1], Claire L. Parkinson[1], Benjamin Poulter[1], Jouni Pulliainen[8], Kimmo Rautiainen[8], Brendan M. Rogers[16], Cecile S. Rousseaux[1,2], Amber J. Soja[10,17], Nicholas Steiner[13], Johanna Tamminen[8], Patrick C. Taylor[10], Maria A. Tzortziou[1,13], Henrik Virta[8], James S. Wang[1,2,18], Jennifer D. Watts[16], David M. Winker[10], and Dong L. Wu[1]

[1]NASA Goddard Space Flight Center, Greenbelt, MD, USA, [2]Goddard Earth Sciences Technology and Research Studies and Investigations, Universities Space Research Association, Columbia, MD, USA, [3]Department of Atmospheric and Oceanic Science, University of Maryland, MD, USA, [4]CEESMO, Chapman University, Orange, CA, USA, [5]Arctic Centre, University of Lapland, Rovaniemi, Finland, [6]School of Geography and Earth Sciences, McMaster University, Hamilton, Ontario, Canada, [7]Earth System Science Interdisciplinary Center, University of Maryland, MS, USA, [8]Finnish Meteorological Institute, Helsinki, Finland, [9]Alaska Fire Science Consortium, University of Alaska, Fairbanks, AK, USA, [10]NASA Langley Research Center, Hampton, VA, USA, [11]Department of Geographical and Historical Studies, University of Eastern Finland, Joensuu, Finland, [12]Department of Geographical Sciences, University of Maryland, College Park, MD, USA, [13]Department of Earth and Atmospheric Sciences, The City College of New York, City University of New York, New York, NY, USA, [14]Science Systems and Applications, Inc., Lanham, MD, USA, [15]Climate Research Division, Environment and Climate Change Canada, Toronto, Ontario, Canada, [16]Woods Hole Research Center, Falmouth, MA, USA, [17]National Institute of Aerospace, Hampton, VA, USA, [18]Now at Institute for Advanced Sustainability Studies e.V. (IASS), Potsdam, Germany

Key Points:
- We review the strengths and limitations of space-based observational capabilities for several important Arctic-Boreal Zone components
- We make recommendations for improving the current Arctic-Boreal Zone observing network and discuss how to build a more comprehensive one

Correspondence to:
B. N. Duncan,
bryan.n.duncan@nasa.gov

Citation:
Duncan, B. N., Ott, L. E., Abshire, J. B., Brucker, L., Carroll, M. L., Carton, J., et al. (2020). Space-based observations for understanding changes in the arctic-boreal zone. *Reviews of Geophysics*, *58*, e2019RG000652. https://doi.org/10.1029/2019RG000652

Received 25 APR 2019
Accepted 4 OCT 2019
Accepted article online 26 OCT 2019

Abstract Observations taken over the last few decades indicate that dramatic changes are occurring in the Arctic-Boreal Zone (ABZ), which are having significant impacts on ABZ inhabitants, infrastructure, flora and fauna, and economies. While suitable for detecting overall change, the current capability is inadequate for systematic monitoring and for improving process-based and large-scale understanding of the integrated components of the ABZ, which includes the cryosphere, biosphere, hydrosphere, and atmosphere. Such knowledge will lead to improvements in Earth system models, enabling more accurate prediction of future changes and development of informed adaptation and mitigation strategies. In this article, we review the strengths and limitations of current space-based observational capabilities for several important ABZ components and make recommendations for improving upon these current capabilities. We recommend an interdisciplinary and stepwise approach to develop a comprehensive ABZ Observing Network (ABZ-ON), beginning with an initial focus on observing networks designed to gain process-based understanding for individual ABZ components and systems that can then serve as the building blocks for a comprehensive ABZ-ON.

Plain Language Summary While numerous scientific datasets of the Arctic Boreal Zone (ABZ) confirm that this region is rapidly changing, the current observational suite is insufficient to understand many of the complex interactions between components of the ABZ, which includes the cryosphere, biosphere, hydrosphere, and atmosphere. Such a process-based understanding is necessary for the development of informed mitigation and adaptation response strategies and the prediction of future change. We review the strengths and limitations of the current suite of observations from satellites, which have the unique advantage of spatial coverage as compared to observations collected from near-surface instruments. We make recommendations for improving satellite observations of individual components of the ABZ and recommend an interdisciplinary and stepwise approach to develop a comprehensive ABZ Observing Network (ABZ-ON).

1. Introduction

Numerous Earth science observations (e.g., surface temperature, sea ice extent and thickness, snow cover extent and seasonality, ocean color, fire regimes, and ice sheet mass) indicate long-term changes are occurring in the Arctic-Boreal Zone (ABZ; e.g., Comiso & Hall, 2014; Osborne et al., 2018), a region that lies north of approximately 50°N and includes the boreal, sub-Arctic, and Arctic climate zones (Figure 1). The Arctic Monitoring and Assessment Programme's (AMAP) Snow, Water, Ice and Permafrost in the Arctic (SWIPA) assessment (AMAP, 2017), Box et al. (2019) and others summarize these observed long-term ABZ changes, which are having profound and complex effects on ABZ inhabitants and their welfare, including flora/fauna, and economies (e.g., Arctic Council, 2016; Larsen et al., 2014; U.S. Global Change Research Program [USGCRP], 2018). Arctic surface temperatures have warmed faster than the Earth as a whole over recent decades (Comiso & Hall, 2014; Overland et al., 2018; USGCRP, 2018), and the Arctic has experienced record high surface air temperatures in the last few years (e.g., Boisvert et al., 2016; Cullather et al., 2016; Osborne et al., 2018), which led to record low winter sea ice extent (Ricker et al., 2017). Change can occur more rapidly in the ABZ than in most other world regions, a phenomenon known as "polar amplification" (e.g., Masson-Delmotte et al., 2013, and references therein; Moon et al., 2019, and references therein). For example, Pistone et al. (2014) estimated that the albedo forcing associated with changes in Arctic sea ice over the last three decades is 25% as large globally as the direct radiative forcing from increased carbon dioxide over the same period. Polar amplification has mainly been attributed to ice-albedo feedback (e.g., Masson-Delmotte et al., 2013, and references therein), which is consistent with satellite observations that show a strong correlation between changes in sea ice extent and surface air temperature in polar regions (e.g., Comiso et al., 2017; Oyle et al., in press). However, there are complex and often poorly understood interactions between the cryosphere, biosphere, hydrosphere, and atmosphere of the ABZ (Figure 2; e.g., McGuire et al., 2006; Ciais et al., 2013; Hinzman et al., 2013; Bhatt et al., 2014; Parmentier et al., 2017a,b), which hamper our ability to predict future ABZ changes (e.g., Serreze & Barry, 2014).

Deficiencies in our understanding of complex interactions between components of the ABZ will also hamper the development of informed mitigation and adaptation response strategies (e.g., AMAP, 2017; Arctic Council, 2016; Arctic Science Ministerial, 2018). Using the economy as an example, the benefits (depending on one's perspective) of a warmer ABZ may include increased access to minerals, oil and natural gas, fisheries, and trans-polar shipping routes (e.g., Northwest and Northeast passages) to better connect country economies. Disadvantages may include increased wildfires, permafrost thaw, and coastal erosion leading to damage to infrastructure, such as buildings, roads, pipelines, ice roads, runways, and ports (e.g., Melvin et al., 2017; Moon et al., 2019). Large uncertainties may also restrict and slow infrastructure development, which is essential for ABZ economic development. Poor predictive capabilities may result in an inability to properly predict teleconnections and longer-term changes. For example, severe weather in the midlatitudes may be influenced as changes in thermodynamic heating associated with sea ice loss influence the position of the jet stream (e.g., Cohen et al., 2014; Francis & Vavrus, 2015; Handorf et al., 2015; Overland & Wang, 2018). Assimilation of sea ice observations can lead to more skillful forecasts of ice extent several months in advance (e.g. Blockley & Peterson, 2018). Over longer timescales, improved process understanding is needed to predict rapid and irreversible changes (e.g., unexpectedly rapid carbon release from thawing of the vast ABZ soil reservoirs; National Research Council, 2013, 2014a; Treat & Frolking, 2013; Schuur et al., 2015; Schuur et al., 2018) that can exacerbate global warming, possibly having unmanageably large, global economic costs and national security implications (e.g., Hope & Schaefer, 2016). Consequently, the effects of observed and potential changes in the ABZ have captured the attention of the world, leading to efforts, such as the formation of the intergovernmental Arctic Council in 1996, for ABZ countries to coordinate their individual research efforts (e.g., as summarized in Arctic Science Ministerial, 2018) and cooperate on common ABZ issues.

While the past and current observing networks of instruments from orbital (i.e., satellite) and suborbital (e.g., surface, aircraft, Unmanned Aerial System [UAS], balloon, boat) platforms confirm that the ABZ is changing (e.g., Box et al., 2019), a more comprehensive and integrated ABZ observing network (ABZ-ON) of orbital and suborbital observations would improve scientific understanding of key processes. Many

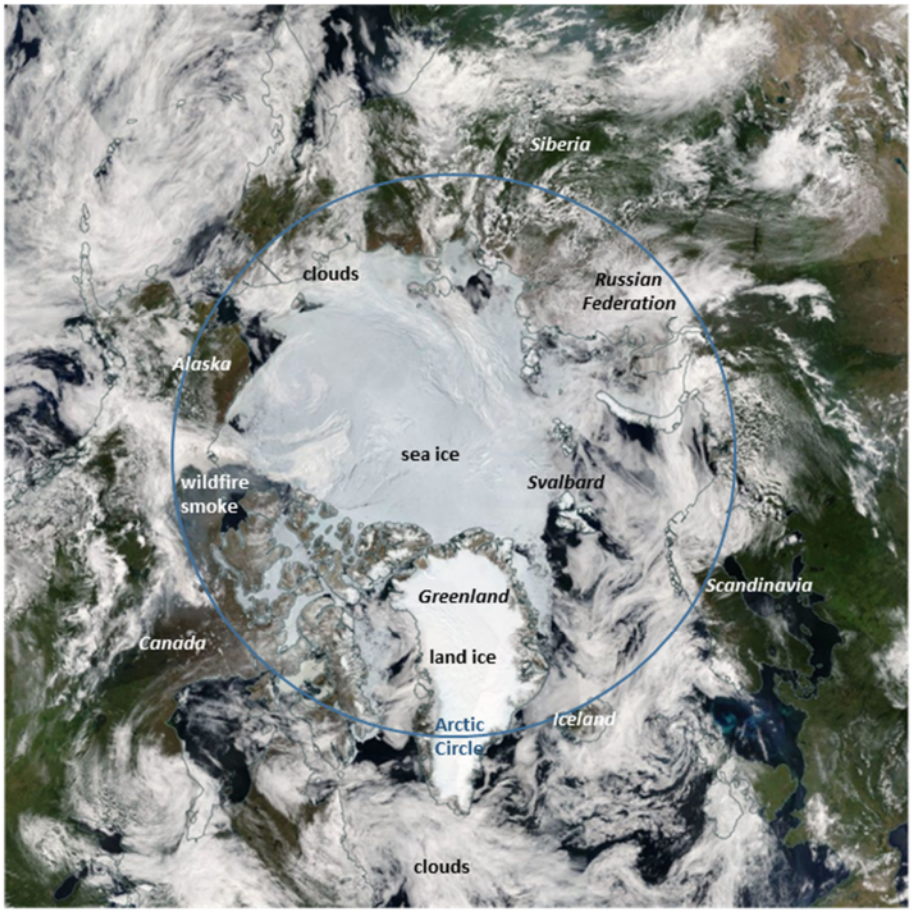

Figure 1. A true color image from the NASA Aqua/Moderate Resolution Imaging Spectroradiometer (MODIS) taken on June 28, 2010. The image captures many of the important ABZ components, including sea ice, glaciers, boreal forests, tundra, smoke from wildfires, clouds, and ocean. Image courtesy of NASA. https://worldview.earthdata.nasa.gov/?v=-6086656,-4689920,6086656,4689920&p=arctic&t=2010-06-28-T18%3A20%3A28Z.

atmospheric general circulation models (AGCMs) and atmosphere-ocean general circulation models are evolving into Earth system models by simulating a more diverse set of interactive processes, incorporating such aspects as ice sheet dynamics, biogeochemical cycles, permafrost thaw, vegetation change, and wetland dynamics (Flato et al., 2013). A well-developed ABZ-ON would provide the data necessary for a comprehensive evaluation of Earth system model performance (e.g., National Research Council, 2014a) and identifying areas where further improvements are needed (e.g., Koenigk et al., 2014; Loranty et al., 2014). It would also support the establishment of long-term, multi-instrument records of ABZ change (Comiso & Hall, 2014). It would have the added benefit of providing a crucial baseline of the present state of the ABZ, against which to compare future change. Very likely, there will be additional economic benefit of ABZ-ON data for commercial and geostrategy applications.

Both orbital and suborbital platforms face unique challenges in the ABZ. Existing suborbital networks are sparse (e.g., Metcalfe et al., 2018) and expensive to operate in the often inaccessible and inhospitable environment (National Research Council, 2003). However limited, these suborbital data have been invaluable for monitoring ABZ change, filling some temporal gaps in satellite coverage, affording detail unobtainable from space, providing the data necessary for validation and interpretation of satellite data, and obtaining a process-based understanding of the ABZ. Earth-observing satellites uniquely provide far more complete spatial coverage than suborbital networks. They are predominately managed by government agencies, including the U.S. National Aeronautics and Space Administration (NASA), U.S. National Oceanic and Atmospheric Administration (NOAA), European Space Agency (ESA), and Japan Aerospace Exploration

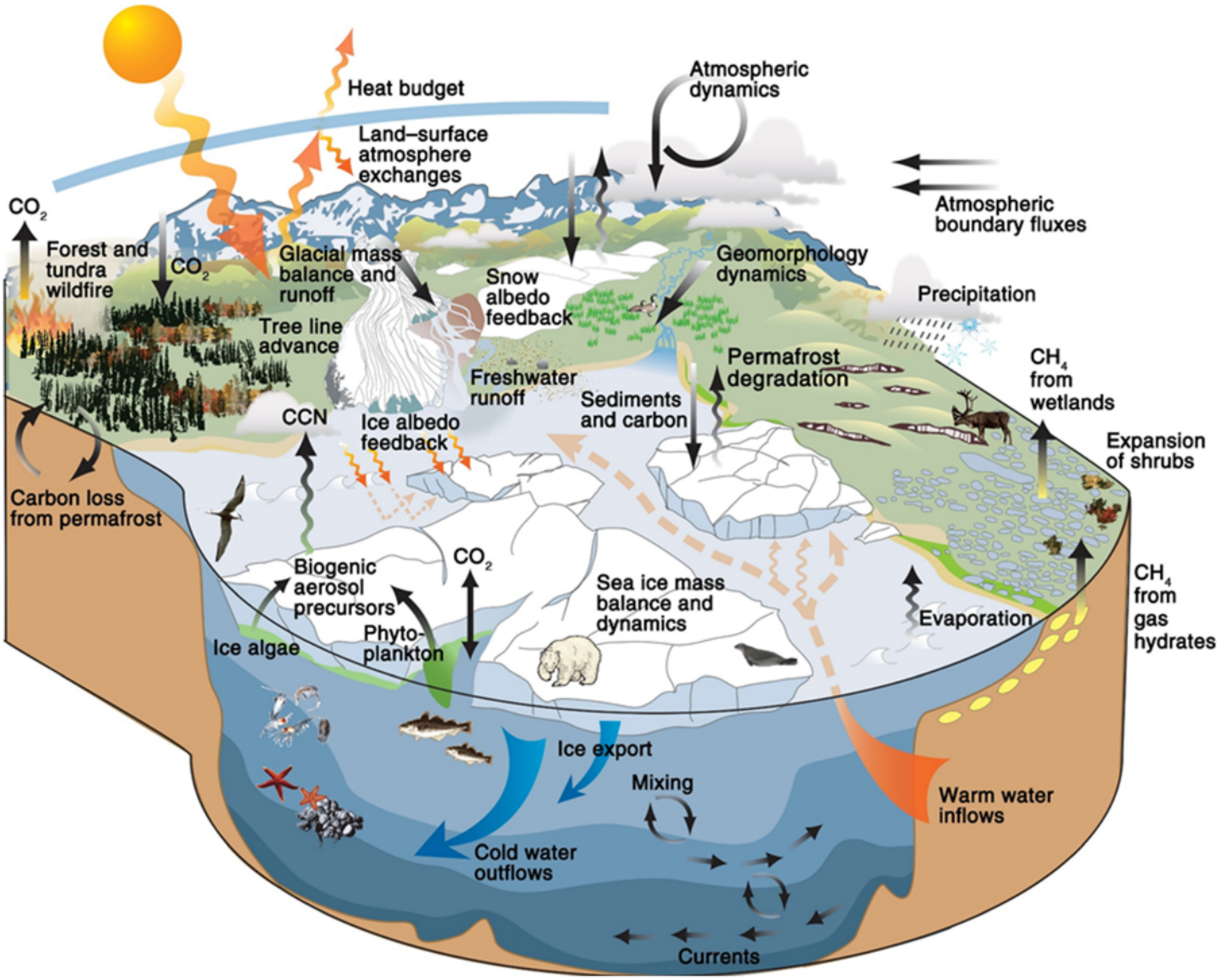

Figure 2. The Arctic Boreal Zone (ABZ) has complex and often poorly understood interactions between the cryosphere, biosphere, hydrosphere, and atmosphere. A change in one process often triggers changes and feedbacks in numerous interconnected processes (e.g., polar amplification). Figure reproduced from Figure 1 of Hinzman, L. D., Deal, C. J., McGuire, A. D., Mernild, S. H., Polyakov, I. V. and Walsh, J. E. (2013), Trajectory of the Arctic as an integrated system. Ecological Applications, 23: 1837-1868. doi:10.1890/11-1498.1.

Agency (JAXA). However, data collection is challenging as the ABZ is characterized by persistent cloudiness, lack of sunlight for months at a time, sea ice, snow and ice covered land surfaces, highly variable air pollution that affects ocean retrievals, and poor thermal contrast between the surface and the air above. Therefore, a complete observing network for the ABZ and key processes would require complementary data collected from space, air, and on the ground (e.g., National Research Council, 2014a) and further satellite and instrument technology development. In addition, a comprehensive suborbital component of an ABZ-ON would provide the crucial data necessary to develop satellite retrieval algorithms and validate satellite observations. Coordination of the establishment of cross-discipline, suborbital ABZ-ON stations and aircraft campaigns would have the benefit of saving operating costs and facilitate information-sharing (e.g., AMAP, 2017). It is important to begin the development of a comprehensive ABZ-ON as the design and deployment of orbital and suborbital networks take time. This development would benefit from observing system simulation experiments (OSSEs) as well as any new high-quality observations, given the paucity of current observations for most components of the ABZ.

In this article, we review the strengths and limitations of current space-based observational capabilities for many of the important components of the ABZ and propose some observational needs, which should be considered in planning future space-based platforms. This review is not meant to be exhaustive, to explicitly cover all ABZ components or satellite data types (e.g., observations relevant to ABZ weather prediction), or to recommend a comprehensive suborbital component of an ABZ-ON. Instead, it is meant to contribute to the ongoing efforts, such as the Integrated Arctic Observation System (INTAROS), the Arctic Research Consortium of the U.S. (ARCUS) and the International Arctic Research Center, to develop a comprehensive ABZ-ON strategy. Other informative reviews and resources on various aspects of the use of satellite data for observing ABZ change and processes include "Remote Sensing of the Cryosphere" (Tedesco, 2015), which provides overviews of remote sensing capabilities including chapters on properties of snow, ice sheets, sea ice, and permafrost, "The Arctic Climate System" (Serreze & Barry, 2014), and several reports by the U.S. National Research Council, including ones on observing Arctic change (National Research Council, 2014a) and specific disciplines, such as permafrost research (National Research Council, 2014b).

We present the historical and current state of satellite observations of individual ABZ components (e.g., permafrost, land ice, ocean temperature) and discuss observational needs going forward. This article begins with surface temperature (section 2), among the most important drivers of ABZ change, and follows with discussions on the ocean (section 3: sea ice, salinity, temperature, circulation, biology, and biogeochemistry), land (section 4: land ice, snow, permafrost, vegetation, wildfires, and wetlands), and atmosphere (section 5: short-lived pollutants, greenhouse gases, clouds, and radiation). The sections are organized around the following questions for the particular variable discussed in the section: Why is observing that ABZ variable important? What suborbital observations do we have of the historical state of the ABZ variable? What is the historical and current state of satellite observations of that variable in the ABZ? What important properties are we currently missing in the ABZ satellite observing network? What are recommendations for an improved, more comprehensive observing strategy (orbital and suborbital) going forward? One section that strays from this format is section 6 on an innovative orbit option for remote sensing of the ABZ.

In section 7, we present our recommendations for prioritizing new satellite observations of the ABZ. In section 7.1, we make general recommendations for satellite observing strategies, and in section 7.2, we discuss specific observational priorities, which are summarized in Table 1, for both orbital and suborbital observations. The focus of our suborbital observational priorities is on the support of the interpretation and validation of satellite data and not necessarily on the development of a comprehensive suborbital component of an ABZ-ON. We prioritize satellite observations with designations of "Most Important," "Very Important," and "Important" based on the following considerations, which are further discussed in section 7.2: (i) "Most Important" observational needs are ones for which the variable is poorly observed currently, and the current process-based understanding of the factors that determine that variable's trends and variations are poorly known (e.g., Hinzman et al., 2013); (ii) "Very Important" observational needs are ones for which the variable is insufficiently observed, and more or better observations are necessary to advance process-based and/or large-scale understanding related to that variable; (iii) "Important" observational needs are ones for which the current and anticipated future observational suite for that variable is adequate in comparison to those for other variables. In section 7.3, we discuss considerations for the development of a comprehensive and integrated ABZ-ON and make a recommendation.

Finally, in this article, we mention numerous satellite instruments and suborbital networks. We recommend the reader to the Committee on Earth Observation Satellites (CEOS) database (http://database.eohandbook.com/) for more detailed information on satellite instrument specifications, history and observations. In addition, the CEOS database website allows the user to search for measurements of specific variables (e.g., ocean salinity, surface albedo, and vegetation). Listings of existing suborbital networks and searchable databases are also available. For example, the Sustain Arctic Observing Networks program (SAON; https://www.arcticobserving.org/; IDA Science and Technology Policy Institute and Sustaining Arctic Observing Networks, 2017) hosts an interactive map that allows the user to search for suborbital networks, such as by region and discipline, and to locate network information, including data access.

Reviews of Geophysics

10.1029/2019RG000652

Table 1
Recommended Satellite Observations, Significant ABZ Drivers and Ancillary Data for Each ABZ Component

Ranking Criteria (as abbreviated from section 7.2)
- ***"Most Important (MI)"*** observational needs are ones for which the variable is poorly observed currently, and the current process-based understanding of the factors that determine that variable's trends and variations are poorly known.
- ***"Very Important (VI)"*** observational needs are ones for which the variable is insufficiently observed, and more or better observations are necessary to advance process-based and/or large-scale understanding related to that variable.
- ***"Important (I)"*** observational needs are ones for which the current and anticipated future observational suite for that variable is adequate in comparison to those for other variables.

ABZ component	Recommended satellite observations	Significant drivers that affect ABZ component	Recommended ancillary data collection
Surface Temperature	(1) *Existing:* Continue thermal infrared observations (I).	(1) Sea ice. (2) Land ice. (3) Snow cover. (4) Permafrost. (5) Fire regimes. (6) Clouds, including for identification of clear-sky conditions.	(1) *Existing, but more required:* Surface stations for validation of satellite surface temperature.
A. Observing Properties of the Oceans			
Sea Ice	(1) *New technology development required:* Finer-resolution (5 km) satellite passive microwave instrument to better define the coast and sea ice edge (MI). (2) *Existing, well-established:* Continue passive-microwave observations of sea ice concentration, distribution, and extent (VI: the current observations are adequate, but there are major concerns regarding whether these observations will be maintained long-term). (3) *Existing, but recent:* Continue sea ice thickness observations from radar and laser altimetry (VI). (4) *New technology development required:* Enhanced SAR for high-resolution, daily determination of sea ice concentration, ice type, ice motion, deformation, ridging, and leads, especially for the operational community (VI; SARs are in orbit but are not providing daily, high resolution coverage of the full Arctic sea ice cover). (5) *Two instruments on same satellite platform:* Radar and laser altimeters for coincident measurements of the thicknesses of the sea ice and the snow on sea ice (VI).	(1) Surface temperature. (2) Atmospheric temperature and winds. (3) Ocean salinity, temperature, and circulation. (4) Incident solar radiation. (5) Freshwater discharge (rivers, land ice). (6) Snowfall.	(1) *Nonexistent*: Solar-powered unmanned aircraft (e.g., large drones) with a snow radar to make repetitive, high-resolution measurements of the snow on sea ice and the snow-ice interface. (2) *Existing but more required:* Field programs to validate the satellite data and address uncertainties.

Reviews of Geophysics

10.1029/2019RG000652

Table 1
(continued)

Ocean Salinity, Temperature and Circulation	(1) *Existing, but new technology required:* sea surface salinity (SSS) observations are too coarse and microwave instruments not sensitive enough. Need microwave radiometers at frequencies lower than 1.4 GHz (VI). (2) *Existing:* Continue infrared and microwave radiometers of sea surface temperature (SST), but higher spatial resolutions desired (I).	(1) Sea ice. (2) Freshwater discharge (rivers and land ice). (3) Precipitation.	(1) *Existing, but more required:* Improve spatiotemporal coverage of suborbital data of salinity and temperature, such as collected by the ARGO network.
Ocean Biology and Biogeochemistry	(1) *New, technology exists:* Extend current instruments to (i) include increased spatial resolution for assessing land-ocean exchanges in the ABZ, and (ii) include ultraviolet wavelengths and higher spectral resolution to assess changes in plankton diversity and carbon quality in the ocean (MI). (2) *Existing:* Continue ocean surface reflectance observations to infer chlorophyll, dissolved organic carbon amount, and suspended particle dynamics (I).	(1) Sea ice thickness and extent. (2) Freshwater discharge (rivers, land/landfast ice, and permafrost thaw) of carbon and nutrients. (3) Coastal erosion. (4) Winds. (5) Ocean salinity, temperature and circulation.	(1) *Existing, but more required:* Field programs that include measurements of water optical and biogeochemical properties from surface platforms (all terrain vehicles, sleds, small boats, research vessels, icebreakers) across the continuum of Arctic rivers, estuaries and the ocean, for validation of satellite products and development of improved ABZ models. (2) *Existing, but more required:* Measurements from autonomous sensors (moorings, floats, buoys, gliders) to sustain continuous *in situ* observations. (3) *Existing, but insufficient*: High spatial resolution remote sensing from airborne sensors. (4) *Existing, but insufficient*: Detailed characterization of atmospheric properties over Arctic rivers, estuaries and ocean for improved atmospheric correction of ocean color.
B. Observing Properties of the Land Biosphere			
Land Ice	(1) *Existing, but new technology required:* Ice and snow albedo (MI). (2) *Existing:* SAR interferometry for ice velocity change (VI). (3) *New:* Meltwater pathways and retention (VI). (4) *Existing:* Radar and lidar altimetry for height change (I). (5) *Existing:* Continue gravimetry for mass change (I).	(1) Clouds. (2) Surface temperature. (3) Ocean temperature and circulation. (4) Anthropogenic short- and long-lived pollutants.	(1) *Existing:* Satellite observations of variables that impact feedback processes involving albedo (e.g., visible, infrared, and near infrared data). (2) *Existing*: Satellite lidar and radar for monitoring ice loss and velocity.
Snow	(1) *New technology required:* snow-water equivalent (SWE) (MI). (2) *New, some technology exists:* Snow cover extent, snow depth, and snow water equivalent from microwave sensors (VI). (3) *Existing:* Continue high-resolution observations of snow cover (I).	(1) Surface temperature. (2) Permafrost. (3) Tundra and boreal vegetation.	(1) *Existing, but more required:* Surface stations exist for validation of snow-covered area, but in most areas the network of meteorological stations in the ABZ is sparsely populated. (2) *Required*: Field programs needed to validate the existing and future satellite data to measure SWE and address uncertainties, especially in forested areas.
Permafrost	Permafrost, which contains large amounts of carbon that may be released to the atmosphere upon thawing, is not directly observable. It may be inferred from satellite observations of	(1) Surface Temperature. (2) Snow extent, snow depth, and water equivalent. (3) Tundra and boreal vegetation.	(1) *Existing:* Satellite active and passive microwave observations to detect freezing and thawing of the surface of the active layer and the behavior of seasonal soil frost.

Reviews of Geophysics

10.1029/2019RG000652

Table 1
(continued)

	soil permittivity changes due to soil freezing in the top of the active layer and by identifying characteristic landforms and surface features (MI).	(4) Fire Regimes. (5) Wetlands, rivers, and lakes.	(2) *Existing, but higher spatiotemporal coverage required:* Data of change detection of surface features (e.g., C-band interferometric SAR). (3) *Existing, but more required:* Surface observations of soil carbon content, ALT.
Tundra Vegetation	(1) *Existing:* Continue observations of land cover trends and anomalies, including greening/browning trends (VI). (2) *New:* Vegetation height observations (VI). (3) *Existing:* Leaf area index (I).	(1) Snow cover and thickness. (2) Fire regimes. (3) Permafrost. (4) Wetlands, rivers and lakes. (5) Surface temperature. (6) Anthropogenic impacts. (7) Large herbivore grazing impacts.	(1) *Existing, but more required:* GPS tracking data of large herbivores to asses grazing impact. (2) *Existing, but more required:* Suborbital data of vegetation cover, biomass, and leaf area index. (3) *Existing, but more required:* Surface albedo data from meteorological stations at remote tundra sites.
Boreal Vegetation	(1) *New, technology exists with some new development*: Improve spatiotemporal resolution of imaging spectroscopy and lidar (VI). (2) *Existing*: Increased coverage and access to very high-resolution visible-shortwave infrared imagery (VI). (3) *New:* repeated (higher temporal frequency) observations of canopy structure from passive optical high-resolution stereo images with standardized viewing geometry (VI). (4) *Existing:* Continue visible-shortwave infrared, microwave observations (I).	(1) Snow cover. (2) Fire regimes. (3) Permafrost. (4) Wetlands, rivers, and lakes. (5) Surface temperature.	(1) *Existing, but coarse spatial resolution:* Satellite data of changing light use efficiency (e.g., SIF). (2) *Existing, but difficult to access, and spatially incomplete:* Internationally-consistent forest inventory (repeatedly measured) of structure and growth, and CO_2/CH_4 flux observations. (3) *Existing, but insufficient*: Suborbital observations of vegetation properties and trace gas concentrations. (4) *Existing, but insufficient*: Consistent multi-temporal and pan-boreal vegetation type layers at moderate resolution (30-500 m) with sufficient physiognomic and floristic detail. (5) *Existing, and rapidly developing*: measurements of patterns of vertical/horizontal boreal structure with high-resolution (2-5 m) pan-boreal Digital Surface/Terrain Models (DSMs/DTMs) and spaceborne lidar (ICESat-2) (6) *Non-existent:* Suborbital observations of vegetation structure in the Russian permafrost larch and other forest domains.
Fire Regimes	(1) *Existing, but beyond lifetime:* Continue observations of smoke plume height, detrainment and the vertical extent of smoke plumes in the atmosphere (VI). (2) *Existing:* Continue active fire detection observations to increase temporal and spatial resolution at the time fires are most active (VI). (3) *Existing*: Develop weather data to define above- and below-ground fuel moisture (dryness or availability) (e.g. SMAP-like L-band radar) (VI). (4) *Existing:* Continue to develop visible observations of burned area and burn severity (I).	(1) Tundra and boreal vegetation. (2) Permafrost. (3) Surface temperature. (4) Wetlands, rivers and lakes. (5) Pollutant and GHG concentrations and fluxes. (6) Radiative feedbacks (land cover, cloud, and ice/snow).	(1) *Existing, but incomplete:* Suborbital data on the depth of duff/peat/soil organic matter contained in an ecosystem (pre-fire fuel) and consumed post fire. (2) *Existing, but incomplete:* Expand suborbital observing network, especially in Russia, to evaluate and interpret satellite-derived fire and fuel properties. (3) *Existing, but more required*: Surface data to validate and interpret satellite and suborbital fire type, burned area, burn severity, fuel structure and burn depth, particularly in Russia.

10.1029/2019RG000652

Table 1
(continued)

Wetlands	(1) *New, technology exists:* longer wavelength microwave radar (L-band) with higher spatial and temporal resolutions (MI). (2) *Existing:* Continue passive microwave, active microwave and visible imagery observations to infer fractional surface-water extent (VI).	(1) Permafrost. (2) Tundra and boreal vegetation. (3) Fire regimes.	(1) *Existing, but more required:* Surface stations for validation of satellite surface temperature. (2) *Existing, but insufficient*: Field programs and surface stations for validation of wetland extent, distribution, vegetation characteristics, and heat/carbon/nutrient exchanges between wetland soil, water, and atmosphere.
C. Observing Chemistry and Composition of the Arctic Atmosphere			
Short-Lived Pollutant Concentrations	(1) *Existing, but well past design life:* Lidar for observations of aerosols in all light conditions (VI). (2) *Existing:* Continue passive ultraviolet/visible and multi-angle instruments in LEO, but finer spatial resolution and better sensitivity, and polarization capability are desired (I). (3) *Existing:* Passive limb observations of aerosols (I). (4) *New, technology exists:* HEO orbits for passive instruments to gain more spatiotemporal coverage than LEO ones for short-lived pollutants (I).	(1) Fire regimes. (2) Clouds (cloud-aerosol interactions).	(1) *Existing, but more required:* Observations of trace gases and aerosols (e.g., lidars for all light observations of aerosols co-located with sun photometers and shortwave and longwave radiometers) for satellite validation as well as the complex vertical structure of the ABZ atmosphere, which is needed as input to retrieval algorithms. (2) *Existing, but more required:* As input to pollutant retrieval algorithms, satellite variables needed include surface reflectivity, vertical profiles of temperature, cloud phase, cloud separation from ice/snow, and cloud top height. (3) *Existing:* Anthropogenic pollutant satellite observations for estimating transport to ABZ. (4) *Required:* Targeted research missions that carry a more comprehensive payload than past and current missions, such as including instruments to measure particle hygroscopicity and mass-extinction efficiency. (5) *Existing, but much too limited*: Direct sampling of light-absorbing aerosol on snow and ice surfaces. (6) *Existing:* Volcanic monitoring.
Long-Lived Greenhouse Gas Concentrations and Fluxes	(1) *New, technology under development:* Lidar for observations of CH_4 and CO_2 in low-light/night/cloudy conditions (MI). (2) *New, technology exists:* HEO orbits for passive instruments to gain more spatiotemporal coverage than LEO ones (VI). (3) *Existing and planned:* Continue passive instruments in LEO (I).	(1) Wetlands, rivers, and lakes. (2) Surface temperature. (3) Fire regimes. (4) Boreal and tundra vegetation. (5) Permafrost.	(1) *Existing, but more required:* Given the complex vertical structure of the ABZ atmosphere, a more comprehensive network of suborbital data of vertical profiles of CH_4 and CO_2 is desired for the inference of surface fluxes from column data. (2) *Existing, but more required:* As input to CH_4 and CO_2 retrieval algorithms, satellite and suborbital data of variables needed include surface reflectivity, vertical profiles of temperature and water vapor, cloud separation from ice/snow, and cloud top height. (3) *Existing, but more required:* suborbital lidars for low-light/night observations.
Clouds	(1) *Existing, but old:* Continue and expand lidar/radar observations to characterize 3-D cloud	(1) Cloud radiative effects and feedbacks. (2) Latent and sensible heat. (3) Surface temperature.	(1) *Existing:* Satellite data of water vapor profiles. (2) *Existing, but sparse spatiotemporal coverage:* In situ suborbital measurements, primarily from

10.1029/2019RG000652

Table 1
(continued)

	distribution and to distinguish transparent and opaque clouds (VI). (2) *Existing, but improve horizontal coverage:* Continue passive, polar-orbiting, multi-sensor observations of cloud properties (I).	(4) Aerosols.	aircraft, of cloud and aerosol microphysical properties and their profiles. Need more frequent sampling in each season to develop robust statistics. (3) *Existing, but sparse spatiotemporal coverage:* Simultaneous surface and top of atmosphere radiation measurements in cloudy and hazy conditions. Need more frequent sampling in each season to develop robust statistics. Also require observations during and after major volcanic events, which can have significant impacts on ABZ radiation.
Surface Ultraviolet Radiation and Stratospheric O_3	Surface ultraviolet radiation is not directly observable, but may be inferred from satellite data of clouds, aerosols, and stratospheric O_3. (1) *Existing:* There are currently sufficient stratospheric O_3 observations of columns and profiles (I).	(1) Clouds. (2) Aerosols.	(1) *Existing:* Continue current suborbital ultraviolet observations at existing ABZ observatories for validation. (2) *Existing, but old:* There are no comprehensive follow-on missions (e.g., MLS) of current instruments that observe the vertical profiles of stratospheric gases that are required to understand the chemical and dynamical causes of the trends and variations of stratospheric O_3.
ABZ Energy Budget	(1) *Existing, well-established:* CERES broadband radiometer instruments since 2000 provide a continuous top of atmosphere energy budget. However, there is no current plan for maintaining these observations long-term, beyond ~2032. Continuity of this record is critical. (VI) (2) *Existing, but more required*: Currently, data on the spectral and angular variation of the surface albedo of snow-covered and sea ice surface (including the bi-directional reflectance function) are available from suborbital measurements, but limited. A targeted satellite mission to provide higher accuracy measurements at increased spectral resolution is needed (technology/instrument development required) (VI). (3) *Future:* The PREFIRE (Polar Radiant Energy in the Far-Infrared Experiment) mission will provide increased spectral resolution in the far infrared (wavelengths longer than 15 μm) for the ABZ energy budget representing the first systematic far infrared measurements to investigate the spectral variation of surface emissivity (I).	(1) Cloud properties. (2) Surface albedo (sea ice, snow cover, vegetation type). (3) Temperature and humidity profiles. (4) Surface skin temperature. (5) Aerosol.	(1) *Existing*: MODIS cloud property retrievals. (2) *Existing*: Temperature and humidity profiles from infrared sounders and meteorological reanalysis. (3) *Existing, but limited*: surface site observations and field campaigns (ship-based and airborne). (4) *Existing, but aging*: active remote sensing (e.g., CALIPSO/CloudSAT) cloud retrievals useful in satellite-retrieved radiative flux validation. (5) *Required*: Acquisition of statistically robust suborbital data sets for validation of satellite-retrieved energy budget.

2. Surface Temperature: A Driver of ABZ Change (Josefino C. Comiso)

Among the most important parameters needed to understand changes in the ABZ is surface temperature as it controls much of the physical and radiative characteristics of the Earth's surface, especially in areas covered by snow, ice or permafrost. For example, surface temperature dictates the onset of melt or freeze-up as well as duration of melt or freeze-up in these areas. In this regard, it is the factor that determines the residence time of snow and how thick the snow can be during winter and how thick the sea ice cover can become before the spring melt begins. Together with surface albedo, it also controls the amount of energy, including turbulent, latent and sensible heat fluxes, that is transferred between the surface and the atmosphere.

Satellite and in situ surface temperature data show that the rate of warming in the Arctic since 1981 is more than three times higher than the global rate (Comiso & Hall, 2014). This is caused in part by ice-albedo feedback which is associated with the decline of high albedo surfaces, such as sea ice and snow in the region (Holland & Bitz, 2003; Stuecker et al., 2018). The amplification in warming is consistent with the observed decline in the Arctic perennial ice cover which went through a dramatic retreat in 2007 when the average sea surface temperatures in the Beaufort Sea and Chukchi Sea regions had record high values (Kashiwase et al., 2017; Shibata et al., 2010). An increasing trend in solar heat input to the upper Arctic Ocean has also been observed and attributed to the rapid decline of the sea ice cover (Perovich et al., 2007).

The key tool used for measuring surface temperature from space has been thermal infrared sensors (around 10 to 14 μm). Examples of such sensors include the Nimbus-7/Thermal Humidity Infrared Radiometer (THIR) launched in 1978, NOAA/Advanced Very High Resolution Radiometer (AVHRR), which has been providing continuous global data since 1981, the ESA/Advanced Along Track Scanning Radiometer (AATSR) launched in 2002, Earth Observing System (EOS)/Terra and EOS/Aqua Moderate Resolution Imaging Spectroradiometer (MODIS) launched in 1999 and 2002, respectively, and ESA/ENVISAT/Medium Resolution Imaging Spectrometer (MERIS) launched in 2002. For time series studies, the sensor that has been used the most is the AVHRR sensor because of comprehensive coverage and the availability of global and continuous data since August 1981. There have been many challenges, however, associated with the creation of time series of global surface temperature data from the AVHRR sensor series. For example, since the expected lifetime of each sensor is about five years, a long data record is possible only if similar and compatible sensors are launched one after another. Although the AVHRR series was designed with that purpose in mind, the different sensors have different calibration and they tend to degrade with time. Furthermore, there were no overlaps in coverage to enable inter-calibration of the different sensors, and, although the system is multispectral, the set of channels available are sometimes not effective for discriminating clouds from snow-covered surfaces.

There were many studies made to overcome these problems, the effectiveness of which varied with season, surface condition, and location (Comiso, 2003; Key & Haefliger, 1992; Simpson & Yhann, 1994; Steffen et al., 1992). One of the key sources of error has been the inability to accurately mask out cloud-covered areas, which is especially difficult in snow-covered regions because of the lack of contrast in both reflected shortwave (SW) and emitted longwave (LW). To minimize errors, spatial techniques have been applied, such as the use of daily differencing of data assuming that the cloud cover changes from one day to the next. Statistical techniques were also used assuming that the statistics of cloud-covered areas are different from those not covered by clouds (Comiso, 2003). To account for the lack of overlapping data between sensors and the apparent degradation of sensors, the calibrations of the different sensors were adjusted for improved consistency through the use of high quality in situ data. Since in situ data usually represent 2-m air temperatures, the 2-m data are first converted to surface temperature data on a monthly basis using coefficients from regression analysis of 2-m air and surface data from year-long measurements (i.e., Perovich et al., 2003) before they were used to improve the temporal consistency of AVHRR data. The uncertainties associated with retrievals have been estimated to be generally about 2 to 3°C (Steffen et al., 1992). However, such estimates are usually based on comparative analysis with in situ data and more recent studies using aircraft thermal infrared data indicate that the accuracies can be as high as 1.5°C. Also, the spatial distribution of temperatures over land, ice sheets, and sea ice as observed by AVHRR is represented more accurately than those provided by reanalysis data, especially in areas where there is a paucity of in situ data (Comiso, 2003).

Among the most important sources of uncertainty in temperature data is the ability to identify observations under clear skies conditions. Some techniques used for cloud masking of AVHRR data assume that the temperature of clouds is lower than that of the surface (e.g., Comiso, 2003). This is generally the case, but not always, because of the effect of temperature inversion, which is a common feature in the Arctic during winter. During inversion, the temperature of the troposphere is higher than that of the surface making it more difficult to discriminate cloud-covered areas from cloud-free ones. The detection of inversion has been made possible by instruments like the Atmospheric Infrared Sounder (AIRS) on board the EOS/Aqua satellite. Refinements in the techniques for cloud detection that make use of this capability to detect the occurrences of inversion would lead to more accurate determination of surface temperature.

Plots of monthly averaged surface temperatures as retrieved from AVHRR data at high-latitude regions (>60° N) in the Northern Hemisphere are shown in Figures 3a and 3b for land and sea ice, respectively. To illustrate how the time series is put together, data from the different NOAA/AVHRR sensors (NOAA-7 to NOAA-19) are indicated in different colors. It is apparent that land surface temperatures are more seasonal than those over sea ice in part because the data from land include those from glaciers and the Greenland ice sheet, which experience extremely low temperatures in winter. To gain insight into the yearly variability and trends, monthly surface temperature anomalies are presented in Figures 3c and 3d, for land and sea ice, respectively. The monthly anomalies were derived by using averages for each month from 1981 to the present as climatological values that are subtracted from the monthly data. It is apparent that the temporal distribution of anomalies over land is similar to those over sea ice. The patterns of dips and peaks are not identical, but they occur at approximately the same time indicating that changes over land areas are coherent with changes over the sea ice covered regions. The trends in temperature are both positive but slightly different with the trend over land being 0.38 ± 0.03°C/decade while the trend over sea ice is about 0.29 ± 0.04°C/decade. The same dataset has also been used to provide a similar record of sea surface temperature (SST). Results from analysis of these data (not shown) indicate a trend in SST of about 0.18°C/decade. It should be noted, however, that the spatial distribution of the trend (not shown) is not uniform since there are some areas where the surface temperature trend is near zero or even negative as in parts of Siberia and the Bering Sea.

When a long-term record is not required, there are other sensors that provide more accurate surface temperatures than AVHRR data. For example, continuous and well-calibrated data are available from EOS/Terra and EOS/Aqua MODIS that have several (36) channels, many of which can be used for atmospheric correction and cloud masking. Such data have been used to create a climate-quality data record of surface temperature over Greenland (Hall et al., 2012; Hall et al., 2018). Similar data sets are also available from ESA/ENVISAT/MERIS and AATSR from 2003 to 2011. The AATSR, and a similar system called Sea and Land Surface Temperature Radiometer (SLSTR) on board Sentinel 3 launched in 2016, makes a couple of measurements for each data point at two different incidence angles for improved atmospheric corrections. It is an especially attractive system and has the potential of providing the most accurate measurement. Although lacking in global coverage, there are also sensors like NASA's Terra Advanced Spaceborne Thermal Emission and Reflection Radiometer (ASTER), Landsat 8, and Satellite Pour l'Observation de la Terre (SPOT) that provide high resolution data (of about 30 m). SST can also be derived using JAXA's Advanced Microwave Scanning Radiometer for the Earth Observing System (AMSR-E) on NASA's Aqua satellite, and JAXA's AMSR2 on Japan's Global Change Observation Mission-Water (GCOM-W) satellite, which is a passive microwave sensor that is able to make continuous measurements even during cloudy conditions. Such data are available from 2003 to 2011 and from 2012 to the present, but the resolution is relatively coarse at about 50 km.

Overall, global surface temperatures, including those in the ABZ, can be measured from space with reasonable accuracy during clear-sky conditions using thermal infrared sensors. The use of the same type of sensor, like AVHRR, over a long term period would be ideal for evaluating long term changes. But in the case of AVHRR, there are shortcomings as indicated previously and the data should be combined with the newer and more capable systems, like MODIS, MERIS, AATSR and SLSTRL, for improved accuracy, better temporal and spatial resolution and more comprehensive coverage. Higher resolution systems, like Landsat 8 and ASTER, should also be used, especially for regional and mesoscale studies. Satellite data should be used to supplement available in situ data sets from meteorological stations and other sources in the ABZ (Rigor et al., 2000). In this regard, studies should take advantage of facilities, like the U.S. Department of Defense Atmospheric Radiation Measurement (ARM) facility in Barrow, Alaska, which provides very

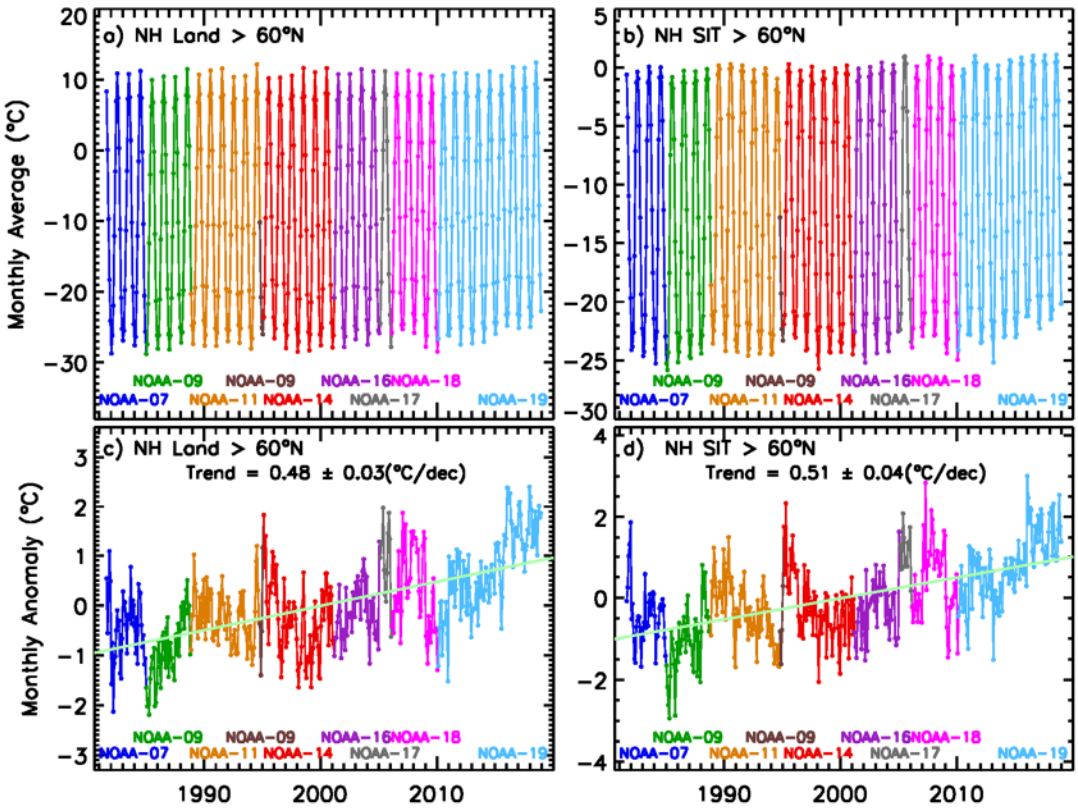

Figure 3. Plots of monthly averaged surface temperature data (>60°N) as derived from Advanced Very High Resolution Radiometer (AVHRR) over (a) land and (b) sea ice. Contributions from the AVHRR sensors from NOAA-07 to NOAA-19 are shown in different colors. Plots of monthly anomalies of surface temperatures over (c) land and (d) sea ice (SIT). The anomalies were derived from the monthly data by subtracting the climatology for each month. The trends as indicated are the result of linear regression.

comprehensive atmospheric and surface measurements, including that of temperature. Such facilities provide excellent validation data for satellite temperatures, and in addition, can collect extensive data of cloud and radiation processes that enable improved understanding of the climate system in the region and proper interpretation of satellite surface temperature data.

Table 1 summarizes our recommendations for improving the orbital and suborbital observations of surface temperature.

3. Observing Properties of the Arctic Ocean

In this section, we discuss the (1) historical and current state of observations of the properties of the Arctic Ocean, including sea ice, salinity, temperature, circulation and ocean productivity and (2) observational needs going forward, which are summarized in Table 1.

3.1. Arctic Sea Ice (Claire L. Parkinson)

Sea ice is a major component of the Arctic climate system, reflecting solar radiation, restricting exchanges of heat, mass, and momentum between the ocean and the atmosphere, and affecting ocean downwelling and circulation through such processes as expelling salt as the ice forms and ages and releasing relatively fresh water as the ice melts. A mass change of particular relevance to discussions of climate change is that of CO_2, as CO_2 uptake by the polar oceans can be expected to increase as sea ice retreats.

Sea ice also affects the life of the Arctic, from the microorganisms living within the ice all the way up through the food chain to the iconic polar bears that live much of their lives on the ice and feed off marine life from the platform that the ice provides. Among the animals affected by sea ice are humans, and among the most discussed impacts on humans of reduced sea ice coverage in recent and forecasted future decades is the

opportunity this provides for increased shipping through the Northwest and Northeast Passages (e.g., Barber et al., 2018; Brigham, 2010; Smith & Stephenson, 2013; Stephenson & Smith, 2015). This opportunity comes with concerns as well, such as increased chance of oil spills and other environmental pollution and increased political tensions. Further, while shipping through the Northwest and Northeast Passages has gotten easier, the increased mobility of the reduced Arctic ice pack has on occasion produced more hazardous ice conditions in other regions (Barber et al., 2018).

The impact of the ice extends well beyond the Arctic itself, as shown through both carefully controlled modeling studies (e.g., Rind et al., 1995) and inferences from observations (e.g., Walsh, 2013). Changes in sea ice are tightly intertwined with changes in temperature and have further been tied to changes in the frequency of severe winters in Eurasia (Mori et al., 2014) and, through changes in the jet stream, to changes in the frequency of many extreme weather events in Northern Hemisphere midlatitudes (Cohen et al., 2014; Francis & Vavrus, 2015). Through their effect on temperature, sea ice decreases are also likely a cause of the increased methane emissions from the Arctic tundra and wetlands (Parmentier et al., 2013; Parmentier et al., 2015). Well illustrating the interconnectedness of the climate system, Nakamura et al. (2016) find that the stratosphere plays a crucial role in some of the connections between sea ice changes and weather changes in lower latitudes.

Sea ice covers approximately 15×10^6 km^2 (i.e., 1.5 times the area of Canada) of Arctic waters in wintertime, retreating to approximately 5×10^6 km^2 in summer, with considerable interannual variability. Prior to the advent of satellite technology, getting an Arctic-wide picture of this enormous expanse of ice was particularly difficult, hindered not only by the large areal extent but also by the dangers imposed by the cold, the dark (in wintertime), and the dynamics of the ice cover, with floes continually breaking up, moving, and crunching against each other.

In great contrast to the in situ difficulties, sea ice has proven particularly amenable to satellite observations, as at many wavelengths the ice is quite readily distinguished from liquid water. Furthermore, it is always liquid water on which the sea ice is floating, in huge contrast to snow cover on land, for which the underlying surface could be concrete, tundra, grass, or many other surfaces. This contrast between the uniformity versus nonuniformity of the underlying surface, plus the fact that snow cover on land can be hidden under trees in the boreal forest, makes it far easier to identify and quantify sea ice from satellite data than to do the same for snow cover.

Sea ice has been observed and studied with data from a wide variety of satellite instruments. First came visible and infrared observations, which can provide readily recognizable images of sea ice under sunny and cloud-free conditions. Such images were available in the early 1960s from NASA's first Television and Infrared Observation Satellite (TIROS), launched in 1960, although these images were limited to latitudes equatorward of 60° N and S, providing a major limitation for sea ice monitoring. Much better coverage came with the 1964 launch of the Nimbus 1 satellite, which was placed in a near polar orbit allowing data coverage poleward to 82.5°N. Further advances in visible and infrared imagery came with the Landsat and AVHRR series, both begun in the 1970s and still continuing today, and with MODIS, launched in December 1999 on the Terra satellite and in May 2002 on the Aqua satellite, and the Visible Infrared Imaging Radiometer Suite (VIIRS), launched in October 2011 on the Suomi National Polar-orbiting Partnership (Suomi NPP) satellite.

Valuable as the visible data are for obtaining readily recognizable, high resolution images of the sea ice cover during periods of sunlight and cloud-free conditions, they are not nearly so valuable during darkness and/or cloudy conditions. In great contrast, with careful choice of wavelength, microwave imagery can avoid both of those limitations, as (1) the microwave radiation derives from the Earth system and does not require sunlight, and (2) at some wavelengths the microwave radiation passes through most clouds unaffected, in significant part because the particle sizes in the clouds are much smaller than the wavelengths of the radiation. These advantages, plus the fact that the microwave signature of sea ice differs significantly from the microwave signature of liquid water, have made satellite passive microwave technology enormously valuable for obtaining climate records of the sea ice cover.

The first major satellite passive microwave imager was the single-channel Electrically Scanning Microwave Radiometer (ESMR) on NASA's Nimbus 5 satellite launched in December 1972 (the Russian COSMOS-243 satellite, launched in 1968, carried a nonimaging passive microwave radiometer; Massom, 1991). The ESMR

instrument was highly successful in demonstrating the value of passive microwave imagery for monitoring sea ice (and other variables), although with only one channel it did not allow sorting through such complications in the sea ice cover as differences in ice type and melt and/or snow on the ice surface. As a result, the follow-on Scanning Multichannel Microwave Radiometer (SMMR) on NASA's Nimbus 7 satellite was a marked improvement. SMMR was launched in October 1978 and provided a sea ice data record from November 1978 through mid-August 1987. SMMR was followed by a series of Special Sensor Microwave Imager (SSMI) and SSMI Sounder (SSMIS) instruments on satellites in the U.S. Department of Defense's Defense Meteorological Satellite Program (DMSP), with the first SSMI launched on the DMSP F8 satellite in June 1987. The SSMI/SSMIS series continues today and has been joined by such additional passive microwave instruments as AMSR-E (no longer operating), AMSR2, and India's Multi-frequency Scanning Microwave Radiometer (MSMR) on India's Oceansat 1, launched in May 1999.

The SMMR/SSMI/SSMIS combination has provided a sea ice record now exceeding four decades in length. By the mid and late 1990s, it was clear from this record that the sea ice coverage of the Arctic was decreasing (e.g., Johannessen et al., 1995; Parkinson et al., 1999). This decrease, overall, has speeded up in the subsequent years (e.g., Comiso et al., 2008; Stroeve et al., 2012) and is reflected also in such additional trends as shortening of the sea ice season (Parkinson, 2014) and earlier onset of melt on the sea ice (Bliss et al., 2017). Figure 4 illustrates the passive microwave record of the Arctic sea ice cover and its depiction of changes that have occurred since the late 1970s, showing stark decreases in sea ice coverage in the mid-winter month of February in the Sea of Okhotsk (off the coast of Siberia) and the Barents Sea (north of Scandinavia and western Russia) and in the mid-summer month of August in the central Arctic. Although there is a large amount of interannual variability, the 1979 and 2018 snapshots appropriately reflect the overall loss of sea ice coverage over the 1979–2018 time period.

One extremely important aspect of the sea ice cover that has not been obtained from passive satellite instruments, whether microwave or otherwise, is ice thickness for the full range of ice thicknesses (for thicknesses up to 0.5 m, see Tian-Kunze et al., 2014). To obtain the total volume of Arctic sea ice, a thickness measurement is needed along with the areal measurement provided by the passive microwave instrumentation. Ice thickness has been obtained from upward-looking sonar on submarines, but these data sets are tremendously limited by where and when the submarines are in the Arctic and taking sonar measurements. Despite the limitations, the submarine data have suggested a substantial thinning of the ice cover (e.g., Rothrock et al., 1999; Yu et al., 2004), and this result nicely complements the ice retreat found from the satellite passive microwave data.

Although we do not yet have a climate-quality ice thickness record, the potential of satellites to obtain weekly ice thickness records throughout the Arctic bodes well for an eventual climate-quality record derived from satellites. Radar altimeters on board the European satellites European Remote Sensing (ERS)-1, ERS-2, and CryoSat2, launched in July 1991, April 1995, and April 2010, respectively, and the Geoscience Laser Altimeter System (GLAS) on NASA's Ice, Cloud, and land Elevation Satellite (ICESat), launched in January 2003, have demonstrated the value of both radar and laser altimetry for ice thickness measurements (Kwok et al., 2009; Laxon et al., 2013). The ICESat mission ended in 2009 and is now followed by the ICESat-2 mission, launched in September 2018.

Another sea ice variable with limited satellite-based results is snow depth on sea ice. Snow cover affects the surface energy balance, with an albedo typically higher than that of snow-free ice and a low thermal conductivity, so that its presence increases the reflection of solar radiation and further restricts heat transfers between the atmosphere and the underlying ocean. Snow depth on sea ice has been estimated from satellite passive microwave data at least since the late 1990s, when Markus and Cavalieri (1998) developed a snow depth algorithm based on two channels of microwave data and an empirically derived linear fit to in situ Antarctic snow depths. Brucker and Markus (2013) used airborne radar data from Operation IceBridge to perform an assessment of snow depth over Arctic seasonal sea ice calculated from AMSR-E data for the period 2009–2011. Although the results varied depending on location, overall the difference between the AMSR-E results and the IceBridge results was 0.00 ± 0.07 m. Still, several regions were identified with errors exceeding 0.10 m (Brucker & Markus, 2013). Comparison of the Operation IceBridge data with in situ snow thickness measurements yielded a root-mean-square error of 5.8 cm (Webster et al., 2014). A subsequent comparison of snow depths derived from IceBridge data through five retrieval algorithms was done explicitly to help inform the development of next-generation algorithms for the data (Kwok et al., 2017).

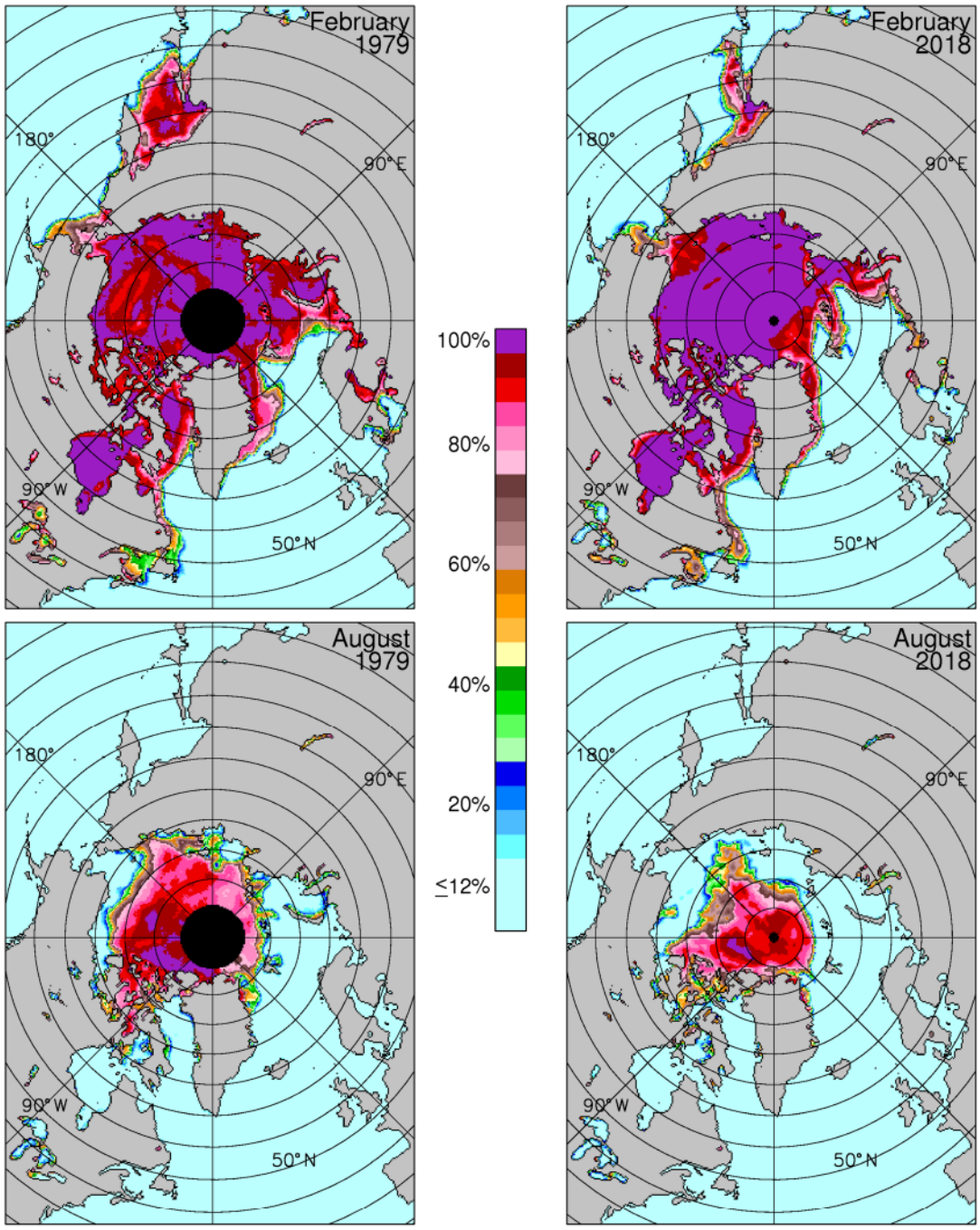

Figure 4. Mapped monthly average sea ice concentrations (percent areal coverage of sea ice) for the mid-winter month of February and the mid-summer month of August, for both 1979 and 2018, the first and last full years to date of the satellite multi-channel passive-microwave sea ice record. The black circles centered on the North Pole in each image identify areas of missing data, due to the satellite orbits not reaching the Pole.

Rostosky et al. (2018) tackled the problem of expanding snow depth retrievals from satellite passive microwave data to include snow depths over multiyear ice, taking advantage of the 6.9 GHz measurements from the AMSR-E and AMSR2 sensors. Comparisons of the derived snow depths with Operation IceBridge springtime measurements yielded good agreement, although better with first-year ice than multiyear ice (Rostosky et al., 2018). Maaß et al. (2013) examined the use of lower frequency passive microwave data, at 1.4 GHz

(L-band), from the ESA's Soil Moisture and Ocean Salinity (SMOS) satellite to retrieve snow thickness estimates over thick Arctic sea ice, detailing both the complications and the sense that this could be an approach worth pursuing further.

The potential exists for satellite-derived Arctic-wide estimates of snow depth on sea ice through subtracting ice freeboard estimates derived from radar altimetry from total snow and ice freeboard estimates derived from laser altimetry. This potential was explored by Kwok and Markus (2018) in anticipation of coincident measurements from CryoSat-2's radar altimeter and ICESat-2's laser altimeter, using an airborne laser altimeter as a proxy for the satellite laser altimeter prior to the ICESat-2 launch. Comparisons with snow depths obtained from an airborne snow radar on Operation IceBridge were encouraging for the eventual derivation of snow thickness from satellite radar and laser altimeters (Kwok & Markus, 2018). Accuracy in the snow depth product is important not just for a measure of climate change but also because the snow depth affects the calculation of sea ice thickness from the altimetry data. More work remains, especially in determining how close the laser reflection is to the top surface of the snow and how close the radar reflection is to the ice-snow interface.

Additional satellite instruments used for sea ice studies include scatterometers and synthetic aperture radars (SARs). Scatterometry data from the European ERS-1 and ERS-2, the Japanese Advanced Earth Observing Satellite-1 (ADEOS-1) and ADEOS-2, launched in 1998 and 2002, respectively, and NASA's Quick Scatterometer (QuikSCAT), launched in 1999, have been used for identifying and monitoring ice type and ice drift and for operational ice-edge detection. Because backscatter is sensitive to salt, scatterometers can be more effective than radiometers in distinguishing first-year versus multi-year ice (e.g., Nghiem et al., 2007), whereas backscatter complications from wind roughening of the ocean can make radiometers more effective than scatterometers in identifying the ice edge (e.g., Meier & Markus, 2015). SAR data from the U.S. Seasat, launched in June 1978, the Russian COSMOS-1870, launched in July 1987, the European ERS-1 and ERS-2, JAXA's Japanese Earth Resources Satellite-1 (JERS-1), launched in February 1992, the Canadian Space Agency's RADARSAT-1 and RADARSAT-2, launched in November 1995 and December 2007, respectively, and the ESA's Sentinel-1 C-band SAR, launched in April 2014, have proven useful in characterizing ice roughness and other details of the sea ice cover.

When considering future needs for satellite observations of sea ice, three high priority items are to: (1) continue the passive microwave record that has obtained so much information about sea ice since the early 1970s and now has a fairly complete record since late 1978, (2) obtain a time series of laser altimeter measurements of ice thickness from the recently launched ICESat-2 satellite, and (3) continue radar altimeter measurements with CryoSat-2 or follow-on missions, for the ice thickness measurements they provide.

For much more on the satellite remote sensing of sea ice, the reader is referred to reviews in Parkinson and Cavalieri (2012) and Meier and Markus (2015).

In view of the highly coupled nature of the Earth system, the changes in Arctic sea ice have many ramifications, from warming the atmosphere and other climate impacts, to causing numerous changes in the polar ecosystem, to impacts on humans, including those living in, working in, or visiting the Arctic region. For all these reasons and additional reasons, the future of the Arctic sea ice matters far beyond the Arctic sea ice itself. Like almost all predictions, the predictions for the future of Arctic sea ice are filled with uncertainties, although the consensus viewpoint of those engaged in climate change studies involving sea ice is that the Arctic sea ice coverage will likely continue to decrease, overall, in the upcoming decades. For a review on modeling the future of Arctic sea ice, including the types of modeling approaches needed to improve the simulations, the reader is referred to Maslowski et al. (2012).

3.2. Arctic Ocean Salinity, Temperature, and Circulation (Emmanuel P. Dinnat, James Carton)

Observing the Arctic Ocean is important because of its fast and amplified response to changes in climate, and its potential impact on future climate change through interactions with the cryosphere, atmosphere, land, and lower latitude oceans. The Arctic Ocean is not only the smallest ocean, but also the shallowest (Figure 5, left). Its average depth is ~1,200 m and most of its water is shallower than 1,000 m, owing to the large extent of the Eurasian continental shelf. Most of its connections with the Pacific and Atlantic (Bering Strait, channels of the Canadian Archipelagos, Barents Sea) are shallow, with the exception of Fram Strait (as deep as 2.5 km). Large exchanges of freshwater (e.g., ice sheet melt, river runoff,

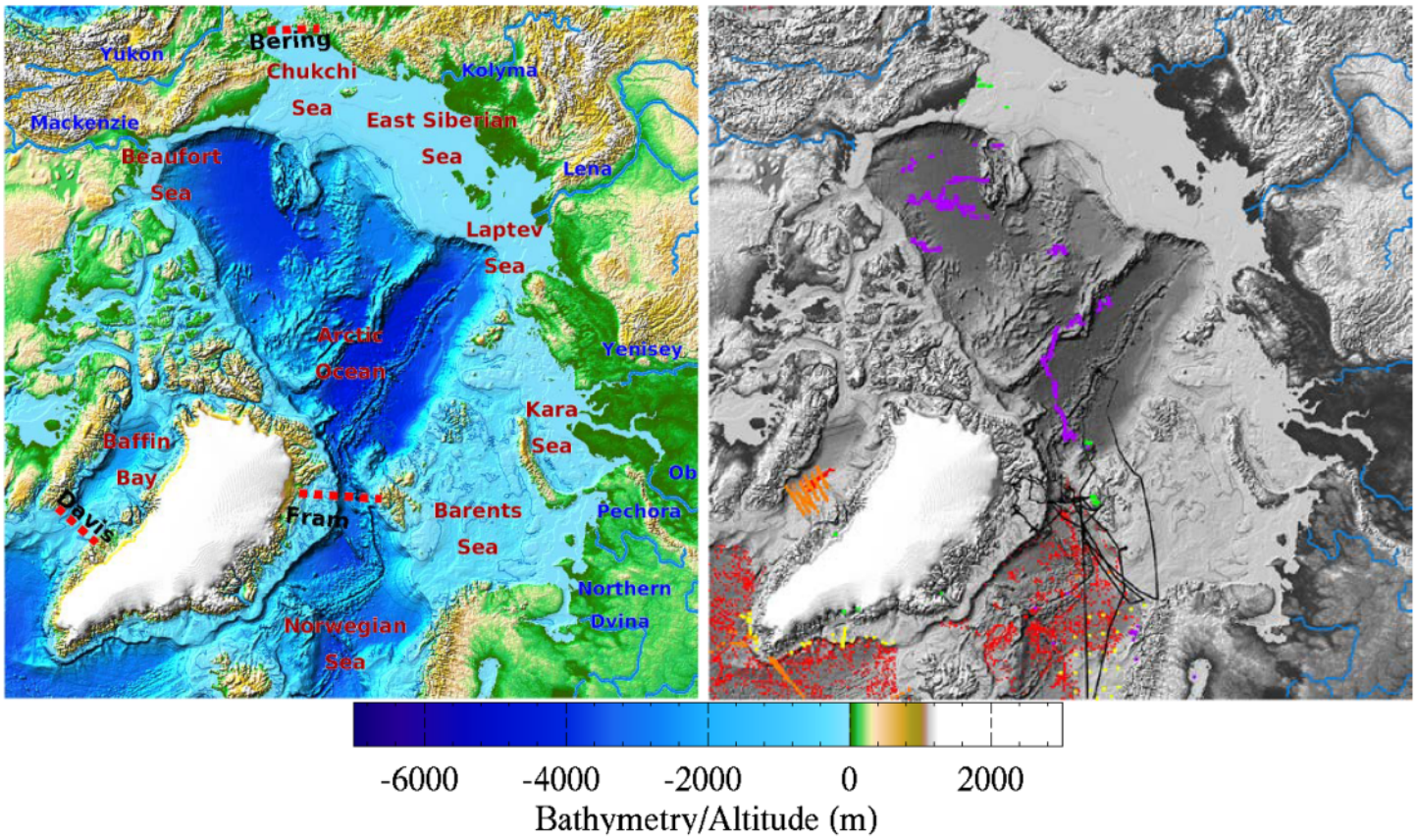

Figure 5. (left) Map of the Arctic Ocean and its marginal seas (red labels), major rivers (blue labels) and major straits (red lines and black labels) in the Arctic Boreal Zone (ABZ). Colors report the bathymetry and topography (data from IBCAO Version 3.0; Jakobsson et al., 2012). (right) Location of in situ measurements of ocean surface (10-m deep or less) salinity and temperature for the year 2016. Measurements are from the Argo network of drifting floats (red dots; Argo, 2019), research vessels or ships of opportunity (e.g., orange tracks in the Baffin Bay and off the southern tip of Greenland, black tracks originating from northern Europe, yellow dots in Norwegian sea). The magenta dots represent observations mostly from Ice Tethered Profilers that measure ocean properties under the sea ice cover. Data are from the Coriolis Ocean database ReAnalysis (CORA) database and the R/V Polarstern (black tracks).

precipitation) and heat (e.g., ocean advection, atmosphere heat fluxes) occur in the Arctic Ocean. Thus the Arctic Ocean can provide extended climate memory to the ABZ such as when sea surface temperature (SST) during one summer leads to a decrease in sea ice growth in the following winter (Steele et al., 2008), which in turns leads to more absorption of SW radiation. Incoming Atlantic Ocean water warms and salinifies the intermediate waters of the Arctic Ocean and likely plays a role in amplification of climate change at high latitudes (Spielhagen et al., 2011). In a warming climate, increased freshwater input from ice melt, continental discharge from the ABZ rivers (Figure 5, left), and changes in precipitation/evaporation can enhance the stability of the Arctic Ocean (along with increasing temperature stratification), reducing deepwater formation and ultimately weakening the Atlantic Meridional Overturning Circulation (AMOC; Fichefet et al., 2003; Yang et al., 2016). Theory suggests that freshening of the higher latitudes can also have effects on the ocean heat and wind regimes in the tropics (Fedorov et al., 2007). Given the importance of these processes and the current large observational uncertainties, there is a strong need for long-term, continuous observations, as well as for improvement in predictive modeling. Among the key variables are salinity, temperature, surface topography, and currents.

In situ observation coverage of the Arctic Ocean has been limited by the distribution of sea ice (Figure 5, right, and Figure 6). Before the 1980s, oceanographic observations relied primarily on a variety of in situ measurement systems, including profiling instruments, buoys, and shipboard measurements (Woodruff et al., 2011). These observations contain a variety of systematic and random errors, which for SST can be

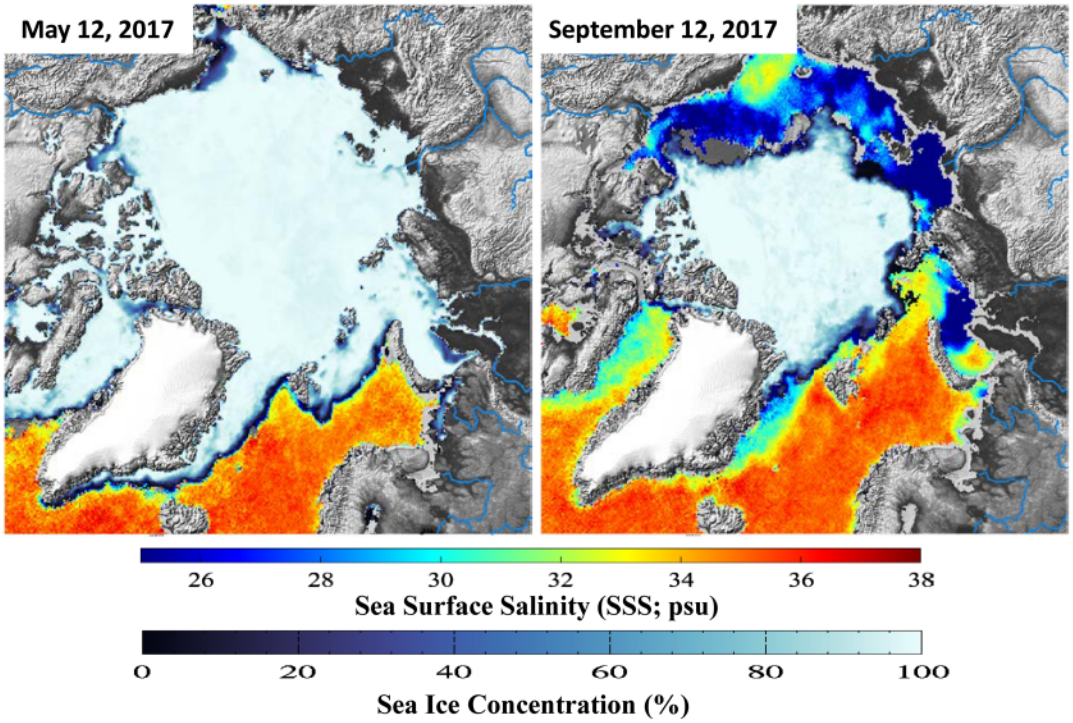

Figure 6. Maps of sea surface salinity (SSS; psu) in (left) midspring (week centered on May 12th) and (right) late summer (week centered on 12 September) of 2017, which were derived from the NASA/JPL/CAP product Level 2 observations from the Soil Moisture Active Passive (SMAP) satellite. Sea ice concentration for the same periods from the AMSR2 Level 3 product from Japan Aerospace Exploration Agency (JAXA) is also shown.

1°C or even larger. Nevertheless, they provide over a century of unique information about changes in ABZ climate, spanning the early twentieth century warm period and the cool period that followed.

In situ observations also form the basis for calibrating satellite observations. Before 2000, the collection of in situ observations relied heavily on ships of opportunity along major shipping lanes in the Northern Hemisphere. For example, SST and sea surface salinity (SSS) have been measured since 1999 along a shipping lane between Denmark and South Greenland onboard the container ship Nuka Arctica (Reverdin et al., 2002). After 2000, the number of measurements and their spatial and temporal coverage increased substantially with the deployment of the Argo network of free drifting profiling floats (Gould et al., 2004). There are now about 4000 Argo floats deployed globally that measure conductivity, temperature and depth/pressure (CTD), from which vertical profiles of salinity and temperature are retrieved from 2000 m deep to 5–10 m below the surface. However, the spatial distribution of Argo instruments is inhomogeneous and regions with even sporadic ice cover are difficult to sample (Figure 5, right) because the floats are programmed to surface every 10 days. The strong stratification of the Arctic Ocean puts high energy demands on an Argo float.

Spurred by the 2007–2008 International Polar Year (IPY), sustained observation systems and international coordination efforts (i.e., Integrated Arctic Ocean Observing System (iAOOS; Dickson, 2006, 2007); Overturning in the Subpolar North Atlantic Program (O-SNAP; www.o-snap.org)) have been put in place during the last decade with the goal to improve monitoring of high-latitude oceans and of their long-term changes. One objective, in particular, is to quantify the mass, heat and freshwater fluxes associated with the AMOC. Observing systems include a multitude of instruments, such as permanent moorings, gliders and CTD deployments at major choke points of ocean exchanges (e.g., Davis and Fram Straits). Technological advances also allow for ice-based observatories, such as Ice Tethered Profiler (ITP; Toole et al., 2011) and Polar Ocean Profiling Systems (POPS; Kikuchi et al., 2007), providing an unprecedented number of temperature and salinity profiles of the ice covered ocean in the inner regions of the Arctic Ocean (e.g., magenta dots in Figure 5, right). The high-latitude capabilities of the floats in the Argo network were

improved with a combination of software to avoid surfacing when ice is present, increased onboard data storage to keep profiles measured under the ice for a later transmission, and use of a better communication network to minimize time spent at the surface (Roemmich et al., 2009).

Despite these expanded in situ networks, the spatial and temporal coverage of the Arctic seas remains sparse, requiring the addition of satellite data to complete the picture. Figure 5 (right) shows locations where the Coriolis Ocean database ReAnalysis (CORA) dataset has salinity and temperature data measured during 2016 (Cabanes et al., 2013), to which are added (in black) ship tracks from the research vessel (R/V) Polarstern that operates yearly rotations in the Arctic (Driemel et al., 2017). While the Argo network samples part of the Arctic, such as the Norwegian Sea and the Baffin Bay, regular observations are lacking elsewhere. Other monitoring systems include permanent mooring and time-limited oceanographic campaigns, and the use of ships of opportunity. However, their spatial coverage is poor and continuous monitoring is not always possible. Fortunately, satellite remote sensing alleviates the limited spatial coverage and provides regular revisit opportunities.

3.2.1. Sea Surface Temperature

SST is the most mature ocean remotely sensed variable, dating from the measurements of upwelling infrared and visible radiation from NOAA polar orbiter satellites beginning in the mid-1970s, which were then adjusted to match in situ observations. High precision infrared radiometers (e.g., AVHRR and AATSR) now provide the highest absolute accuracy satellite SST (Kilpatrick et al., 2001). Their advantages over in situ measurements include greatly improved spatial coverage at or below the 10 km Arctic Ocean eddy scale (Høyer et al., 2012; Stroh et al., 2015). They also provide twice-daily temporal coverage and the virtues of using a single instrument. But these infrared wavelengths can be obstructed by clouds and contaminated by aerosols and sea ice bits within a satellite footprint in the marginal ice zone (Donlon et al., 2012; Le Traon et al., 2015). Another source of error is the variable humidity of the air column, which affects the atmospheric corrections. Also, these infrared observations measure temperature in a shallow 0.1- to 1-mm thick skin layer, whereas in situ instruments typically make measurements at a depth of 1–10 m.

AVHRR observations have been complemented by the MODIS infrared radiometer capabilities and a succession of European radiometers including the Spinning Enhanced Visible and InfraRed Imager (SEVIRI) instrument aboard the geostationary Meteosat Second Generation satellites. Use of longer microwave wavelengths avoids the problem of cloud masking. The first of these microwave instruments in a near-polar orbit was AMSR-E, launched in 2002, followed by the Naval Research Laboratory's WindSat, AMSR2, and GPM Microwave Imager (GMI), the latter of which are still functioning. These sensors use frequencies above 5 GHz for which the impact of salinity on emissivity is small (see Figure 3 of Le Vine et al., 2010) and can be corrected for using SSS from climatology (Shibata, 2013). Although these instruments provide more frequent sampling because of their all-weather observation capability, their accuracy is lower than the infrared instruments and they have larger (25–50 km) spatial footprints. Using a 29 year record primarily based on infrared satellites, Chepurin and Carton (2012) derived a trend in Arctic SST of 0.04°C/year (± 0.01°C/year) for ice free regions (errors increase near ice edge).

3.2.2. Sea Surface Salinity

SSS has been monitored from space since 2010 using L-band (1.4 GHz) microwave radiometers onboard the SMOS and Aquarius (onboard SAC-D) missions (Lagerloef et al., 2008; Kerr et al., 2010; Brucker et al., 2014a, b; Le Vine et al., 2015). In June 2015, the Aquarius mission was lost because of a spacecraft failure. An L-band radiometer on SMAP, launched in January 2015, also allows for SSS retrievals even though its primary objective was to measure soil moisture and land freeze/thaw. Example maps of SSS observed from space are shown in Figure 6 for mid-spring when the sea ice cover is at its maximum and for late summer when sea ice extent is at its minimum. In spring, only the Labrador Sea south of the Baffin Bay, the Norwegian Sea, and the Barents Sea are clearly observable, with SSS mostly falling in the range of 33–36 psu. North of the Pacific Ocean, small regions with reduced ice concentration occur, but the accuracy of satellite retrievals is questionable. In late summer when sea ice retreats to its minimum extent, marginal seas are mostly open waters. Salinity in the Beaufort (25–28 psu), East Siberian, Laptev and (part of) the Kara Seas (18–28 psu) is much lower than over most of the rest of the global oceans due to the large influx of fresh water from rivers and ice melt. Salinity in the Chukchi Sea is also low (30–33 psu), but it is still larger than the surrounding waters due to salinification by intrusions of Pacific Ocean water. Waters of the Atlantic

Subpolar Gyre and northward (Barents, Norwegian, Labrador Sea and Baffin Bay) are substantially saltier than the other Arctic waters. The Barents Sea has two salinity and temperature regimes, with warmer and saltier (~35 psu) Atlantic water in the south and fresh stratified polar water in the North where the sea ice extends during the winter. SSS in the northern Barents Sea is about 34 psu, which is 1.5 psu higher than two decades ago (SST increased by 2°C during the same period). This reduction in freshwater content, likely related to a weakened stratification triggered by the reduced freshwater input due to declining sea-ice (Lind et al., 2018), illustrates the tight coupling between sea ice extent, water mass formation, and circulation.

River runoff from Arctic and subarctic drainage basins is another major aspect of Arctic Ocean interactions with the rest of the ABZ. Rivers are the main source of Arctic freshwater (Carmack et al., 2016) and SSS in the resulting plumes can be as low as 20 psu, or even lower close to the river mouths. Changes in this river input result from changes in ice and snow melt on land thousands of kilometers away. Also, the spatial distribution of the riverine freshwater can be influenced by changes in atmospheric circulation. Satellite SSS data from Aquarius have been used to monitor the shape of the large river plume in the Kara Sea in all weather conditions since L-band microwave wavelengths are not impacted by clouds; these observations thus provide an advantage over the limited coverage of MODIS observations of chlorophyll-a (Kubryakov et al., 2014). The extent and direction of plume propagation is influenced by the prevailing wind regime. However, the coarse spatial resolution of the Aquarius SSS maps hinders an accurate definition of plume boundaries, which in reality exhibits sharp SSS gradients over sub-100-km scales. When plume waters propagate toward the east along the coast, it is no wider than 100 km. River plumes in the Arctic tend to be deflected to the right and to form a Riverine Coastal Domain of low salinity in a narrow (~10–60 km) and shallow current (Carmack et al., 2015). The width of the currents and the salinity gradient (e.g., 6 psu) are larger in summer as a result of the spring freshet. As shown in Figure 6, satellite SSS observations are missing close to the coasts, or, if present, they tend to be biased due to land contamination of the relatively coarse footprints of current sensors. Another source of bias for satellite SSS is sea ice. Garcia-Eidell et al. (2017) compare several satellite SSS products in the northern high latitudes and show good agreement with in situ data, and freshening cycles consistent with ice melt. They also identify discrepancies in the products due to the treatment of the sea ice. Improving the characterization of sea ice (concentration and age) on the satellite measurements has a very large impact (Dinnat & Brucker, 2017). L-band radiometric measurements are also used to retrieve the thickness of thin sea ice, thinner than 1 m, and thus complements alternative altimeter-based sea ice thickness measurements which require thicker sea ice (Tian-Kunze et al., 2014).

SSS monitoring by satellite in the ABZ is hindered by the coarse spatial resolution and reduced sensitivity of existing sensors. The latest Aquarius product has a global RMS error of ~0.17 psu (Lagerloef et al., 2015), but that error increases to 0.2–0.3 psu at high latitudes where water temperature is low. Biases of 1 psu or more are also observed for a distance of up to 100 km away from coasts and ice boundaries. This is due to the relative large footprint of the low frequency radiometers used for SSS retrieval, which have a spatial resolution of the order of 40 km (SMOS and SMAP) and 100–150 km (Aquarius). In situ data are also lacking near coasts and ice margins, in part because they tend to be shallow waters that limit opportunities for ship-borne observations. As a result, regular monitoring of the SSS of coastal currents, such as the East and West Greenland Currents, is not yet possible despite their importance for the stratification of the Subpolar Gyre, including the Labrador Sea (Luo et al., 2016). Monitoring of the salinity of these currents is also needed to project the impact of the melting ice sheet on future climate. Such coastal currents are typically only ~45–85 km wide (Fratantoni & Pickart, 2007; Sutherland & Pickart, 2008), with SSS fresher by 1 psu or more compared to surrounding waters which requires spatial resolution finer than 20 km, with revisit times of the order of days. Another challenge to SSS retrievals over cold waters is the decreased sensitivity of radiometric measurements to salinity as compared to warmer waters (see Figures 1b and 1c in Garcia-Eidell et al., 2017). This temperature effect results in larger errors and, when combined with the larger uncertainty on SST at high latitude, in regional biases. New technologies (e.g., microwave radiometers at frequencies lower than 1.4 GHz) need to be developed to increase the accuracy of SSS measurements.

3.2.3. Sea Level

There are two main sources of sea level information with which to constrain the geostrophic circulation in the Arctic: the 70 reliable coastal tide gauges (Proshutinsky et al., 2004) and satellite altimetry. The era of continuous satellite altimetry began with the launches of ESA's European Remote Sensing (ERS-1) satellite in 1991 and Topex/Poseidon in 1992. The former was the first of a succession of European satellites

maintaining a 35-day high inclination orbit. The latter was the first of another series of satellites, the latest being the multinational Jason-3 mission, in a 10-day repeat orbit with a more southerly turning latitude of 66°N. Additional satellites, such as the U.S. Navy's Geosat Follow-On (GFO) satellite (17-day repeat), NASA's ICESat and ICESat2, ESA's CryoSat-2, China's HY-1B and HY-2 (14-day and 168-day), and the joint ISRO and France's Centre National d'Études Spatiales (CNES) Satellite with ARgos and ALtiKa (SARAL; 35 days), have added to the data density. When combined with ocean bottom pressure estimates from NASA's and DLR's GRACE and GRACE-FO, the measurements effectively constrain the barotropic and baroclinic circulation patterns (Kwok & Morison, 2016). Trends in sea surface height derived from satellite measurements of the Arctic are between 0.002 and 0.005 m/y (± 0.001–0.002 m/year; Volkov & Pujol, 2012; Armitage et al., 2016). Error estimates are reported for the Norwegian coast. Further north, the signal to noise ratio is one or less partly due to the decrease in the number of available satellites.

Conventional satellite altimeters require open water and thus are unable to monitor sea level in the ice-covered portion of the Arctic. However, new satellites technologies and new processing techniques offer the promise of making routine sea level measurements through leads (large linear fractures) in the sea ice, and thus providing estimates of sea ice thickness as well (e.g., Giles et al., 2008).

Going forward, continuity and expanded capabilities of SSS, SST, and surface topography are two of the main objectives for satellite observations of the oceans. With the loss of the Aquarius instrument in June 2015, and given the age of SMOS (operating since late 2009), the continuity of SSS observations is uncertain. The recent SMAP L-band radiometer shows promise for observing SSS, but the instrument was optimized for soil moisture and its radiometric accuracy on footprint measurement is lower than Aquarius'. SMAP also suffers from the loss of its radar, which is needed to estimate surface roughness. As a result, the accuracy of SMAP SSS retrievals is degraded and the roughness must be estimated from noncolocated estimates of wind speed. Future salinity observations should aim for higher spatial resolution (10–20 km) with daily to weekly temporal resolution and increased sensitivity over cold waters to improve data quality at high latitude and near land and ice margins. Such improvements would open the way to improved monitoring of circulation in high latitudes, including, for example, the coastal currents around Greenland which transport fresh water into the subpolar North Atlantic. Together with subsurface profile measurements (e.g., the Argo network), this would permit the assessment of the total amount of freshwater contributed from ice melt.

Although SST is the most mature ocean remote sensing measurement, accurate calibration in the ABZ, cloud masking, and the need for fine few-kilometer resolution remain important. Large differences between high-latitude SST products remain and have been attributed to differences in the treatment of ice-contaminated data and bias correction schemes (Dash et al., 2012).

The highest priority for the future is to continue to refine the record of high quality well-calibrated infrared and microwave observations, and to combine these observations in a way to exploit both the fine resolution of the infrared observations and the spatial coverage of the microwave observations. Improvements in the inter-calibration of the various sensors are also necessary to better assess the SST diurnal cycle. Finally, theoretical analyses and laboratory demonstrations show that retrieving vertical profiles of temperature from lidar measurements can be expected in the future (Churnside, 2014; Rudolf & Walther, 2014; Rupp et al., 2017).

3.3. Ocean Biology and Biogeochemistry (Cecile S. Rousseaux, Watson W. Gregg, Maria A. Tzortziou)

Changes in ocean temperature, salinity, circulation and sea ice coverage, freshwater fluxes and permafrost, atmospheric composition and deposition of pollutants can directly impact the biogeochemistry of the oceans. Permafrost thawing, changing hydrology patterns, and land erosion alter the amount and quality of sediments, organic matter and nutrient loadings to rivers and the ocean, modifying marine biological activity, microbial processes, and overall ecosystem functioning. Changes in terrestrial inputs and in the water column stratification can directly impact the amount of nutrients available for primary producers. Similarly, sea ice coverage can change the amount and spectral properties of light available for primary production.

Over the last 30 years, large areas of the Arctic ocean have become free of sea ice in the summer (Comiso & Hall, 2014). This has led to many documented changes in marine biota, ranging from benthic algae to

seabirds (Wassmann et al., 2011). As the base of the food chain, phytoplankton produce organic carbon necessary for higher trophic levels to thrive. The concentration and composition of phytoplankton depends on the amount of light, nutrients and predators present. Their variability is indicative of changes in physical and biogeochemical conditions. Any changes in phytoplankton concentration and composition can in turn affect the physical, biogeochemical conditions and recruitment of higher trophic levels. Despite the challenges and intrinsic limitations of satellite observations in high-latitude regions, ocean color remote sensing has provided a unique tool for monitoring these changes in phytoplankton concentration, dissolved organic carbon amounts, and suspended particle dynamics from space by relating surface ocean reflectance to in-water composition (Devred et al., 2015). Since the 1990s, measurements from SeaWiFS, MODIS, MERIS, VIIRS, OLCI, and other ocean color sensors have provided continuous datasets that are critical for assessing changes in Arctic ocean biology, biogeochemistry and biodiversity over the past decades and linking these changes to anthropogenic and natural pressures.

Using ocean chlorophyll from these satellites, Arrigo et al. (2008; Arrigo & van Dijken, 2011; Arrigo & van Dijken, 2015) have reported an increase in annual primary production in the ABZ of 134 Tg C or, 38% over the last two decades, with the largest increase on the continental shelf. MODIS (Aqua) retrievals of dissolved organic matter distribution over the past decade, revealed a change in the routing of the Mackenzie River discharge from an alongshore, eastward path through the Canadian Arctic Archipelago in 2002 to a cross-shelf, northwestward path to the Canada Basin since 2006 (Fichot et al., 2013), with important implications for the fate and processing of North American runoff. Satellite observations combined with modeling showed that photochemical production of CO_2, through oxidation of colored dissolved organic matter in the southeastern Beaufort Sea increased over the period 1979 to 2003 by ~15% in response to decreasing sea ice extent (Bélanger et al., 2006).

Remote sensing of primary production and other ecological and biogeochemical processes in the Arctic Ocean faces unique challenges, including strong seasonality in terrestrial inputs of materials, under-ice phytoplankton blooms, insufficient understanding of Arctic phytoplankton physiology, and highly dynamic atmospheric properties (associated with the distinct seasonality of Arctic Haze, long range transport of anthropogenic pollution, as well as seasonally and regionally dependent forest and tundra fire emissions) that require new approaches for atmospheric correction of space-based ocean color retrievals (IOCCG, 2015). At the same time, seasonal darkness, low sun elevation, persistent clouds and fog, pixel 'contamination' by ice, and the remoteness and harshness of the region result in a limited number of matchups between field measurements and satellite overpasses (Chaves et al., 2015; Lund-Hansen et al., 2015; Matsuoka et al., 2015). Remote sensing observations from different platforms and both passive and active sensors are required for studying ocean processes in these regions and improving predictions of ABZ ecosystem responses to climate change. Lidar systems can retrieve the vertical structure in plankton communities and provide measurements between clouds, through significant fog and cloud cover, and at all times of the year (both day and night observations; e.g., Behrenfeld et al., 2013, 2017). Multiple polar orbiting satellites would also increase the number of successful overpasses in the coastal Arctic therefore decreasing the effects that clouds may have on the data.

Extending the spectral range into the ultraviolet and increasing the spectral resolution of remote sensing measurements from orbital or suborbital platforms will improve monitoring of key biogeochemical variables in the ocean. In particular, higher spectral resolution and extended spectral range enable remote sensing algorithms to distinguish between dissolved organic carbon, nonalgal particles, and phytoplankton pigments, monitor different phytoplankton taxonomic groups, and assess changes in carbon quality across systems. High spatial resolution, new generation optical imagers, such as the Sentinel 2/MultiSpectral Instrument (MSI) and Landsat 8, offer new opportunities to monitor biogeochemical processes in Arctic coastal waters, and improve understanding of climate change effects, such as permafrost thawing, changing riverine fluxes and coastal erosion, on ABZ ecology.

Comprehensive field observations across seasonal and spatial scales are, thus, critical for understanding variability and change in ocean processes and ecosystems, improving development and validation of satellite products, such as phytoplankton pigments, dissolved organic carbon, and primary production in this region (Hill et al., 2013; Lee et al., 2015; Matrai et al., 2013), and developing improved parameterizations as well as evaluating model simulations of biological processes and biogeochemical fluxes across multiple temporal and spatial scales. Previous field campaigns have collected bio-optical data to support satellite remote

sensing observations in the Arctic Ocean. The NSF-funded Shelf-Basin Interactions (SBI) program (https://www.eol.ucar.Edu/projects/sbi/index.html) focused on understanding the physical and biogeochemical processes that link the Arctic shelves, slopes, and deep basins within the context of global change. The MALINA project (http://malina.obs-vlfr.fr/index.html) was launched in 2008 and included an expedition in 2009 to document the stocks, processes and boundary fluxes over a network of sampling stations. In 2010–2011, the Impacts of Climate on the Eco-Systems and Chemistry of the Arctic Pacific Environment (ICESCAPE; http://ocean.stanford.edu/icescape/) project, a multi-year project funded by NASA, focused on addressing the impact of climate change (natural and anthropogenic) on the biogeochemistry and ecology of the Chukchi and Beaufort Seas. Yet, our understanding of the ocean biogeochemistry in the Arctic Ocean remains limited. As highlighted in many reports, including the U.S. National Academies of Sciences, Engineering and Medicine (NASEM; "Thriving on Our Changing Planet: A Decadal Strategy for Earth Observation from Space," National Academies of Sciences, Engineering, and Medicine, 2018) and the NASA Arctic COLORS community consensus report (Mannino et al., 2018; Tzortziou et al., 2019), more measurements are urgently needed to assess vulnerability, response, feedback, and resilience of Arctic ecosystems, communities, and natural resources to current and future pressures.

The ABZ is a challenging region for remote sensing of ocean biology. The importance of ocean biology, and its rate of recent change, however, necessitates that monitoring activities be continued and intensified. Remote sensing is an essential component of this monitoring, but the challenges are such that an integrated and comprehensive ABZ-ON is required in order to achieve the goal of understanding how the ABZ is changing and why. Enhanced remote sensing capabilities, such as lidar and higher spectral, temporal and spatial resolution sensors, and modeling development would contribute to this important effort.

4. Observing Properties of the ABZ Land

In this section, we discuss the (1) historical and current state of observations of the properties of the ABZ land biosphere, including land ice, snow, permafrost, tundra and boreal vegetation, wildfires, and wetlands, and (2) observational needs going forward, which are summarized in Table 1.

4.1. ABZ Land Ice (Ludovic Brucker)

ABZ land ice, which includes mountain glaciers (e.g., in Alaska and Svalbard), ice caps (e.g., on Iceland and Baffin Island), and one ice sheet (i.e., on Greenland), has experienced significant melting in recent decades, contributing to sea level rise (e.g., Fettweis et al., 2017; Gardner et al., 2013; Moon et al., 2018; Shepherd et al., 2012; van den Broeke et al., 2016). There are concerns about continued melting as, for instance, a sea level rise of 2 m would displace about 200 million people globally (Willis & Church, 2012). In addition, ABZ land ice masses, especially the Greenland ice sheet, release freshwater, which affects the ocean thermohaline circulation and may have far-reaching impacts on Earth's climate (e.g., Bamber et al., 2012; Frajka-Williams et al., 2016; Luo, Castelao, et al., 2016). Melting also alters Earth's climate through significant changes in albedo and therefore energy fluxes across multiple spatial and temporal scales (e.g., Casey et al., 2017; Ryan et al., 2017). There are articles in the literature that give a more exhaustive list of land ice components at play in Earth's climate system (e.g., Fyke et al., 2018; Vizcaino, 2014).

Greenland suborbital observations started as early as the 1930s, and allowed the first photogrammetry studies to estimate terminal ice flow and thickness (e.g., Higgins, 1991; Korsgaard et al., 2016). Decades later, more sophisticated instruments were operated with flight lines repeated annually using a lidar altimeter and a coherent radar depth sounder to obtain extensive ice sheet elevation (Krabill et al., 1995) and ice thickness (Gogineni et al., 1998) measurements. These airborne observations enabled the collection of data in areas too difficult to access during a field traverse. Moreover, the data gave a first three-dimensional view of the ice sheet without drilling into ice several kilometers thick.

Among the first properties monitored over land ice masses were surface melt using microwave radiometers (section 3.1), surface temperature, and albedo using spectroradiometers (section 2). For more details on these techniques and retrieved geophysical properties, the reader is referred to the following books: Bamber and Payne (2004), Massom and Lubin (2006), and Tedesco (2015).

Remote sensing techniques commonly used to assess the Greenland ice sheet mass balance are radar and lidar altimetry for height change measurements (e.g., McMillan et al., 2016; Zwally et al., 2011),

gravimetry for mass change measurements (e.g., van den Broeke et al., 2009; Velicogna et al., 2014), and SAR interferometry (InSAR) for ice velocity change measurements (Joughin et al., 2010). Each technique presents pros and cons, and each is often combined with in situ measurements and model simulations (e.g., van den Broeke et al., 2016, and references therein). However, independent satellite-derived ice mass loss estimates from satellite observations agree on accelerated ice mass loss (e.g., Shepherd et al., 2012).

Altimetry (radar and lidar) gives an estimate of ice sheet height, or elevation, from which ice-mass variations may be inferred with some assumptions on snow density and compaction. Gravity measurements give a more direct estimate of mass change, but offer a coarse resolution, and they are affected by ocean, land, and atmosphere mass changes. Satellite InSAR gives an estimate of ice velocity, which in conjunction with altimeter-derived ice thickness makes it possible to quantify ice flux. Altimetry for ice mass studies spans several decades, with the radar altimeters on ESA's European Remote Sensing (ERS; 1992–1996), ERS2 (2003), and Envisat (2002–2012), and the laser altimeter on ICESat (2003–2009). Current missions include the ESA CryoSat-2 (since 2010), AltiKa (since 2013), and Sentinel-3 (since 2015). The ICESat-2 laser altimeter was launched in 2018.

Studies using gravimetry, from NASA's and Deutsche Forschungsanstalt für Luft und Raumfahrt (DLR's) Gravity Recovery and Climate Experiment (GRACE) satellites (since 2003) reached the same conclusion that there is an increasing loss of land ice (e.g., van den Broeke et al., 2009, Velicogna et al., 2014). GRACE-FO, the follow-on mission, was launched in mid-2018.

To determine ice velocity, InSAR observations can be used from the Canadian Space Agency's RADARSAT, JAXA's Advanced Land Observing Satellite (ALOS) Phased Array type L-band Synthetic Aperture Radar (PALSAR), or DLR's TerraSAR-X (e.g., Joughin et al., 2010) and clear-sky visible imagery can be used, for example, from Landsat time series (e.g., Fahnestock et al., 2016; Mouginot et al., 2017). Space-based technologies and algorithms to monitor ice flow are in place, but there is no dedicated mission for monitoring ice dynamics beyond the NASA-Indian Space Research Organisation (ISRO) SAR (NISAR) instrument, which is scheduled for a 3-year nominal mission starting in 2020.

Together, these satellite observations have allowed for the estimation of Greenland ice sheet mass loss. According to Rignot et al. (2008), it was losing 110±70 Gt/year in the 1960s, 30±50 Gt/year in the 1970s–1980s (when the ice sheet was near balance), and 97±47 Gt/year in 1996, increasing to 267±38 Gt/year in 2007. Another comprehensive study using an ensemble of different satellite observations revealed that the Greenland ice sheet lost 142±49 Gt/year between 1992 and 2011 (Shepherd et al., 2012). This occurred primarily through surface meltwater runoff and ice dynamics, both of which have increased mass loss since the end of the 1990s (e.g., van den Broeke et al., 2016). Surface melt appears to be the dominant process, leading to >60% of the mass loss in recent years (Enderlin et al., 2014). Meltwater can flow directly on the land ice surface to the coast, and it can alternatively drain to the bottom of the outlet glaciers, lubricating their base and resulting in ice flow acceleration and hence more ice discharge into the ocean. Either way, this meltwater contributes directly to sea level rise. In contrast, meltwater may also be stored in sub/supra glacial lakes (e.g., Hoffman et al., 2011; Morriss et al., 2013), or as an aquifer in the ice sheet (e.g., Forster et al., 2014; Miège et al., 2016; Miller et al., 2017), buffering temporarily sea level increase (Koenig et al., 2013; Poinar et al., 2017). The increased mass loss through ice dynamics in recent decades is complex, and likely a consequence of both the recent increase in surface melt lubricating the glacier-bedrock interface and ocean warming (Fettweis et al., 2017).

While melt extent and duration were among the first variables monitored over Greenland from satellites, melt intensity or the amount of liquid water produced for a given area/duration remain unknown. This lack of information makes it challenging to assess modeling results (e.g., Cullather et al., 2016). Interestingly, surface meltwater runoff and ice dynamics exhibit rapid short-term fluctuations and large spatial variability, indicating the complexity of surface processes and the ice sheet response to climate forcing (Csatho et al., 2014). Also, it appears that gaining knowledge about Greenland hydrology (meltwater pathways [e.g., Smith et al., 2015] and retention [e.g., Miège et al., 2016]) from satellites is of increasing importance.

Currently, there are two multi-year airborne missions that have as one of their goals to investigate the processes that determine mass loss of the Greenland ice sheet. Both missions are sponsored by NASA: Operation IceBridge (OIB; Koenig et al., 2010) and Oceans Melting Greenland (OMG; Fenty et al., 2016).

OIB (2009–2019) surveyed extensively the Greenland ice sheet, as well as ice caps in the Canadian Arctic Archipelago and Svalbard, and glaciers in Alaska (as well as many ice masses in the Southern Hemisphere). There is typically a deployment to the Arctic every spring, with repeat observations, to monitor thickness and accumulation changes using lidar and radar altimeters; for several years, a gravimeter was also used. The OIB mission was designed to fill the gap in the spaceborne laser altimetry time series between ICESat (2003–2009) and its successor ICESat-2. IceBridge observations led to significant discoveries about ice sheet thickness and bedrock topography (e.g., Bamber et al., 2013; Morlighem et al., 2014). Studies using IceBridge observations have characterized annual changes in mass (and therefore the response of the land ice masses to climate change and resulting increase in sea level) and improved understanding of complex processes that may connect the ABZ with the global climate system.

OMG, started in 2015 and expected to be a five-year mission, surveys ocean conditions and ice loss from outlet glaciers around Greenland, providing critical information about ocean-driven ice mass loss in a warming climate. There is a focus on marine-terminated glaciers to understand their response to the presence of warmer Atlantic water. Based on bathymetric surveys, many glaciers terminate in deep water and are hence vulnerable to increased melting caused by ocean-ice interaction (Fenty et al., 2016). Several marine-based sectors of the Greenland ice sheet totaling 1.1 m sea level equivalent are retreating rapidly (Mouginot et al., 2015). As marine-based glaciers start retreating inland, the dominant process of ablation will be ice calving. OMG operates the Glacier and Ice Surface Topography Interferometer (GLISTIN-A) in order to generate high resolution, high precision elevation measurements of Greenland's coastal glaciers.

In the next decade, to reduce uncertainties in sea level rise projections, there is a need to understand changes occurring both in the margin and in the interior of the Greenland ice sheet, and satellite observations should help in both areas. While changes in the interior are likely to be subtle compared to the meter-scale vertical changes measured on the ice sheet margin and other glaciers in the ABZ, the volume of interior ice and the area of its interface with the atmosphere are large. Temporally continuous or overlapping satellite laser altimetry, gravimetry, photogrammetry, and InSAR missions are required. These satellite missions will be for quantifying changes in Greenland ice flow regime (and fluxes into the ocean), for improving our understanding of glacier calving dynamics, and for measuring the present rate of change of each component of land ice with high-enough temporal and spatial resolutions required for investigating the forcing (atmospheric, oceanic, or internal). These satellite instruments are fundamental for monitoring ice topography, elevation change, and ice mass balance during the next decades.

For investigating feedback processes involving albedo (e.g., surface composition, presence of impurities and biota, and deposition processes), it is important to maintain the visible, infrared and near infrared instruments, such as VIIRS, MODIS, or the Landsat series. Finally, for constraining snow accumulation and mass redistribution processes (e.g., blowing snow, snow depth) and their impacts on mass balance and on snow-atmosphere heat, recent studies highlighted the benefit of using instruments (lidar and radar) primarily designed for atmospheric research, such as NASA's Cloud-Aerosol Lidar and Infrared Pathfinder Satellite Observation (CALIPSO; Palm et al., 2011, Palm et al., 2017) and NASA's/JAXA's Global Precipitation Mission (GPM), but with orbits better covering the ABZ (section 7).

4.2. Mapping Seasonal Snow Cover in the ABZ (Dorothy K. Hall)

Seasonal snow cover is a highly variable component of the Earth's climate system, having a strong positive feedback with Earth's radiation balance. Because of the very high reflectivity of snow, especially fresh snow, 80% or more of the incident solar radiation can be reflected back to space. This has an overall cooling effect on the Earth's surface, and is especially important in the Northern Hemisphere springtime (e.g., Déry & Brown, 2007; Groisman et al., 1994; Kukla, 1981; Lettenmaier et al., 2015).

In years with extensive snow cover, approximately one third of the Earth's total land area can be snow covered during the boreal winter (Dahlman, 2018). When there is a significant snowpack, the temperature of the surface and near surface of the ground may be warmer than the temperature of the air. Changes in timing, density, and thickness of snow cover influence the exchange of heat between the air and underlying ground (e.g., Goodrich, 1982). If there is a sustained change in the timing of snow onset or snow melt with climate change, this will lead to changes in the thermal regime of the underlying ground. Snow cover, because of its

low thermal conductivity, is an excellent insulator especially when it is dry and deep, and can affect the presence of frozen ground or permafrost and the thickness of the active layer.

In fact, changes in the timing and duration of snowfall and snow cover in the Northern Hemisphere have already led to changes in the thermal state of the underlying ground according to modeling studies (Park et al., 2015). On the North Slope of Alaska there is a trend toward increased snowfall and warming of permafrost (Osterkamp & Romanovsky, 1996; Zhang et al., 1996). Modeling results for the period 1977–1998 revealed that permafrost warming, even at a depth of 20 m, was attributable to both the effect of increased snow depth and increased air temperature at Barrow, which is on the northern coast of Alaska. Changes in permafrost temperatures on the North Slope of Alaska between 1983 and 1998 are consistent with decadal scale variability in snow cover (Stieglitz et al., 2003). Warming of the near-surface ground in permafrost regions can increase the rate of organic decomposition, and the resulting loss of terrestrial carbon (Stieglitz et al., 2000).

The presence, extent and character of snow cover exert a major influence on life on Earth. About one sixth of the Earth's population relies on water derived from snowmelt for agriculture and consumption (Barnett et al., 2005). In the forest, a thick snow cover may be retained causing warmer conditions, or, alternatively, snow can be intercepted by the forest canopy, where it may remain without reaching the ground, although the canopy often unloads the snow to the ground later if the air temperature warms. Whether the snow stays on the canopy or falls to the ground, this will influence the intensity of the snow albedo feedback (Thackeray et al., 2014). Snow cover may also be important agriculturally and for wildlife habitat and feeding. Additionally, the snow cover enables a variety of recreational activities during the winter months and is economically significant (Sturm et al., 2017).

The documented warming trend in the ABZ of the Northern Hemisphere causes earlier spring recovery which increases carbon uptake. Recent work by Pulliainen et al. (2017) combined passive microwave satellite-derived estimates of snow clearance, with continuous in situ CO_2 flux measurements to retrieve the trends of boreal forest spring recovery for North America and Eurasia. They found a statistically significant positive trend of advanced spring recovery of carbon uptake across the Northern Hemisphere boreal evergreen forest zone of 2.3 days per decade over a 36-year study period (1979–2014).

Earth-observing satellites carrying increasingly sophisticated sensors have revolutionized the mapping and monitoring of the Earth's snow cover over about the last 50 years (Lettenmaier et al., 2015). Snow cover was first observed from space from TIROS-1, on 1 April 1960. Snow was easily distinguishable from most other natural features because of its high albedo, though it was, and still can be difficult to distinguish snow from clouds and even from some other features.

The second major breakthrough came in 1966 when NOAA started the production of maps of Northern Hemisphere snow cover using a variety of satellites and ground measurements (Matson et al., 1986). At first, these snow maps were produced manually once a week, and later, in 1999, digital production was started. Today twice-daily maps are produced by NOAA's National Ice Center (NIC) in the Interactive Multisensor Snow and Ice Mapping System (IMS; Ramsay, 1998; Helfrich et al., 2007), at a spatial resolution of up to 1 km, serving the needs of NOAA's operational government customers, the National Centers for Environmental Prediction (NCEP)/Environmental Modeling Center and the NCEP/Climate Prediction Center, as well as many other government and nongovernment users.

Using NOAA's 52-year snow-cover record, the Rutgers University Global Snow Lab (RUGSL) produces and maintains a climate data record of Northern Hemisphere snow cover (http://climate.rutgers.edu/snowcover/; Robinson, 1993; Frei & Robinson, 1999; Robinson, 2013; Estilow et al., 2015). The NIC also produces a 4-km resolution fully automated product. Both the IMS and the automated product are derived from several data sources including the Polar-orbiting Operational Environmental Satellites (POES), and the AVHRR, MODIS, AMSR (-E and -2), Advanced Microwave Sounding Unit (AMSU) and VIIRS instruments. In situ observations from the Global Telecommunications System (GTS), Surface Radar, and U.S. domestic surface observation networks have been applied since the 1990s to augment the satellite-derived snow observations when clouds obscure the surface.

Another breakthrough in satellite snow mapping occurred with the launch of the first of the Landsat series of sensors, called the Multispectral Scanner (MSS) in 1972. Using MSS images, snow cover could be measured at 80-m spatial resolution from space (Rango et al., 1977), permitting snow-cover buildup and

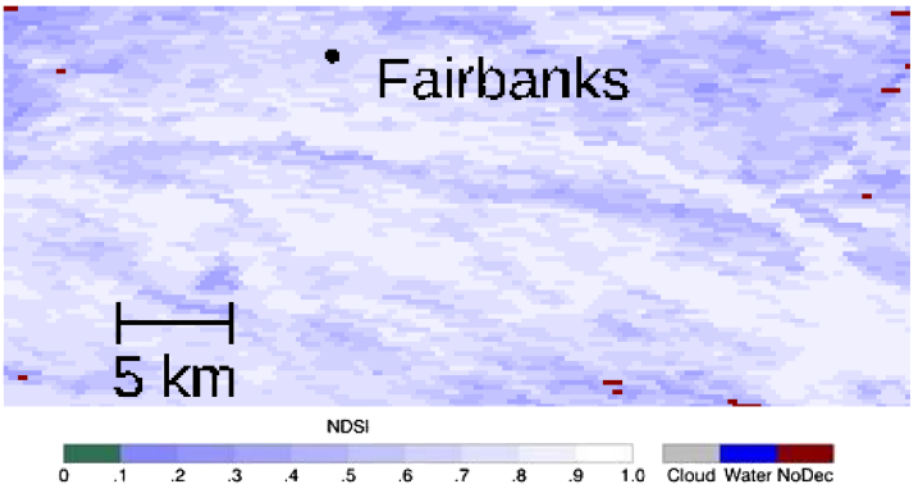

Figure 7. Terra Moderate Resolution Imaging Spectroradiometer (MODIS) Collection 6 (C6) Normalized Difference Snow Index (NDSI) snow-cover map of a 1,685-km^2 area of the boreal forest in central Alaska, acquired on 1 March 2016. The NDSI provides information that can be tuned to a specific study area to estimate fractional snow cover (FSC) in each pixel if a user has detailed information about the snow cover in their study area. The red areas represent "no decision" by the snow-mapping algorithm.

depletion to be observed and snow-cover depletion curves to be constructed, though only once every 18 days, cloud-cover permitting from Landsats-1, 2, and 3 (http://landsat.usgs.gov/band_designations_landsat_satellites.php). The Thematic Mapper sensor on the Landsat-4 satellite, with a 16-day repeat and a spatial resolution of 30 m, was launched in 1982 with a SW infrared band centered at 1.6 μm, permitting a major improvement in our ability to discriminate snow and clouds. In the SW-infrared bands, the reflectance of snow declines, while the reflectance of most clouds remains high (because cloud particles are smaller than surface snow grains), thus permitting snow and most clouds to be distinguished.

Additional Landsat sensors were launched throughout the 1980s and 1990s, and the Landsat series continues today with the 2013 launch of the Landsat-8 satellite, allowing still-more detailed satellite snow-cover mapping at the basin scale. With a repeat time of once every 16 days, as compared to 18 days for Landsats-1, -2, and -3, and a spatial resolution of 30 m (or better for some bands) as compared to Landsats-1, -2, and -3, incremental improvements in our ability to map snow cover and snow melt are continuing to be made. Additionally, when more than one Landsat is in orbit, more-frequent observations are possible (from different satellites).

The 1999 launch of the MODIS on the Terra satellite enabled another breakthrough in satellite snow-cover mapping (Figure 7). A second, nearly identical MODIS was launched in 2002 on the Aqua satellite. These products permit twice-daily views of snow cover for most parts of the Northern Hemisphere, when both Terra and Aqua data are available, cloud-cover permitting. With 36 channels, of which seven are dedicated to land remote sensing, automated global snow-mapping algorithms were developed (Hall et al., 1995), based on heritage work using Landsat (e.g., Dozier, 1989; Dozier & Marks, 1987) and MODIS Airborne Simulator (MAS) data (Hall et al., 1995). A suite of MODIS standard snow-cover products was produced that continues today, serving hundreds of users internationally (Hall et al., 2002; Riggs et al., 2015, 2017). And thanks to the Earth Observing System Data and Information System (EOSDIS), anyone in the world can download and use the snow maps for free (Wolfe & Ramapriyan, 2010). The snow maps are archived and distributed through the National Snow and Ice Data Center.

VIIRS, launched in 2011, has added another tool for mapping global snow cover from space. With its 375-m spatial resolution and 22 bands in the visible, near thermal infrared and infrared parts of the spectrum, automated algorithms are being developed by NASA to extend the snow cover data record of MODIS (Justice et al., 2013; Riggs et al., 2016, 2017).

The 50-year RUGSL climate data record of snow-cover extent (SCE; Robinson, 2013) has enabled breakthrough climate research to show that the maximum extent of seasonal snow cover has been decreasing,

and that snow cover has been melting earlier in springtime (e.g., Derksen & Brown, 2012; Déry & Brown, 2007; Stone et al., 2002), contributing to climate warming in the Northern Hemisphere. Earlier snowmelt has been especially evident since the mid-twentieth century (Hamlet et al., 2005; Mote et al., 2005). In fact, Foster (1989) and Foster et al. (1992) found that the date on which the tundra became snow-free in Barrow, Alaska, had occurred progressively earlier since the 1940s. Now, spring weather is arriving about 2 ½ weeks earlier than it did 50 years ago in parts of the Arctic (Sturm et al., undated). As more lower-albedo land area is exposed, more incoming solar radiation can be absorbed by Earth's surface, and re-emitted as LW radiation or heat.

Though earlier snowmelt has been documented for the Northern Hemisphere as a whole using the RUGSL climate data record (Figure 8), increasing temperature and earlier snowmelt in the western United States has also been documented using other observations and higher-resolution imagery, and the date of snowmelt onset has been reported to be earlier by 20 days or more, as compared to the middle of the last century (e.g., Cayan et al., 2001; Dettinger et al., 2004; Frei et al., 2012; Liston & Hiemstra, 2011; Lundquist et al., 2009; Stewart et al., 2005). Using 44 years of Landsat-derived snow maps, earlier snowmelt by ~16 days has been documented in parts of the Wind River Range, Wyoming (Hall et al., 2015).

The more-elusive measurement that is most desired by hydrologists is snow water equivalent (SWE). The volume of water contained in the snowpack, the SWE, can vary greatly from year to year even in the same location. Algorithms to map snow depth and SWE have been developed and time series have been created since 1978 following the launch of passive microwave sensors on the SSMI, providing estimates of SCE and SWE in snow-covered regions throughout the world (e.g., Chang et al., 1987; Kelly et al., 2003). Important advantages of passive microwave remote sensing of snow cover are its ability to map snow through cloud cover and to sense radiation emanating from the snow/soil interface thus permitting the measurement of SWE. However, there are many factors that confound passive microwave measurements of SWE from space, including (but not limited to) coarse resolution, obscuration by dense vegetation and forest cover, snowpack layering and snowpack wetness. For these and other reasons, the measurement of snow depth and SWE from space is not feasible using the passive microwave instruments that are currently available from satellites. In addition, Takala et al. (2011) have developed an algorithm that assimilates synoptic weather station data of snow depth along with satellite passive microwave radiometer data for the Northern Hemisphere. The retrieval performance for SWE is increased using this approach especially for SWE <150 mm. However, the measurement of SWE in the Northern Hemisphere is greatly hampered by confounding factors, such as forest cover (e.g., Foster et al., 2005). Both passive microwave sensors, such as the SSMI, and active sensors, such as the SeaWinds on QuikSCAT (e.g., Nghiem & Tsai, 2001), are also useful for measuring snow-covered area albeit at a coarse resolution of ~25 km. Higher-resolution sensors operating in the visible and near-infrared wavelength ranges are still the primary sensors used for snow mapping in spite of the major limitation of their inability to obtain data through darkness and cloud cover.

Looking toward the future, it is desirable to extend the 19-year global data record of the NASA MODIS standard snow-cover maps, with VIIRS standard snow-cover maps that began in 2011, to enable development of a CDR at a spatial resolution of 375 to 500 m to complement the longer, but coarser-resolution RUGSL CDR of SCE of the Northern Hemisphere. The next breakthrough in satellite remote sensing of snow may not be possible without the launch of satellite-borne microwave sensors that allow mapping of snow extent, depth and SWE globally.

4.3. Permafrost (Jouni Pulliainen, Kimmo Rautiainen)

The warming ABZ is causing shorter periods of seasonal ground frost and degrading permafrost, which is defined as ground that stays below 0°C for two or more consecutive years and covers about a quarter of the Northern Hemisphere land area (Smith & Brown, 2009; Van Everdingen, 1998). Warming has caused an overall increase of permafrost temperature (Biskaborn et al., 2019), decrease of permafrost depth and an increase of active layer thickness (ALT; Luo, Castelao, et al., 2016), which is defined as the soil layer above the permafrost exposed to seasonal soil freezing and thawing, in summer. The rate of permafrost thaw will depend on factors that determine the thermal dynamics of permafrost soils. As reviewed by Loranty et al. (2018), these factors include vegetation (sections 4.4 and 4.5), soil composition, snow cover (section 4.2), hydrology (section 4.7), wildfire (section 4.6), and animal and human activities, and their interactions are expected to evolve as the climate warms. Thawing permafrost will likely have a significant impact on

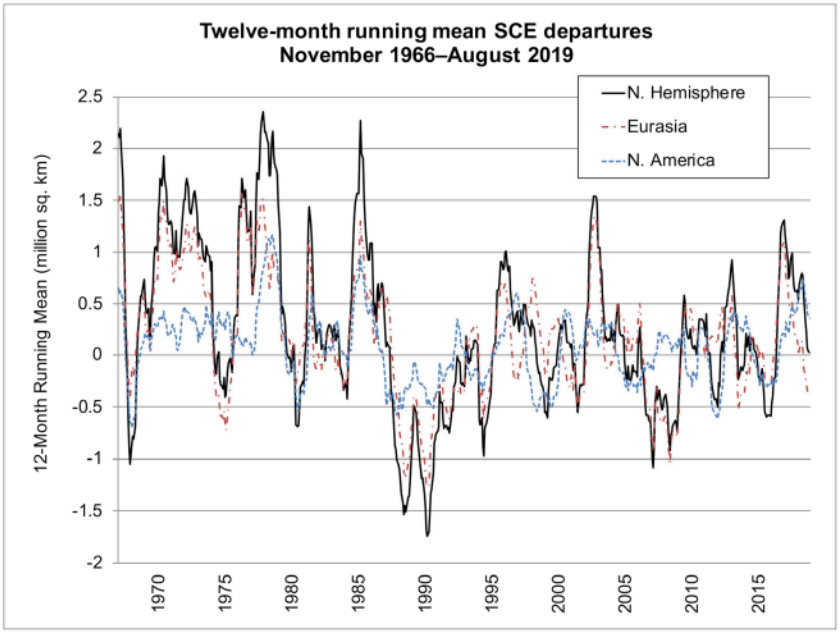

Figure 8. Twelve-month running mean snow-cover extent (SCE) departures from the 1981–2010 mean for the Northern Hemisphere, 1967–2019. Note the decline in snow cover beginning around 1985 and continuing to the present. Figure courtesy of Rutgers University Global Snow Lab.

biogeochemical cycles, including soil carbon reservoirs (e.g., Grosse et al., 2016, and references therein; references in section 4.5). Seasonal soil freeze has an important effect on annual surface energy balance, surface and subsurface water flows—contributing to possible inundation, and impacts on the carbon cycle (e.g., Skogland et al., 1988; Zhang et al., 2003; Langer et al., 2011). Soil freezing also affects biogeochemical processes, the photosynthetic activity of plants and the microbial activity within soils (Hollinger et al., 1999; Liebner et al., 2015). Vegetation characteristics, top-soil organic layer thickness, snow cover properties, soil type and soil moisture conditions have a significant influence on soil freezing and thawing processes.

An important concern of permafrost thaw is the carbon stored in ABZ frozen soils (e.g., Turetsky et al., 2019), a reservoir estimated to be large (Hugelius et al., 2014; Tarnocai et al., 2009). This reservoir is 4–5 times greater than the amount of carbon estimated to have been released to the atmosphere from anthropogenic activities since 1750 (Flato et al., 2013), and has been dubbed a potential "carbon bomb" that will greatly exacerbate global warming if rapidly released (e.g., Treat & Frolking, 2013). The rate and depth of permafrost thaw will likely vary substantially from region to region (e.g., Loranty et al., 2018; Schaefer et al., 2014) and be driven mainly by air temperatures and exacerbated by wildfires (Zhang et al., 2015a, and references therein; Abbott et al., 2016; Minsley et al., 2016; Loranty et al., 2018). However, carbon release is currently expected to be relatively slow (e.g., National Research Council, 2013; Schuur et al., 2018) and, thus, overshadowed by anthropogenic releases of carbon from fossil fuel burning and global deforestation (Schuur et al., 2015). The potential offset by photosynthetic uptake caused by increasing vegetation density or "greening" of a warmer Arctic is uncertain (e.g., Abbott et al., 2016; Parazoo et al., 2018; Pearson et al., 2013).

The Earth system models used for the IPCC AR5 did not simulate permafrost thaw and the concomitant release of carbon to the atmosphere. Models that do simulate these processes need improvements to credibly account for the complex interactions that are observed (Loranty et al., 2018; Schuur et al., 2015) as they show a wide range of present-day permafrost extent as well as predicted permafrost degradation (e.g., Schaefer et al., 2014). Recently, several studies have been conducted to simulate and predict the effect of climate change on permafrost using climate models from the fifth phase of the Coupled Model Intercomparison Project (CMIP5; e.g., Koven et al., 2013; Slater & Lawrence, 2013; Guo & Wang, 2016; McGuire et al., 2018). The predictions are highly dependent on the Representative Concentration Pathways (RCP) future greenhouse gas emission scenarios used. Though all studies predict losses in

permafrost extent, there are large variations in the results. The most recent study by McGuire et al. (2018) estimates the permafrost areal losses from 2010 to 2299 to be between 3 and 5 million km^2 and between 6 and 16 million km^2 for RCP4.5 and RCP8.5, respectively. Despite these differences in predictions between the CMIP5 models, the models consistently show that the decrease in permafrost extent is linked to warming air temperature (Slater & Lawrence, 2013).

The key parameters defining the permafrost physical state are the extent and temperature of the permafrost. ALT is also a useful parameter. Systematic permafrost measurements began in the late 1970s (Osterkamp, 2007; Smith et al., 2010; Zhou et al., 2000), although some measurements in Russia were conducted as early as the early 1930s (Romanovsky et al., 2010) and in North America in the late 1940s (Brewer, 1958). The permafrost temperature is measured from the boreholes drilled into the permafrost. ALT has been historically observed using thaw tubes or by measuring the soil temperature profiles. Measurements of seasonal soil frost are identical with ALT, but the tube is called a frost tube. A frost/thaw tube is filled with liquid having a freezing point at 0°C, typically added with a color indicator.

The permafrost temperature at depth of zero annual amplitude (ZAA; i.e., where permafrost temperature is not affected by seasonal variations in surface air temperature) has been used as an indicator for detecting the long-term variations in permafrost physical state. At most borehole sites, the long-term trend in permafrost ZAA temperature has been increasing (e.g., Biskaborn et al., 2019; Vaughan et al., 2013). The Global Terrestrial Network for Permafrost (GTN-P) was developed in the 1990s "with the long-term goal of obtaining a comprehensive view of the spatial structure, trends and variability of changes in the active layer thickness and permafrost temperature." (http://gtnp.arcticportal.org). The GTN-P has two components: the Circumpolar Active Layer Monitoring (CALM) network, focusing on active-layer characteristics, and the Thermal State of Permafrost (TSP) network, focusing on measurement of ground temperatures in boreholes. Currently, TSP includes 1091 boreholes, whereas CALM has 242.

While permafrost cannot be directly observed using satellite remote sensing techniques, freezing and thawing of the surface of the active layer and, in general, the behavior of seasonal soil frost can be monitored using active and/or passive microwave instruments. The detection is based on soil permittivity changes due to soil freezing. The large permittivity contrast between liquid water and ice at low microwave frequencies is used to detect the soil transitions between frozen and thaw states. Several studies have been conducted to detect soil or landscape freezing and thawing. Global products have been developed using active microwave data, such as from the Advanced Scatterometer (ASCAT; Naeimi et al., 2012), or passive microwave data at either high frequencies (e.g., 37-GHz records from SMMR, SSMI, and SSMIS at 25-km resolution from 1970 to 2016 (Kim et al., 2017) and 19- to 37-GHz records from AMSR-E and AMSR2) or very low frequencies (L band; 1.4 GHz) with the Soil Moisture and Ocean Salinity (SMOS 35- to 50-km resolution; Rautiainen et al., 2016) and Soil Moisture Active Passive (SMAP 3- to 9-km resolution; Dunbar et al., 2015; Derksen et al., 2017) missions. Additionally, many studies are concentrating on regional scale freeze/thaw detection using both high spatial resolution SAR instruments and lower resolution radiometers and scatterometers (Chimitdorzhiev et al., 2016; Colliander et al., 2012; Du et al., 2015; Du et al., 2015; Jagdhuber et al., 2014; Podest et al., 2014; Roy et al., 2015; Xu et al., 2016). The L-band missions, SMOS (2010-present), Aquarius (2011–2015) and SMAP (2015-present), have shown the greatest potential for monitoring the surface soil state globally (Brucker et al., 2014a, b; Roy et al., 2015; Rautiainen et al., 2016; Derksen et al., 2017). Figure 9 shows the date of soil freezing onset for 2012 as determined from the SMOS freeze/thaw product. For comparison, the map of Northern Hemisphere permafrost areas is also shown.

Indirect methods to map and assess changes in permafrost are typically based on the identification and change detection of characteristic landforms and surface features (e.g., Westermann et al., 2015). Additionally, characteristic vegetation types can be mapped by optical satellite instruments in some regions (Westermann et al., 2015). Since dynamic permafrost processes include phase changes of water, they often induce changes in surface characteristics over time. This makes interferometric SAR and other methods feasible to generate digital elevation models (DEM) and map changes in elevation or surface roughness characteristics applicable for permafrost monitoring (Alasset et al., 2010; Kääb et al., 2005). The InSAR method is a powerful tool to monitor both (1) short term changes in landscape (summer surface displacements) due to soil freeze/thaw cycle in the active layer (Rouyet et al., 2019; Strozzi et al., 2018) and long-term changes

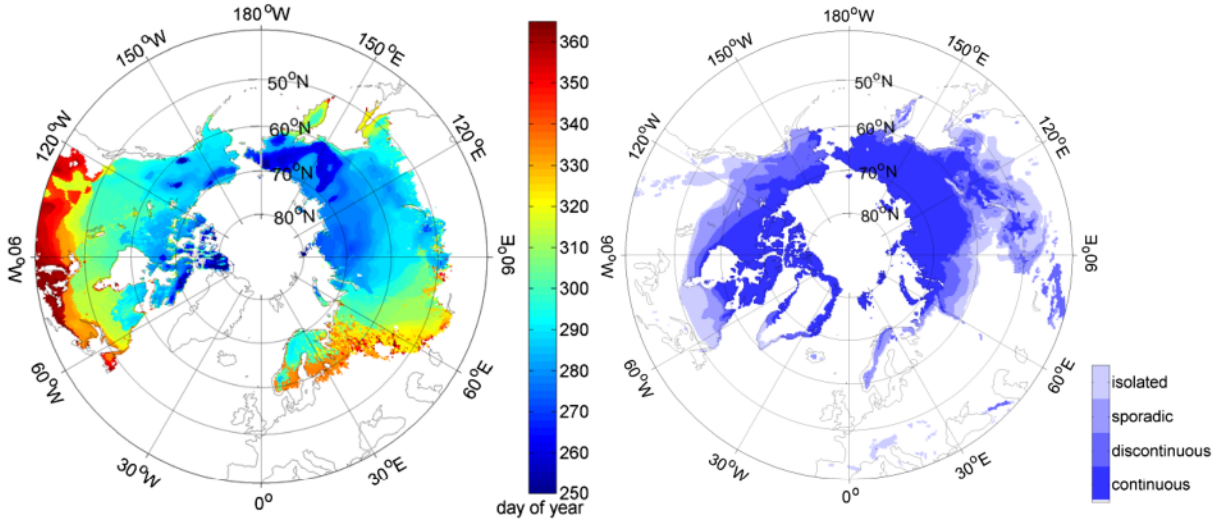

Figure 9. (left) Date of onset of soil freezing inferred from SMOS freeze/thaw product for 2012 (note that for Eurasian central latitudes SMOS data are not available). (right) The distribution of permafrost (Brown et al., 2002).

in landscape potentially due to the changes in permafrost condition (Liu et al., 2010; Rouyet et al., 2019). Rouyet et al. (2019) also show that InSAR observations can be used to contribute to investigations of geomorphology and ground thermal conditions. Even larger degradation effects include surface deformations due to landslides, formations of thermokarst terrain and expansions of thaw lakes. Additionally, instruments measuring land surface temperature and snow cover properties provide quantitative information relevant to the modelling of permafrost processes (Langer et al., 2013; Marchenko et al., 2009).

Monitoring permafrost in a changing climate is recognized to be important and, as such, permafrost is included in the Essential Climate Variable lists (World Meteorological Organization (WMO) and United Nations Framework Convention on Climate Change (UNFCCC)). ESA's GlobPermafrost was initiated in 2016 with one objective to develop and validate means of indirect permafrost monitoring with multi-sensor satellites (https://www.globpermafrost.info/). WMO's Polar Space Task Group (PSTG) founded a SAR Coordination Working Group (CWG) to organize space agencies to establish a collection of SAR satellite data for cryospheric research and applications, one thematic area being permafrost (Polar Space Task Group, 2016). Currently, many satellites are providing satellite data for indirect permafrost monitoring (e.g., ESA's Sentinel series of high resolution SAR data and optical data). However, no dedicated mission for permafrost has been established.

The main deficiency in current satellite data regarding the indirect monitoring of permafrost is low spatial coverage and infrequent, irregular observations. Typically, for example, SAR missions have a repetition time of many days and narrow antenna swaths, a configuration not suitable for providing high spatial and temporal resolution data. The L-band radiometer missions, SMOS, Aquarius, and SMAP, have shown potential for global monitoring of the cryosphere (e.g., seasonal frost and active layer surface freeze/thaw state; Brucker et al., 2014a, b; Roy et al., 2015; Rautiainen et al., 2016; Derksen et al., 2017). The deficiency of these satellite datasets is their coarse spatial resolution (i.e., tens of kilometers) and the short temporal history. Additionally, no new passive L-band satellite missions have been confirmed, potentially jeopardizing the continuity of the passive L-band observations. Even though coarse spatial resolution restricts the feasibility of radiometry, observations by L-band sensors are potentially highly useful for permafrost thermal models through the use of data assimilation techniques, thus reducing the limitations induced by the coarse spatial resolution.

Ideally, to further improve thermal permafrost models and the general understanding of permafrost processes, a suite of satellite sensors optimized for monitoring the cryosphere needs to be established to provide global, daily data sufficient for assimilation (i.e., measurements that are influenced by snow extent, snow

water equivalent, surface soil status or soil moisture, and that are accompanied with in situ monitoring data for calibration and validation). A plan for continuously maintained missions is required in order to avoid possible data gaps between satellites. An ideal cryospheric satellite network could include several high resolution SAR satellites for monitoring landscape changes with a high repetition frequency (e.g., C- and/or L-band interferometric single pass SAR tandem missions).

4.4. Tundra Vegetation: Drivers, Feedbacks and Indicators of Systemic Change (Bruce C. Forbes, Timo Kumpula)

The low arctic portions of the ABZ tundra biome exist as a relatively narrow strip of land typically within 100–300 km from the margins of the Arctic Ocean (Walker et al., 2005). It is characterized by low temperatures and precipitation, low biotic diversity, permafrost soils with limited nutrient availability, and short growing seasons and reproduction cycles. Vegetation structure is simple and monotonous relative to more temperate regions. However, the ecotone between closed low arctic tundra vegetation and the boreal forest to the south varies widely. Transitions can be relatively sharp, such as in the deciduous boreal highlands of northern Fennoscandia, or extend 100–200 km or more, such as in the coniferous lichen-woodland lowlands of the West Siberian Plain (Virtanen et al., 2016). To the north, mainly on islands in the High Arctic of Canada and Russia, except for the mainland Taimyr Peninsula where they are contiguous with low arctic tundra, polar deserts occur. Polar deserts lie geographically within the tundra biome *sensu lato*, but are characterized by open ground with patches of vegetation where there is enough moisture (cf. Serreze & Barry, 2005, Figure 2.12; Forbes, 2013).

Expected diminishment of the extent of the tundra biome as a whole is of strong interest given the huge potential loss of habitat for plants, animals and humans who depend on them, as well as potential positive feedback to global climate change (Larsen et al., 2014; Osborne et al., 2018). Major terrestrial feedback are expected: (1) northward migration of the treeline into the tundra and increases in tundra shrub height and cover, all of which would act to decrease Arctic tundra albedo and further increase regional warming (Callaghan et al., 2005; te Beest et al., 2016); (2) stores of greenhouse gases are believed to have highly significant potential to accelerate climate change (Larsen et al., 2014); and (3) the massive reservoirs of soil organic matter in the northern boreal and tundra biomes may be vulnerable both to permafrost thawing and warming (Karhu et al., 2014; Schuur et al., 2015), as well as to encroachment by plant communities, which may accelerate decomposition and loss of soil carbon to the atmosphere (Hartley et al., 2012; Loranty et al., 2018). There are also several studies where satellite time series have shown arctic browning. Browning can be caused by a number of factors, such as the effect of 1) herbivory (e.g., reindeer grazing, lemmings, geese, insect damage, including autumnal moth outbreaks in Northern Fennoscandia, for example), 2) winter rain-on-snow (ROS) events when deep freezing of the ground layer damages dwarf shrubs, and 3) fire ignited by lightning or anthropogenic activity (Bjerke et al., 2017; Phoenix & Bjerke, 2016; Treharne et al., 2018; Veraverbeke et al., 2017).

Even without a warming climate, vegetation composition, cover and height in the ABZ are typically highly dynamic over diverse temporal and spatial scales. These are the properties most commonly measured at ground level in both stand-alone and shared protocol studies throughout much of the circumpolar Arctic (e.g., International Tundra Experiment; Elmendorf et al., 2012a, b). Patterns and processes of vegetation change are best understood in the context of various local and regional disturbance regimes. Disturbance ecology encompasses natural and cyclic phenomena, such as fires and insect outbreaks, but also anthropogenic forces like large-scale oil and gas extraction (Kumpula et al., 2011; Kumpula et al., 2012) and the huge semi-domesticated reindeer herds of Northwest Eurasia (Forbes et al., 2016; Forbes & Kumpula, 2009). This vegetation shift is expected to have a positive feedback on climate warming as taller vegetation protrudes above the snowpack and decreases landscape albedo (Ménard et al., 2014).

Our understanding of tundra vegetation dynamics has advanced greatly in recent decades, particularly in the West, because of the advent of experimental population and community ecology. Permanent plots came into vogue in the 1970s and now have proved their value since the 2007–2008 International Polar Year led to resurveying many of the oldest and most carefully sampled sites. In a review of circumpolar studies (Callaghan et al., 2011), the majority of the plots were in the range of 40 years old, which encompasses the era of late 20th century ABZ warming. Elmendorf et al. (2012a, b) provide a complement to the latter by focusing on population—and community-scale experimental warming trials,

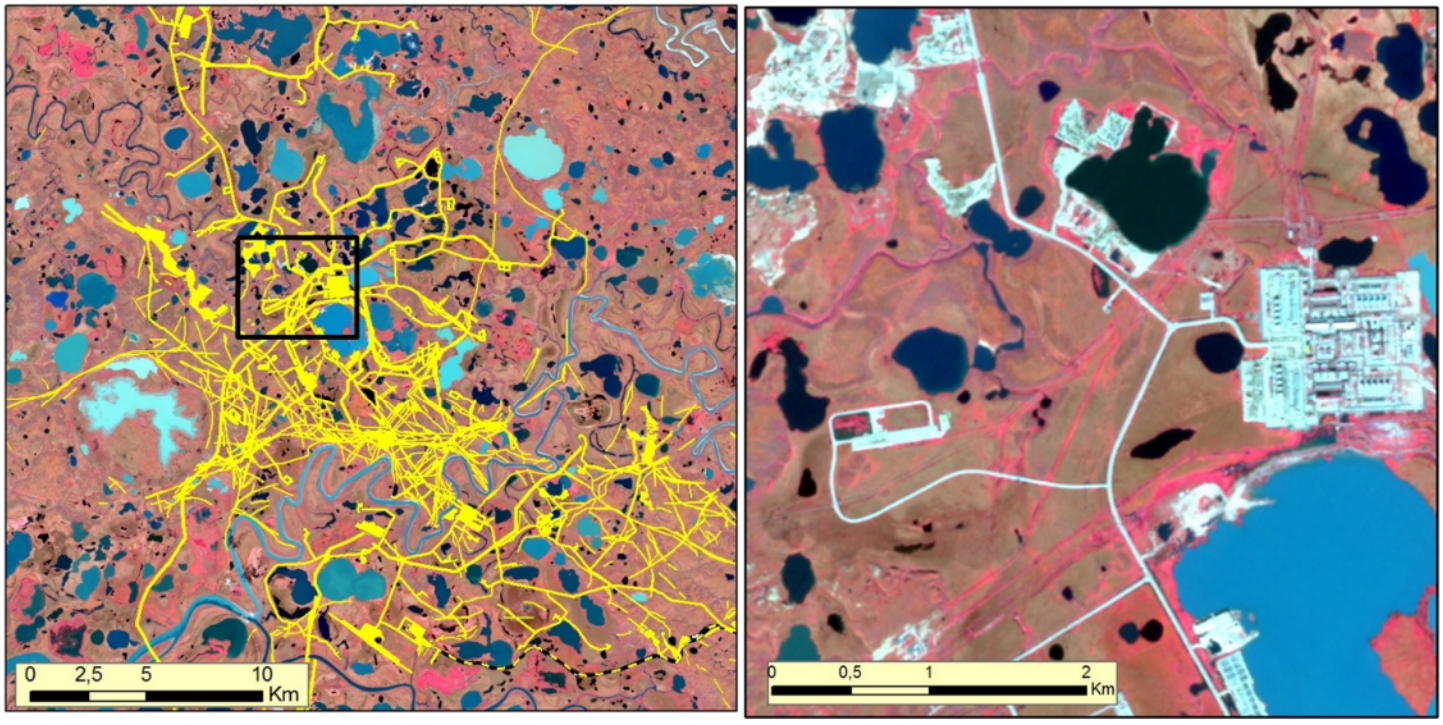

Figure 10. Sentinel-2 image (false color composition NIR, Red and Green bands, note that the colors of the lakes range from black to almost light cyan, due to differences in lake turbidity) from Bovanenkovo gas field Yamal Peninsula, West Siberia, Russia dated 1 September 2016, with 10-m multispectral resolution. (left) Infrastructure expansion can be studied with various optical satellite imageries, where yellow represents different types of anthropogenic disturbance visibly affecting land cover. Landsat and SPOT data cover the period from the early 1970s to late 1990s with 20- to 60-m resolution. Since early 2000, very high resolution imagery, such as IKONOS-2 and Quickbird-2, has allowed detailed study of infrastructure development (Kumpula et al., 2010). (inset right) A portion of the image on the left (inside the square box) is enlarged, showing a gas condensation plant with buildings.

albeit of shorter duration, pointing to a future decline in tundra biodiversity. However, while the latter two syntheses claim to be "circumpolar," there are no sites in Russia, which comprises nearly half of the tundra biome.

Satellite imagery archives have an extensive legacy (e.g., Corona, Keyhole (KH-9), Landsat, Satellite Pour l'Observation de la Terre (SPOT), Advanced Spaceborne Thermal Emission and Reflection Radiometer (ASTER), and AVHRR-based products like Global Inventory Monitoring and Modelling System (GIMMS) Normalized Difference Vegetation Index (NDVI = [NIR – Red]/[NIR + Red], where "NIR" is spectral reflectance data in the near-infrared region and "Red" is in the visible region) third generation GIMMS NDVI3g, MODIS, Sea-Viewing Wide Field-of-View Sensor (SeaWiFS) and recent Sentinel-1/2 imagery; e.g., Figure 10) that enable detection and examination of land cover trends and anomalies over the past 60 years. Capabilities for tundra vegetation classification and photosynthetic activity/biomass have advanced considerably since the Landsat era. Long-term observations and datasets mean that most spatial patterns can be analyzed at decadal time scales. However, we currently lack a reliable method for detecting changes in the height of tundra vegetation, in particular erect shrubs, the annual growth of which appears to be increasing in several regions (Macias Fauria et al., 2012; Myers-Smith et al., 2015). Novel approaches include also the applied use of very high-resolution satellite imagery (e.g., IKONOS-2, Quickbird-2, Worldview-2/3, and Pleiades; e.g., Figure 11), and newly launched (October 2016) WorldView-4 data with a spatial multispectral resolution of 1.24 m (Kumpula, 2006; Virtanen & Ek, 2014). Aerial photograph archives enable examination of land cover trends over the past 60–70 years, although availability and spatial coverage allow rather small scale and local studies. New radar and lidar products like Terra Synthetic Aperture Radar X-band wavelength (TerraSAR-X) data have high potential to be used in vegetation cover change applications, for example permafrost thaw-caused landslides and Arctic lake drainage, and other environmental modelling applications (Stettner et al., 2017).

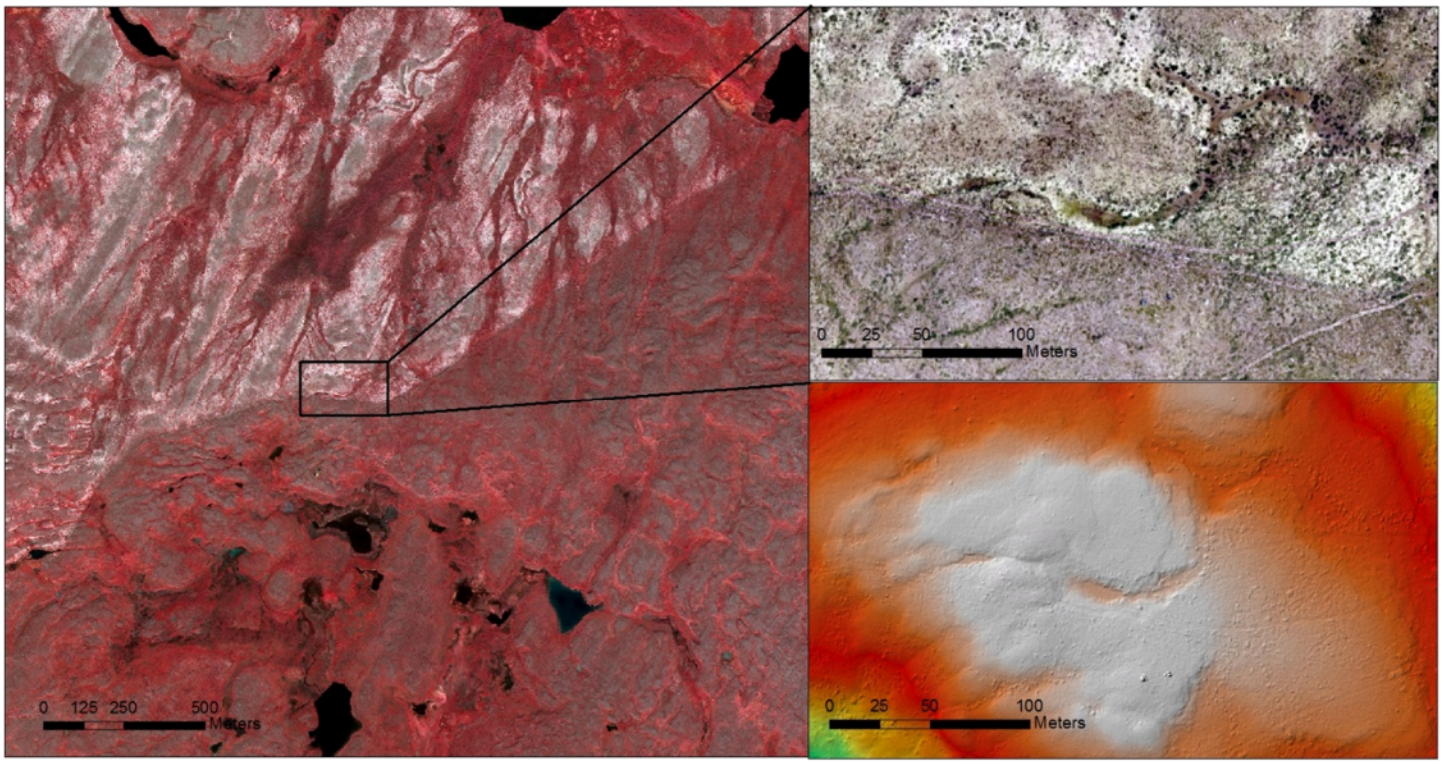

Figure 11. (left) WorldView-3 image (NIR-Red-Green) from July 22, 2015 from the Norwegian-Finnish border area showing lichen-rich pastures (lighter color) on the Norwegian side. A reindeer fence separates the border's pastures. The Norwegian pastures are only grazed in winter, when snow provides some protection for the lichens, while the Finnish pastures are grazed in summer. (inset top right) UAS-based orthomosaic (RGB) of July 28, 2016 clearly demonstrates variations in lichen coverage also on Norwegian pastures, where lichen is heavily grazed in areas where snow depth is less than approximately 1 m. (inset bottom right, same area as above) A digital elevation model (DEM) map created from UAS image acquisition. Fine-scale DEM datasets combined with other very high resolution data allow detailed habitat analysis.

A serious challenge of earlier remote sensing approaches for detecting climate-induced vegetation changes has been the reliability of datasets describing greening and browning trends as well as choosing the suitable spatial resolution for mapping change in different geographic regions. NDVI is a widely used proxy of vegetation productivity in global and regional remote sensing studies (Beck et al., 2011; Beck & Goetz, 2011; Bjerke et al., 2014; Raynolds et al., 2008; Verbyla, 2008; Walker et al., 2009). However, a major drawback of the earlier studies has been the rather coarse resolution of NDVI products (8×8 km^2 grid size) that do not allow detection of land cover change at more detailed scales. This has resulted in difficulties in distinguishing climate-induced vegetation change from interannual phenological differences related to variations in short-term climate and weather conditions. Interannual fluctuations include variations in snow melting, the intensity and duration of the annual flood season, seasonal variations in the extent of lakes, variations in permafrost melting, and human activities (Lara et al., 2018; Rocha et al., 2018). As an example, Guay et al. (2014) reported notable differences between NDVI datasets in greening and browning trends that describe increases and decreases in vegetation productivity, respectively. The difficulties in resolving these cross-scale issues still remain, yet UAS (see below) will likely facilitate reconciliation between ground-level and satellite-based productivity sensors in the near future.

Another major challenge in detection of climate-induced vegetation transitions is the impacts of different forms of land use on vegetation in circumpolar areas. For example, reindeer grazing can significantly constrain the shrubification process and result in lower NDVI values in intensively grazed regions. Lichen-dominated tundra with whitish reindeer lichens has high albedo, however intensive reindeer grazing has also been observed to enhance tree and shrub growth (Tømmervik et al., 2009; Tømmervik et al., 2012). Grazing-induced changes in vegetation may also influence the local greenhouse gas balance (Cahoon et al., 2012; Väisänen et al., 2014; Ylänne et al., 2015), in particular on wetlands where grazing may also

alter methane (CH_4) emissions (Stark & Ylänne, 2015). Compared to reindeer grazing, more localized land use impacts can be caused by, for example, mining and related infrastructure development that denude vegetation cover (Forbes & Kumpula, 2009; Kumpula et al., 2011; Kumpula et al., 2012). At the southern tundra border, forestry also creates a continuously changing mosaic of clear-cuts and forest patches with different age structure that strongly affect NDVI trends (e.g., with MODIS vegetation indices—250 m spatial resolution and 16-day composites for each instrument or 8-day composites if instrument data are combined; Kivinen & Kumpula, 2014). Satellite instruments with finer spatial resolution and more frequent revisit times than MODIS would better allow the quantification of land use on vegetation.

We recommend that the suborbital network be enhanced as it is essential in understanding the spatiotemporal dynamics of ongoing and future changes in the ABZ and for interpreting and evaluating satellite data. The study of spectral signature characteristics (e.g., spectral libraries, leaf area index (LAI)) of the various tundra vegetation cover types can be used in interpretation of satellite data. Also other ground measurements of vegetation cover, biomass, carbon release with eddy towers, etc. are needed to link in situ field sampling and satellite observations. UAS remote sensing used with new hyperspectral, thermal and lidar sensors allows the building of clear linkages between ground and coarser-scale remote sensing data.

In addition, an enhanced suborbital network, in combination with satellite data, will enable advances in process-based understanding. For instance, reliable quantification of changes in high-latitude ecosystem productivity and land-atmosphere carbon balance form a cornerstone in understanding and estimating future climate-induced change. So far, previous studies have combined biotope-scale NDVI-values with carbon balance data (Shaver et al., 2013) or incorporated models of carbon cycling to scenarios of global warming over vast areas (Abbott et al., 2016; Sitch et al., 2007). However, the interpolated scale has been large and does not account for small-scale differences in land use. Combining satellite data of vegetation with in situ measurements of land–atmosphere carbon fluxes provides a way to quantify greenhouse gas balances over vast landscapes. The fine-scale imagery of novel approaches (e.g., UAS and lidar data) provides a tool to link in situ measurements of local carbon balance to land-use patterns, such as grazing.

We recommend that there is continuity of satellite data, which is essential for ecological studies. Various polar orbiting satellites with multiple resolution and spectral characteristics are needed to follow and quantify changes in albedo, NDVI, snow, water, vegetation, phenological state, etc. in the ABZ. These parameters can be used to explain changes caused by either natural processes or anthropogenic activity (e.g., reindeer herding, petroleum and other extraction industry activities). MODIS data at a coarser resolution and Sentinel-2 data with a finer resolution provide adequate satellite coverage of the ABZ, although clouds coverage is still a limiting factor in high quality data acquisition.

Sensors change over time, which potentially limits their utility for long-term ecological studies. It is important that data continuity is thoroughly evaluated when new satellite sensors and systems are developed. Ideally, sensors (old and new) should operate and overlap for a period that is long enough for data to be reliably calibrated. Landsat, as the longest running program since 1972, has changed throughout the mission, yet continues to be invaluable. There is an enormous amount of data to run ABZ vegetation monitoring from various platforms with multiple scales. Further applications will increasingly combine optical and passive data for analyzing vegetation-cryosphere-climate interactions for ABZ ecosystem change research.

4.5. Boreal Vegetation (Brendan M. Rogers, Alemu Gonsamo, Paul M. Montesano, Christopher S. R. Neigh, Jennifer D. Watts, Amber J. Soja)

"Taiga" is the Russian term often used to describe the conifer forests that dominate ABZ vegetation. These boreal forests cover roughly one third of Earth's forested area and have enormous importance for regional and global climate (Gauthier et al., 2015). Although biodiversity is relatively low as compared to forests at lower latitudes, the structure and composition of boreal forests is complex and varies dramatically by environmental conditions, such as permafrost prevalence, nutrient availability, soil moisture, temperature, disturbance history, and evolutionary process (Rogers et al., 2015; Ranson et al., 2011; Montesano et al., 2009: Shugart et al., 1991). Local interactions between microclimate, topography, snow depth, wind, and edaphic conditions impact forest canopy height and cover (Callaghan et al., 2002; Elmendorf et al., 2012a; Holtmeier & Broll, 2005). Boreal vegetation has experienced rapid environmental change during the last half-century, but remains poorly represented by in situ monitoring networks (Schimel et al., 2015). Along

with ABZ temperature trends roughly double the rest of the globe (Hartmann et al., 2013), it has responded to increasing atmospheric CO_2 concentrations, nitrogen deposition, intensifying fire regimes, and changes in hydrology and nutrient availability as a result of deepening active layers and thawing permafrost (AMAP, 2017; Thomas et al., 2017; Xia et al., 2017).

Observations of ABZ vegetation from remote sensing platforms began as early as the 1920s, largely based on aerial photograph interpretation. Aerial photography, mostly in Canada, complemented ground surveys for forest type classification with topographic information from stereoscope images and visible characteristics of vegetation (Johnston & Sharpe, 1922; Losee, 1942). Decades later, the contrast in reflectance of infrared and visible wavelengths by vegetation was leveraged through color infrared photograph films (CIR) to characterize vegetation types, soil moisture, and vegetation stress. Beginning in the mid-1980s, active laser technology (lidar) emerged as a powerful technology to directly estimate properties relevant for forest inventory and monitoring (Wulder et al., 2012). Airborne lidar sampling was initially conducted for management practices in Canada, but has since evolved into a fundamental tool for large-scale science applications. Russian boreal forests remain challenging for western scientists to access, even though they represent roughly two thirds of the boreal forest biome (Hare & Ritchie, 1972). Nonetheless, these forests have been extensively surveyed, primarily during the twentieth century using Gulag settlement workers, which resulted in extensive maps and carbon accounting databases (Alexeyev & Birdsey, 1998; Isachenko et al., 1988; Isaev, 1990).

In the early 1990s, the landmark Boreal Ecosystem Atmosphere Study (BOREAS) campaign was initiated by NASA with support from the Canada Centre for Remote Sensing (CCRS) and the Natural Sciences and Engineering Research Council of Canada (NSERC; Sellers et al., 1997). BOREAS was actively funded for eight years and included a wide array of field and remote sensing scientists. BOREAS tested the limitations of which boreal vegetation properties can be characterized by remote sensing and advanced the capability of multiple sensors, algorithms, and models (Gamon et al., 2004). NASA has continued to fund coordinated airborne campaigns in the ABZ, including the Carbon in Arctic Reservoirs Vulnerability Experiment (CARVE; Miller et al., 2016) and the Arctic-Boreal Vulnerability Experiment (ABoVE), which together have improved our ability to understand large-scale ABZ vegetation dynamics and advanced fundamental remote sensing science (Miller et al., 2019). For instance, ABoVE has provided a high level of detail in Alaska and western Canada using multiple sensors including image spectrometers for broad applications (AVIRIS-NG) and solar-induced fluorescence (CFIS), L- and P-band radar, and lidar.

Although field and airborne observations are fundamental, our ability to monitor large-scale changes in boreal vegetation is only truly possible through long-term and continuous observations from space-based platforms. Their success for monitoring boreal vegetation relies primarily on: (i) visible through SW-infrared; and (ii) microwave wavelengths. Visible through SW-infrared science has mostly used passive multispectral imagery, although imaging spectroscopy and active lidar have been used and are promising for future satellite missions (see below). Vegetation indices calculated directly from multispectral surface reflectance, such as the NDVI, enhanced vegetation index (EVI), and photochemical reflectance index (PRI), are correlated with many ecosystem properties related to vegetation extent, composition, and productivity. Directional spectral reflectances captured by multi-angle observations can also be used to derive bidirectional reflectance distribution functions (BRDFs) and land surface albedo, which is an essential and changing climate variable (Liang & Strahler, 1994; Lucht et al., 2000). Either through direct correlations or by constraining forward process models (e.g., radiative transfer and geometric-optical reflectance models), multispectral imagery can be used to estimate key boreal vegetation properties, although there are inevitable issues related to view angles, understory vegetation, cloud cover, and consistency between sensors. For example, LAI and the fraction of absorbed photosynthetically active radiation (fAPAR) are critical constraints on carbon cycling and have been derived from a variety of sensors (Myneni et al., 2015; Zhu et al., 2013). Properties such as percent tree cover (Montesano et al., 2016) and land cover type, including forest genera and even species (Beaudoin et al., 2014), are essential for quantifying large-scale vegetation distributions and their changes. Finally, forest volume characteristics, such as biomass, tree height, and related canopy properties, can be derived most successfully from lidar (Neigh et al., 2013).

Long-term datasets from multispectral sensors now span 30–40 years. The Landsat satellites have been the primary data source at relatively high spatial resolution (~30 m). Landsat science was revolutionized in 2008 when the USGS provided open access to the archive in a consistent and user-friendly format (Kennedy et al.,

2014; Wulder et al., 2012). With subsequent consolidation of the Landsat archive (Wulder et al., 2016) and increases in computing power, a variety of processing tools (e.g., Google Earth Engine) and circumpolar data products related to tree cover, productivity, and disturbance history (e.g., Hansen et al., 2013; Ju & Masek, 2016; Montesano, Sun, et al., 2016; Sexton et al., 2013; White et al., 2017) are now available to the community. Although at a much coarser spatial resolution (1–8 km), the AVHRR family of satellites has provided continuous data since 1978, and particularly since 1981 with the operation of AVHRR/2 on board NOAA-7. AVHRR was used for circumpolar assessments much sooner than Landsat (e.g., Angert et al., 2005; Fung et al., 1987; Goetz et al., 2005; Myneni et al., 1997; Walker et al., 2003) because of its smaller computing requirements and consistent global area coverage; Landsat has a considerably longer revisit frequency of 16 days as compared to every day with AVHRR and more variable spatial coverage due to sparse downlink stations across the ABZ, especially prior to 2000. However, the long-time series of AVHRR comes at the cost of very coarse spatial resolution and inconsistent estimates of vegetation indices with higher resolution MODIS (Jiang et al., 2017). Although not as long-running (2000-present), MODIS has become the gold standard for land-based remote sensing at a moderate resolution (250 m–1 km) in terms of radiometric fidelity and configuration for terrestrial science, as well as open access to well-documented products spanning a range of boreal vegetation properties. The launch of the Visible Infrared Imaging Radiometer Suite (VIIRS) on the Suomi NPP satellite in 2011 and on NOAA-20 (formerly JPSS-1) in 2017 continues the MODIS record. Finally, European sensors, such as VEGETATION on SPOT 4 and 5 (1998-present, ~1-km resolution) and MERIS on Envisat (2002–2012, 300-m resolution), have offered a similar standard of high-quality moderate-resolution observations and data products for relatively long time periods.

Microwave remote sensing, both active and passive, has been equally valuable for quantifying ABZ vegetation properties and long-term changes. Passive radiometry detects microwave energy naturally emitted from the Earth but requires a relatively large, frequency-dependent field of view (5 to > 40 km) for adequate signal detection (Woodhouse, 2006). Radar sensors actively emit pulses of microwave radiation and detect the backscattered portion of the signal, thereby improving the spatial resolution of the signal (McDonald & Kimball, 2006). One of the most robust properties that can be calculated from microwaves in the ABZ is landscape freeze-thaw state, given the strong sensitivity of the dielectric constant to the abundance of liquid water (as discussed in section 4.3; e.g., Hoekstra & Cappillino, 1971; Warren, 2019). Freeze-thaw state represents a fundamental control on land surface water mobility, vegetation phenology, and carbon cycling (Kim et al., 2012; section 4.3).

In addition to freeze-thaw, long-term records of snow water equivalent (e.g., Derksen et al., 2005; Rawlins et al., 2007; Takala et al., 2011; section 4.2), soil moisture (Bartsch et al., 2011; Colliander et al., 2017; Dorigo et al., 2017; Du et al., 2016), boreal wetland community types and characterization of flooded land (Watts et al., 2014; Du et al., 2016; Prigent et al., 2016; section 4.7) have been obtained from combinations of the SMMR, SMMI, SSMIS, AMSR-E, AMSR2, and TRMM Microwave Imager (TMI) sensors, including calibration with the FY3B Microwave Radiation Imager (MWRI; Du et al., 2017). These key landscape indicators provide necessary insight into highly dynamic landscape conditions that strongly influence vegetation carbon assimilation, growth, structure and resistance or vulnerability to ecosystem change.

Vegetation optical depth (VOD) is also an important contribution from passive microwave sensing. The presence of snow can confound optical signals from satellites, making it challenging to detect changes in vegetation greenness using traditional optical/NIR based remote sensing indices (e.g. NDVI) in spring and autumn. Some success has been achieved using the Normalized Difference Water Index (NDWI; e.g. ratios of near-infrared and SW infrared; Gao, 1996) to detect onset of green-up for boreal deciduous and needleleaf forests (Delbart et al., 2005). NDWI infers changes in water availability within the vegetation that occur during transition seasons. Microwave VOD presents an alternative to NDVI and NDWI and is derived from daily 10.7 GHz (Ku band) brightness temperatures (e.g. from AMSR-E; Jones et al., 2011). Satellite VOD has shown greater sensitivity to changes in leaf water content, including those occurring during the seasonal changes in photosynthesis and following drought stress, relative to optical and infrared methods. The VOD indicator has also tracked well with vegetation growth and post-fire recovery in boreal forests (Jones et al., 2013). Yet microwave VOD is less often used for local ecosystem assessments because of the coarse 25-km spatial footprint. A site level alternative to VOD are L-band (1.5 GHz) microwave signals detected at GPS (global positioning system) ground stations. Changes in vegetation canopy water content are

determined through the Normalized Microwave Reflection Index (NMRI) which accounts for the canopy water interference of signals communicated between GPS stations and satellites (Larson & Small, 2014). Taking advantage of differential backscatter between forest and nonforest vegetation, microwave remote sensing can also be used to estimate vegetation land cover types (Dobson et al., 1996; Engdahl & Hyyppa, 2003; Maghsoudi et al., 2012), characterize the distribution of water bodies and wetlands (Bartsch et al., 2012; Clewley et al., 2015), detect disturbance events (Pantze et al., 2014), and study post-disturbance recovery (Kasischke et al., 2007; Jones et al., 2013).

Two primary examples of changing boreal vegetation dynamics that have been explored using these long-term data sources are (i) land surface phenology (LSP) and (ii) peak plant productivity. Long-term satellite observations show a warming-induced lengthening of the growing season due to both earlier plant activity in the spring and delayed senescence in the fall (Figure 12; Barichivich et al., 2013, Gonsamo & Chen, 2016; Kim et al., 2012), as well as associated shifts in peak productivity (Gonsamo et al., 2017). Although these changes have increased peak productivity in many temperature-constrained ABZ landscapes, the opposite has been observed in moisture-constrained areas (Barichivich et al., 2014; Kim et al., 2014; Zhu et al., 2016). This is especially the case in the interior boreal forests of Alaska and western Canada (Angert et al., 2005; Beck & Goetz, 2011; Goetz et al., 2005), where warmer and earlier springs tend to cause higher immediate productivity but result in drought stress and decreased productivity later in the summer (Barichivich et al., 2014; Buermann et al., 2013; Parida & Buermann, 2014), ultimately leading to increases in regional tree mortality (Chen & Luo, 2015; Hember et al., 2017; Peng et al., 2011; Zhang et al., 2015). Indeed, the overall impacts of lengthening growing seasons on net carbon uptake are uncertain due to longer and drier summers (lack of sustained productivity) and increased soil respiration (McDonald et al., 2004; Angert et al., 2005; Piao et al., 2007, Piao et al., 2008; Barichivich et al., 2012).

New improvements in sensor technology and processing techniques offer tremendous promise for understanding changing ABZ vegetation dynamics, and potential for the initiation of new long-term data products. Improvements have generally increased spectral and spatial resolution for land-specific properties and have been aided by more receiving stations and increased on-board storage. For example, the Sentinel-2 visible-near infrared satellite sensors offer improved spatial (visible bands 2–4 and 8, 10 m; red-edge bands 5–7, 20 m) and spectral resolution compared to Landsat, particularly in the red edge. Emerging techniques to merge Landsat 8 and Sentinel-2 data (e.g., Claverie et al., 2017) promise global coverage every 2–3 days at 30-m resolution. Imaging spectroscopy measurements offer the potential to observe ABZ vegetation at a much higher spectral frequency, enabling for example consistent tree species mapping. The Hyperion instrument, on the NASA Earth Observing One (EO-1) satellite, demonstrated this technology (Middleton et al., 2013), which may become operational with the upcoming NASA Surface Biology and Geology mission (HyspSIRI, 2018). High-resolution radar measurements (e.g., L-band ALOS PALSAR 1/2, C-band RADARSAT 1/2, C-band Sentinel-1, X-band TerraSAR, and S- and L-band NISAR), including the use of SAR and InSAR data, have shown enormous capabilities to map ABZ land surface deformation (Liu et al., 2014; Short et al., 2011) and changing vegetation properties (Antropov et al., 2016; Chen et al., 2018) at high spatial resolution (5–100 m).

Recent advances in space-based observations of solar induced fluorescence (SIF) by chlorophyll (Frankenberg et al., 2011; Joiner et al., 2011) and enhanced retrieval of biochemical properties of boreal plant leaves may also aid the study of the climate sensitivity of boreal vegetation. In the case of SIF, all current observations are derived from satellites (GOME-2, SCIAMACHY, GOSAT, OCO-2) that were initially intended to measure trace gases in the atmosphere, but spectra contained the SIF signature in the visible-near infrared region. SIF is of interest because it can be used as an indicator of the start, end, and intensity of the growing season, can provide information on vegetation stress, and correlates well with GPP. Finally, space-based lidar measurements offer enormous benefits in terms of quantifying ABZ vegetation properties such as vegetation height, biomass, LAI, and class. However, we have yet to have consistent lidar coverage at high latitudes with an optimal wavelength for vegetation properties. The Geoscience Laser Altimeter System (GLAS) on ICEsat was the closest, but it was not explicitly designed for land vegetation (Harding & Carabajal, 2005). ICESat2 will offer more coverage, with improved in-track sampling using photon-counting technology. Unfortunately, the dedicated lidar mission to estimate forest structure, NASA Global Ecosystem Dynamics Investigation (GEDI), is limited to ±51.6° latitude from being based on the international space station. However, the ESA BIOMASS

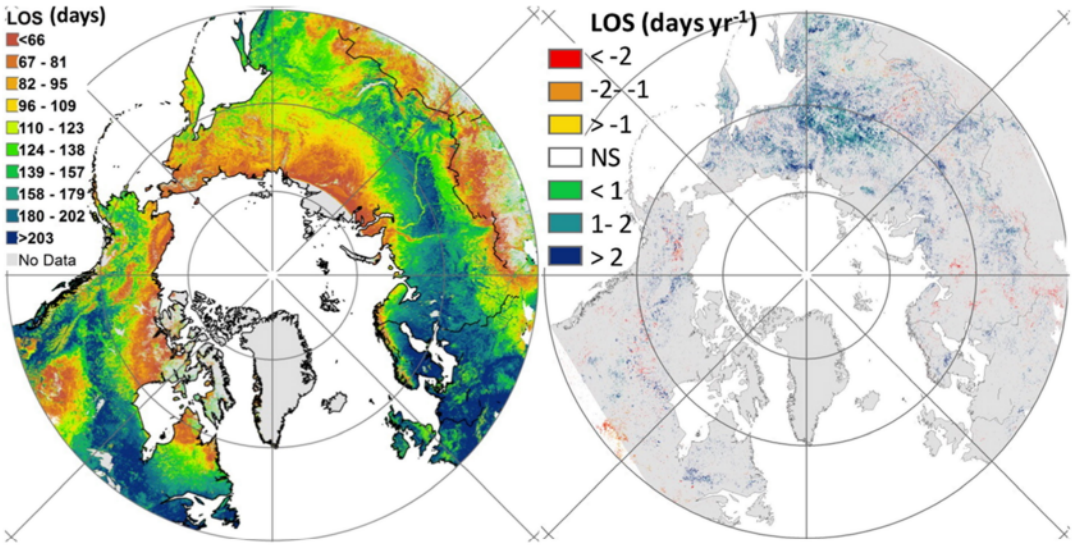

Figure 12. Spatial distributions of the mean length (LOS) of the growing season (left) and LOS trends (right) extracted from the circumpolar vegetation dynamics product (Gonsamo & Chen, 2016) during 1999–2013 at 4-km spatial resolution. Categories in the left panel are mapped in 10 equal quantile classes, meaning each category of the legend contains 10% of the valid circumpolar land pixels. "NS" is not significant trend at $p = 0.05$ (two tailed Student's t test). Reprinted from Gonsamo and Chen (2016) with permission from Elsevier.

satellite mission (planned launch in 2020) using P-band (435 MHz) SAR will aid in measuring boreal forest structure (Le Toan et al., 2011).

Unlike the above mentioned satellite instruments, fine-scale spatial variability can be resolved with commercial very high-resolution spaceborne sensors (0.3–4 m), first available commercially from the IKONOS satellite in 2000 and expanding to a variety of others in the late 2000s (e.g., DigitalGlobe Worldview-1, -2, -3, and -4; GeoEye-1; RapidEye; and Planet). The emerging use of these data comes after decades of airborne photographic analysis of forest extents, which included photogrammetry, and has continued with digital aerial photogrammetry (DAP). Recent access by some to commercial submeter data (Neigh et al., 2013) has enabled fine-scale investigations with mono and stereo image acquisitions. These passive optical data have similar spectral wavelengths to Landsat (visible and near infrared channels), but they have important fundamental differences due to image acquisition characteristics. The differences can be seen as limitations, as sun-sensor geometry, pixel resolution, and irregular image extent, but these observations can also provide new features to exploit (Montesano et al., 2017). Methods that capitalize on the new features of these data will provide a means for resolving detailed patterns of vertical and horizontal vegetation structure across remote portions of the boreal forest (Montesano et al., 2019). Structural parameters, such as height, cover, stem density, and aboveground biomass, can be informed by textural characteristics, which quantify the variation in contrast according to the illumination of image features and their scattering (Berner et al., 2012; Kayitakire et al., 2006; Montesano et al., 2016; Wood et al., 2012; Wulder et al., 2000; Wulder et al., 2008). These fine-scale properties will provide new insight into the distribution of plant functional types, disturbances, productivity, land-atmosphere interactions, and their changes through time.

Looking forward, it is a priority to maintain and update the long-term databases from space-based remote sensing that capture both dramatic and subtle changes in boreal vegetation. There will always be tension within the scientific community and funding agencies between ensuring data continuity and providing new sensor improvements. In some instances, the two can be accomplished in tandem by including instrument refinements that improve acquisition but also maintain compatibility (e.g., Landsat OLI, SSM/I, and AMSR2). Nonetheless, key vegetation properties have remained difficult or impossible for space-based remote sensing to capture at large scales, and that would greatly improve our understanding and ability to understand and project boreal vegetation. Among these include stand age (Lutz et al., 2008), species composition (which is theoretically feasible for circumpolar boreal forests because of low species diversity), fine-

scale moisture and hydrologic properties (e.g., site moisture as in Johnstone et al., 2008), and changing light use efficiency (either from SIF or PRI photoprotection mechanisms; see Hilker et al., 2008). Thus, we recommend the continued development and deployment of sensors that could provide information on these properties, such as imaging spectroscopy, lidar, combined information from radar and radiometer L-band, and high-resolution dual-frequency radar (e.g., L- and P-bands) with adequate revisit frequency. We also recommend an increased focus on the Eurasian ABZ, which remains significantly understudied compared to North America (Soja & Groisman, 2018, and references therein), as well as expanded and strategically placed in situ networks of vegetation properties and trace gas fluxes to better calibrate and extrapolate existing remotely sensed metrics across the boreal zone. Improving the spatial resolution of SIF observations should occur with the next generation of satellite missions, yet reducing uncertainties on the relationship with GPP requires improvements in temporal resolution. Finally, increased access to very high-resolution imagery will facilitate a greater understanding of boreal vegetation properties and changes at more ecologically relevant resolutions.

4.6. Fire Regimes: An Agent of Rapid ABZ Change (Amber J. Soja, Tatiana V. Loboda, Randi Jandt)

Fire acts to cycle carbon and nutrients, initialize ecosystem succession, and is the dominant disturbance across ABZ lands. However, given the diversity of interacting systems (e.g., section 4.3–4.5), understanding how one ecosystem responds to fire does not equate to another, especially on disparate continents. Fire is largely under the control of short-term weather (~7 days) and large-scale climate. Climate determines the composition and structure of boreal forest cohorts, each of which is associated with a fire return interval (e.g., *P. sylvestris* – lichen vaccinium understory 10–70 years; dark coniferous forest 70–600 years; Soja et al., 2006, and references therein). Additionally, severe fire seasons have been associated with the Arctic Oscillation in central Siberia (Balzter et al., 2005) and the Pacific Decadal Oscillation in Alaska (Duffy et al., 2005). Moreover, fire impacts weather and climate systems by altering radiative forcing (e.g., via smoke and land cover change), inducing permafrost degradation (e.g., minimally two to five decades to recover), as well as direct and indirect emissions of aerosols and greenhouse gases to the atmosphere (e.g., sections 4.3–4.5 and 5.1–5.2; Michaelides et al., 2019). In addition to the potentially devastating effects on communities and local economies (e.g., the 2016 Fort McMurray fire, the costliest disaster in Canadian history with $9.9 billion in losses), fire smoke degrades air quality (Figure 1), affecting human health (e.g., the 2010 Moscow peatland fires caused an estimated 56,000 deaths and $15 billion in losses; Rappold et al., 2011; Thelen et al., 2013). It is predicted that fire will increase with respect to burned area and fire frequency, fire severity, fire season length, fire weather severity, and ignitions from lighting (Price & Rind, 1994; Stocks et al., 1998; Flannigan et al., 2001; Flannigan et al., 2009; Wotton et al., 2010; Flannigan et al., 2013; Hu et al., 2015). Additionally, the initial signs of fire-induced change are already evident across the boreal landscape (Soja et al., 2007).

Observations can be categorized as prefire, active-fire and post-fire. Prefire information is required to understand fire potential (e.g., growth, direction, and severity) and these include information on prefire fuels (e.g., above- and below-ground biomass, availability, structure, and health) and fire weather (e.g., preceding temperature, precipitation, wind speed, lightning, and relative humidity). Prefire vulnerabilities, such as fuel availability and fire weather, are not discussed in this work. ABZ vegetation, or prefire "fuel," is discussed in sections 4.4 and 4.5. Active-fire data include fire location, severity or depth of burn, fire radiative power, and smoke plume injection height, detrainment, and transport, all of which are used by fire scientists, operational fire management, and air quality communities. Post-fire analysis (e.g., Figure 13) includes fire severity and burn scar mapping (i.e., burned area), evaluating relevant patterns of change (e.g., fire return intervals and severity), smoke transport, deposition, and other potential impacts (e.g., changes in landscape and atmospheric albedo, landslide and debris flow potential, and air quality).

Estimates of long-term (~70 years), large fire (>200 ha) burned area data exist for Canada and Alaska (Figure 14). Burned area has more than doubled across North America, when comparing the first (1950–1979) and last (1987–2016) 30 years of the record. In Russia, historic fire records were under-reported before 1988 for economic and political reasons, and fire was not monitored, controlled, or documented in about 40% of the remote Russian Forest Fund region (Shvidenko & Nilsson, 2000; Sofronov et al., 1998; Soja et al., 2004). In addition, fire data are not complete across the Arctic tundra, because these data are difficult to obtain and the fire return interval is large (from 180 to 1,500 years; Soja et al., 2006; Hu et al., 2015).

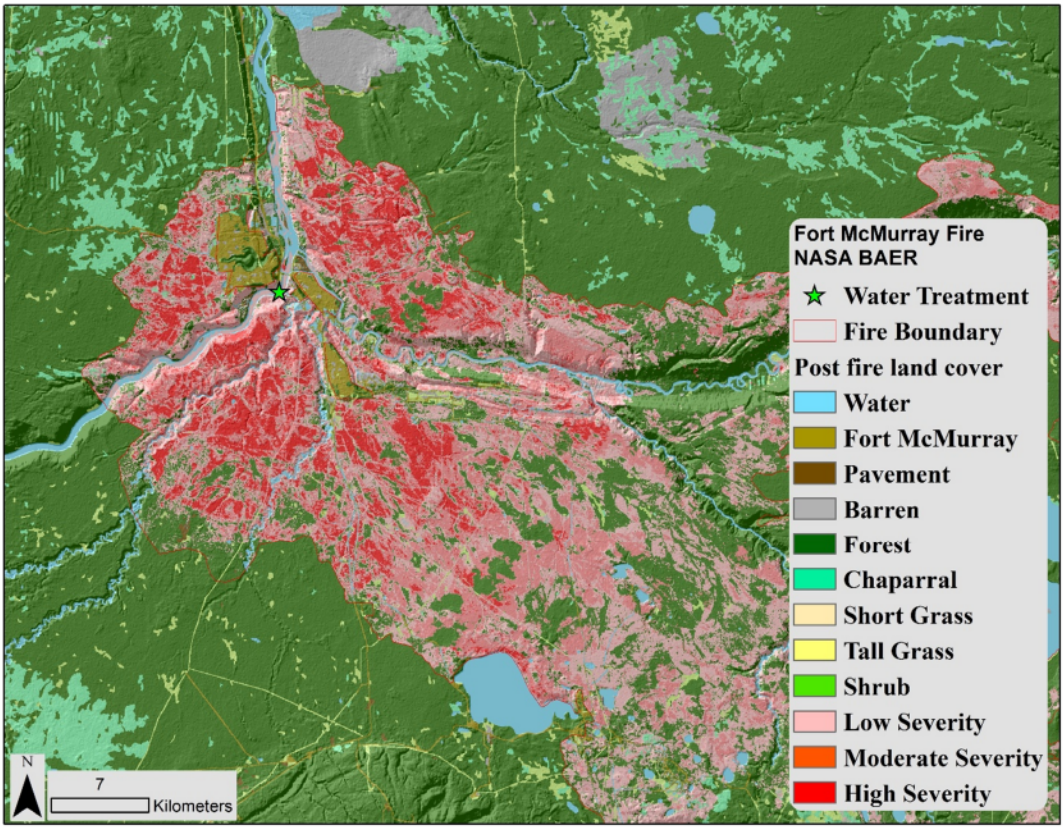

Figure 13. Map highlighting land cover in Fort McMurray, Alberta following the 2016 Horse River Fire. This map was created by combining burn severity from Landsat 8 OLI imagery with land cover data. Land cover, topography, climate and soils data were used to predict post-fire erosion with the Water Erosion Prediction Project (Dr. Mary Ellen Miller; http://www.mtri.org/post_fire.html).

Between 1995 and 2001, NASA participated in the controlled crown fire experiment in Canada's Northwest Territories, the International Crown Fire Modelling Experiment (ICFME), which was led by Canada and the United States (Stocks et al., 2004). The ICFME team provided innovative data and insights into the characteristics of crowning forest fires, while NASA suborbital aircraft measured some of the first boreal crown fire emissions and emission factors. Following the opening of Russia to the western world, NASA collaborated with Russian and other scientists to contribute to the historic 1996 Fire Research Campaign Asia-North (FIRESCAN) experiment (Goldammer et al., 1996). The goal of Firescan was to quantitatively understand the role of fire in boreal ecosystems, motivated by the International Boreal Forest Research Association

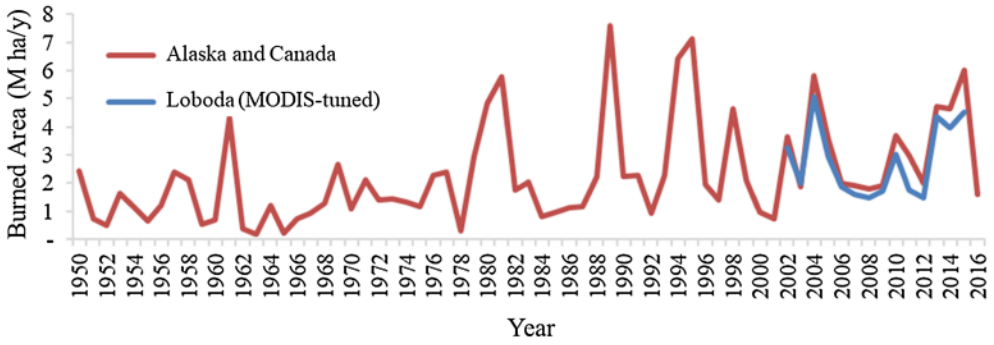

Figure 14. Historic burned area (M ha/y; red line) for Alaska and Canada compared with the satellite record (blue line) that has been optimized specifically for these ecosystems as described in Loboda et al. (2011).

(IBFRA) and the International Global Atmospheric Chemistry (IGAC) organizations. During this campaign, an interdisciplinary team of scientists conducted a large forest fire experiment on Bor Island, Krasnoyarsk, Russia on July 06, 1993. Then, also in this window of opportunity in Central Siberia, the NASA FIRE BEAR (Fire Effects in the Boreal Eurasia Region) project began in the late 1990s and continued for over a decade, with the goal of investigating the complex interactive effects of fire, weather, fire severity, fuel consumption, fire behavior and ecosystem succession. These projects and the suite of scientific instruments, including sub-orbital and satellite data, offered an unprecedented view of fire regimes, burned areas, ecosystem recovery, trace gas and aerosol emissions, feedback to climate systems, and carbon storage in these unique boreal forests.

Historic satellite data that have been used to derive patterns of fire are the U.S. Corona secret military reconnaissance program (1959–1972) and the Operational Linescan System (OLS) on the U.S. Department of Defense Defense Meteorological Satellite Program satellites (DMSP, polar orbit, first launch 1962). The Corona program series of satellites took photographs and released the film canisters in capsules on parachutes that were retrieved by aircraft mid-air. These data were declassified under the Gore-Chernomyrdin agreement in 1995 and could be used to identify and quantify large fire scars that predate the historic sub-orbital fire databases (available through the U.S. Geological Survey [USGS]). DMSP satellites were declassified in 1973, and the first systematic inventory of fire was produced using these data (Cahoon et al., 1992). DMSP satellites continue to orbit.

Satellite instruments on polar orbiters and geostationary satellites have been used to locate or detect active fires ("hot spots" spectral maximum ~3.7 μm) and map fire scars (visible and near infrared wavelengths) since these capabilities were first observed (Matson et al., 1984; Matson & Dozier, 1981; Muirhead & Cracknell, 1984, 1985). In 1972, the first satellite in the polar-orbiting Landsat series (Earth Resources Technology Satellite (ERTS)) was launched, which provided the capability to detect and measure fire scars (80-m resolution, return interval 18 days). Subsequent Landsat satellites were launched with improved capabilities (15- to 30-m resolution, return interval 16 days and additional channels). Landsat has provided an unprecedented historic record of healthy vegetation and burned area, and currently Landsat provides data that are used to assess fire severity and monitor active fire (Schroeder et al., 2016). NASA and the USGS have started to design Landsat 9, which is targeted for a launch date of 2020.

In 1978, NOAA launched a meteorological satellite, TIROS-N, with the AVHRR instrument onboard (polar orbit; ~1.1 km^2 at nadir; ~1 day, 1 night view), which unexpectedly proved to be instrumental in detecting active fire and defining burned area from space. Finding hot spots in water bodies using the 3.8-μm channel was unexpected, and Matson and Dozier (1981) used nighttime imagery to conclude these high temperature fields were from steel mills and gas flares (Smith & Rao, 1971). Since 1978, a series of AVHRR instruments has provided the capability to identify active fire and quantify burn scars, even though the instrument was not designed for these purposes. However, because of limited storage capability and the lack of downlink stations (until ~late 1990s), consistent long-term global AVHRR coverage only exist as Global Area Coverage data (GAC – mean value of 4 pixels stored for every 15 pixels). Still, because most of the burned area in boreal regions is by large fires, AVHRR GAC data can be used to quantify historic ABZ burned area.

Data from the two MODIS instruments provide improved active-fire locations, increased saturation temperatures, higher spatial resolution (500–1,000 m) and a new fire measurement, Fire Radiative Power (FRP). Both these instruments are in extended operations, functioning well beyond their 6-year design time. Thermal anomalies or active-fire detection data are consistently provided in near-real-time, which makes these data valuable for both scientific analyses and fire and smoke management (MOD14/MYD14; Giglio et al., 2003; Giglio, Csiszar, & Justice, 2006). With each fire location, valuable ancillary data are provided, such as time, fire confidence and FRP (1 day, 1 night view from each MODIS instrument (Terra 10:30 and Aqua 13:30 equatorial crossing time), swath overlap at high latitudes). Fire radiative energy is derived using FRP and takes advantage of the energy released from a fire to evaluate fuel consumption, emissions and plume injection heights (Ichoku et al., 2008; Ichoku & Ellison, 2014; Val Martin et al., 2010; Wooster et al., 2005).

Burned area provides the basis for fire emission estimates and a consistent database for fire science, management and change analysis. Two official MODIS global fire products exist, one optimized for the tropics and savannahs (MCD45 (Roy et al., 2005, Roy et al., 2008)) and the other optimized for northern forests (MCD64;

Giglio, van der Werf, et al., 2006, Giglio et al., 2009). MCD64 provides more accurate estimates in the ABZ, however, a regionally optimized MODIS-based burned area algorithm provides estimates that compare best to ground-based data (Figure 14; Loboda et al., 2011). A comparison of the regionally optimized product to official statistics in North America results in mean differences of 19%, which demonstrates the ability of satellite data to provide long-term accurate and consistent data in remote regions. However, Northern Eurasian burned area products do not compare well (e.g., mean differences ~39%), which highlights challenges that result from differences in ecosystems, fire regimes (e.g., dominant surface fires as opposed to crown fires), and algorithms. These discrepancies in products also suggest that there is a need for a comprehensive evaluation (Ponomarev et al., 2016; Sukhinin et al., 2004).

VIIRS active-fire detection data (375- and 750-m resolution for the IR bands; Schroeder et al., 2014) provide higher resolution in comparison to MODIS data (1,000 m for the IR bands), although the VIIRS instrument equator crossing times are not optimized for morning or late afternoon fire detection (~13:30 local time, at a location ~50 min apart with different view angles). There are currently two VIIRS instruments (on S-NPP and NOAA-20), and these data are actively used by operational agencies in the United States and globally to locate and manage fire. Additionally, because of enhanced spatial resolution, these data are being used to initialize predictive fire behavior models (Coen & Schroeder, 2013), which could provide higher resolution meteorological information to Incident Meteorologists, and this could translate to increased situational awareness.

Cloud cover is pervasive in the ABZ, and thick cloud cover or smoke can inhibit active-fire detection. However, the high pressure weather systems that act to dry fuels are synonymous with clear skies, and high-pressure systems precede and often endure during large fires. During the day, smoke is detrained, so smoke does not typically inhibit active-fire detection, but smoke can limit the strength of FRP and impede near-field precipitation (Andreae et al., 2004; Lu & Sokolik, 2013). Concurrently, the energy, moisture, and smoke particulates produced by large fires can alter and generate weather (pyro-generated cumulus (pyroCu) and cumulonimbus (pyroCb)), which can inhibit active-fire detection. Additionally, continuous tree cover often limits or prevents the detection of surface fires, which is the dominate fire type in boreal Eurasia (Korovin, 1996; Rogers et al., 2015). Reflective snow, ice or water bodies can be a source of false fire detection, although algorithms have been developed that mask continuously reflective surfaces. Post-fire burn scar mapping is straightforward in the ABZ where burn scars persist on the landscape for months to years, yet burn scar mapping is challenging in boreal grasslands that green-up quickly and following surface fires, where the forest can continue to remain green.

Currently, there are two aging satellite instruments that are capable of capturing plume injection height: Multi-angle Imaging SpectroRadiometer (MISR) and Cloud-Aerosol LIdar with Orthogonal Polarization (CALIOP). Both instruments provide essential and unique information. MISR has a larger swath width, thus a greater ability to estimate near-fire plumes, and the MISR smoke plume injection height database is advanced (Kahn et al., 2007; Val Martin et al., 2010). However, MISR is on Terra, which is a morning overpass, so the largest smoke plume injection heights are missed because fires and smoke plumes peak in the late afternoon when fuels are the driest and relative humidity is the lowest. Additionally, MISR requires distinct boundaries to estimate plume heights, and large fires tend to lie down at night, where smoke is trapped in the boundary layer, resulting in no distinct boundaries. CALIOP (active lidar, 30-m vertical resolution) has an increased capability to detect optically thin smoke plumes and plumes from extensive ambiguous smoke fields. When CALIOP data are paired with a back trajectory model, these can enhance the MISR morning database, by defining afternoon plumes (Omar et al., 2009; Soja et al., 2012).

Over recent years, the hemispheric transport of large smoke plumes has been recognized as occurring on a regular basis (Damoah et al., 2004), and it has been suggested pyroCu and pyroCb clouds may be more common than had been initially imagined (Fromm et al., 2010; Guan et al., 2010). These largely unexplored pyroCb's inject a huge amount of aerosols and greenhouse gases into the upper troposphere and lower stratosphere and at times are equivalent to volcanic eruptions (Peterson et al., 2018). Case studies have associated individual pyroCb events with twofold to fivefold increases in zonal stratospheric aerosol optical depth (AOD; Fromm et al., 2000, 2005). Persistence of stratospheric AOD enhancements following fire events (Fromm et al., 2008; Fromm et al., 2008), make this phenomenon the largest perturbation to stratospheric aerosol apart from large volcanic eruptions and a noteworthy force on the climate system (Fromm et al., 2000; Fromm & Servranckx, 2003).

It is challenging to infer the depth and extent of carbon stored below ground in the ABZ from satellites or from the ground in these remote regions. As discussed in section 4.3, this is significant because the boreal zone holds the largest reservoir of carbon on Earth (minimum 27% of global terrestrial carbon), which is predominantly stored belowground (permafrost, peatlands and carbon-rich soil organic matter; Apps et al., 1993; Zoltai & Martikainen, 1996; Alexeyev & Birdsey, 1998; Tarnocai et al., 2009; Scharlemann et al., 2014). Therefore, more extensive fires or deeper consumption of organic forest floor by wildfires has the potential to release vast amounts of carbon that has been stored for millennia (e.g., Figure 15; Walker et al., 2018, Walker et al., 2019). For instance, the West Siberian lowlands are the largest bog region on Earth, and they hold ~40% of the Earth's peat (Walter, 1979). Additionally, about two-thirds of the world's boreal forests are located in Russia (Hare & Ritchie, 1972), however these critical ABZ ecosystems are under studied due to the political environment, their extent, and remote location.

Because fire is a key driver of landscape change, consistent long-term fire data records are an integral component to environmental studies in the ABZ. Going forward, the larger air quality, fire management and science communities have recommended an expansion of the number of polar orbiters and/or higher-resolution geostationary satellites that can quantify ABZ fire, which is important for assessing fire timing (e.g., time of day, season), quantifying short-lived or understory fires, defining burn scars (area, severity), calculating fire emissions, and for assessing overall fire regimes. Because fires can be small and short-lived (morning cropland burning) or travel rapidly (~10–22 km/hr, spotting to 35 km), the time an instrument is overhead is significant to understanding fire regimes. Concurrently, instrument spatial resolution is important for fire detection, burn scar and severity accuracy, but spatial resolution has often been necessarily sacrificed for temporal resolution.

In order to evaluate and interpret satellite-derived fire and fuel (live vegetation and ground carbon) properties, we also recommend an expansion of the suborbital observing network, which is currently sparse in the ABZ, particularly in the Russian ABZ. Notably in 2019, there are ongoing field campaigns that are expected to provide substantial insights, ABoVE (e.g., section 4.5) and the NASA/NOAA Fire Influence on Regional to Global Environments and Air Quality (FIREX-AQ) focused on linking fuels to the chemical transport of emission in North America, which is the first NASA fire-fuel-atmosphere focused campaign, although fire smoke has always presented itself for opportunistic sampling. Fire weather paired with detailed biospheric mapping and SMAP-like data could hold promise for our ability to quantify the depth, severity and extent of carbon consumed during fires. Even though the boreal zone is floristically simple, Siberian ecosystems evolved separately from those in North America and respond differently to the complicated interactions with soils, hydrology, fire regimes and climate. For instance, surface fires, that burn under canopies, dominate fire regimes in Northern Eurasia, and these burned areas are not currently accurately quantified.

Consistent long-term fire and fuel records are imperative to understanding the past, current and future ABZ, because fire is integral to both initiating land and atmospheric change and serving as an initial indicator of change (Soja et al., 2007). Instruments that are capable of defining plume injection height and the vertical distribution of smoke in the atmosphere are in extended operations, and there are currently no replacements. These data are important for constraining models that would aid in predicting aerosol and cloud impacts on the climate. Additionally, emissions factors are based on limited case studies and vary widely, likely due to the limited number of studies and the exclusion of contributing influences, such as detailed ecosystem fuels and fire weather. Finally, improved estimates for FRP are promising for linking fire energy to emissions, fire severity and smoke plume injection heights. However, FRP currently saturates, so this potential has not been fully explored.

4.7. ABZ Wetlands (Ben Poulter, Nicholas Steiner, Kyle C. McDonald, Mark L. Carroll)

ABZ wetlands include inland water bodies, such as shallow lakes, ponds and rivers, as well as seasonally inundated systems characterized by emergent vegetation adapted to hydric soil conditions, as well as by treed or shrubby vegetation, such as peatlands (Cowardin et al., 1979). From a remote sensing perspective, monitoring and mapping of inundated ABZ wetlands involve classifying a continuum of ecosystems defined by both the duration and the areal extent of surface flooding and inundation. Combined with differences in terminology for how wetlands are defined, as well as challenges in observing small-scale and temporally varying hydrologic conditions, there remains a large gap in the ABZ-ON that has led to uncertainties in monitoring the location and dynamics of ABZ wetlands (Bohn et al., 2015; McGuire et al., 2012). These

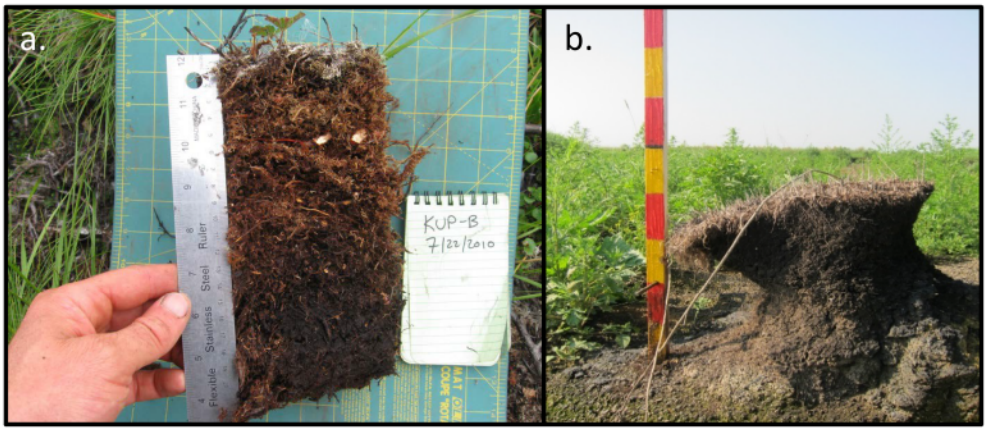

Figure 15. (a) Residual soil organic material (SOM) or peat in an Alaska tundra burn (photo: E. Miller, BLM-Alaska Fire Service). About 20 cm of organic material remained after a light severity burn. (b) Burned SOM and peat in Shushenskoe, Russia, showing the depth of burn in this region was greater than 40 cm (photo Dr. Elena Kukavskaya, V.N. Sukachev Institute of Forest).

uncertainties have led to concerns that wetland area, and thus CH_4 emissions and other ecosystem services, are easily "double counted" (Thornton et al., 2016). The double-counting problem is partly due to the broad definition of wetlands in the "Cowardin" classification, which includes both vegetated "palustrine" wetlands and inland-waters or water bodies that are included in the "lacustrine" category of Cowardin et al. (1979), but also due to remote sensing limitations that stem from the use of coarse-spatial resolution satellites (e.g., passive microwave instruments and scatterometers) as compared to moderate or fine-resolution optical satellites (e.g., Landsat or Worldview) or Synthetic Aperture Radars (SARs) that are needed to detect small isolated ponds or streams. In addition, monitoring of year-to-year changes in wetland area associated with permafrost thaw (section 4.3) and the creation of thermokarst lakes has stymied biogeochemical accounting, particularly for assessing climate-driven changes in high latitude CH_4 emissions (section 5.2; Saunois et al., 2017). ABZ wetlands play an important role in the Earth system and for a variety of ecosystem services (MEA, 2005), which include regulating biogeochemical processes (e.g., carbon storage, CH_4 emissions), biodiversity (e.g., providing habitat for migratory waterfowl), and biophysical properties (e.g., albedo and Arctic amplification). Thus documenting recent trends and remote sensing opportunities for improved monitoring of wetlands is particularly important given their vulnerability to climate change (Melillo et al., 2014).

The first efforts to document the distribution of ABZ wetlands were made by compiling ground-based national inventories of vegetation and soil type, and combining this information with a patchwork of aerial photograph interpretations of inundation, leading to an estimate of ~2.7 Mkm^2 of wetlands above 60°N (Matthews & Fung, 1987). The approach of Matthews and Fung et al. (1987) was intended to provide a globally consistent methodology to map wetlands, yet was limited to using coarse spatial resolution databases (1° resolution) that did not effectively partition inland waters from vegetated wetlands. Global wetland area updates using the inventory approach were carried out by Kaplan in Bergamaschi et al. (2007) and by Lehner and Doll (2004); i.e., the Global Lakes and Wetlands Dataset, GLWD), which classified wetlands based on eleven categories related to duration of flooding, vegetation type, salinity and other factors and by using higher spatial resolution information. The inventory approaches only provide approximate snapshots in time rather than temporal dynamics because the delineation of wetland features is carried out over multi-annual periods (e.g., HydroLAKES (Messager et al., 2016) contains 1.43 million polygons entered into a Geographic Information System). More recent efforts have attempted to capture both seasonal and interannual variability, as well as separate inland waters and vegetated wetlands by using remote sensing.

Fractional surface-water extent (Fw) is a measure of surface inundation dynamics and is derived by combining various microwave instruments in Low Earth Orbit (LEO) to create daily time series from 1992 to present. The geophysical variable "surface inundation" is only one aspect of features that represent wetlands and for wetlands where surface water is not present, or where dense vegetation canopies are present, the

surface inundation datasets only partly reveal the location of wetlands. These passive sensors include SSMI at 37 GHz (0.81 cm), SSMIS, and AMSR-E at 6.9 GHz, 18.7 and 23.8 GHz and the active sensors include the C-band ERS-1 scatterometer (5.25 GHz, 5.71 cm), QuikSCAT (Ku band, 13.4 GHz) and ASCAT (C-band, 5.25 GHz). There are various algorithms for relating brightness temperature to measure surface inundation, and for fusing the datasets from the different instruments together. There are currently three global Fw datasets available: the Surface WAter Microwave Product Series (SWAMPS; Schroeder et al., 2015; Jensen & McDonald, 2019), the Global Inundation Extent from Multi Satellites (GIEMS; Prigent et al., 2001), and the Land Parameter Data Record (LPDR; Watts et al., 2014; Du et al., 2017). Of these, SWAMPS and GIEMS employ a mixture model to infer Fw based on endmembers selected from salient landcover classes. The derivation of the LPDR employs a radiometrically derived retrieval that uses multi-frequency, multi-polarization microwave brightness temperatures to classify Fw. ABZ surface inundation varies seasonally following freeze-thaw processes and interannually with climate variability; for 1992–2012, SWAMPS estimates surface inundation >50°N of ~1.7 Mkm^2, and GIEMS estimates <1 Mkm^2 above 55°N. As compared to the MODIS Open Water Bodies and permanent wetlands dataset (i.e., MODIS LC and MOD44W) discussed below, the SWAMPS and GIEMS ABZ surface inundation estimates are lower by about 0.5 and 1.2 Mkm^2, respectively. The difference between SWAMPS and GIEMS estimates with the MODIS-based estimate points to the challenge of integrating heterogeneous surface inundation information within a 0.25° resolution pixel versus a 250-m pixel. SWAMPS retrievals are generally in agreement with the results from the LPDR.

SARs are active microwave imaging instruments that measure backscattered energy (backscatter) from surfaces they illuminate. When observed off-nadir, open water surfaces are generally characterized by low backscatter. When vegetation is present, scattering processes enhance backscatter and enable determination of vegetation structure and inundation under vegetation canopies. SARs benefit from high spatial resolution (10–50 m) and are able to support measurement of wetlands day and night, independent of solar illumination and largely unaffected by cloud cover, thus supporting consistent, multi-temporal characterization of inundation regimes. The L-band (1.275 GHz) HH-polarization JERS SAR operated from 1992 to 1998, providing the first synoptically collected imaging radar datasets appropriate for mapping continental-scale landcover. Dual-season imagery from the JERS SAR was thus employed in development of the first consistent mapping of wetlands across Alaska (Whitcomb et al., 2009). ALOS, launched by JAXA, operated from 2006 to 2011. It carried the successor to JERS, PALSAR. PALSAR incorporated a multi-polarization capability and a ScanSAR mode, allowing broad, regional coverage across a 350-km-wide swath and providing new data sets suitable for seasonal inundation monitoring and vegetation mapping. PALSAR datasets are of sufficient extent and temporal frequency of coverage to support regional to continental-scale mapping and monitoring of changing ABZ wetlands (Clewley et al., 2015; Clewley, Whitcomb, Moghaddam, & McDonald, 2015) and differentiation of CH_4 source areas in boreal landscapes (Bohn et al., 2007). Presently, the availability of L-band SAR datasets continues with the ALOS successor mission ALOS-2/PALSAR-2, launched in 2014. ESA's C-band Sentinel-1A (launched in 2014) and -1B (launched in 2016) SARs have two imaging radar systems, providing a combined capability for advancing the monitoring capability of imaging radars. With the Sentinel-1C and -1D instruments presently in development, these spacecraft establish a sustained long-term presence of SARs for the monitoring of wetlands environments.

Optical remote sensing at moderate spatial resolution has been used successfully at global scales to create static maps of open/inland water bodies, (e.g., MOD44W; Carroll et al., 2009) and wetland vegetation (Friedl et al., 2010). More recently, high resolution data using GeoCover2000 (i.e., GLOWaBo; Verpoorter et al., 2014) and Landsat (i.e., G3WBM; Yamazaki et al., 2015) have been used to map seasonal dynamics of lakes, ponds and rivers. Using similar algorithms and harnessing the full power of Google Earth Engine with the full Landsat archive, Pekel et al. (2016) created the Global Surface Water (GSW) dataset, producing more than 30 years of surface-water dynamics and associated metrics at 30-m resolution. The moderate and high resolution mapping approaches are consistent with the inventory and microwave-based approaches, for example the GSW dataset estimates permanent surface water in Canada, Russia, Norway and Sweden to cover >1.9 Mkm^2 in comparison with the MOD44W estimate of 2.1 Mkm^2. Despite the high resolution provided by Landsat, approximately 90 million lakes worldwide are less than 0.01 km^2 in size (Verpoorter et al., 2014) and thus 30-m resolution introduces significant co-registration, spectral mixing, and other

issues in mapping smaller inland waters directly. These issues are partly overcome by using hybrid mapping approaches. For example, using a combination of remote sensing observations, topography, inventory and expert elicitation, Olefeldt et al. (2016) mapped up to 3.6 Mkm^2 of thermokarst wetlands, which is larger than the sum of the separate inland waters and vegetated wetlands estimates provided by remote sensing alone. Optical remote sensing has also been applied to global mapping of river and stream networks to enhance or provide additional insight into topographically derived networks. For example, the Global Width Database for Large Rivers (GWD-LR) applied hydrologic routines to a 90-m digital elevation model to map bank-to-bank river widths (Yamazaki et al., 2014). More recently, Allen and Pavelsky (2018) mapped river and stream networks using Landsat finding more river extent that previous regional estimates for the Arctic.

The GSW dataset is the most robust global moderate resolution dataset depicting all types of waterbodies because it uses multiple observations per year to map the waterbodies which helps avoid anomalous conditions caused by drought and/or flood. Comparison of the GSW with a locally derived product shows that many small waterbodies and edges are missed with the global algorithm (Carroll & Loboda, 2017). The ABoVE field campaign funded decadal water maps covering the periods 1991, 2001, and 2011 to provide a regional estimate with lower uncertainties for the region (Carroll et al., 2016). A database of local and regional water products for the circum-Arctic permafrost region is being maintained in Europe (Muster et al., 2017). Cooley et al. (2017) used near daily data from Planet at 5-m resolution to track intra-seasonal changes in inland water bodies over the course of a year. Very high resolution stereo imagery has also been used to generate a fine resolution (2-m posting) Digital Elevation Model which can be used to map connectivity between inland waterbodies and wetlands (PGC, 2017). Expanded coverage from cubesats offers new possibilities for identifying and monitoring seasonally inundated areas as possible CO_2 and CH_4 emissions hotspots.

Determining how ABZ warming has affected CO_2 and CH_4 emissions requires a combination of remote sensing observations coupled with biogeochemical models as also discussed in section 5.2. Direct observations of surface concentration records do not yet show trends in ABZ CH_4 emissions, despite significant warming (Cooper et al., 2017; Sweeney et al., 2016). Possible drying of wetland soils is exposing soil carbon to oxidation (Commane et al., 2017) leading to increases in CO_2 emissions, but the monitoring network for CH_4 emissions is sparse and does not fully capture pulses of emissions that occur during the zero-curtain period (Mastepanov et al., 2008; Zona et al., 2016). Surface inundation trends from GIEMS and SWAMPS qualitatively agree in a global decline in Fw (Prigent et al., 2012; Schroeder et al., 2015). Between 1992 and 2012, SWAMPS detected ABZ declines in wetland area of 145 km^2/year found mainly over Asia and Europe, with a slight positive increase in Fw in parts of Canada north of the Hudson Bay. In contrast, the GSW Landsat-based approach show inland-waters potentially increasing in area from the 1980s to 2014/15, with Russian inland waters increasing from 0.45 to 0.47 Mkm^2 and Canadian inland waters decreasing by 40,000 km^2 (Pekel et al., 2016).

Presently, remote sensing of wetland area and dynamics is contributing to large uncertainties in monitoring and modeling (Bloom et al., 2016; Poulter et al., 2017; Zhang et al., 2017), preventing a robust attribution to how wetlands are responding to climate change. Current observing systems for ABZ wetlands are confronted by several key challenges that ongoing and upcoming NASA LEO and airborne missions (e.g., SMAP, ABOVE and SWOT) and synthesis research activities (e.g., the Global Carbon Project CH_4 budget; Saunois et al., 2016) have the potential to reconcile. The main observing system gaps include (i) terminology over what constitutes a wetland and how to include wetlands that are not flooded at the surface and thus not detectable by passive remote sensing, (ii) tools to improve detection of surface inundation below closed vegetation canopies, (iii) multi-sensor integrated approaches that harmonize time series of radar, optical, lidar, and inventory simultaneously (Guo et al., 2017), and (iv) high-resolution topographic retrievals to better understand hydrologic and biogeochemical relationships (Davidson et al., 2017). Ideally, longer wavelength microwave radar (i.e., L-Band) would be combined with orbits that provide higher spatial resolution and temporal frequency than the current array of active and passive microwave instruments provide. Higher spatial resolution imagery would help separate inland water bodies from vegetation wetlands (following the standard definition of Cowardin et al. (1979) for wetlands), and longer wavelength would penetrate closed canopy or dense vegetation more effectively than C-Band wavelengths, for example. The NASA-ISRO SAR (NISAR) is a joint mission planned for launch in 2020. A primary objective of NISAR is the

monitoring of inundated landscapes with repeat coverage of 12 days. NISAR will continue advancing L-band SAR remote sensing of wetlands environments.

The NASA SWOT mission, a Ka-Band radar mission, will provide 5.5 × 10- to 60-m resolution with 21-day frequency, and is designed to map surface inundation and water-surface elevation. Applications from SWOT airborne emulator, AIRSWOT, as part of the NASA ABOVE campaign may yield useful insights for how SWOT can help quantify Fw more effectively. To fully address the observation gap of monitoring ABZ wetlands, multi-sensor approaches need to be more completely used to fuse data that can improve temporal resolution (e.g., combining Sentinel 2A and 2B with Landsat Climate Data Records) and to extract finer scale features associated with topographic variation, surface waters, and vegetation properties (both structural and spectral characteristics). The recent expansion of commercial high resolution data coupled with the extended long term climate data record from moderate resolution instruments offers new possibilities for future quantification of changes in surface water extent that were not previously feasible. In addition to lentic waters, there are major rivers that flow into the Arctic Ocean that account for over 10% of the freshwater discharge into the global oceans (https://arcticgreatrivers.org/) and provide a critical link for the transport of carbon and other constituents from land to the ocean (Cole et al., 2007; White et al., 2007). The discharge from these rivers has been increasing in recent decades (Rawlins et al., 2010; Serreze et al., 2006), which has an impact on both freshwater content and sea ice concentration (Stroeve et al., 2011). The upcoming SWOT mission will provide a new way to obtain discharge measurements for these rivers, filling a critical measurement gap in the data record (Alsdorf et al., 2003; Biancamaria et al., 2016).

5. Observing Chemistry and Composition of the ABZ Atmosphere

In this section, we discuss the (1) historical and current state of observations of the properties of the ABZ atmosphere, including short-lived pollutants (e.g., nitrogen oxides [NO_x = NO + NO_2], carbon monoxide [CO], aerosols, and ozone [O_3]), greenhouse gases (e.g., CH_4, CO_2), clouds, surface UV radiation and stratospheric ozone, and the Arctic energy balance, and (2) observational needs going forward, which are summarized in Table 1.

5.1. Short-lived Pollutants in the ABZ (Ralph A. Kahn, Bryan N. Duncan)

Airborne particles (or aerosols) and trace gas pollutants affect the ABZ in a variety of ways. First, light-absorbing particles can reduce the albedo of ice and snow, especially after deposition occurs, accelerating melting and altering the ABZ's radiative balance (Clarke & Noone, 1985; Doherty et al., 2010; Qian et al., 2015; Stone et al., 2014; Warren & Wiscombe, 1980). Second, aerosols affect the microphysical properties of clouds, changing the concentrations of cloud condensation nuclei and ice nucleating particulates (e.g., Borys, 1989) and, thus, indirectly affecting cloud SW albedo and LW thermal emissivity (e.g., Zhao & Garrett, 2015, and references therein; Zamora et al., 2016, 2018), as well as on precipitation and possibly cloud lifetime (e.g., Morrison et al., 2012; Zamora et al., 2017, 2018). Third, light-absorbing aerosols, such as black and organic carbon, are expected to have the greatest effect among the pollutant species on the ABZ's radiation budget, with O_3 and CH_4 also contributing (Breider et al., 2014; Quinn et al., 2008).

The presence of widespread Arctic haze and cryoconite (i.e., powdery dust that is deposited on and builds up on ice) was first recognized over a century ago (e.g., Garrett & Verzella, 2008). The haze is composed of well-aged, anthropogenic particulates, primarily sulfate and organic matter, with contributions from black carbon, mineral dust, ammonium and nitrate (Quinn et al., 2007, and references therein). It accumulates during winter and early spring when removal processes are slow in the cold, dark ABZ and the lower troposphere is relatively isolated from mixing with lower latitude air masses (e.g., Barrie, 1986; Quinn et al., 2007; Shaw, 1995, and references therein). This wintertime dynamical isolation is referred to as the "polar dome," which is shallow (generally <2 km) and bounded by the "Arctic front" (Stohl, 2006). Pollutants emitted within the polar dome are primarily emitted at lower latitudes, especially in northern Eurasia, where the polar dome can extend down to 40°N (e.g., Hirdman et al., 2010; Klonecki et al., 2003; Law & Stohl, 2007; Stohl, 2006).

Pollution emitted outside the polar dome typically ascends above the polar dome as it moves northward, creating layers of aerosols and trace gases that vary by source region (e.g., Law & Stohl, 2007; Willis et al., 2019). Warm Conveyor Belts, which occur preferentially east of Asia and North America in the midlatitudes

in colder months (Eckhardt et al., 2004), frequently loft pollution well into the free troposphere, where it may then impact the ABZ free troposphere (e.g., Law et al., 2017). The amount of pollution arriving to the ABZ varies from year to year. For example, pollution from North America and Europe typically maximizes in winter and spring when the North Atlantic Oscillation (NAO) meteorological phenomenon is in the positive phase; the contribution from East Asia is not significantly dependent on the NAO phase (Duncan & Bey, 2004; Eckhardt et al., 2003). Fisher et al. (2010) suggest that the El Niño phenomenon may also play a role in the transport of anthropogenic pollution from East Asia to the ABZ.

Surface observations of some air pollutants (e.g., aerosols, CO, and O_3) were established at a few high-latitude sites in the late 1970s and 1980s, and the data records are often short or incomplete (e.g., Helmig et al., 2007; Novelli et al., 1998; Quinn et al., 2007; Stone et al., 2014). Nevertheless, they indicate that levels of Arctic haze and some trace gases have decreased over the past few decades (e.g., Sharma et al., 2004, Sharma et al., 2006, Sharma et al., 2013; Quinn et al., 2007, and references therein; Hirdman et al., 2010). These decreases may be associated with the economic contraction of the former Soviet Union and restrictions on emissions in North America and Western Europe (e.g., Duncan & Logan, 2008; Gong et al., 2010; Mackie et al., 2016). There have been several field campaigns in the ABZ over the last few decades (e.g., as presented by Law et al., 2014) which had the goal of identifying pollution sources affecting ABZ atmospheric composition. For example, the Arctic Research of the Composition of the Troposphere from Aircraft and Satellites (ARCTAS) and Polar Study using Aircraft, Remote Sensing, Surface Measurements and Models, Climate, Chemistry, Aerosols and Transport (POLARCAT) field campaigns took place in 2008 (Fuelberg et al., 2010; Jacob et al., 2010; Law et al., 2014). These two campaigns highlighted that important sources of pollutants in the ABZ include boreal wildfires and the long-range transport of pollution from East Asian anthropogenic sources. The suite of scientific instruments, including those on satellites, offered an unprecedented look at the spatial distribution of trace gases and aerosols, including those relevant for climate, in the ABZ troposphere. Satellite observations indicate that in just the last decade, air quality improved significantly over much of East Asia, North America and Europe (e.g., Duncan et al., 2016; Krotkov et al., 2016), presumably with a concomitant decrease in pollution transported to the ABZ from these anthropogenic sources.

There may be an increase in future pollution emissions within the ABZ given the likely increase in wildfires, agricultural fires, and anthropogenic activities (e.g., shipping, oil and natural gas extraction, fishing) in the warmer and increasingly accessible ABZ (e.g., Arnold et al., 2016; Corbett et al., 2010; Gong et al., 2018; Hegg et al., 2010; Law et al., 2017; Marelle et al., 2018; McKuin & Campbell, 2016; Peters et al., 2011; Schmale et al., 2018). There are several international efforts that have as part of their design to observe these changes. For instance, the Arctic Climate Change, Economy, and Society (ACCESS) project has a goal of studying the impact of anthropogenic ABZ emissions, such as oil and gas extraction and shipping, on Arctic air quality and climate (Roiger et al., 2015). Additionally, the International Arctic Systems for Observing the Atmosphere (IASOA) is currently working to strengthen international cooperation to build a collaborative network of Arctic observatories, including "supersite" observatories," for aerosols, trace gases, clouds, radiation and other parameters (Uttal et al., 2016). Yet, mining and industrial development in the warming Arctic, along with increased high-latitude wildfire activity, have the potential to overwhelm the decreases in transported pollution from lower latitudes.

In general, ABZ conditions (e.g., very bright surfaces at ultraviolet/visible wavelengths, low light levels, steep sun angles, and persistent clouds, including thin cirrus) create challenges for trace gas and aerosol retrievals from satellite instruments. For instance, detecting clouds over sea ice or snow, a necessary input for retrieval algorithms that use ultraviolet/visible wavelengths, is difficult (Eastman & Warren, 2010b). Similarly, it is unlikely that black carbon deposits on snow and ice surfaces can be identified using remote-sensing techniques alone (Warren, 2013). Individual observations of SO_2 and formaldehyde (HCHO) are associated with relatively high uncertainties. Another remaining challenge is retrieving surface O_3 (e.g., Duncan et al., 2014). Similar to retrievals of CH_4 and CO_2 (section 5.2), retrieving CO at thermal infrared wavelengths is challenging under ABZ conditions (e.g., Monks et al., 2015; Pommier et al., 2010). Additionally, for both aerosols and most trace gases, their ABZ levels are typically too low, except during large wildfires or near large point sources, for current instruments/retrieval algorithms to resolve with confidence. An additional challenge for all satellite observations is the paucity of independent, suborbital data with which to validate and improve retrieval algorithms for high latitudes.

Passive imagers that measure ultraviolet, visible and infrared wavelengths give information directly related to particulates, such as aerosol optical depth (AOD) and other light scattering properties. Examples include MODIS, MISR, and the upcoming European Organisation for the Exploitation of Meteorological Satellites (EUMETSAT) Multi-Viewing-Channel-Polarisation Imager (3MI), which are on polar-orbiting satellites. They provide broader and more frequent spatial coverage than active sensors and most sounding instruments, making event-resolved studies of aerosols possible (e.g., wildfires; Mielonen et al., 2012, Mielonen et al., 2013). Passive instruments that measure ultraviolet, visible and infrared wavelengths also provide information on several trace gas air pollutants, including atmospheric columns (i.e., molecules/unit area) of NO_2, HCHO, CO, and SO_2, which can serve as smoke and particulate pollution tracers for constraining transport model simulations. Instruments that measure trace gas pollutants include the EUMETSAT MetOp-A and MetOp-B Global Ozone Monitoring Experiment (GOME-2), NOAA Ozone Mapping and Profiler Suite (OMPS), Canadian Space Agency (CSA)-NASA Measurements Of Pollution In The Troposphere (MOPITT), and the Dutch-Finnish Ozone Monitoring Instrument (OMI), which are on polar-orbiting satellites. Currently, large sources (e.g., smelters, volcanoes, gas flaring; Theys et al., 2015; Ialongo et al., 2014, 2015; Schmidt et al., 2015; Li et al., 2016; Kashkin et al., 2018) are detected by these instruments. Figure 16 shows that OMI NO_2 data averaged over a single summer in Finland are noisy, but when averaged over multiple years, the signals of small cities become detectable. Relative to current similar satellites, the recently launched ESA Sentinel-5 Precursor TROPOspheric Monitoring Instrument (TROPOMI) offers a larger spectral range, better signal-to-noise ratio, and finer footprint (3.6×5.6–7.2 km^2), which improve the detection of emission sources. TROPOMI NO_2 data averaged over a single season (Figure 16) allow for improved detection of emission sources at a finer spatial resolution and with less noise. As compared to OMI (Figure 16), TROPOMI NO_2 tropospheric columns show higher values overall, as expected from the instrument's increased resolution and sensitivity, and because of differences in the retrieval algorithms.

Active satellite instruments have clear advantages over passive ones in the ABZ, and one such system for aerosols currently exists. NASA's CALIPSO lidar, in orbit since April 2006, is the most sensitive and best available space-based source of total column and height-resolved Arctic aerosol observations, especially at night, when signal/noise is highest (Figure 17). Despite limited coverage from its very narrow cross-track sampling swath (~100 m), coverage is aided by the polar orbit of this spacecraft, as the orbit tracks converge at high latitudes. Nevertheless, data usually need to be spatially and/or temporally averaged to obtain statistical significance. CALIPSO also allows for aerosol type classification based on spectral and depolarization ratios (Omar et al., 2009). CALIPSO continues to operate well past its design life, yet there is no follow-on capability planned within the U.S. program. There are active instruments, such as ESA's Earth Cloud Aerosol and Radiation Explorer (EarthCARE), planned by other programs.

Given the strengths and limitations of each approach, the combination of active and passive satellite measurements, suborbital observations for validation and providing additional detail, and transport modeling constrained by observations, is required to complete the ABZ aerosol picture. For example, Di Pierro et al. (2013) analyzed the spatial distribution of CALIPSO layer-resolved ABZ seasonal aerosol extinction measurements between 2006 and 2012, along with surface and aircraft measurements and results from global aerosol transport models, to create a general map of ABZ aerosol behavior. Generoso et al. (2007) used AOD from MODIS and ESA's Polarization and Directionality of the Earth Reflectance (POLDER) instrument, mainly in the boreal sub-Arctic, along with MOPITT CO as a smoke tracer, to constrain an atmospheric chemistry and transport model, allowing them to plot the advance of biomass burning aerosols from Russia into the high Arctic during summer 2003. Zamora et al. (2017, 2018) used the combination of lidar data from CALIPSO, radar data from CloudSat, and an aerosol transport model, to quantify regional-scale aerosol-cloud microphysical interactions, including changes in cloud phase and cloud fraction, under polar nighttime conditions, favorable to active remote-sensing.

Despite the extensive spatial and temporal coverage offered by polar-orbiting satellites, observing conditions in the ABZ severely limit the capabilities of many satellite instruments, which create an even greater need for suborbital measurements in the ABZ than in more favorable observing environments. Additionally, black carbon in Arctic snow is not likely detectable by remote sensing (Warren, 2013). Many surface-based instruments, such as sun photometers and radiometers sampling the visible and near-infrared, can operate only when there is sufficient sunlight, but they can complement ground-based lidars, which perform best at

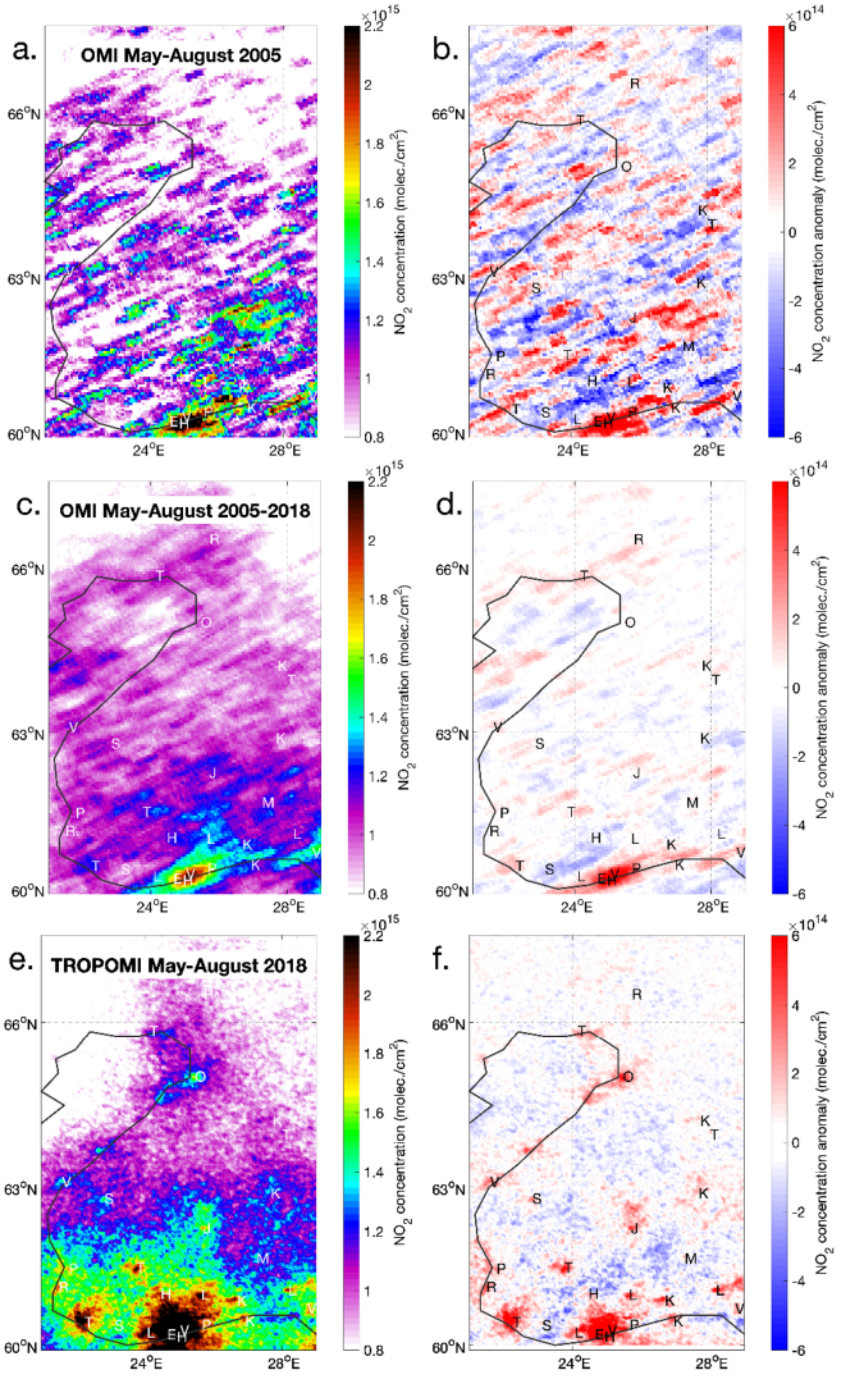

Figure 16. (a) Ozone Monitoring Instrument (OMI) NO_2 data (molecules/cm^2) for May-August 2005 over Finland at 0.05° latitude × 0.05° longitude resolution. The data were filtered by wind speed (<5 m/s) to minimize the effect of dispersion. The letters correspond to the locations of cities. Because of relatively low signal-to-noise, the data are noisy. (b) To improve the detectability of small sources, the average signal of surrounding pixels (1° latitude × 1° longitude) is removed from every grid pixel so that red pixels correspond to NO_2 levels larger than the local background. This procedure leads to the small cities around Helsinki, the largest source in Finland, to appear below background levels. (c and d) The same as the top row, but as the average of May-August 2005–2018. The average of multiple years reduces noise, allowing smaller sources to become apparent. (e and f) The same as the top row but using TROPOMI NO_2 tropospheric columns averaged over the period May–August 2018 at 0.02° latitude × 0.02° longitude resolution. TROPOMI smaller pixels and higher signal-to-noise ratio improve the detection of emission sources (cities).

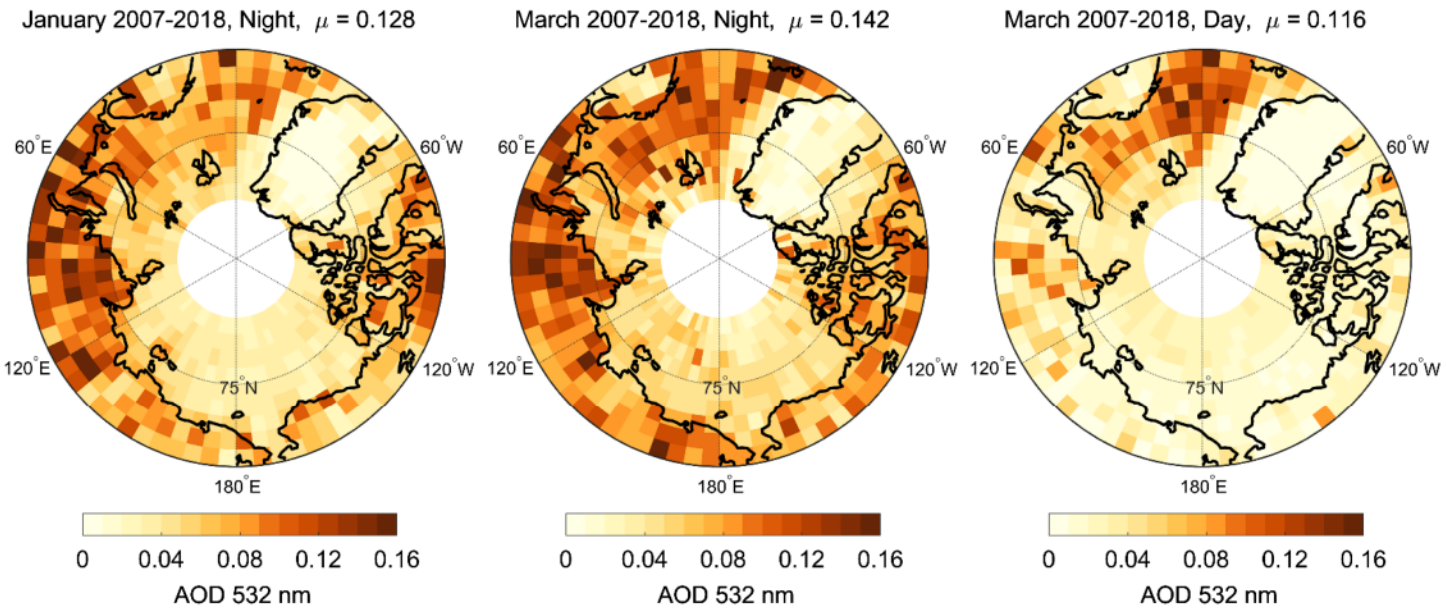

Figure 17. Mean aerosol optical depth (AOD; unitless) from the Cloud-Aerosol Lidar and Infrared Pathfinder Satellite Observation (CALIPSO) satellite for (left) January during night, (center) March during night, and (right) March during day. The mean data are for "all-sky" conditions and averaged from 2007 to 2018. CALIPSO does not detect AOD values below a detection threshold, so the mean AOD is biased to higher AOD events in spatial and temporal averages. It has lower detection sensitivity in daylight, only detecting the strongest Arctic aerosol events (center and right). Consequently, the daytime data are systematically biased low (Di Pierro et al., 2013). CALIPSO's detection sensitivity is lowest in summer, which leads to a large low bias (not shown) that is compounded by the fact that AOD values tend to be seasonally lowest in summer. There are missing data over the pole because the instrument is on a satellite in sun-synchronous orbit and because of instrument design.

night, provided these instruments can be maintained under severe weather conditions. Research stations at Ny Alesund in Svalbard, Norway, Pallas-Sodankylä, Finland, Eureka, Canada, and Barrow, Alaska, are examples of the few sites with experience operating atmospheric observatories at high-latitudes (e.g., Stone et al., 2014).

There are a number of ongoing efforts to develop collaborative, comprehensive and multi-disciplinary observing networks for air pollutants (this section), greenhouse gases (section 5.2), clouds (section 5.3) and ultraviolet radiation (section 5.4), such as by ARCUS, the WMO Global Atmospheric Watch (GAW) programme, the European Research Infrastructure for the observation of Aerosol, Clouds, and Trace gases (ACTRIS) program, and IASOA (Uttal et al., 2016). The PEEX "Pan-Eurasian Experiment" aims, in particular, to enhance surface-based observations in Russia and China (Kulmala et al., 2015). This development is often guided by international efforts to prioritize air pollution research, such as the International Global Atmospheric Chemistry (IGAC) Air Pollution in the Arctic: Climate, Environment and Societies (PACES) project (https://pacesproject.org/).

From the satellite perspective, we recommend that the siting of surface instruments also consider the need for evaluating and interpreting satellite observations. First, there is a need for a network of instruments that measures surface levels and the vertical profiles of aerosols and trace gases, given the highly complex vertical structure often observed in the stably stratified ABZ atmosphere, as discussed in this section. Co-located spectrometers and instruments that measure surface pollutant concentrations (e.g., AOD and surface particulates; column NO_2 and surface levels of NO_2) will be particularly valuable to aid in the interpretation of satellite data. Second, additional long-term, continuous observations of aerosols and trace gases should be established to aid in the evaluation and interpretation of long-term trends observed from space-based platforms. This should include direct measurements of light-absorbing aerosol concentrations on snow and ice surfaces. Third, a coordinated effort to include, in an ABZ-ON, observations of input parameters to retrieval algorithms, which are necessary to optimize algorithms for ABZ high latitudes. These parameters include surface reflectivity, vertical profiles of temperature, cloud separation from ice/snow, and cloud top height. This recommendation has important implications for the creation of long-term data records and

estimating trends. Improper accounting of changes in input parameters over space and time can introduce space- and time-dependent biases. Although this recommendation applies to all satellite observations of atmospheric gases globally, it is particularly relevant as the ABZ has experienced rapid change over the last few decades, which is anticipated to continue in the coming decades. Fourth, siting of additional coastal monitors near potential new ABZ shipping lanes, ports, areas of mining and industry, etc. should be considered; concentrated human activity at such locations would also help in finding staff to maintain the instruments. These recommendations will also benefit scientific research (e.g., source apportionment studies) and aid monitoring potential ABZ pollutant changes.

Finally, an innovative orbit option of ABZ aerosols and trace gases is discussed in section 6.

5.2. Long-Lived Greenhouse Gases in the ABZ (Bryan N. Duncan, Stephen R. Kawa, James B. Abshire, James S. Wang, Lesley E. Ott, Ray Nassar)

CO_2 and CH_4 are the two dominant anthropogenic, radiatively important gases driving Arctic and global warming. Although CO_2 is a larger contributor to climate change overall because of its higher abundance, the 100-year and 20-year global warming potentials (GWP) of CH_4 are 28–32 times and 84–86 times larger than those of CO_2 (Holmes et al., 2013; Myhre et al., 2013). Therefore, both anthropogenic CO_2 and CH_4 are seen as critical targets for climate change mitigation (e.g., Kirschke et al., 2013). Anthropogenic sources of CO_2 and CH_4 may increase in a more accessible ABZ because of increased access to areas with oil, natural gas, and minerals, the development of new ports and industry, and increased shipping. Possible changes in natural ABZ sources and sinks, which include vegetation changes (sections 4.4 and 4.5), wildfires (section 4.6), wetlands (section 4.7), and permafrost thaw (section 4.3), are highly uncertain (e.g., Pastick et al., 2017). The rate at which the vast stores of soil organic carbon are being released and their feedback to the rapidly warming ABZ are a major uncertainty and potential "tipping point" in climate projections. A key challenge of constraining ABZ CO_2 and CH_4 emissions and sinks is that they often have high spatiotemporal variability and different source/sink types are often co-located.

While direct observations of atmospheric CO_2 and CH_4 at Arctic baseline observatories have been and will continue to be essential, the characterization of carbon fluxes will benefit from ancillary observations of the hydrological, atmospheric and terrestrial factors, many of which can be observed from space, that control these carbon fluxes. Large uncertainties associated with process-based understanding of natural carbon source fluxes have seriously limited our ability to estimate future fluxes in a warmer and more hydrologically active world (e.g., McGuire et al., 2009). For example, present-day ABZ wetland CH_4 emissions, as shown in a recent model inter-comparison of the West Siberian Lowlands that included process-based models and inversions, are not well constrained (Bohn et al., 2015). The large spread of emission estimates results because, for instance, the factors that affect microbial CH_4 production are not well constrained (e.g., Meng et al., 2012), and land cover, including wetlands, is not well categorized (e.g., Frey & Smith, 2007). Though the ABZ is currently a net sink for CO_2 because ecosystems absorb more carbon than they emit (McGuire et al., 2009), studies differ on whether the magnitude of this sink is increasing (e.g., Rawlins et al., 2015) or decreasing (Hayes et al., 2011). Substantial uncertainties also exist for carbon emissions associated with permafrost thaw (section 4.3; e.g., Schuur et al., 2015, 2018; Gao et al., 2013; Zhu et al., 2013; National Research Council, 2014b; Koven et al., 2013; Lawrence et al., 2015; McGuire et al., 2016), lake sediments (e.g., Tan & Zhuang, 2015), and ocean hydrates (e.g., Kort et al., 2012; Ruppel & Kessler, 2017) in a warmer ABZ.

Before the satellite era, ABZ data on CH_4 and CO_2 concentrations were sparse and mostly from a handful of high-latitude stations established mainly after 1980 (Dlugokencky et al., 2015; Worthy et al., 2009). While these data are invaluable, including in the satellite era, the small number of stations are not sufficient to reveal a complete picture of the heterogeneity in sources and sinks throughout the ABZ and are insufficient for attribution to specific anthropogenic or natural sources/sinks. Independent data that could be used to differentiate historical CO_2 and CH_4 source/sink types are also limited, complicating efforts to disentangle the relative roles of changes in ABZ vegetation (e.g., solar-induced fluorescence), fossil fuel combustion (e.g., NO_x, isotopic measurements), ocean, wetlands (e.g., fluctuations in wetland extent and temperature), wildfires (e.g., annual area burned), and fugitive emissions from natural gas production and transport (e.g., Uvarova et al., 2014), such as in the former Soviet Union (e.g., Reshetnikov et al., 2000). For example,

there are only a few recent observations of carbon fluxes from Eurasian Arctic wetlands, which indicate that wetland CH_4 emissions may be higher than previously thought (e.g., Schneider et al., 2016).

Current satellite retrievals of CO_2 and CH_4 are from polar-orbiting passive instruments that observe spectra using thermal infrared or reflected solar near infrared/SW infrared wavelengths (e.g., Sellers et al., 2018). CO_2 and CH_4 observations from thermal infrared instruments, such as the NASA Aqua AIRS (Chahine et al., 2008; Xiong et al., 2008), NASA Aura Tropospheric Emission Spectrometer (TES; Payne et al., 2009; Kulawik et al., 2010) and EUMETSAT MetOp Infrared Atmospheric Sounding Interferometer (IASI; Crevoisier et al., 2009; Razavi et al., 2009; Turquety et al., 2004), provide limited information on the vertical structure of concentrations in the mid- and upper troposphere, but lack sensitivity in the lower troposphere where concentrations respond most strongly to surface fluxes.

CH_4 and CO_2 satellite retrievals from near infrared/SW infrared wavelengths give total atmospheric columns that can be used in conjunction with models to infer CH_4 and CO_2 fluxes (e.g., Butz et al., 2011; Chevallier et al., 2014; Eldering et al., 2017; Eldering et al., 2017; Houweling et al., 2015; Schepers et al., 2012; Turner et al., 2015; Yokota et al., 2009; Zhang et al., 2013). Retrievals are only possible during daylight, cloud-free conditions. Initial long-term column CH_4 and CO_2 products are from the ESA Envisat SCanning Imaging Absorption SpectroMeter for Atmospheric CHartographY (SCIAMACHY; 2002–2012; e.g., Schneising et al., 2011, Schneising et al., 2012) and the JAXA Greenhouse gases Observing Satellite (GOSAT; 2009–present) Thermal and Near Infrared Sensor for carbon Observation instrument (TANSO; e.g., Yokota et al., 2009; Butz et al., 2011; Schepers et al., 2012). Though the two instruments overlapped in time, SCIAMACHY experienced detector degradation in October 2005, resulting in lower sensitivity thereafter (e.g., Frankenberg et al., 2011; Schneising et al., 2012). Buchwitz et al. (2015) describe the efforts to reconcile differences and biases among current SCIAMACHY and GOSAT CH_4 and CO_2 retrieval algorithms so as to improve accuracy of the data products. Despite observational uncertainties, the time series analysis of GOSAT CO_2 data compare well to ground-based measurements, showing that the seasonal cycle, both the amplitude and the phase, of CO_2 can be detected at high latitudes (Lindqvist et al., 2015). The NASA Orbiting Carbon Observatory-2 (OCO-2) was launched in 2014, with the goal to provide CO_2 column data with the precision, resolution, and coverage needed to characterize regional sources and sinks (Eldering, O'Dell, et al., 2017, Eldering, Wennberg, et al., 2017). Obtaining robust flux estimates remains challenging, especially at high latitudes (Chevallier et al., 2014; Houweling et al., 2015; Wang et al., 2018). Initial flux inversion results using OCO-2 data are largely focused on low latitude regions (Eldering, O'Dell, et al., 2017, Eldering, Wennberg, et al., 2017 and references within). GOSAT and OCO-2 were joined in orbit by the Chinese Carbon Dioxide Observation Satellite Mission (TanSat; Liu et al., 2013; CO_2) launched in December 2016 and the Chinese Feng-Yun 3D Greenhouse-gases Absorption Spectrometer (GAS; CO_2, CH_4) launched in November 2017. TROPOMI was launched in October 2017 and observes CH_4 (Hu et al., 2018), among other species. JAXA's GOSAT-2 (CO_2, CH_4) was launched in October 2018 and CNES's MicroCarb (CO_2) is expected to launch by ~2021. NASA's newest greenhouse gas mission, OCO-3 (launched in May 2019; CO_2) and its next one, GeoCarb (CO_2, CH_4), will not observe latitudes greater than about 52°N, because OCO-3 is on the International Space Station (Eldering et al., 2018) and GeoCarb will use a geostationary orbit (Moore et al., 2018). Jacob et al. (2016) provide a table comparing the capabilities of various CH_4 past, current, and near-term instruments.

There remain substantial observing challenges that result in sparse high-quality data over the ABZ relative to lower latitudes. This occurs even though current passive instruments are on polar-orbiting satellites, which have more frequent and overlapping overpasses over the ABZ than over the tropics. Detecting CH_4 and CO_2 over the ABZ is particularly difficult for passive sensors, which rely on reflected sunlight, because of low sun elevation angles in spring and fall and no sun in winter, and because of atmospheric scatter from clouds and aerosols. Early inversion results from OCO-2 suggest that it is challenging to accurately infer fluxes in high-latitude regions because of seasonal changes in coverage (e.g., Crowell et al., 2018). Although the surface albedo of snow and ice are high in the visible and near infrared regions, they are very low in the SW infrared CO_2 and CH_4 bands, resulting in lower signal-to-noise ratios from passive sensors when observing over these surfaces. These challenges are minimized in mid-summer, but the ABZ is a cloudy region and aerosols from boreal fires in summer often lead to hazy conditions. All near infrared passive datasets have contained biases in raw retrieved data (e.g., because of aerosols, solar zenith angle, or

observing mode) that do not meet the very strict accuracy requirements needed for flux inversions (~0.25% for CO_2) and therefore require correction before they can be used to infer fluxes (e.g., Wunch et al., 2017). This is currently done using data collected by the Total Column Carbon Observing Network (TCCON), which is a system of ground-based, high spectral resolution Fourier Transform Spectrometers at more than 20 sites globally that records direct solar spectra in the SW infrared (Wunch et al., 2011). Despite these efforts, biases that remain in the data can exert a strong influence in resulting flux estimates making new calibration and validation datasets and techniques particularly critical.

Because they do not depend on reflected sunlight, the planned polar-orbiting active sensors (i.e., lidar) will significantly augment the data from polar-orbiting passive sensors in the ABZ by providing more precise CH_4 and CO_2 column data with better temporal coverage and complementary spatial coverage (e.g., Crowell et al., 2018; Hammerling et al., 2015; Kawa et al., 2010; Kawa et al., 2018). This is important as carbon fluxes in the ABZ occur in all seasons, times of day, and sky conditions (e.g., Oechel et al., 2014; Treat et al., 2018; Zona et al., 2016). The first CH_4 lidar mission, called the MEthane Remote sensing Lidar missioN (MERLIN; Kiemle et al., 2014; Ehret et al., 2017) expected to launch in 2024, will demonstrate the capability to constrain CH_4 fluxes in cloudy and/or low-light environments, such as the ABZ, although its 3-year design lifetime may not address the need for long-term, continuous observations. As part of a potential active mission to measure CO_2 (NASA Active Sensing of CO_2 Emissions over Nights, Days, and Seasons [ASCENDS] mission; National Research Council, 2007), NASA has supported the development of several lidar technologies, as well as a series of flight campaigns to demonstrate the capabilities of airborne precursor instruments (Kawa et al., 2018, and references within). Data from these flights has also been used to demonstrate retrieving column CO_2 to several types of cloud tops (e.g., Mao et al., 2018), though the errors are larger than for measurements to the ground.

As mentioned above, there is an important need for observations of the factors that control CH_4 and CO_2 fluxes, which will allow for a better process-based understanding of these fluxes and enhance the predictive capability of Earth system models. As discussed in section 4.7 and relevant to CH_4, data of gravity anomalies, such as NASA's and DLR's GRACE (2002-present), and from microwave instruments, such as AMSR-E (2002–2011) and SMOS (2009-present), provide soil moisture data that may also be used as proxies for inundation (e.g., Bloom et al., 2010; Watts et al., 2012). For observing in the ABZ, microwave instruments have the advantage that they do not rely on reflected solar radiation and are not hampered by clouds. Observations of vegetation (sections 4.5 and 4.6) continue to provide critical information on the trends and spatiotemporal variability of CO_2 flux. The strategy of measuring both carbon greenhouse gases and factors that control their fluxes is integral to the NASA Carbon in Arctic Reservoirs Vulnerability Experiment (CARVE; http://science.nasa.gov/missions/carve/; Miller & Dinardo, 2012) and Arctic Boreal Vulnerability Experiment (ABoVE; http://above.nasa.gov/) suborbital missions.

Similar to the recommendations in section 5.1 for pollutants, we recommend that the siting of surface instruments also consider the need for evaluating and interpreting satellite observations. First, a comprehensive ABZ suborbital observing network of instruments that measure surface concentrations and give vertical profile information of CH_4 and CO_2 is essential for evaluating and interpreting satellite observations. The primary network that measures both gases for validating satellite observations is TCCON (Wunch et al., 2011). Some operating ABZ sites include East Trout Lake (54.4°N) and Eureka (80.0°N) in Canada, and Sodankylä, Finland (67.4°N). There are sparse observations of the vertical structure of CH_4 and CO_2 concentrations from a relatively new technique, the AirCore system (Karion et al., 2010). Second, a coordinated effort to include, in an ABZ-ON, observations of input parameters to retrieval algorithms, which are necessary to optimize algorithms for ABZ high latitudes.

Finally, an innovative orbit for observing ABZ CH_4, CO_2, SIF and other observables is discussed in section 6.

5.3. ABZ Clouds (Dong Wu)

The significant changes in the ABZ, including reduction of sea ice and albedo (section 3.1), Greenland ice sheet loss (section 4.1), and increases in atmospheric water vapor (Serreze et al., 2012), have affected ABZ cloud formation. To what extent ABZ clouds interact with large-scale dynamics, temperature, and moisture has been an active area of research. Generally speaking, the Arctic experiences a warming effect from LW radiation in all seasons except summer when its SW cooling effect offsets the LW warming (Curry &

Ebert, 1992). The warming to the surface from low-level semi-transparent liquid clouds is thought to be very effective, because these clouds allow the incoming SW solar radiation to heat the surface while trapping the outgoing LW radiation (Bennartz et al., 2013). However, overall cloud-radiative feedback on the Arctic warming appear to be complex and coupled with other processes (Curry et al., 1996). Current climate model simulations still disagree in terms of the estimated cloud amount and radiative fluxes over the Arctic (Klein et al., 2009; Vavrus et al., 2009). Observations of cloud properties and their variations on a basin scale are critically needed for improving our understanding of cloud roles in the Arctic amplification and associated feedback processes.

A long-term cloud climatology has been derived from ground-based visual observations, which are limited to monthly statistics from weather stations primarily on land (Hahn & Warren, 2007). Reports from drifting stations on sea ice are used for the ocean. The stations from the high Arctic report a dominance of low stratiform clouds, showing more cloudiness in summer than winter and significant correlations of interannual variability with surface air temperature, total sea ice extent, and the Arctic Oscillation (Eastman & Warren, 2010a). There is an increasing trend in cloud cover over the Arctic Ocean in all seasons, but this trend is most significant during spring and autumn. In addition to the station observations, several extensive sea-ice-based, ship-based and airborne campaigns were conducted over the Arctic including the Surface Heat Budget of the Arctic Ocean (SHEBA) in 1997–1998 in the Beaufort and Chukchi seas (Uttal et al., 2002), Arctic Ocean summertime expeditions from Japanese research vessel Mirai (Inoue et al., 2015), the Mixed Phase Arctic Cloud Experiment (M-PACE, Verlinde et al., 2007), and the Arctic Summer Cloud Ocean Study (ASCOS) on the central Arctic sea-ice pack in late summer 2008 (Tjernström et al., 2014).

Polar-orbiting satellite sensors play an essential role in determining cloud cover and variations in the ABZ. Using the thermal infrared sounding channels from AVHRR, Comiso (2003) and Wang and Key (2003) were able to estimate surface, cloud, and radiation properties, but reported conflicting trends in the retrieved Arctic cloudiness for the period of 1982–2000. The trends of Wang and Key (2003) also differed markedly from the trends obtained from visual surface observations (Eastman & Warren, 2010b). The AVHRR data also constitute the most polar coverage of a global data set from the International Satellite Cloud Climatology Project (ISCCP), which formulated cloud detection using narrowband channels at 0.6 and 11 μm (Rossow & Garder, 1993). Beginning in 2000, NASA has been providing much improved cloud measurements at a high (1 km) spatial resolution from the multi-channel MODIS (Ackerman et al., 1998; Frey et al., 2008; Platnick et al., 2003) and MISR (Wu & Lee, 2012). The MODIS cloud fraction is more robust in daytime detection but exhibits a systematic dependence on sea ice concentration at night (Liu et al., 2010). The MISR stereo technique is most skillful for boundary-layer cloud detection among passive satellite sensors (Wu et al., 2009). Analyzing the AIRS data from 2002 to 2015, Boisvert and Stroeve (2015) show that the Arctic atmosphere has become warmer and wetter. In addition, the Clouds and the Earth's Radiant Energy System (CERES) sensor on Terra and Aqua satellites is used to estimate Arctic cloud radiative properties at the top of atmosphere (TOA) and the surface (Kato et al., 2006; Loeb et al., 2009).

The most complete characterization of Arctic 3-D cloud distribution is from active satellite sensors, namely, the CloudSat 94-GHz radar and CALIOP. Despite limited sampling from their nadir views, the combined radar/lidar observations are able to produce valuable global cloud climatology on a monthly basis (Mace & Zhang, 2014). Studying the CloudSat/CALIOP data of the 2006–08 period, Kay and Gettelman (2009) found more low clouds over open water in the Arctic autumn than summer. The observed vertical cloud profiles help to further constrain radiative flux calculations at the TOA as well as at the surface; the dominant error source is from cloud uncertainty. Analyzing data of observed TOA radiative fluxes from Clouds and the Earth's Radiant Energy System-Energy Balanced and Filled (CERES-EBAF) and observationally constrained radiative flux calculations (2B-FLXHR-LIDAR), Kay and L'Ecuyer (2013) obtained a more reliable cloud and radiation climatology over the Arctic Ocean, showing an annual cloud warming (+10 W/m^2) at the surface and cooling (−12 W/m^2) at the TOA.

While low-level clouds play a more important role than high clouds in warming the surface, their radiative effects are complicated by their mixed-phase type (Morrison et al., 2012) and semi-transparent layers (Bennartz et al., 2013). When upper-level clouds do not hide lower levels, satellite sensors have some skill in distinguishing between liquid and ice types (Baum et al., 2000; Hu et al., 2010). The space-borne lidar systems are able to classify transparent and opaque clouds, based on the absence of surface echoes (Vaughan

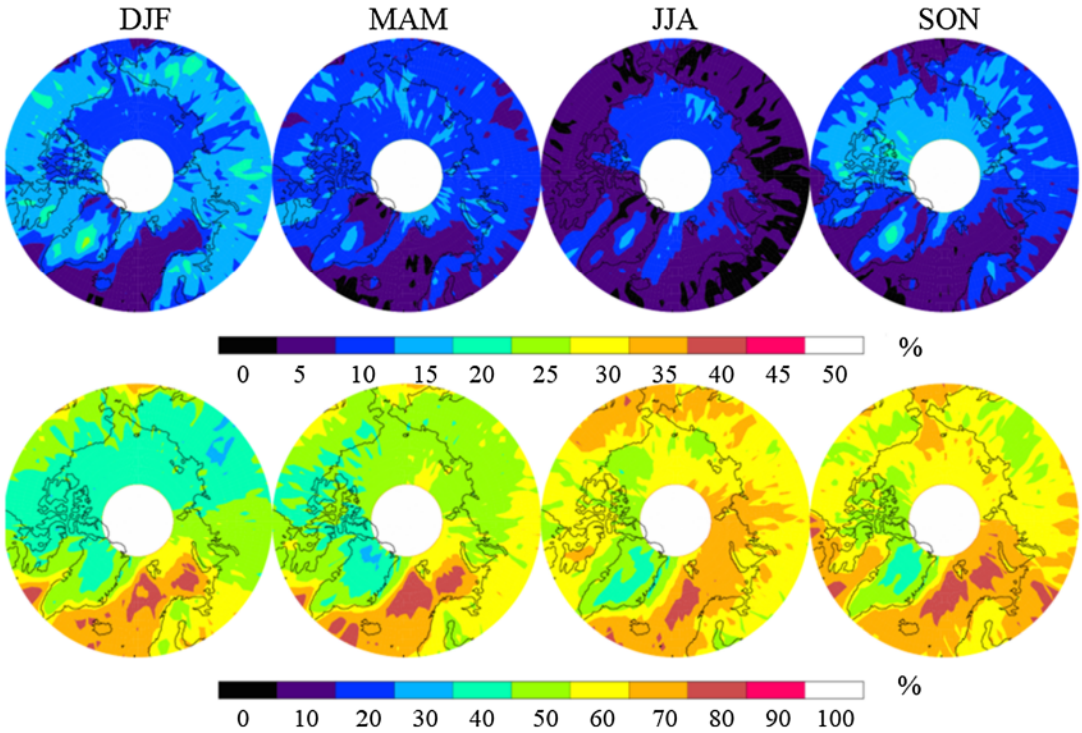

Figure 18. Transparent (top row) and opaque (bottom row) Arctic cloud climatology from the Cloud-Aerosol LIdar with Orthogonal Polarization (CALIOP) instrument for DJF (December-February), MAM (March-May), JJA (June-August), and SON (September-November) in 2008–2014. Over Greenland, the ICESat digital elevation model (DEM) is used to reduce systematic false detection of low-level clouds seen from the previous DEMs.

et al., 2009). Figure 18 shows a climatology of Arctic transparent and opaque clouds from CALIOP, showing dominance of opaque clouds during all seasons.

Arctic clouds and their processes, especially cloud radiative effects, remain poorly represented in most modern-era climate models. Reliable observations on a basin-scale are still lacking, including cloud properties (e.g., water and ice content and particle size), formation, and interactions with aerosol and precipitation processes. Because the majority of Arctic clouds reside in the PBL and vary dramatically across surfaces of different types, orbital and suborbital sensors with high vertical resolution, as well as horizontal coverage, are critically needed.

5.4. Surface Ultraviolet Radiation and Stratospheric Ozone (Johanna Tamminen, Erkki Kyrölä, Alexey Karpechko)

Biologically harmful surface ultraviolet radiation (UV-B; 280–320 nm) has both positive and negative effects on humans and the biosphere, and plays an important role in tropospheric chemistry. Atmospheric O_3 attenuates solar UV radiation reaching the surface with stratospheric O_3 having a large effect on surface UV-B. For example, the effects of the large springtime O_3 depletion over the Arctic in 2011 lasted through the following summer and increased cumulative spring-summer UV-B radiation by up to 4% (Karpechko et al., 2013). Year-to-year variations in UV-B radiation are largely caused by variations in stratospheric O_3 and cloudiness, though it is also modulated by aerosols and surface albedo. For instance, Bernhard et al. (2007) show that in Barrow, Alaska, clouds reduce UV radiation (at 345 nm) by 4% in spring (when surface albedo is high from snow) and by more than 40% in autumn (when cloud cover is higher). Aerosols reduce UV radiation by ~5%, but the decrease can be larger in ABZ haze events.

Very little data of surface UV radiation and O_3 exist before the expansion of observations following the discovery of the Antarctic "ozone hole" (Farman et al., 1985). Surface O_3 was measured at about 300 sites in Europe after 1850. By 1881, it was realized that there is more O_3 in the middle atmosphere than near the surface. The first high quality surface O_3 measurements were collected in 1918 and accurate total vertical

columns of O_3 (3 mm in STP) were measured in 1921 as determined by the Umkehr method, which led to the discovery of the ozone layer in 1934. Since then, O_3 in the middle atmosphere has been monitored using optical and in situ methods from special observatories. Systematic measurements, which are archived by the World Ozone and Ultraviolet Data Centre (WOUDC), began in the early 1950s. Many new O_3 monitoring stations were established in the Arctic during the 1957–1958 Polar Year. The international Network for the Detection of Atmospheric Composition Change (NDACC) includes 17 Arctic measurement stations, with data records starting mainly in the 1990s.

Estimates of surface UV radiation can be derived globally using satellite observations of O_3, aerosols and cloudiness. The GOME-2 and OMI surface UV radiation products include, for example, spectral irradiance at selected wavelengths and erythemally weighted daily maximum dose rate (Tanskanen et al., 2006; Kujanpää & Kalakoski, 2015). Recent validation of satellite UV radiance at high northern latitudes by Bernhard et al. (2015) shows relatively good agreement (within 20%) with satellite and ground-based observations, except when albedo values used in satellite estimates are uncertain. The satellite-based surface UV radiation data sets will be extended with data from the recently launched TROPOMI (Lindfors et al., 2018).

The first orbital total vertical column O_3 measurements were collected by the Nimbus-4 Backscatter UltraViolet (BUV) instrument in 1970 (e.g., Singh & Fabian, 2003; Grant, 1989) and followed by the Solar Backscatter Ultraviolet (SBUV) instrument and Total Ozone Mapping Spectrometer (TOMS), which were launched on Nimbus-7 in 1978. Versions of these two latter instruments have been flown nearly continuously since on a series of Nimbus and NOAA satellites. Several instruments, including GOME, GOME-2, SCIAMACHY, OMI, and OMPS, have measured total vertical column O_3 over the last twenty years with the more recent instruments having increased spatial resolution. TROPOMI continues the record and has even finer spatial resolution. All these instruments use back-scattered solar light and, therefore, cannot collect observations during night and Arctic winter.

While the distribution of O_3 within a vertical column has some direct impact on the amount of UV radiation reaching the surface, knowledge of O_3's vertical profile is important for identification of causes of variations in the total vertical column O_3 which lead to variations in UV surface radiation. Additionally, O_3's vertical distribution may influence surface UV radiation indirectly as it affects stratospheric dynamics, which influences tropospheric composition and weather (e.g., clouds), such as through the Arctic Oscillation phenomenon. Links between cryospheric changes and surface climate variability via polar stratospheric variability have recently been investigated in several modeling studies (e.g., Kim et al., 2014; Sun et al., 2015; Seviour, 2017). The somewhat diverse results of these studies emphasize the importance of continued monitoring of upper tropospheric and stratospheric composition, especially O_3 and water vapor, as well as temperature.

Satellite instruments measure O_3's vertical profile in the stratosphere using a limb-viewing technique and several wavelength regions. They use scattered solar light, stellar light or thermal emission from the atmosphere as a source of radiation. Instruments using scattered or occulted solar light are not able to measure through the Arctic winter whereas stellar occultation or thermal emission instruments can. The first instrument in this category was the NASA Explorer 60 Stratospheric Aerosol and Gas Experiment (SAGE-I) instrument (1979–1981), but a more important instrument was the Earth Radiation Budget Satellite (ERBS) SAGE-II instrument, which measured O_3 profiles from 1984 to 2004. These data have been combined with more recent O_3 measurements for trend studies (Kyrölä et al., 2013; Harris et al., 2015; Sofieva et al., 2017). In addition to O_3 profiles, SAGE-II provided stratospheric NO_2, H_2O, and aerosol profiles.

Observations of some trace gases (e.g., hydrochloric acid (HCl), bromine monoxide (BrO)) and aerosols provide insight into the complex chemistry and dynamics that influence stratospheric O_3, and subsequently, surface UV radiation. Many of these relevant trace gases and aerosols in the stratosphere have been measured at least for a limited time by SAGE-II and the instruments that followed (e.g., SPARC, 2017). These instruments include the NASA Upper Atmosphere Research Satellite (UARS) Halogen Occultation Experiment (HALOE), MLS, CSA Odin Optical Spectrograph and InfraRed Imager System (OSIRIS), Swedish National Space Board Odin Sub-Millimeter Radiometer (SMR), ESA Global Ozone Monitoring by Occultation of Stars (GOMOS), ESA Envisat Michelson Interferometric Passive Atmosphere Sounder (MIPAS), SCIAMACHY, AIRS, SAGE III, NASA Thermosphere Ionosphere Mesosphere Energetics Dynamics (TIMED) Sounding of the Atmosphere using Broadband Emission Radiometry (SABER)

instrument, and CSA Atmospheric Chemistry Experiment (ACE) Fourier Transform Spectrometer (ACE-FTS). Data from these instruments raised stratospheric composition studies to a new level. For instance, Manney et al. (2011) use MLS and OMI data to show that, for the first time in the observational record, constituent evolution within the 2010/2011 Arctic polar vortex approached that in the Antarctic. As another example, the SAGE data indicate a seasonal decrease in Arctic particle size from ~0.35 to ~0.25 μm from spring to summer, based on the ratio of mid-visible—1-μm limb observations (Treffeisen et al., 2006).

Arctic UV-B radiation levels are expected to decrease by 2100 from a few percent to some tens of percent as compared to 1950 because of decreasing Arctic sea ice and surface reflectivity together with increased cloudiness and the expected O_3 "super recovery" (due to both removal of O_3-destroying chlorofluorocarbons (CFCs) and acceleration of the Brewer-Dobson circulation; e.g., Watanabe et al., 2011; Fountoulakis et al., 2014). However, as compared to the decrease in UV-B irradiance at the surface, a far greater increase is projected for UV-B irradiance entering the ocean by 2100 because of sea ice loss (Fountoulakis et al., 2014). Therefore, a comprehensive and internally consistent suite of observations, including clouds, surface albedo, aerosols, and ozone, is necessary to attribute the causes of trends and variations in ABZ UV-B radiation.

Going forward, there is an important need to continue observations with MLS and MIPAS types of instruments, which provide important data of the vertical distributions of a number of trace gases which are used to study the chemical and dynamical processes that determine Arctic ozone variations and trends. These instruments are able to measure during day and night, which is important for Arctic studies. Similarly, solar occultation instruments that observe UV-visible wavelengths (e.g., SAGE II) are needed for estimating long-term trends and as a transfer standard between different instruments and over data gaps. The Atmospheric Limb Tracker for the Investigation of the Upcoming Stratosphere (ALTIUS) instrument promises to extend limb scatter, solar and stellar occultation observations (Fussen et al., 2016). It is being developed in collaboration with Belgium and ESA with an expected launch date in 2021. NASA's/NOAA's OMPS limb scatter observations of O_3 are also planned for continuation in upcoming JPSS missions. Finally, it is important to continue data collection at existing ABZ observatories, which is critical for satellite validation activities.

5.5. Observing the Arctic-Boreal Energy Budget (Patrick C. Taylor, Seiji Kato)

The energy budget is a critical variable for understanding changes in the ABZ. For instance, the annual mean top-of-the-atmosphere (TOA) budget of incoming and outgoing radiation is approximately balanced by large-scale horizontal transports of the ocean and atmosphere because the storage term (i.e., the energy used to melt sea ice and warm the ABZ) is negligible at time scales longer than annual. The energy budget at the surface, including radiative and turbulent fluxes and surface temperature, determines the seasonal timing of sea ice and snow melt/freeze-up. The TOA and surface energy budgets are also influenced by ABZ climate feedback processes, including the surface albedo feedback, the lapse rate feedback, and the permafrost carbon-feedback (Pithan & Mauritsen, 2014; Schuur et al., 2015; Screen & Simmonds, 2010; Serreze & Barry, 2011; Stuecker et al., 2018). As a consequence, the uncertainty in the ABZ surface energy budget is, in part, responsible for the inter-model spread in Arctic climate projections (Boeke & Taylor, 2018). Monitoring changes in the ABZ energy budget is necessary for observationally determining the causes and consequences of amplified ABZ climate change and to constrain models and projections.

Observations indicate that energy budget fluxes have changed over the last 30 years across the ABZ. Most evident is the increase in absorbed SW radiation (sunlight) at the surface and TOA associated with the decreases in sea ice and snow cover (Brown & Robinson, 2011; Stroeve et al., 2012). Pistone et al. (2014) used both the Clouds and the Earth's Radiant Energy System (CERES) and the passive microwave measurements to estimate that an additional 6.4 ± 0.9 W/m^2 of SW radiation was absorbed by the ABZ since 1979. Considering the CERES Energy Balanced and Filled (EBAF; Loeb et al., 2018; Kato et al., 2018) data product alone, a -1.3 ± 0.6 W $\cdot$ m^{-2} $\cdot$ decade^{-1} trend in reflected solar radiation at TOA is found since 2000 (Figure 19a), consistent with Pistone et al. (2014). The observed greening of Arctic tundra and the shift in boreal vegetation type are also contributing to changes in the ABZ surface albedo and energy budget (Mao et al., 2016; Myers-Smith et al., 2011), evident in the CERES data as a -1.1 ± 0.3%/decade in surface albedo over land regions poleward of 60°N (Figure 19b).

Significant changes are also evident in the LW radiative fluxes. Increased downwelling LW radiation at the surface has received the most attention because of its connection to the hypothesized Arctic amplification

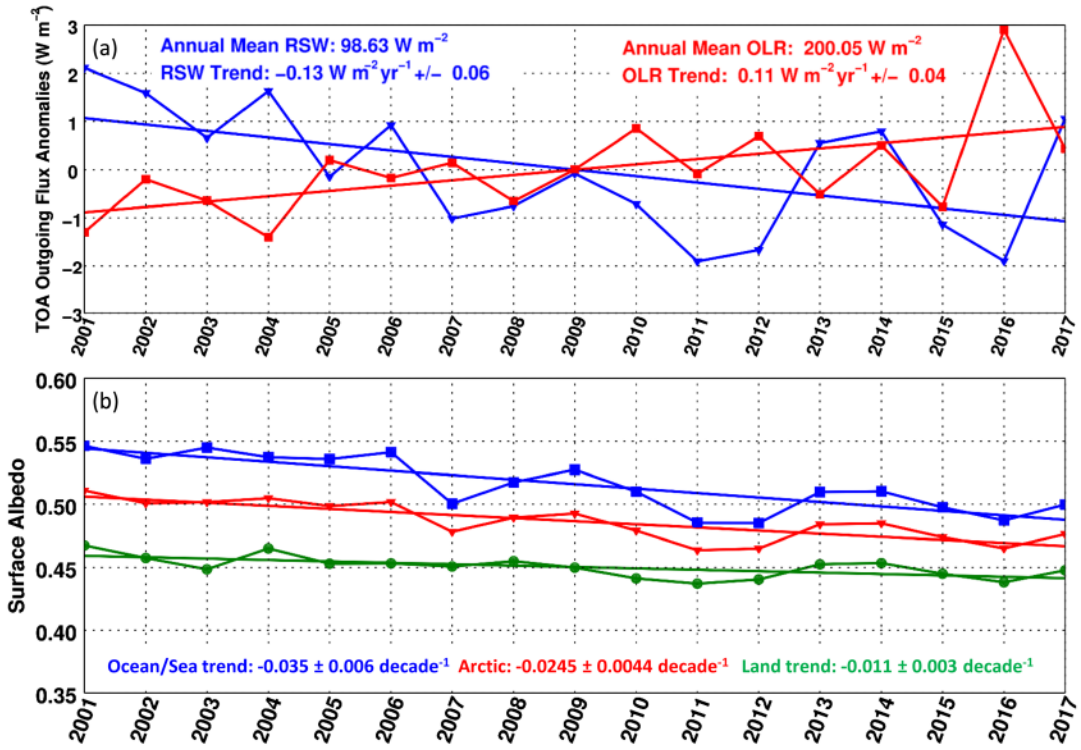

Figure 19. Time series of the annual (a) top of atmosphere (TOA) reflected shortwave (RSW; blue) and outgoing longwave radiation (OLR; red) anomalies and (b) the TOA mean albedo for the Arctic Ocean (blue), ABZ land (green), and the total ABZ region poleward of 60°N (red) from CERES TOA EBAF-Edition 4.0. Numerical values provided in the panels correspond to the annual mean TOA radiative fluxes and the linear regression trends with 1σ uncertainty bounds. (Figure courtesy of Robyn Boeke, SSAI).

process (e.g., Boeke & Taylor, 2018), a signal that also appears in reanalysis data sets (Lee et al., 2017). At TOA, CERES data indicate an increase in outgoing LW radiation of 1.1±0.4 W · m^{-2} · decade^{-1} in association with warmer ABZ temperatures (Loeb et al., 2018). A recent study by Peterson et al. (2019) exploits spectral data from AIRS, revealing that increased surface temperatures contribute more than increased atmospheric temperature and humidity to the observed broadband LW fluxes changes.

Changes in surface turbulent fluxes across the ABZ are much more uncertain than radiative fluxes (Bourassa et al., 2013). However, all indications are that significant changes are occurring during fall and winter in the regions of the Arctic Ocean that are experiencing delayed sea ice freeze onset (Barents-Kara Sea and Beaufort Chukchi Sea regions). These trends are supported by both satellite retrievals of surface turbulent fluxes (Boisvert et al., 2013; Taylor et al., 2018) and from meteorological reanalysis (Screen & Simmonds, 2010). The significance of ABZ energy budget changes and their central role in understanding and credibly predicting ABZ climate change warrants long-term, high quality observations of these variables.

Suborbital observations from surface sites provide detailed information of the ABZ energy budget at specific locations and within the ABZ; however, few sites exist. Examples of surface energy budget observation networks for the Greenland ice sheet include the Greenland Climate Network beginning in 1996 (GC-Net; Steffen et al., 1996) and the Programme for Monitoring of the Greenland Ice Sheet (PROMICE; van As & Fausto, 2011) beginning in 2007. In addition, the Baseline Surface Radiation Network (BSRN; 64 global sites) is a global network of high-quality surface radiation budget data and has the goal to monitor change in LW and SW surface radiation by providing validation data for satellite retrievals and global climate models. Even though seven BSRN sites exist poleward of 60°N, only four of these are currently operating and have at least 10 years of observations. These sites include Alert, Canada, Ny-Ålesund, Spitsbergen, Barrow, AK, US, and Lerwick, Shetland Island, UK. Similar to BSRN, FLUXNET is also a global network of surface flux towers to measure surface turbulent and gas flux exchanges between the atmosphere and ecosystem using eddy

covariance techniques (https://fluxnet.fluxdata.org). Data from 20 FLUXNET sites have been collected within the ABZ and many also provide surface radiation flux data. FLUXNET data have been used to evaluate satellite measurements and climate models, representing critical data to assess the exchanges of energy and gases between the atmosphere and ecosystems (Baldocchi, 2014).

Observations of the ABZ surface energy fluxes at these surface sites are difficult to maintain. High-quality surface energy flux observations are challenging in the unique ABZ meteorological conditions, such as strong winds that tilt/damage sensors, riming on sensors, severe cold temperatures, and snowfall covering sensors. Moreover, the remoteness of the ABZ limits access to these sites to repair instrumentation, especially during winter. Despite these challenges, suborbital observations are critical for validating satellite data products. Increasing the number of these high-quality ground sites is needed to improve our ability to monitor changes in the ABZ surface energy budget and to validate satellite-based surface energy budget data.

Since permanent surface sites are confined to land, periodic suborbital observations over the Arctic Ocean are needed to constrain the ABZ surface energy budget. These periodic suborbital missions take the shape of airborne campaigns, ice camps, drifting stations, and buoys (e.g., Rigor et al., 2002; Taylor et al., 2018). More than 20 suborbital field campaigns have provided surface energy budget observations across the ABZ since 1975. Here, two campaigns are highlighted. Arguably the most important modern suborbital field campaign to date was the Surface Heat Budget of the Arctic (SHEBA) experiment (Uttal et al., 2002). The first of its kind, SHEBA established an ice camp in the Beaufort Sea and maintained it for a full year from October 1997 through September 1998; these data provided the first annual cycle of the ABZ surface energy budget over sea ice (Persson et al., 2002). More recently, the Arctic Radiation IceBridge Sea ice Experiment (ARISE; Smith et al., 2017) took place in September 2014 as a radiation-focused mission designed to evaluate CERES radiative fluxes and provide data to understand how cloud radiative effects are influencing the ABZ surface energy budget over sea ice. Readers are referred to Taylor et al. (2018) for a more complete list of ABZ field missions gathering surface energy budget data. More campaigns like ARISE and SHEBA are needed to accumulate the statistics required to reduce uncertainty in our understanding and our ABZ surface energy budget data sets. The Multidisciplinary drifting Observatory for the Study of Arctic Climate (MOSAiC; https://www.mosaic-expedition.org) set to deploy into the eastern Arctic in Fall 2019 and drift for one-year with the sea ice is an example of such a field mission. MOSAiC is expected to produce an unprecedented data set to understand the surface energy budget in the ABZ.

Observing the ABZ energy budget from space is challenging. The unique thermodynamic conditions of the ABZ (e.g., frequent surface-based temperature inversions), low thermal contrast between the ABZ atmosphere and surface, and highly reflective snow and ice surfaces creating a small brightness contrast between clouds and the surface make passive remote sensing of the ABZ difficult. Moreover, the dynamic nature of sea ice and its albedo, especially its spectral character, adds uncertainty because of noisy and inaccurate boundary conditions for satellite retrievals.

Despite the challenges of observing the ABZ from space, long-term satellite observations represent the only feasible option for monitoring change of the energy budget at broad spatial scales required to address climate change science. Satellite observations of the ABZ TOA energy budget have been measured by the Earth Radiation Budget Experiment (ERBE) on NOAA-9 (February 1985 to June 1988), NOAA-10 (November 1986 to May 1989), and since 2000 with the six CERES instruments aboard Terra, Aqua, and NPP. Retrieval of TOA fluxes from the ERBE scanner and CERES instruments requires the inversion of radiances to fluxes using empirical angular distribution models. The angular distribution of radiances depends upon the specifics of the scene, including surface type and cloud properties. Key error sources in the retrievals of ABZ TOA energy fluxes include instrument calibration, angular distribution models and scene identification (Loeb et al., 2009).

Alternatively, ABZ TOA and surface radiation flux information has been obtained using radiative transfer model calculations constrained with satellite retrievals of clouds, sea ice cover, and thermodynamic properties (e.g., Zhang et al., 1995; Rossow & Zhang, 1995; Zhang et al., 2004). Uncertainty in the radiative fluxes computed from the International Satellite Cloud Climatology Project (ISCCP) cloud property retrievals is estimated to be 10–15 W/m^2 at the surface and 5–10 W/m^2 at TOA (Zhang et al., 2004). However, these values refer to global flux uncertainty and do not represent the ABZ. CERES data products also use

radiative transfer model calculations and satellite retrievals to provide surface radiative fluxes; these calculations serve as the basis for the CERES Surface EBAF dataset. Kato et al. (2018) estimate uncertainty values for individual ABZ surface radiative flux terms ranging from 12 to 16 W/m^2 (1σ) at the monthly mean 1°×1° gridded scale.

Satellite measurements of ABZ surface turbulent fluxes are more limited than their radiative flux counterparts. Traditional satellite-retrieved surface turbulent fluxes (such as SEAFLUX; Curry et al., 2004 or OAFLUX; Yu & Weller, 2007) do not allow for retrievals over sea ice. Boisvert et al. (2013, 2015) demonstrate a methodology tailored to the ABZ using thermodynamic profile information from AIRS to retrieve ABZ surface turbulent fluxes. Comparisons of satellite-retrieved surface turbulent fluxes with available buoy and ship data indicate root mean square errors of 0.74 and 5.32 W/m^2 in latent and sensible heat fluxes, respectively. Taylor et al. (2018) also show that variability in the air-surface temperature difference drives variability in ABZ surface turbulent fluxes over both sea ice and ocean. Improved, satellite-retrieved surface turbulent fluxes require an improved ability to detect the air-surface temperature difference from space. Meteorological reanalysis has also been used to provide surface turbulent flux information, however, the accuracy of these data is unknown and discrete jumps and discontinuities in the record make it inappropriate for trend analysis (Taylor et al., 2018).

The current satellite observing system provides the data required to make reasonable estimates of the ABZ energy budget. However, some key issues need to be highlighted in order to monitor the ABZ energy budget with an accuracy to accelerate climate research. First and foremost, continuity of the TOA radiative flux measurements and climate data record from space must be maintained to advance ABZ energy budget science. A multi-decadal record of the ABZ TOA energy budget provides an understanding of how the ABZ is changing during times when the radiative forcing is increasing and serves as a valuable constraint on Arctic climate projections. Overall, ABZ TOA energy fluxes are well observed since the launch of CERES aboard Terra with the record starting in March 2000 and continuing this record is vital.

Second, ABZ energy budget science requires reduction in the uncertainty of surface fluxes determined using satellite instruments. Larger uncertainty in the satellite-derived TOA and surface fluxes as compared to the uncertainty for tropics and midlatitude occurs because of the uncertainty in input variables used to compute surface fluxes. Specifically, the bias (with unknown sign) in fluxes comes from large uncertainties associated with surface conditions (e.g., snow and ice cover), cloud properties (especially during polar night), and thermodynamic profiles (especially near the surface). The first step to reduce the bias in these properties is to quantify these individual contributions. To obtain statistically significant results in quantifying the bias, a single campaign or a few surface sites with short record lengths are insufficient because of diverse range of surface types (e.g., ocean, land, and with and without snow and sea ice) and dependence of key variables on the surface type. Over the Arctic Ocean, this requires a series of carefully designed suborbital airborne and/or ship-based campaigns to accumulate observations of key variables over a wide range of scene types (e.g., clear-sky ocean, clear-sky sea ice, partly cloudy sea ice, etc.). These suborbital campaigns should be coordinated with satellite observations, in special cases incorporating unique satellite instrument scan modes, as was done in ARISE (Smith et al., 2017), to focus on specific scene types or variables. When possible, field campaigns should leverage existing surface sites (e.g., ARM facilities in Barrow, AK and Ny-Alesund, Spitsbergen) to provide context and a full-characterization of the atmospheric column. In addition, suborbital instruments can observe variables that are difficult to derive from satellite instruments. These variables include temperature and humidity profiles under clouds or surface skin temperature under overcast conditions. Because of radiative cooling during clear polar nights, we expect that near surface temperature and humidity would be different from those under cloudy conditions, much larger than the differences occurring in the tropics and midlatitudes. In addition, there is a surface type dependence of the skin temperature uncertainty, such that uncertainty is larger over sea ice than ice-free ocean.

Over ABZ land, irradiance observations at surface sites are important to assess CERES EBAF surface flux uncertainty. However, the number of these high-quality (e.g., BSRN) surface radiometer sites is limited (i.e., four across the Arctic). More sites in a more diverse set of locations would enable the quantification of the uncertainty in the ABZ surface radiation budget. Placing instruments on buoys to observe near surface variables over the Arctic Ocean is ideal to obtain measurements at remote sites. Overcoming the harsh environment and technical difficulties to maintain the accuracy is, however, challenging, if not impossible. A

complete strategy should include at least one surface site in each ABZ surface type (open water, sea ice, tundra, boreal forest, etc.). Then, surface and satellite observations can be used together to assess changes in the ABZ energy budget.

Uncertainties currently exist in our knowledge of surface albedo and its spectral and angular variations, especially in the presence of melt ponds and over first-year sea ice. Improved modeling of spectral and angular variations of sea ice surface albedo would enable reduced uncertainty in satellite cloud retrievals and therefore TOA and surface radiative fluxes. Moreover, continued effort and validation of satellite-retrieved surface turbulent fluxes is needed.

6. Highly Elliptical Orbits for Remote Sensing of the ABZ (Ray Nassar)

Low Earth Orbit (LEO) satellites typically orbit in a plane near Earth's poles to provide global sampling. For a Sun-synchronous LEO, observations at a given location are repeatedly made at the same time of day. Geostationary Earth Orbit (GEO) satellites orbit at Earth's equatorial plane from a much farther distance of 35,786 km and are synchronized with the Earth's rotation, enabling continuous observations over a given region. From GEO, the temporal evolution of the atmosphere can be observed with a revisit time on the order of minutes to hours (instead of days from LEO), but viewing angles become too large at latitudes poleward of ~55°. The constellation of satellites supporting modern weather forecasting consists of multiple LEO and GEO satellites. Observations of atmospheric composition focused on air quality are now moving from only LEO missions to include an internationally coordinated GEO component to the constellation that will be in place in the early 2020s (CEOS-ACC, 2011). A coordinated GEO component to a constellation of greenhouse gas missions from multiple nations may soon materialize (Crisp et al., 2018), beginning with NASA's planned Geostationary Carbon Cycle Observatory (GeoCARB; Moore et al., 2018). For both air quality and greenhouse gases, the synergy of a LEO-GEO constellation is highly desirable, but results in a gap in continuous observations at high latitudes over the ABZ. Observations from a highly elliptical orbit (HEO) have the potential to fill this gap to complement the measurements from LEO and GEO.

The use of HEOs for Earth observation was first suggested by Kidder and Vonder Haar (1990). More recently, the value of this class of orbits for high-latitude observations has been recognized in the WMO Vision for a Global Observing System in 2025 (WMO, 2009), the follow-on vision for 2040, which will soon be finalized, and CEOS air quality and greenhouse gas strategy papers (CEOS-ACC, 2011; Crisp et al., 2018). How exactly do HEO satellites provide quasi-geostationary observations? Figure 20 illustrates the orbital path of a satellite in an HEO. Since angular momentum is conserved in any satellite orbit, a satellite in an elliptical orbit with the Earth at one focus will move quickly when it is close to the Earth and slowly when it is far from the Earth. Near the farthest point in the orbit from Earth (the apogee) the satellite will move very slowly and dwell over a given spot enabling geostationary-like observations. By selecting the inclination of the orbit to situate the apogee near the critical inclination of 63.44°N, a single satellite can make quasi-geostationary observations of the ABZ for a limited time before accelerating toward perigee, where it no longer views the ABZ. With two HEO satellites, continuous GEO-like viewing is possible (aside from external factors like the available sunlight) with a number of different HEO options with periods typically in the range of 12–24 hr and apogee altitudes that are comparable to GEO (Trishchenko et al., 2011; Tritchtchenko et al., 2014).

The Canadian government considered a HEO mission called Polar Communications and Weather (PCW) that would provide meteorological observations of the high latitudes (Garand et al., 2014), using similar instrumentation as the NOAA Geostationary Operational Environmental Satellite system (GOES). Mission enhancements were also considered to measure CO_2, CH_4, CO, O_3, NO_2, SO_2, aerosols, temperature and water vapor (LaChance et al., 2012; McConnell et al., 2012). An OSSE demonstrated that the CO_2 observations from HEO would provide much improved constraints on ABZ terrestrial biospheric CO_2 fluxes relative to GOSAT (Nassar et al., 2014), especially during the summer months when the expected CO_2 fluxes (due to boreal forest growth or disturbances or permafrost thaw) and their uncertainties would both be largest. Other advantages, including the diurnal coverage available from HEO and imaging capability, were not assessed in the OSSE, but would contribute further information needed to reduce uncertainty in ABZ CO_2 and CH_4 fluxes.

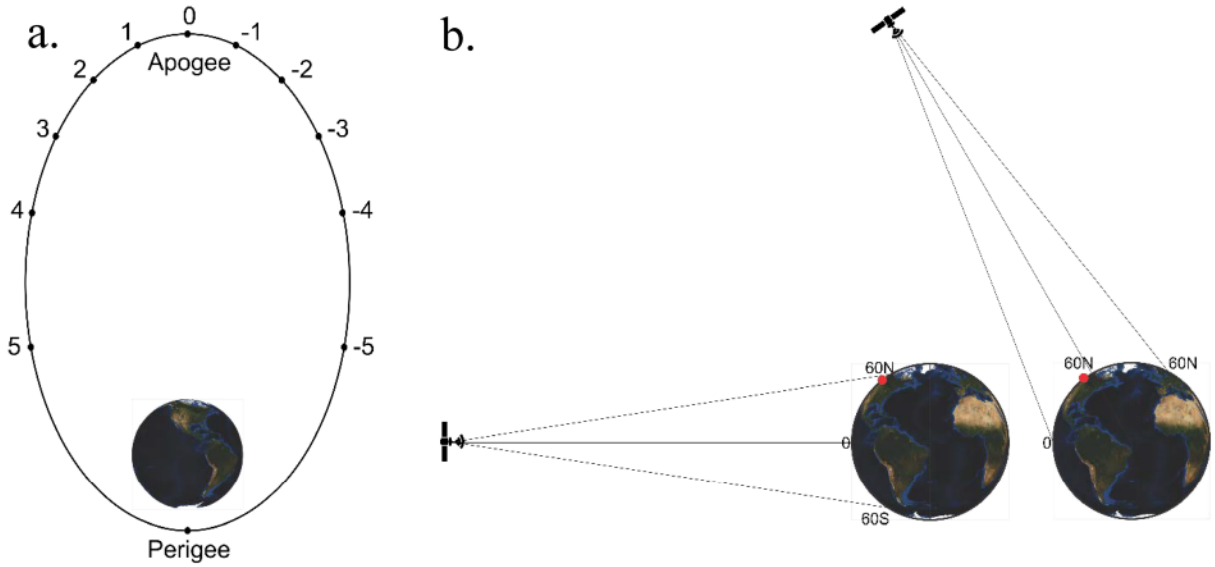

Figure 20. (a) A 12-hr HEO or Molniya orbit with an apogee altitude of ~39,000 km and perigee altitude of ~800 km. The number of hours before/after apogee for the satellite in the orbit is indicated on the figure, showing that for at least 6–8 hr of the 12-hr period, the satellite would have a favorable view of the north. (b) The nadir and ±60° from the nadir for GEO and HEO are indicated by lines in the figure. The red dot is a point of interest at ~57°N. From GEO, the viewing angle for a point at this latitude is very large and far from vertical, while from a HEO near the critical inclination (i=63.44°N), the point is viewed with a favorable viewing angle when the satellite is near apogee. Any longitude offset (not shown) increases the viewing angle further, compounding the difficulty of high latitude viewing from GEO.

The Atmospheric Imaging Mission for Northern regions (AIM-North, www.aim-north.ca) is a new HEO concept currently undergoing Phase 0 studies for the CSA (Nassar et al., 2019). AIM-North would measure CO_2, CH_4, CO, SIF, NO_2, O_3, BrO, HCHO, SO_2, aerosols, clouds, and other species. AIM-North has stricter precision requirements for greenhouse gases and air quality gases than earlier HEO plans and smaller proposed image pixel size (4×4 km^2), which would enable better quantification of localized sources (natural or anthropogenic) in the ABZ.

Due to the high altitude of HEO as compared to LEO, much more of the Earth is visible from the satellite vantage point at any given instant, which can be a major advantage for dealing with clouds. At any given moment, about 70% of the Earth is covered by clouds (Stubenrauch et al., 2013), which results in a loss of greater than 70% of observations for species like CO_2 for which retrievals are very sensitive to clouds. During the Arctic summer, monthly mean cloud cover may reach 85% (Kay et al., 2016), suggesting that it is an even bigger challenge for the ABZ. With information on cloud cover from a cloud imager (or another source) to inform pointing from HEO, instruments making observations very sensitive to clouds can spend their time observing only the clearer regions, resulting in less data loss due to clouds than from LEO, for which pointing options are much more limited.

Although a particular set of observables has been proposed for AIM-North, the list of species or parameters that could be measured from HEO is almost limitless and could be extended to clouds, winds, vegetation and wildfire parameters, snow cover, sea ice, etc., but like GEO, active measurements (radar or lidar) are especially challenging due to the high orbit altitude. The European Copernicus Programme, ESA, and EUMETSAT along with industrial partners, are currently investigating measuring other ABZ variables from HEO in a series of ongoing studies, such as the Nordic and Arctic Imager Mission Requirements Consolidation (Kennedy & Arthurs, 2018). Ultimately, international partnership on a HEO mission dedicated to multiple observables may be the best way to obtain enhanced observations of the ABZ.

7. Synthesis of ABZ Satellite Observation Priorities

In this section, we present our recommendations for prioritizing new satellite observations of the ABZ. In section 7.1, we make general recommendations for satellite observing strategies, and, in section 7.2, we discuss specific observational priorities, which are summarized in Table 1. Finally, in section 7.3, we discuss

considerations for the development of a comprehensive and integrated ABZ Observing Network (ABZ-ON) and make a recommendation. Application of these recommendations will require international and interagency collaboration on satellite mission design through existing initiatives (e.g., CEOS).

7.1. Recommendations Common to All ABZ Components

In this section, we make the following general recommendations that are common to all satellite observations of ABZ components, including those in a comprehensive ABZ-ON. Many of our general recommendations echo the recommendations given in the scientific literature and reports for the ABZ, such as those discussed in various sections (e.g., section 1) of this review, and for the Earth system (e.g., Simmons et al., 2016).

7.1.1. Enhanced and Coordinated Suborbital Network

We recommend the development of a comprehensive and robust suborbital portion of an ABZ-ON, which can act to fill some temporal gaps in satellite coverage, can provide detail unobtainable from space, and is necessary for validation and interpretation of satellite data. This suborbital network would complement the satellite data via strategic sampling and coordinated satellite "underpass" measurements. To achieve this goal, we recommend the establishment of international and multi-disciplinary observing ground sites and other platforms (e.g., aircraft), which will constrain and distribute the costs of building and maintaining observational platforms in the challenging ABZ research environment. The development of this suborbital network to support space-based observations should leverage existing efforts to coordinate the development of a suborbital observing network and data sharing, such as the Integrated Arctic Observation System (INTAROS), U.S. National Science Foundation's Arctic Observing Network (AON) program, the International Arctic Systems for Observing the Atmosphere (IASOA; Uttal et al., 2016), the Arctic Science Ministerial (Arctic Science Ministerial, 2018), and Sustain Arctic Observing Networks (SAON; IDA Science and Technology Policy Institute and Sustaining Arctic Observing Networks, 2017).

7.1.2. Multi-Generational Datasets

We recommend that a priority be the continuation, enhancement, and/or creation of long-term, multi-satellite, climate-quality, and self-consistent data records of ABZ components, such as surface temperature, energy fluxes, or sea ice extent and volume, for improved quantitative determination of ABZ trends. Long-term passive satellite observations currently represent the only feasible option for monitoring change of the ABZ at broad spatial scales required to address pressing climate change science challenges. Application of consistent retrieval algorithms to multiple satellite data sets, as well as a careful characterization of satellite instruments and their temporal evolution, helps to ensure data quality and cross-sensor consistency.

Urgency: We recommend that development of a comprehensive ABZ-ON begin immediately given the time necessary to design, build and implement an ABZ-ON. For example, the time from initial concept to launch of a satellite is typically years and often more than a decade.

7.1.3. Community Engagement and Capacity Building

We recommend that Earth scientists work in parallel with policy and other decision-support organizations and stakeholders to formulate strategies that pursue innovative, informed, and practical uses for Earth science data in science-based decision-making (e.g., the development of tools that support mitigation and adaptation strategies). We acknowledge that a high degree of technical skill is often required to access, process, and properly interpret ABZ satellite datasets and Earth System model output. As a result, some governmental and nongovernmental entities, such as the NASA Applied Sciences Program and others mentioned above, have initiated programs to foster capacity building. At the same time, we understand that governments, nongovernmental agencies, and private companies have existing structure under which decisions are made. The goal is to integrate Earth science, technology, and data into stakeholder organizations as seamlessly as possible, so that mitigation and adaptation decisions are based on sound, comprehensive science.

7.2. Specific ABZ Observational Priorities

In this section and Table 1, we summarize the information and recommendations in sections 2–5, in which we reviewed the strengths and limitations of current satellite observations for various ABZ components, identified important ABZ properties that are not observed at all or are observed inadequately, and discussed the potential of some upcoming satellite missions and observing strategies. We also prioritize observational capabilities with the goal to address observational deficiencies in an ABZ-ON that hinder process-based understanding of the ABZ, especially for those processes that have the potential to impact human society

in profound ways. Our recommendations include for current observational capabilities to be improved upon for many specific ABZ components, which may be achieved with existing technological improvements (as compared to current instruments) and ones feasible in the near-term (e.g., <10 years) with further development. The observational priorities in Table 1 should be reassessed periodically as the ABZ evolves in a warming world.

Prioritization is necessary and pragmatic given the large expense associated with satellite mission design and operation. To be clear, we believe that all satellite observations discussed in sections 2–5 are important for the creation of a comprehensive and integrated ABZ-ON. In Table 1, we prioritize our 44 satellite recommendations with designations of "Most Important," "Very Important," and "Important" based on the following considerations:

- "Most Important" observational needs are ones for which the variable is poorly observed currently, and the current process-based understanding of the factors that determine that variable's trends and variations are poorly known (e.g., Hinzman et al., 2013). Seven (16%) recommendations ranked as "Most Important".
- "Very Important" observational needs are ones for which the variable is insufficiently observed, and more or better observations are necessary to advance process-based and/or large-scale understanding related to that variable. Twenty-two (50%) recommendations ranked as "Very Important".
- "Important" observational needs are ones for which the current and anticipated future observational suite for that variable is adequate in comparison to those for other variables. Fifteen (34%) recommendations ranked as "Important". As discussed in section 7.1, we recommend the creation of multi-generational datasets that necessarily requires the continuation of the capabilities (at a minimum) of current satellite instruments. However, based on our criteria, some of these highly valuable observations are ranked as "Important," such as thermal infrared observations of surface temperature, visible observations of burned area, and gravimetry for land ice mass change (Table 1).

Among the observational needs that are ranked as "Most Important" are those associated with gaining a process-based and large-scale understanding of the ABZ carbon cycle and hydrologic cycle (which includes sea level rise) as they have the potential to affect a large portion of Earth's population via economic loss, displacement, etc. For the carbon cycle, these observational priorities are (1) CH_4 and CO_2 lidar instruments (technology exists) to observe their atmospheric concentrations, which will allow for the inference of fluxes from ABZ wetlands, permafrost, and wildfires in the low-light conditions that are typical of the ABZ; (2) microwave radars (L-Band) with higher spatiotemporal resolution to develop consistent, multi-temporal characterization of wetland inundation regimes; (3) enhanced spectral range (to include ultraviolet) and spatiotemporal resolution of ocean color sensors for assessing changes in plankton diversity and carbon quality, and increased spatial resolution for assessing land-ocean exchanges; and (4) improved spatial resolution for observations to detect surface-feature changes (e.g., L-band interferometric SAR) and more suborbital observations of soil carbon content to better characterize permafrost. For the hydrologic cycle, the observational priorities are 1) finer spatial observations from passive microwave instruments to better define the coast and sea ice edge; 2) new technology to better observe ice and snow albedo and snow-water equivalent; and 3) improved observations of wetlands and permafrost as discussed for the carbon cycle.

The satellite recommendations in Table 1 highlight the importance of active sensors (e.g., lidar) in ABZ-ON design going forward. Active sensors do not depend on reflected sunlight and so join passive microwave sensors in having a significant advantage over passive visible and infrared sensors in the low-light conditions that are typical of the ABZ for several months of the year. Lidar measurements provide other advantages. First, the spatial footprint is smaller for active than passive instruments, allowing more opportunity of observing clear skies between clouds. Second, lidar observes in a single nadir-zenith path over both land and oceans (i.e., no changes with surface or latitude). Third, this single path is less impacted by clouds than the two separate paths (i.e., illumination and observation) required by some passive sensors. Furthermore, the lidar measurements are range-gated which minimizes the impact of scattering from thin clouds, haze and aerosols. And, fourth, lidar observations are independent of sun angle and so are available over all local times of year and at different times of day (e.g., once at night and once in the daytime).

Our prioritization of observational needs is largely consistent with the science and application priorities presented in the recent consensus study from the U.S. National Academies of Sciences, Engineering, and Medicine (NASEM; "Thriving on Our Changing Planet: A Decadal Strategy for Earth Observation from

Space," National Academies of Sciences, Engineering, and Medicine, 2018), even though the study used a different set of prioritization criteria (i.e., Chapter 3 of the NASEM study) than we employ in this review article. While the charge of the study did not include making recommendations explicitly for a comprehensive ABZ-ON, it emphasized the critical need for a comprehensive suite of ABZ observations: 'The Arctic has never been static, but recent changes have been exceptionally dramatic. The needed scientific exploration has only begun, and the practical capabilities necessary to successfully manage and adapt to these changes require additional development. With the scientific, economic, political, and strategic landscape evolving so rapidly, the need for frequently updated, large-scale information about the ice, ocean, land, and atmosphere in this remote region has never been greater." The NASEM recommendations include a set of global observational capabilities that require ABZ observations to "enable substantial progress" in science and application areas, such as the following:

- "Understanding the sources and sinks of carbon dioxide and methane and the processes that will affect their concentrations in the future."
- "Determining the extent to which the shrinking of glaciers and ice sheets, and their contributions to sea level rise, is accelerating, decelerating, or remaining unchanged."
- "Improving understanding of ocean circulation, the exchanges between the ocean and atmosphere, and their impacts on weather and climate."
- "Assessing the evolving characteristics and health of terrestrial and aquatic ecosystems, which is important for understanding key consequences such as crop yields, carbon uptake, and biodiversity."

7.3. Recommendation and Considerations for Designing an ABZ-ON

Building Blocks: We recommend an interdisciplinary and stepwise approach to developing an ABZ-ON, beginning with an initial focus on observing networks designed to gain process-based understanding for individual ABZ components. The justification for the recommendation to initially focus on individual ABZ components is based on a desire to keep early development efforts feasible and to recognize pragmatic financial constraints. This approach should help to lay the foundation for designing observing networks for more complex ABZ subsystems (e.g., the hydrological cycle) that could, at some point in the future, serve as the building blocks for a comprehensive ABZ-ON and, ultimately, an Earth system observing network. We emphasize that a systems approach to observing is necessary to support a predictive understanding of Earth system science and to ensure a strong return on investment for future ABZ-relevant satellite missions.

To aid in the identification of variables that should be monitored for a specific complex ABZ subsystem, we list in Table 1 the primary drivers of change for each ABZ component discussed in sections 2–5 and ancillary data for variables that cannot be observed or observed well from space, including the desired spatial and temporal scales. To illustrate this concept, we briefly discuss the carbon and hydrologic cycles because of their complexity and potential to impact regions far beyond the ABZ. Both cycles were recognized as important in the NASEM consensus study as discussed above. For the carbon cycle, observations of atmospheric chemical concentrations with greater spatial and seasonal coverage are required to monitor changes in carbon dioxide and methane fluxes (section 5.2). Tracking atmospheric changes of greenhouse gas concentrations to integrated ecosystem components requires advanced measurements of vegetation (sections 4.4 and 4.5), fire regimes (section 4.6), wetlands (section 4.7), ocean biology and biogeochemistry (section 3.3) and the geophysical variables influencing these subsystems, including soil moisture, surface inundation, and air and sea temperatures, all of which are observable from space. To complement satellite data, the collection of suborbital data on active layer thickness (ALT) and carbon content of soils is critical. For the ABZ hydrologic cycle, simulating and predicting sea level rise requires a process-based understanding of the snow lifecycle. Observations of surface temperature (section 2), land ice velocity and mass change (section 4.1), observations of precipitation, snow accumulation and redistribution (section 4.2) are all required to simulate possible future sea level.

Acknowledgments
This version benefited from the reviews of the first and second submissions. We gratefully acknowledge upper management, especially Dr. Piers Sellers (deceased), at NASA Goddard Space Flight Center who encourage the Center's scientists to better communicate across disciplines on ABZ issues. Thanks to Sean Helfrich of NOAA National Ice Center for updated information on NOAA's IMS snow product. Brendan Rogers acknowledges support from NASA ABoVE and Carbon Cycle Science (NNX17AE13G). Numerous datasets are discussed in this review, so it is not feasible to list where each may be accessed. Instead, we refer the reader to international efforts to organize Arctic-relevant datasets. For instance, the Arctic Data Committee (https://arcticdc.org/) has the mission to "to promote and facilitate international collaboration towards the goal of free, ethically open, sustained and timely access to Arctic data through useful, usable, and interoperable systems." On their website, numerous international, national and nongovernmental data archives are listed, such as the U.S. National Snow and Ice Data Center (NSIDC; http://nsidc.org/) and the WMO Global Cryosphere Watch (GCW; http://globalcryospherewatch.org/). Most satellite and field campaign datasets funded by NASA and ESA may be found at the Earthdata (https://earthdata.nasa.gov/) and Earth Online (https://earth.esa.int/) archives, respectively.

References

Abbott, B. W., Jones, J. B., Schuur, E. A. G., Chapin, F. S. III, Bowden, W. B., Bret-Harte, M. S., & Zimov, S. (2016). Biomass offsets little or none of permafrost carbon release from soils, streams, and wildfire: An expert assessment. *Environmental Research Letters*, *11*, 034014. https://doi.org/10.1088/1748-9326/11/3/034014

Ackerman, S. A., Strabala, K. I., Menzel, W. P., Frey, R. A., Moeller, C. C., & Gumley, L. E. (1998). Discriminating clear sky from clouds with MODIS. *Journal of Geophysical Research*, *103*(D24), 32,141–32,157. https://doi.org/10.1029/1998JD200032

Alasset, P.-J., Chamberland, J., English, J., Power, D., & Volkov, N. (2010). *Monitoring and Assessing Geohazards in Permafrost Terrain using Spaceborne Synthetic Aperture Radar (SAR), GEO 2010, Calgary, Alberta* (pp. 1329–1337). Richmond, BC Canada: Canadian Geotechnical Society. https://www.worldcat.org/title/geocalgary-2010-proceeedings/oclc/690009825

Alexeyev, V. A., & Birdsey, R. A. (1998). Carbon storage in forests and peatlands of Russia. *Gen. Tech. Rep. NE* 244, U.S.D.A. Forest Service Northeastern Research Station, Radnor, 137.

Allen, G. H., & Pavelsky, T. M. (2018). Global extent of rivers and streams. *Science*, *361*(6402), 585–588. https://doi.org/10.1126/science.aat0636

Alsdorf, D., Lettenmaier, D., & Vörösmarty, C. (2003). The need for global, satellite-based observations of terrestrial surface waters. *Eos, Transactions American Geophysical Union*, *84*(29), 269–276. https://doi.org/10.1029/2003EO290001

AMAP (2017). *Snow, Water, Ice and Permafrost. Summary for Policy-makers*. Oslo, Norway: Arctic Monitoring and Assessment Programme (AMAP). 20 pp

Andreae, M. O., Rosenfeld, D., Artaxo, P., Costa, A. A., Frank, G. P., Longo, K. M., & Silva-Dias, M. A. F. (2004). Smoking Rain Clouds over the Amazon. *Science*, *303*(5662), 1337–1342. https://doi.org/10.1126/science.1092779

Angert, A., Biraud, S., Bonfils, C., Henning, C. C., Buermann, W., Pinzon, J., et al. (2005). Drier summers cancel out the CO_2 uptake enhancement induced by warmer springs. *Proceedings of the National Academy of Sciences of the United States of America*, *102*(31), 10823–10827. https://doi.org/10.1073/pnas.0501647102

Antropov, O., Rauste, Y., Vaananen, A., Mutanen, T., & Hame, T. (2016). Mapping forest disturbance using long time series of Sentinel-1 data: Case studies over boreal and tropical forests. IEEE International Geoscience and Remote Sensing Symposium.

Apps, M. J., Kurz, W. A., Luxmoore, R. J., Nilsson, L. O., Sedjo, R. A., Schmidt, R., et al. (1993). Boreal forests and tundra. *Water Air and Soil Pollution*, *70*(1-4), 39–53. https://doi.org/10.1007/BF01104987

Arctic Council (2016). In M. Carson, & G. Peterson (Eds.), *Arctic Resilience Report*. Stockholm: Stockholm Environment Institute and Stockholm Resilience Centre. http://www.arctic-council.org/arr

Arctic Science Ministerial (2018). Report of the 2nd Arctic Science Ministerial, Co-operation in Arctic Science – Challenges and Joint Actions, published by Federal Ministry of Education and Research (BMBF), Germany, https://www.arcticscienceministerial.org/files/BMBF_ASM2_Broschuere_V1_A4_webRZ_bf.pdf

Argo (2019). Argo float data and metadata from Global Data Assembly Centre (Argo GDAC). *SEANOE*. https://doi.org/10.17882/42182

Armitage, T. W. K., Bacon, S., Ridout, A. L., Thomas, S. F., Aksenov, Y., & Wingham, D. J. (2016). Arctic sea surface height variability and change from satellite radar altimetry and GRACE, 2003–2014. *Journal of Geophysical Research: Oceans*, *121*(6), 4303–4322. https://doi.org/10.1002/2015JC011579

Arnold, S. R., Law, K. S., Brock, C. A., Thomas, J. L., Starkweather, S. M., von Salzen, K., et al. (2016). Arctic air pollution: Challenges and opportunities for the next decade. *Elementa Science of the Anthropocene*, *4*, 000104. https://doi.org/10.12952/journal.elementa.000104

Arrigo, K. R., van Dijken, G., & Pabi, S. (2008). Impact of a shrinking Arctic ice cover on marine primary production. *Geophysical Research Letters*, *35*, L19603. https://doi.org/10.1029/2008GL035028

Arrigo, K. R., & van Dijken, G. L. (2011). Secular trends in Arctic Ocean net primary production. *Journal of Geophysical Research*, *116*(C9), C09011. https://doi.org/10.1029/2011JC007151

Arrigo, K. R., & van Dijken, G. L. (2015). Continued increases in Arctic Ocean primary production. *Progress in Oceanography*, *136*, 60–70. https://doi.org/10.1016/j.pocean.2015.05.002

Baldocchi, D. (2014). Measuring fluxes of trace gases and energy between ecosystems and the atmosphere – the state and future of the eddy covariance method. *Global Change Biology*, *20*, 3600–3609. https://doi.org/10.1111/gcb.12649

Balzter, H., Gerard, F. F., George, C. T., Rowland, C. S., Jupp, T. E., McCallum, I., et al. (2005). Impact of the Arctic Oscillation pattern on interannual forest fire variability in Central Siberia. *Geophysical Research Letters*, *32*, n/a. https://doi.org/10.1029/2005GL023027

Bamber, J., vanden Broeke, M., Ettema, J., Lenaerts, J., & Rignot, E. (2012). Recent large increases in freshwater fluxes from Greenland into the North Atlantic. *Geophysical Research Letters*, *39*, L19501. https://doi.org/10.1029/2012GL052552

Bamber, J. L., & Payne, A. J. (2004). *Mass Balance of the Cryosphere: Observations and Modelling of Contemporary and Future Changes*. Cambridge, UK: Cambridge University Press. https://doi.org/10.1017/CBO9780511535659

Bamber, J. L., Siegert, M. J., Griggs, J. A., Marshall, S. J., & Spada, G. (2013). Paleofluvial Mega-Canyon Beneath the Central Greenland Ice Sheet. *Science*, *341*(6149), 997–999. https://doi.org/10.1126/science.1239794

Barber, D. G., Babb, D. G., Ehn, J. K., Chan, W., Matthes, L., Dalman, L. A., et al. (2018). Increasing mobility of high Arctic sea ice increases marine hazards off the east coast of Newfoundland. *Geophysical Research Letters*, *45*(5), 2370–2379. https://doi.org/10.1002/2017GL076587

Barichivich, J., Briffa, K. R., Myneni, R., van der Schrier, G., Dorigo, W., Tucker, C. J., et al. (2014). Temperature and Snow-Mediated Moisture Controls of Summer Photosynthetic Activity in Northern Terrestrial Ecosystems between 1982 and 2011. *Remote Sensing*, *6*(2), 1390–1431. https://doi.org/10.3390/rs6021390

Barichivich, J., Briffa, K. R., Myneni, R. B., Osborn, T. J., Melvin, T. M., Ciais, P., et al. (2013). Large-scale variations in the vegetation growing season and annual cycle of atmospheric CO_2 at high northern latitudes from 1950 to 2011. *Global Change Biology*, *19*(10), 3167–3183. https://doi.org/10.1111/gcb.12283

Barichivich, J., Briffa, K. R., Osborn, T. J., Melvin, T. M., & Caesar, J. (2012). Thermal growing season and timing of biospheric carbon uptake across the Northern Hemisphere. *Global Biogeochemical Cycles*, *26*, GB4015. https://doi.org/10.1029/2012GB004312

Barnett, T. P., Adam, J. C., & Lettenmaier, D. P. (2005). Potential impacts of a warming climate on water availability in snow-dominated regions. *Nature*, *438*(7066), 303–309. https://doi.org/10.1038/nature04141

Barrie, L. A. (1986). Arctic air pollution: An overview of current knowledge. *Atmospheric Environment*, *20*(4), 643–663. https://doi.org/10.1016/0004-6981(86)90180-0

Bartsch, A., Sabel, D., Wagner, W., & Park, S.-E. (2011). Considerations for derivation and use of soil moisture data from active microwave satellites at high latitudes. *IEEE International Geoscience and Remote Sensing Symposium*, 3132–3135.

Bartsch, A., Trofaier, A. M., Hayman, G., Sabel, D., Schlaffer, S., Clark, D. B., & Blyth, E. (2012). Detection of open water dynamics with ENVISAT ASAR in support of land surface modelling at high latitudes. *Biogeosciences*, *9*(2), 703–714. https://doi.org/10.5194/bg-9-703-2012

Baum, B. A., Soulen, P. F., Strabala, K. I., King, M. D., Ackerman, S. A., Menzel, W. P., & Yang, P. (2000). Remote sensing of cloud properties using MODIS airborne simulator imagery during SUCCESS: 2. Cloud thermodynamic phase. *Journal of Geophysical Research*, *105*(D9), 11,781–11,792. https://doi.org/10.1029/1999JD901090

Beaudoin, A., Bernier, P. Y., Guindon, L., Villemaire, P., Guo, X. J., Stinson, G., et al. (2014). Mapping attributes of Canada's forests at moderate resolution through kNN and MODIS imagery. *Canadian Journal of Forest Research*, *44*(5), 521–532. https://doi.org/10.1139/cjfr-2013-0401

Beck, H., Mcvicar, T., van Dijk, A., Schellekens, J., de Jeu, R., & Bruijnzeel, L. A. (2011). Global evaluation of four AVHRR–NDVI data sets: Intercomparison and assessment against Landsat imagery. *Remote Sensing of Environment*, *115*(10), 2547–2563. https://doi.org/10.1016/j.rse.2011.05.012

Beck, P. S. A., & Goetz, S. J. (2011). Satellite observations of high northern latitude vegetation productivity changes between 1982 and 2008: Ecological variability and regional differences. *Environmental Research Letters*, *6*(4), 045501. https://doi.org/10.1088/1748-9326/6/4/045501

Behrenfeld, M. J., Hu, Y., Hostetler, C. A., Dall'Olmo, G., Rodier, S. D., Hair, J. W., & Trepte, C. R. (2013). Space-based lidar measurements of global ocean carbon stocks. *Geophysical Research Letters*, *40*, 4355–4360. https://doi.org/10.1002/grl.50816

Behrenfeld, M. J., Hu, Y., O'Malley, R. T., Boss, E. S., Hostetler, C. A., Siegel, D. A., et al. (2017). Annual boom-bust cycles of polar phytoplankton biomass revealed by space-based lidar. *Nature Geoscience*, *10*(2), 118–122. https://doi.org/10.1038/ngeo2861

Bélanger, S., Xie, H., Krotkov, N., Larouche, P., Vincent, W. F., & Babin, M. (2006). Photomineralization of terrigenous dissolved organic matter in Arctic coastal waters from 1979 to 2003: Interannual variability and implications of climate change. *Global Biogeochemical Cycles*, *20*, GB4005. https://doi.org/10.1029/2006GB002708

Bennartz, R., Shupe, M. D., Turner, D. D., Walden, V. P., Steffen, K., Cox, C. J., et al. (2013). July 2012 Greenland melt extent enhanced by low-level liquid clouds. *Nature*, *496*(7443), 83–86. https://doi.org/10.1038/nature12002

Bergamaschi, P., Frankenberg, C., Meirink, J. F., Krol, M., Dentener, F., Wagner, T., et al. (2007). Satellite chartography of atmospheric methane from SCIAMACHY on board ENVISAT: 2. Evaluation based on inverse model simulations. *Journal of Geophysical Research*, *112*(D2), D02304. https://doi.org/10.1029/2006JD007268

Berner, L. T., Beck, P. S. A., Loranty, M. M., Alexander, H. D., Mack, M. C., & Goetz, S. J. (2012). Cajander larch (Larix cajanderi) biomass distribution, fire regime and post-fire recovery in northeastern Siberia. *Biogeosciences*, *9*(10), 3943–3959. https://doi.org/10.5194/bg-9-3943-2012

Bernhard, G., Arola, A., Dahlback, A., Fioletov, V., Heikkilä, A., Johnsen, B., et al. (2015). Comparison of OMI UV observations with ground-based measurements at high northern latitudes. *Atmospheric Chemistry and Physics*, *15*, 7391–7412. https://doi.org/10.5194/acp-15-7391-2015

Bernhard, G., Booth, C. R., Ehramjian, J. C., Stone, R., & Dutton, E. G. (2007). Ultraviolet and visible radiation at Barrow, Alaska: Climatology and influencing factors on the basis of version 2 National Science Foundation network data. *Journal of Geophysical Research*, *112*(D9), D09101. https://doi.org/10.1029/2006JD007865

Bhatt, U. S., Walker, D. A., Walsh, J. E., Carmack, E. C., Frey, K. E., Meier, W. N., et al. (2014). Implications of Arctic Sea Ice Decline for the Earth System. *Annual Review of Environment and Resources*, *39*(1), 57–89. https://doi.org/10.1146/annurev-environ-122012-094357

Biancamaria, S., Lettenmaier, D. P., & Pavelsky, T. M. (2016). The SWOT Mission and Its Capabilities for Land Hydrology. In A. Cazenave, N. Champollion, J. Benveniste, & J. Chen (Eds.), *Remote Sensing and Water Resources*, *Space Sciences Series of ISSI* (Vol. 55, pp. 117–147). Cham: Springer. https://doi.org/10.1007/978-3-319-32449-4_6

Biskaborn, B. K., Smith, S. L., Noetzli, J., Matthes, H., Vieira, G., Streletskiy, D. A., et al. (2019). Permafrost is warming at a global scale. *Nature Communications*, *10*(1), 264. https://doi.org/10.1038/s41467-018-08240-4

Bjerke, J. W., Karlsen, S. R., Høgda, K. A., Malnes, E., Jepsen, J. U., Lovibond, S., et al. (2014). Record-low primary productivity and high plant damage in the Nordic Arctic Region in 2012 caused by multiple weather events and pest outbreaks. *Environmental Research Letters*, *9*(8), 8. https://doi.org/10.1088/1748-9326/9/8/084006

Bjerke, J. W., Treharne, R., Vikhamar-Schuler, D., Karlsen, S. R., Ravolainen, V., Bokhorst, S., et al. (2017). Understanding the drivers of extensive plant damage in boreal and Arctic ecosystems: Insights from field surveys in the aftermath of damage. *Science of the Total Environment*, *599-600*(599-600), 1965–1976. https://doi.org/10.1016/j.scitotenv.2017.05.050

Bliss, A. C., Miller, J. A., & Meier, W. N. (2017). Comparison of passive microwave-derived early melt onset records on Arctic sea ice. *Remote Sensing*, *9*(3), 199. https://doi.org/10.3390/rs9030199

Blockley, E. W., & Peterson, K. A. (2018). Improving Met Office seasonal predictions of Arctic sea ice using assimilation of CryoSat-2 thickness. *The Cryosphere*, *12*(11), 3419–3438. https://doi.org/10.5194/tc-12-3419-2018

Bloom, A. A., Lauvaux, T., Worden, J., Yadav, V., Duren, R., Sander, S. P., & Schimel, D. S. (2016). What are the greenhouse gas observing system requirements for reducing fundamental biogeochemical process uncertainty? Amazon wetland CH_4 emissions as a case study. *Atmospheric Chemistry and Physics*, *16*(23), 15,199–15,218. https://doi.org/10.5194/acp-16-15199-2016

Bloom, A. A., Palmer, P. I., Fraser, A., Reay, D. S., & Frankenberg, C. (2010). Large-scale controls of methanogenesis inferred from methane and gravity spaceborne data. *Science*, *327*, January 15(5963), 322–325. https://doi.org/10.1126/science.1175176

Boeke, R. C., & Taylor, P. C. (2018). Seasonal energy exchange in sea ice retreat regions contributes to differences in projected Arctic warming. *Nature Comminications*, *9*(1), 5017. https://doi.org/10.1038/s41467-018-07061-9

Bohn, T. J., Lettenmaier, D. P., Sathulur, K., Bowling, L. C., Podest, E., McDonald, K. C., & Friborg, T. (2007). Methane emissions from western Siberian wetlands: Heterogeneity and sensitivity to climate change. *Environmental Research Letters*, *2*(4), 045015 (9pp). https://doi.org/10.1088/1748-9326/2/4/045015

Bohn, T. J., Melton, J. R., Ito, A., Kleinen, T., Spahni, R., Stocker, B. D., et al. (2015). WETCHIMP-WSL: Intercomparison of wetland methane emissions models over West Siberia. *Biogeosciences*, *12*(11), 3321–3349. https://doi.org/10.5194/bg-12-3321-2015

Boisvert, L. N., Markus, T., & Vihma, T. (2013). Moisture flux changes and trends for the entire Arctic in 2003-2011 derived from EOS Aqua data. *Journal of Geophysical Research*, *118*(10), 5829–5843. https://doi.org/10.1002/jgrc.20414

Boisvert, L. N., Petty, A. A., & Stroeve, J. C. (2016). The Impact of the Extreme Winter 2015/16 Arctic Cyclone on the Barents–Kara Seas. *Monthly Weather Review*, *144*(11), 4279–4287. https://doi.org/10.1175/MWR-D-16-0234.1

Boisvert, L. N., & Stroeve, J. C. (2015). The Arctic is becoming warmer and wetter as revealed by the Atmospheric Infrared Sounder. *Geophysical Research Letters*, *42*, 4439–4446. https://doi.org/10.1002/2015GL063775

Boisvert, L. N., Wu, D. L., & Shie, C.-L. (2015). Increasing evaporation amounts seen in the Artic between 2003 and 2013 from AIRS data. *Journal of Geophysical Research*, *120*, 6865–6881. https://doi.org/10.1002/2015/JD023258

Borys, R. D. (1989). Studies of ice nucleation by Arctic aerosol on AGASP-II. *Journal of Atmospheric Chemistry*, *9*(1–3), 169–185. https://doi.org/10.1007/BF00052831

Bourassa, M. A., Gille, S. T., Bitz, C., Carlson, D., Cerovecki, I., Clayson, C. A., et al. (2013). High-Latitude Oceans and Sea Ice Surface Fluxes: Challenges for Climate Research. *Bulletin of the American Meteorological Society*, *94*(3), 403–423. https://doi.org/10.1175/BAMS-D-11-00244.1

Box, J. E., Colgan, W. T., Christensen, T. R., Schmidt, N. M., Lund, M., Parmentier, F.-J. W., et al. (2019). Key indicators of Arctic climate change: 1971-2017. *Environmental Research Letters*, *14*(4), 045010. https://doi.org/10.1088/1748-9326/aafc1b

Breider, T. J., Mickley, L. J., Jacob, D. J., Wang, Q., Fisher, J. A., Chang, R. Y.-W., & Alexander, B. (2014). Annual distributions and sources of Arctic aerosol components, aerosol optical depth, and aerosol absorption. *Journal of Geophysical Research: Atmospheres*, *119*, 4107–4124. https://doi.org/10.1002/2013JD020996

Brewer, M. C. (1958). Some results of geothermal investigations of permafrost. *American Geophysical Union Transactions*, *39*(1), 19–26. https://doi.org/10.1029/TR039i001p00019

Brigham, L. W. (2010). Think Again: The Arctic. *Foreign Policy*, September/October 2010 issue, 70–74.

Brown, J., Ferrians, O., Heginbottom, J. A., & Melnikov, E. (2002). *Circum-Arctic Map of Permafrost and Ground-Ice Conditions, Version 2. Boulder, Colorado USA*. NSIDC: National Snow and Ice Data Center.

Brown, R. D., & Robinson, D. A. (2011). Northern Hemisphere spring snow cover variability and change over 1922-2010 including an assessment of uncertainty. *The Cryosphere*, *5*(1), 219–229. https://doi.org/10.5194/tc-5-219-2011

Brucker, L., Dinnat, E. P., & Koenig, L. S. (2014a). Weekly gridded Aquarius L-band radiometer/scatterometer observations and salinity retrievals over the polar regions—Part 1: Product description. *Cryosphere*, *8*(3), 905–913. https://doi.org/10.5194/tc-8-905-2014

Brucker, L., Dinnat, E. P., & Koenig, L. S. (2014b). Weekly gridded Aquarius L-band radiometer/scatterometer observations and salinity retrievals over the polar regions-Part 2: Initial product analysis. *Cryosphere*, *8*(3), 915–930. https://doi.org/10.5194/tc-8-915-2014

Brucker, L., & Markus, T. (2013). Arctic-scale assessment of satellite passive microwave-derived snow depth on sea ice using Operation IceBridge airborne data. *Journal of Geophysical Research: Oceans*, *118*, 2892–2905. https://doi.org/10.1002/jgrc.20228

Buchwitz, M., Reuter, M., Schneising, O., Boesch, H., Guerlet, S., Dils, B., et al. (2015). The Greenhouse Gas Climate Change Initiative (GHG-CCI): Comparison and quality assessment of near-surface-sensitive satellite-derived CO_2 and CH_4 global data sets. *Remote Sensing of Environment.*, *162*, 344–362. https://doi.org/10.1016/j.rse.2013.04.024

Buermann, W., Bikash, P. R., Jung, M., Burn, D. H., & Reichstein, M. (2013). Earlier springs decrease peak summer productivity in North American boreal forests. *Environmental Research Letters*, *8*(2), 024027. https://doi.org/10.1088/1748-9326/8/2/024027

Butz, A., Guerlet, S., Hasekamp, O., Schepers, D., Galli, A., Aben, I., et al. (2011). Toward accurate CO_2 and CH_4 observations from GOSAT. *Geophysical Research Letters*, *38*, L14812. https://doi.org/10.1029/2011GL047888

Cabanes, C., Grouazel, A., von Schuckmann, K., Hamon, M., Turpin, V., Coatanoan, C., et al. (2013). The CORA dataset: Validation and diagnostics of in-situ ocean temperature and salinity measurements. *Ocean Science*, *9*(1), 1–18. https://doi.org/10.5194/os-9-1-2013

Cahoon, D. R. Jr., Stocks, B. J., Levine, J. S., Cofer, W. R. III, & O'neill, K. P. (1992). Seasonal distribution of African savanna fires. *Nature*, *359*(6398), 812–815. https://doi.org/10.1038/359812a0

Cahoon, S. M. P., Sullivan, P. F., Post, E., & Welker, J. M. (2012). Large herbivores limit CO_2 uptake and suppress carbon cycle responses to warming in west Greenland. *Global Change Biology*, *18*(2), 469–479. https://doi.org/10.1111/j.1365-2486.2011.02528.x

Callaghan, T. V., Björn, L. O., Chapin, F. S. III, Chernov, Y., Christensen, T. R., Huntley, B., et al. (2005). Arctic tundra and polar desert ecosystems. In C. Symon, L. Arris, & B. Heal (Eds.), *Arctic Climate Impact Assessment* (pp. 243–352). Cambridge: Cambridge University Press.

Callaghan, T. V., Crawford, R. M. M., Eronen, M., Hofgaard, A., Payette, S., Rees, W. G., et al. (2002). The dynamics of the tundra-taiga boundary: An overview and suggested coordinated and integrated approach to research. *Ambio*, 3–5.

Callaghan, T. V., Tweedie, C. E., & Webber, P. J. (2011). Multi-decadal changes in tundra environments and ecosystems: The International Polar Year-Back to the Future Project (IPY-BTF). *Ambio*, *40*(6), 705–716. https://doi.org/10.1007/s13280-011-0179-8

Carmack, E., Winsor, P., & Williams, W. (2015). The contiguous panarctic Riverine Coastal Domain: A unifying concept. *Progress in Oceanography*, *139*, 13–23. https://doi.org/10.1016/j.pocean.2015.07.014

Carmack, E. C., Yamamoto-Kawai, M., Haine, T. W. N., Bacon, S., Bluhm, B. A., Lique, C., et al. (2016). Freshwater and its role in the Arctic Marine System: Sources, disposition, storage, export, and physical and biogeochemical consequences in the Arctic and global oceans. *Journal Geophysical Research Biogeosciences*, *121*(3), 675–717. https://doi.org/10.1002/2015JG003140

Carroll, M., & Loboda, T. (2017). Multi-Decadal Surface Water Dynamics in North American Tundra. *Remote Sensing*, *9*(5), 497. https://doi.org/10.3390/rs9050497

Carroll, M., Wooten, M., DiMiceli, C., Sohlberg, R., & Kelly, M. (2016). Quantifying Surface Water Dynamics at 30 Meter Spatial Resolution in the North American High Northern Latitudes 1991–2011. *Remote Sensing*, *8*(8), 622. https://doi.org/10.3390/rs8080622

Carroll, M. L., Townshend, J. R., DiMiceli, C. M., Noojipady, P., & Sohlberg, R. A. (2009). A new global raster water mask at 250 m resolution. *International Journal of Digital Earth*, *2*(4), 291–308. https://doi.org/10.1080/17538940902951401

Casey, K. A., Polashenski, C. M., Chen, J., & Tedesco, M. (2017). Impact of MODIS sensor calibration updates on Greenland Ice Sheetsurface reflectance and albedo trends. *The Cryosphere*, *11*(4), 1781–1795. https://doi.org/10.5194/tc-11-1781-2017

Cayan, D. R., Dettinger, M. D., Kammerdiener, S. A., Caprio, J. M., & Peterson, D. H. (2001). Changes in the onset of spring in the western United States. *Bulletin of the American Meteorological Society*, *82*(3), 399–415. https://doi.org/10.1175/1520-0477(2001)082<0399:CITOOS>2.3.CO;2

CEOS-ACC (2011). A Geostationary Satellite Constellation for Observing Global Air Quality: An International Path Forward. http://ceos.org/document_management/Virtual_Constellations/ACC/Documents/AC-VC_Geostationary-Cx-for-Global-AQ-final_Apr2011.pdf.

Chahine, M. T., Chen, L., Dimotakis, P., Jiang, X., Li, Q., Olsen, E. T., et al. (2008). Satellite remote sounding of mid-tropospheric CO_2. *Geophysical Research Letters*, *35*, L17807. https://doi.org/10.1029/2008GL035022

Chang, A. T. C., Foster, J. L., & Hall, D. K. (1987). Nimbus-7 SMMR derived global snow cover parameters. *Annals of Glaciology*, *9*, 9–44.

Chaves, J. E., Werdell, P. J., Proctor, C. W., Neeley, A. R., Freeman, S. A., Thomas, C. S., & Hooker, S. B. (2015). Assessment of ocean color data records from MODIS-Aqua in the western Arctic Ocean. *Deep Sea Research Part II: Topical Studies in Oceanography*, *118*, 32–43. https://doi.org/10.1016/j.dsr2.2015.02.011

Chen, H. Y. H., & Luo, Y. (2015). Net aboveground biomass declines of four major forest types with forest ageing and climate change in western Canada's boreal forests. *Global Change Biology*, *21*(10), 3675–3684. https://doi.org/10.1111/gcb.12994

Chen, W., Jiang, H., Moriya, K., Sakai, T., & Cao, C. (2018). Monitoring of post-fire forest regeneration under different restoration treatments based on ALOS/PALSAR data. *New Forests*, *49*(1), 105–121. https://doi.org/10.1007/s11056-017-9608-2

Chepurin, G. A., & Carton, J. A. (2012). Subarctic and Arctic sea surface temperature and its relation to ocean heat content 1982-2010. *Journal of Geophysical Research*, *117*(C6), C06019. https://doi.org/10.1029/2011JC007770

Chevallier, F., Palmer, P. I., Feng, L., Boesch, H., O'Dell, C. W., & Bousquet, P. (2014). Toward robust and consistent regional CO_2 flux estimates from in situ and spaceborne measurements of atmospheric CO_2. *Geophysical Research Letters*, *41*, 1065–1070. https://doi.org/10.1002/2013GL058772

Chimitdorzhiev, T. N., Dagurov, P. N., Bykov, M. E., Dmitriev, A. V., & Kirbizhekova, I. I. (2016). Comparison of ALOS PALSAR interferometry and field geodetic leveling for marshy soil thaw/freeze monitoring, case study from Baikal lake region, Russia. *Journal of Applied Remote Sensing*, *10*(1), 016006. https://doi.org/10.1117/1.JRS.10.016006

Churnside, J. H. (2014). Review of profiling oceanographic lidar. *Optical Engineering*, *53*(5), 051405. https://doi.org/10.1117/1.OE.53.5.051405

Ciais, P., Sabine, C., Bala, G., Bopp, L., Brovkin, V., Canadell, J., et al. (2013). Carbon and Other Biogeochemical Cycles. In: *Climate Change 2013: The Physical Science Basis. Contribution of Working Group I to the Fifth Assessment Report of the Intergovernmental Panel on Climate Change* (Stocker, T.F., D. Qin, G.-K. Plattner, M. Tignor, S.K. Allen, J. Boschung, A. Nauels, Y. Xia, V. Bex & P.M. Midgley (eds.)). Cambridge University Press, Cambridge, United Kingdom and New York, NY, USA.

Clarke, A. D., & Noone, K. J. (1985). Soot In The Arctic Snowpack—A Cause For Perturbations In Radiative-Transfer. *Atmospheric Environment*, *19*(12), 2045–2053. https://doi.org/10.1016/0004-6981(85)90113-1

Claverie, M., Masek, J. G., Junchang, J., & Dungan, J. L. (2017). Harmonized Landsat-8 Sentinel-2 (HLS) Product User's Guide, *version 1.3*. Retrieved from http://hls.gsfc.nasa.gov/

Clewley, D., Whitcomb, J., Moghaddam, M., & McDonald, K. (2015). In R. Tiner, M. Lang, & V. Klemas (Eds.), *"Mapping the State and Dynamics of Boreal Wetlands using Synthetic Aperture Radar," in Remote Sensing of Wetlands: Applications and Advances*. Boca Raton, FL: CRC Press, March 2015. ISBN: 9781482237382.

Clewley, D., Whitcomb, J., Moghaddam, M., McDonald, K., Chapman, B., & Bunting, P. (2015). Evaluation of ALOS PALSAR Data for High-Resolution Mapping of Vegetated Wetlands in Alaska. *Remote Sensing*, *7*(6), 7272–7297. https://doi.org/10.3390/rs70607272

Coen, J. L., & Schroeder, W. (2013). Use of spatially refined satellite remote sensing fire detection data to initialize and evaluate coupled weather-wildfire growth model simulations. *Geophysical Research Letters*, *40*, 5536–5541. https://doi.org/10.1002/2013GL057868

Cohen, J., Screen, J. A., Furtado, J. C., Barlow, M., Whittleston, D., Coumou, D., et al. (2014). Recent Arctic amplification and extreme mid-latitude weather. *Nature Geoscience*, *7*(9), 627–637. https://doi.org/10.1038/ngeo2234

Cole, J. J., Prairie, Y. T., Caraco, N. F., McDowell, W. H., Tranvik, L. J., Striegl, R. G., et al. (2007). Plumbing the global carbon cycle: Integrating inland waters into the terrestrial carbon budget. *Ecosystems*, *10*(1), 172–185. https://doi.org/10.1007/s10021-006-9013-8

Colliander, A., Jackson, T. J., Bindlish, R., Chan, S., Das, N., Kim, S. B., et al. (2017). Validation of SMAP surface soil moisture products with core validation sites. *Remote Sensing of Environment*, *191*, 215–231. https://doi.org/10.1016/j.rse.2017.01.021

Colliander, A., McDonald, K., Zimmermann, R., Schroeder, R., Kimball, J. S., & Njoku, E. G. (2012). Application of QuikSCAT Backscatter to SMAP Validation Planning: Freeze/Thaw State Over ALECTRA Sites in Alaska From 2000 to 2007, (2012). *IEEE Transactions on Geoscience and Remote Sensing*, *50*(2), 461–468. https://doi.org/10.1109/TGRS.2011.2174368

Comiso, J. C. (2003). Warming trends in the Arctic from clear sky satellite observations. *Journal of Climate*, *16*(21), 3498–3510. https://doi.org/10.1175/1520-0442(2003)016<3498:WTITAF>2.0.CO;2

Comiso, J. C., Gersten, R., Stock, L., Turner, J., Perez, G. J., & Cho, K. (2017). Positive trends in the Antarctic sea ice cover and associated changes in surface temperature. *Journal of Climate*, *30*(6), 2251–2267. https://doi.org/10.1175/JCLI-D-16-0408.1

Comiso, J. C., & Hall, D. K. (2014). Climate trends in the Arctic as observed from space. *WIREs Climate Change*, *5*(3), 389–409. https://doi.org/10.1002/wcc.277

Comiso, J. C., Parkinson, C. L., Gersten, R., & Stock, L. (2008). Accelerated decline in the Arctic sea ice cover. *Geophysical Research Letters*, *35*, L01703. https://doi.org/10.1029/2007GL031972

Commane, R., Lindaas, J., Benmergui, J., Luus, K. A., Chang, R. Y.-W., Daube, B. C., et al. (2017). Carbon dioxide sources from Alaska driven by increasing early winter respiration from Arctic tundra. *Proceedings of the National Academy of Sciences*, *114*(21), 5361–5366. https://doi.org/10.1073/pnas.1618567114

Cooley, S., Smith, L., Stepan, L., & Mascaro, J. (2017). Tracking Dynamic Northern Surface Water Changes with High-Frequency Planet CubeSat Imagery. *Remote Sensing*, *9*(12), 1306. https://doi.org/10.3390/rs9121306

Cooper, M. D. A., Estop-Aragonés, C., Fisher, J. P., Thierry, A., Garnett, M. H., Charman, D. J., et al. (2017). Limited contribution of permafrost carbon to methane release from thawing peatlands. *Nature Climate Change*, *7*(7), 507–511. https://doi.org/10.1038/NCLIMATE3328

Corbett, J. J., Lack, D. A., Winebrake, J. J., Harder, S., Silberman, J. A., & Gold, M. (2010). Arctic shipping emissions inventories and future scenarios. *Atmospheric Chemistry and Physics*, *10*(19), 9689–9704. https://doi.org/10.5194/acp-10-9689-2010

Cowardin, L. M., V. Carter, F. C. Golet, & E. T. LaRoe (1979). *Classification of wetlands and deepwater habitat of the United States*. in U. S. F. A. W. Service, editor., Washington, DC: U. S. Department of the Interior, Fish and Wildlife Service.

Crevoisier, C., Nobileau, D., Fiore, A. M., Armante, R., Chédin, A., & Scott, N. A. (2009). Tropospheric methane in the tropics – first year from IASI hyperspectral infrared observations. *Atmospheric Chemistry Physics*, *9*(17), 6337–6350. https://doi.org/10.5194/acp-9-6337-2009

Crisp, D., Meijer, Y., Munro, R., Bowman, K., Chatterjee, A., Baker, D., ... & Zehner, C. (2018). A Constellation Architecture for Monitoring Carbon Dioxide and Methane from Space. http://ceos.org/document_management/Virtual_Constellations/ACC/Documents/CEOS_AC-VC_GHG_White_Paper_Version_1_20181009.pdf.

Crowell, S. M. R., Kawa, S. R., Browell, E. V., Hammerling, D. M., Moore, B., Schaefer, K., & Doney, S. C. (2018). On the ability of space-based passive and active remote sensing observations of CO_2 to detect flux perturbations to the carbon cycle. *Journal of Geophysical Research: Atmospheres*, *123*(2), 1460–1477. https://doi.org/10.1002/2017JD027836

Csatho, B. M., Schenk, A. F., van der Veen, C. J., Babonis, G., Duncan, K., Rezvanbehbahani, S., et al. (2014). Laser altimetry reveals complex pattern of Greenland ice sheet dynamics. *Proceedings of the National Academy of Sciences*, *111*(52), 18478–18483. https://doi.org/10.1073/pnas.1411680112

Cullather, R. I., Lim, Y.-K., Boisvert, L. N., Brucker, L., Lee, J. N., & Nowicki, S. M. J. (2016). Analysis of the warmest Arctic winter, 2015–2016. *Geophysical Research Letters*, *43*, 10,808–10,816. https://doi.org/10.1002/2016GL071228

Cullather, R. I., Nowicki, S. M. J., Zhao, B., & Koenig, L. S. (2016). A Characterization of Greenland Ice Sheet Surface Melt and Runoff in Contemporary Reanalyses and a Regional Climate Model. *Frontiers in Earth Science*, *4*. https://doi.org//10.3389/feart.2016.00010

Curry, J. A., Bentamy, A., Bourassa, M. A., Bourras, D., Bradley, E. F., Brunke, M., et al. (2004). SEAFLUX. *Bulletin of the American Meteorological Society*, *85*(3), 409–424. https://doi.org/10.1175/BAMS-85-3-409

Curry, J. A., & Ebert, E. E. (1992). Annual cycle of radiation fluxes over the Arctic Ocean: Sensitivity to cloud optical properties. *Journal of Climate*, *5*(11), 1267–1280. https://doi.org/10.1175/1520-0442(1992)005<1267:ACORFO>2.0.CO;2

Curry, J. A., Rossow, W. B., Randall, D., & Schramm, J. L. (1996). Overview of Arctic cloud and radiation characteristics. *Journal of Climate*, *9*(8), 1731–1764. https://doi.org/10.1175/1520-0442(1996)009<1731:OOACAR>2.0.CO;2

Dahlman, L. (2018): Climate Change: Spring Snow Cover. https://www.climate.gov/news-features/understanding-climate/climate-change-spring-snow-cover.

Damoah, R., Spichtinger, N., Forster, C., James, P., Mattis, I., Wandinger, U., et al. (2004). Around the world in 17 days—Hemispheric-scale transport of forest fire smoke from Russia in May 2003. *Atmospheric Chemistry and Physics*, *4*(5), 1311–1321. https://doi.org/10.5194/acp-4-1311-2004

Dash, P., Ignatov, A., Martin, M., Donlon, C., Brasnett, B., Reynolds, R. W., et al. (2012). Group for High Resolution Sea Surface Temperature (GHRSST) analysis fields inter-comparisons-Part 2: Near real time web-based level 4 SST Quality Monitor (L4-SQUAM). *Deep-Research. Part II: Topical Studies in Oceanography*, *77-80*, 31–43. https://doi.org/10.1016/j.dsr2.2012.04.002

Davidson, J. S., Santos, J. M., Sloan, L. V., Reuss-Schmidt, K., Phoenix, K. G., Oechel, C. W., & Zona, D. (2017). Upscaling CH_4 Fluxes Using High-Resolution Imagery in Arctic Tundra Ecosystems. *Remote Sensing*, *9*(12), 1227. https://doi.org/10.3390/rs9121227

Delbart, N., Kergoat, L., Le Toan, T., Lhermitte, J., & Picard, G. (2005). Determination of phenological dates in boreal regions using a normalized difference water index. *Remote Sensing of Environment*, *97*(1), 26–38. https://doi.org/10.1016/j.rse.2005.03.011

Derksen, C., & Brown, R. (2012). Spring snow cover extent reductions in the 2008–2012 period exceeding climate projections. *Geophysical Research Letters*, *39*, L19504. https://doi.org/10.1029/2012GL053387

Derksen, C., Walker, A., & Goodison, B. (2005). Evaluation of passive microwave snow water equivalent retrievals across the boreal forest/tundra transition of western Canada. *Remote Sensing of Environment*, *96*(3-4), 315–327. https://doi.org/10.1016/j.rse.2005.02.014

Derksen, C., Xu, X., Dunbar, R. S., Colliander, A., Kim, Y., Kimball, J. S., et al. (2017). Retrieving landscape freeze/thaw state from Soil Moisture Active Passive (SMAP) radar and radiometer measurements. *Remote Sensing of Environment*, *194*, 48–62. https://doi.org/10.1016/j.rse.2017.03.007

Déry, S. J., & Brown, R. D. (2007). Northern Hemisphere snow cover extent trends and implications for the snow-albedo feedback. *Geophysical Research Letters*, *34*, L22504. https://doi.org/10.1029/2007GL031474

Dettinger, M. D., Cayan, D. R., Meyer, M., & Jeton, A. E. (2004). Simulated hydrologic responses to climate variations and change in the Merced, Carson, and American River basins, Sierra Nevada, California, 1900–2099. *Climatic Change*, *62*(1-3), 283–317. https://doi.org/10.1023/B:CLIM.0000013683.13346.4f

Devred E., Tzortziou, M., Hirawake, T., Mannino, A., & Reynolds, R. (2015). "Ocean colour remote sensing in high latitudes areas," Workshop Report, International Ocean Colour Science Conference, 2015.

Di Pierro, M., Jaegle, L., Eloranta, E. W., & Sharma, S. (2013). Spatial and seasonal distribution of Arctic aerosols observed by the CALIOP satellite instrument (2006–2012). *Atmospheric Chemistry and Physics*, *13*(14), 7075–7095. https://doi.org/10.5194/acp-13-7075-2013

Dickson, B. (2006). The integrated Arctic Ocean Observing System (iAOOS): An AOSB-CliC Observing Plan for the International Polar Year. *Oceanologia*, *48*(1), 5–21. https://doi.org/10.1117/12.536820

Dickson, R. R. (2007). *The integrated Arctic Ocean Observing System (iAOOS) in 2007*. Arctic Ocean Sciences Board. https://www.arcus.org/files/page/documents/19695/iaoos_document.pdf

Dinnat, E. P., & Brucker, L. (2017). Improved sea ice fraction characterization for L-band observations by the Aquarius radiometers. *IEEE Transactions on Geoscience and Remote Sensing*, *55*(3), 1285–1304. https://doi.org/10.1109/TGRS.2016.2622011

Dlugokencky, E.J., Lang, P.M., Masarie, K.A., Crotwell, A.M., & Crotwell, M.J. (2015). Atmospheric Carbon Dioxide Dry Air Mole Fractions from the NOAA ESRL Carbon Cycle Cooperative Global Air Sampling Network, 1968-2014, Version: 2015-08-03, ftp://aftp.cmdl.noaa.gov/data/trace_gases/co2/flask/surface/.

Dobson, M. C., Pierce, L. E., & Ulaby, F. T. (1996). Knowledge-based land-cover classification using ERS-1/JERS-1 SAR composites. *IEEE Transactions on Geoscience and Remote Sensing*, *34*(1), 83–99. https://doi.org/10.1109/36.481896

Doherty, S. J., Warren, S. G., Grenfell, T. C., Clarke, A. D., & Brandt, R. E. (2010). Light-absorbing impurities in Arctic snow. *Atmospheric Chemistry and Physics*, *10*(23), 11647–11680. https://doi.org/10.5194/acp-10-11647-2010

Donlon, C. J., Martin, M., Stark, J., Roberts-Jones, J., Fiedler, E., & Wimmer, W. (2012). The Operational Sea Surface Temperature and Sea Ice Analysis (OSTIA) system. *Remote Sensing of Environment*, *116*, 140–158. https://doi.org/10.1016/j.rse.2010.10.017

Dorigo, W. A., Wagner, W., Albergel, C., Albrecht, F., Balsamo, G., Brocca, L., et al. (2017). ESA CCI soil moisture for improved Earth system understanding: State-of-the art and futuredirections. *Remote Sensing of Environment*, *203*, 185–215. https://doi.org/10.1016/j.rse.2017.07.001

Dozier, J. (1989). Spectral signature of alpine snow cover from the Landsat thematic mapper. *Remote Sensing of Environment*, *28*(1), 9–22. https://doi.org/10.1016/0034-4257(89)90101-6

Dozier, J., & Marks, D. (1987). Snow mapping and classification from Landsat Thematic Mapper data. *Annals of Glaciology*, *9*, 1–7.

Driemel, A., Fahrbach, E., Rohardt, G., Beszczynska-Möller, A., Boetius, A., Budéus, G., et al. (2017). From pole to pole: 33 years of physical oceanography onboard R/V Polarstern. *Earth System Science Data*, *9*(1), 211–220. https://doi.org/10.5194/essd-9-211-2017

Du, J., Kimball, J. S., Azarderakhsh, M., Dunbar, R. S., Moghaddam, M., & McDonald, K. C. (2015). Classification of Alaska spring thaw characteristics using satellite L-band radar remote sensing. *IEEE Transactions on Geoscience and Remote Sensing*, *53*, 542–556.

Du, J., Kimball, J. S., & Jones, L. A. (2016). Passive microwave remote sensing of soil moisture based on dynamic vegetation scattering properties of AMSR-E. *IEEE Transactions on Geoscience and Remote Sensing*, *54*(1), 597–608. https://doi.org/10.1109/TGRS.2015.2462758

Du, J., Kimball, J. S., Jones, L. A., Kim, Y., Glassy, J., & Watts, J. D. (2017). A global satellite environmental data record derived from AMSR-E and AMSR2 microwave Earth observations. *Earth System Science Data*, *9*(2), 791–808. https://doi.org/10.5194/essd-9-791-2017

Du, J., Kimball, J. S., Jones, L. A., & Watts, J. D. (2016). Implementation of satellite based fractional water cover indices in the pan-Arctic region using AMSR-E and MODIS. *Remote Sensing of Environment*, *184*, 469–481. https://doi.org/10.1016/j.rse.2016.07.029

Du, J., Kimball, J. S., & Moghaddam, M. (2015). Theoretical modeling and analysis of L- and P-band radar backscatter sensitivity to soil active layer dielectric variations. *Remote Sensing*, *7*(7), 9450–9472. https://doi.org/10.3390/rs70709450

Duffy, P. A., Walsh, J. E., Graham, J. M., Mann, D. H., & Rupp, T. S. (2005). Impacts Of Large-Scale Atmospheric–Ocean Variability On Alaskan Fire Season Severity. *Ecological Applications*, *15*(4), 1317–1330. https://doi.org/10.1890/04-0739

Dunbar, S., Xu, X., Colliander, A., McDonald, K., Podest, E., Njoku, E., et al. (2015). Soil Moisture Active Passive (SMAP) L3 Radar Freeze/Thaw (Active) Algorithm Theoretical Basis Document. Release v3.2. Jet Propulsion Laboratory Technical Document. 56 Pages.

Duncan, B. N., & Bey, I. (2004). A Modeling Study of the Export Pathways of Pollution from Europe: Seasonal and Interannual Variations (1987-1997). *Journal of Geophysical Research*, *109*(D8), D08301. https://doi.org/10.1029/2003JD004079

Duncan, B. N., Lamsal, L. N., Thompson, A. M., Yoshida, Y., Lu, Z., Streets, D. G., et al. (2016). A space-based, high-resolution view of notable changes in urban NO_x pollution around the world (2005-2014). *Journal Geophysical Research*, *121*(2), 976–996. https://doi.org/10.1002/2015JD024121

Duncan, B. N., & Logan, J. A. (2008). Model analysis of the factors regulating the trends of carbon monoxide, 1988-1997. *Atmospheric Chemistry and Physics*, *8*(24), 7389–7403. https://doi.org/10.5194/acp-8-7389-2008

Duncan, B. N., Prados, A. I., Lamsal, L., Liu, Y., Streets, D., Gupta, P., et al. (2014). Satellite Data of Atmospheric Pollution for U.S. Air Quality Applications: Examples of Applications, Summary of Data End-User Resources, Answers to FAQs, and Common Mistakes to Avoid. *Atmospheric Environment*, *94*, 647–662. https://doi.org/10.1016/j.atmosenv.2014.05.061

Eastman, R., & Warren, S. G. (2010a). Interannual variations of arctic cloud types in relation to sea ice. *Journal of Climate*, *23*(15), 4216–4232. https://doi.org/10.1175/2010JCLI3492.1

Eastman, R., & Warren, S. G. (2010b). Arctic cloud changes from surface and satellite observations. *Journal of Climate*, *23*(15), 4233–4242. https://doi.org/10.1175/2010JCLI3544.1

Eckhardt, S., Stohl, A., Beirle, S., Spichtinger, N., James, P., Forster, C., et al. (2003). The North Atlantic Oscillation controls air pollution transport to the Arctic. *Atmospheric Chemistry and Physics*, *3*(5), 1769–1778. https://doi.org/10.5194/acp-3-1769-2003

Eckhardt, S., Stohl, A., Wernli, H., James, P., Forster, C., & Spichtinger, N. (2004). A 15-Year Climatology of Warm Conveyor Belts. *Journal of Climate*, *17*(1), 218–237. https://doi.org/10.1175/1520-0442(2004)017<0218:AYCOWC>2.0.CO;2

Ehret, G., Bousquet, P., Pierangelo, C., Alpers, M., Millet, B., Abshire, J. B., et al. (2017). MERLIN: A French-German Space Lidar Mission Dedicated to Atmospheric Methane. *Remote Sensing*, *9*(10), 1052. https://doi.org/10.3390/rs9101052

Eldering, A., O'Dell, C. W., Wennberg, P. O., Crisp, D., Gunson, M. R., Viatte, C., et al. (2017). The Orbiting Carbon Observatory-2: First 18 months of science data products. *Atmospheric Measurement Techniques*, *10*(2), 549–563. https://doi.org/10.5194/amt-10-549-2017

Eldering, A., Taylor, T. E., O'Dell, C. W., & Pavlick, R. (2018). The OCO-3 mission; measurement objectives and expected performance based on one year of simulated data. *Atmospheric Measurement Techniques Discussions.*. https://doi.org/10.5194/amt-2018-357

Eldering, A., Wennberg, P. O., Crisp, D., Schimel, D. S., Gunson, M. R., Chatterjee, A., et al. (2017). The Orbiting Carbon Observatory-2 early science investigations of regional carbon dioxide fluxes. *Science*, *358*(6360), eaam5745. https://doi.org/10.1126/science.aam5745

Elmendorf, S. C., Henry, G. H. R., Hollister, R. D., Bjork, R. G., Bjorkman, A. D., Callaghan, T. V., et al. (2012a). Global assessment of experimental climate warming on tundra vegetation: Heterogeneity over space and time. *Ecology Letters*, *15*(2), 164–175. https://doi.org/10.1111/j.1461-0248.2011.01716.x

Elmendorf, S. C., Henry, G. H. R., Hollister, R. D., Bjork, R. G., Boulanger-Lapointe, N., Cooper, E. J., et al. (2012b). Plot-scale evidence of tundra vegetation change and links to recent summer warming. *Nature Climate Change*, *2*(6), 453–457. https://doi.org/10.1038/NCLIMATE1465

Enderlin, E. M., Howat, I. M., Jeong, S., Noh, M. J., Angelen, J. H., & van den Broeke, M. R. (2014). An improved mass budget for the Greenland ice sheet. *Geophysical Research Letters*, *41*, 866–872. https://doi.org/10.1002/2013GL059010

Engdahl, M. E., & Hyyppa, J. M. (2003). Land-cover classification using multitemporal ERS-1/2 InSAR data. *IEEE Transactions on Geoscience and Remote Sensing*, *41*(7), 1620–1628. https://doi.org/10.1109/TGRS.2003.813271

Estilow, T., Young, A. H., & Robinson, D. R. (2015). A long-term Northern Hemisphere snow cover extent data record for climate studies and monitoring. *Earth System Science Data*, *7*(1), 137–142. https://doi.org/10.5194/essd-7-137-2015

Fahnestock, M., Scambos, T., Moon, T., Gardner, A., Haran, T., & Klinger, M. (2016). Rapid large-area mapping of ice flow using Landsat 8. *Remote Sensing of Environment*, *185*(2016), 84–94, ISSN 0034-4257. https://doi.org/10.1016/j.rse.2015.11.023

Farman, J. C., Gardiner, B. G., & Shanklin, J. D. (1985). Large losses of total ozone in Antarctica reveal seasonal ClO_x/NO_x interaction. *Nature*, *315*(6016), 207–210. https://doi.org/10.1038/315207a0

Fedorov, A., Barreiro, M., Boccaletti, G., Pacanowski, R., & Philander, S. G. (2007). The Freshening of Surface Waters in High Latitudes: Effects on the Thermohaline and Wind-Driven Circulations. *Journal of Physical Oceanography*, *37*(4), 896–907. https://doi.org/10.1175/JPO3033.1

Fenty, I., Willis, J. K., Khazendar, A., Dinardo, S., Forsberg, R., Fukumori, I., et al. (2016). Oceans Melting Greenland: Early results from NASA's ocean-ice mission in Greenland. *Oceanography*, *29*(4), 72–83. https://doi.org/10.5670/oceanog.2016.100

Fettweis, X., Box, J. E., Agosta, C., Amory, C., Kittel, C., Lang, C., et al. (2017). Reconstructions of the 1900–2015 Greenland ice sheet surface mass balance using the regional climate MAR model. *The Cryosphere*, *11*(2), 1015–1033. https://doi.org/10.5194/tc-11-1015-2017

Fichefet, T., Poncin, C., Goosse, H., Huybrechts, P., Janssens, I., & Le Treut, H. (2003). Implications of changes in freshwater flux from the Greenland ice sheet for the climate of the 21st century. *Geophysical Research Letters*, *30*(17), 1911. https://doi.org/10.1029/2003GL017826

Fichot, C. G., Kaiser, K., Hooker, S. B., Amon, R. M. W., Babin, M., Bélanger, S., et al. (2013). Pan-Arctic distributions of continental runoff in the Arctic Ocean. *Nature: Scientific Reports*, *3*(1), 1053. https://doi.org/10.1038/srep01053

Fisher, J. A., Jacob, D. J., Purdy, M. T., Kopacz, M., Le Sager, P., Carouge, C., et al. (2010). Source attribution and interannual variability of Arctic pollution in spring constrained by aircraft (ARCTAS, ARCPAC) and satellite (AIRS) observations of carbon monoxide. *Atmospheric Chemistry and Physics*, *10*(3), 977–996. https://doi.org/10.5194/acp-10-977-2010

Flannigan, M., Cantin, A. S., deGroot, W. J., Wotton, M., Newbery, A., & Gowman, L. M. (2013). Global wildland fire season severity in the 21st century. *Forest Ecology and Management*, *294*, 54–61. https://doi.org/10.1016/j.foreco.2012.10.022

Flannigan, M. D., Cambell, I., Wotton,B. M., Carcaillet, C., Richard, P., & Bergeron, Y. (2001). Future fire in Canada's boreal forest: Paleoecology results and General Circulation Model-Regional Climate Model simulations. *Canadian Journal of Forest Research*, *31*, 854–864. https://doi.org/810.1139/x1101-1010

Flannigan, M. D., Krawchuk, M. A., de Groot, W. J., Wotton, B. M., & Gowman, L. M. (2009). Implications of changing climate for global wildland fire. *International Journal of Wildland Fire*, *18*(5), 483–507. https://doi.org/10.1071/WF08187

Flato, G., Marotzke, J., Abiodun, B., Braconnot, P., Chou, S. C., Collins, W., et al. (2013). In T. F. Stocker, D. Qin, G.-K. Plattner, M. Tignor, S. K. Allen, J. Boschung, A. Nauels, Y. Xia, V. Bex, & P. M. Midgley (Eds.), *Evaluation of Climate Models. In: Climate Change 2013: The Physical Science Basis. Contribution of Working Group I to the Fifth Assessment Report of the Intergovernmental Panel on Climate Change*. Cambridge, United Kingdom and New York, NY, USA: Cambridge University Press.

Forbes, B. C. (2013). Tundra biome. In D. Gibson (Ed.), *Oxford Bibliographies in Ecology*. New York: Oxford University Press. https://doi.org/10.1093/obo/9780199830060-0097

Forbes, B. C., & Kumpula, T. (2009). The ecological role and geography of reindeer (Rangifer tarandus) in northern Eurasia. *Geography Compass*, *3*(4), 1356–1380. https://doi.org/10.1111/j.1749-8198.2009.00250.x

Forbes, B. C., Kumpula, T., Meschtyb, N., Laptander, R., Macias-Fauria, M., Zetterberg, P., et al. (2016). Sea ice, rain-on-snow and tundra reindeer nomadism in Arctic Russia. *Biology Letters*, *12*(11), 20160466. https://doi.org/10.1098/rsbl.2016.0466

Forster, R. R., Box, J. E., van den Broeke, M. R., Miège, C., Burgess, E. W., van Angelen, J. H., et al. (2014). Extensive liquid meltwater storage in firn within the Greenland ice sheet. *Nature Geoscience*, *7*(2), 95–98. https://doi.org/10.1038/ngeo2043

Foster, J. L. (1989). The significance of the date of snow disappearance on the arctic tundra as a possible indicator of climate change. *Arctic and Alpine Research*, *21*(1), 60–70. https://doi.org/10.2307/1551517

Foster, J. L., Sun, C., Walker, J. P., Kelly, R., Chang, A., Dong, J., & Powell, H. (2005). Quantifying the uncertainty in passive microwave snow water equivalent observations. *Remote Sensing of Environment*, *94*(2), 187–203. https://doi.org/10.1016/j.rse.2004.09.012

Foster, J. L., Winchester, J. W., & Dutton, E. G. (1992). The date of snow disappearance on the Arctic Tundra as determined from satellite, meteorological Station and Radiometric In situ Observations. *IEEE Transactions on Geoscience and Remote Sensing*, *30*(4), 793–798. https://doi.org/10.1109/36.158874

Fountoulakis, I., Bais, A. F., Tourpali, K., Fragkos, K., & Misios, S. (2014). Projected changes in solar UV radiation in the Arctic and sub-Arctic Oceans: Effects from changes in reflectivity, ice transmittance, clouds, and ozone. *Journal of Geophysical Research: Atmospheres*, *119*, 8073–8090. https://doi.org/10.1002/2014JD021918

Frajka-Williams, E., Bamber, J. L., & Våge, K. (2016). Greenland melt and the Atlantic meridional overturning circulation. *Oceanography*, *29*(4), 22–33. https://doi.org/10.5670/oceanog.2016.96

Francis, J. A., & Vavrus, S. J. (2015). Evidence for a wavier jet stream in response to rapid Arctic warming. *Environmental Research Letters*, *10*(1), 014005. https://doi.org/10.1088/1748-9326/10/1/014005

Frankenberg, C., Aben, I., Bergamaschi, P., Dlugokencky, E. J., van Hees, R., Houweling, S., et al. (2011). Globe column-averaged methane mixing ratios from 2003 to 2009 as derived from SCIAMACHY: Trends and variability. *Journal of Geophysical Research*, *116*, D04302. https://doi.org/10.1029/2010D014849

Frankenberg, C., Fisher, J. B., Worden, J., Badgley, G., Saatchi, S. S., Lee, J.-E., et al. (2011). New global observations of the terrestrial carbon cycle from GOSAT: Patterns of plant fluorescence with gross primary productivity. *Geophysical Research Letters*, *38*, L17706. https://doi.org/10.1029/2011GL048738

Fratantoni, P. S., & Pickart, R. S. (2007). The Western North Atlantic Shelfbreak Current System in Summer. *Journal of Physical Oceanography*, *37*(10), 2509–2533. https://doi.org/10.1175/JPO3123.1

Frei, A., & Robinson, D. A. (1999). Northern hemisphere snow extent—Regional variability 1972–1994. *International Journal of Climatology*, *19*(14), 1535–1560. https://doi.org/10.1002/(SICI)1097-0088(19991130)19:14<1535::AID-JOC438>3.0.CO;2-J

Frei, A., Tedesco, M., Lee, S., Foster, J., Hall, D., Kelly, R., & Robinson, R. (2012). A review of global satellite-derived snow products. *Advances in Space Research*, *50*(8), 1007–1029. https://doi.org/10.1016/j.src.2011.12.021

Frey, K., & Smith, L. (2007). How well do we know northern land cover? Comparison of four global vegetation and wetland products with a new ground-truth database for West Siberia. *Global Biogeochemical Cycles*, *21*, GB1016. https://doi.org/10.1029/2006GB002706

Frey, R. A., Ackerman, S. A., Liu, Y., Strabala, K. I., Zhang, H., Key, J. R., & Wang, X. (2008). Cloud Detection with MODIS. Part I: Improvements in the MODIS Cloud Mask for Collection 5. *Journal of Atmospheric and Oceanic Technology*, *25*(7), 1057–1072. https://doi.org/10.1175/2008JTECHA1052.1

Friedl, M. A., Sulla-Menashe, D., Tan, B., Schneider, A., Ramankutty, N., Sibley, A., & Huang, X. (2010). MODIS Collection 5 Global Land Cover: Algorithm refinements and characterization of new datasets. *Remote Sensing of Environment*, *114*(1), 168–182. https://doi.org/10.1016/j.rse.2009.08.016

Fromm, M., Alfred, J., Hoppel, K., Hornstein, J., Bevilacqua, R., Shettle, E., et al. (2000). Observations of boreal forest fire smoke in the stratosphere by POAM III, SAGE II, and lidar in 1998. *Geophysical Research Letters*, *27*(9), 1407–1410. https://doi.org/10.1029/1999GL011200

Fromm, M., Bevilacqua, R., Servranckx, R., Rosen, J., Thayer, J., Herman, J., & Larko, D. (2005). Pyro-cumulonimbus injection of smoke to the stratosphere: Observations and impact of a super blowup in northwestern Canada on 3-4 August 1998. *Journal of Geophysical Research*, *110*(D8), D08205. https://doi.org/10.1029/2004JD005350

Fromm, M., Lindsey, D. T., Servranckx, R., Yue, G., Trickl, T., Sica, R., et al. (2010). The untold story of pyrocumulonimbus. *Bulletin of the American Meteorological Society, American Meteorological Society*, *91*(9), 1193–1210. https://doi.org/10.1175/2010BAMS3004.1

Fromm, M., Shettle, E. P., Fricke, K. H., Ritter, C., Trickl, T., Giehl, H., et al. (2008). Stratospheric impact of the Chisholm pyrocumulonimbus eruption: 2. Vertical profile perspective. *Journal of Geophysical Research*, *113*(D8), D08203. https://doi.org/10.1029/2007JD009147

Fromm, M., Torres, O., Diner, D., Lindsey, D., Vant Hull, B., Servranckx, R., et al. (2008). Stratospheric impact of the Chisholm pyrocumulonimbus eruption: 1. Earth-viewing satellite perspective. *Journal of Geophysical Research*, *113*(D8), D08202. https://doi.org/10.1029/2007JD009153

Fromm, M. D., & Servranckx, R. (2003). Transport of forest fire smoke above the tropopause by supercell convection. *Geophysical Research Letters*, *30*(10), 1542. https://doi.org/10.1029/2002GL016820

Fuelberg, H. E., Harrigan, D. L., & Sessions, W. (2010). A meteorological overview of the ARCTAS 2008 mission. *Atmospheric Chemistry and Physics*, *10*(2), 817–842. https://doi.org/10.5194/acp-10-817-2010

Fung, I. Y., Tucker, C. J., & Prentice, K. C. (1987). Application of Advanced Very High-Resolution Radiometer Vegetation Index. *Journal of Geophysical Research-Atmospheres*, *92*(D3), 2999–3015. https://doi.org/10.1029/JD092iD03p02999

Fussen, D., Dekemper, E., Errera, Q., Franssens, G., Mateshvili, N., Pieroux, D., & Vanhellemont, F. (2016). The ALTIUS mission. *Atmospheric Measurement Techniques Discussions*, 1–40. https://doi.org/10.5194/amt-2016-213

Fyke, J., Sergienko, O., Löfverström, M., Price, S., & Lenaerts, J. T. M. (2018). An overview of interactions and feedbacks between ice sheets and the Earth system. *Reviews of Geophysics*, *56*(2), 361–408. https://doi.org/10.1029/2018RG000600

Gamon, J. A., Huemmrich, K. F., Peddle, D. R., Chen, J., Fuentes, D., Hall, F. G., et al. (2004). Remote sensing in BOREAS: Lessons learned. *Remote Sensing of Environment*, *89*(2), 139–162. https://doi.org/10.1016/j.rse.2003.08.017

Gao, B. (1996). NDWI -A normalized difference water index for remote sensing of vegetation liquid water from space. *Remote Sensing of Environment*, *58*(3), 257–266. https://doi.org/10.1016/S0034-4257(96)00067-3

Gao, X., Schlosser, C. A., Sokolov, A., Anthony, K. W., Zhuang, Q., & Kicklighter, D. (2013). Permafrost degradation and methane: Low risk of biogeochemical climate-warming feedback. *Environmental Research Letters*, *8*(3), 035014. https://doi.org/10.1088/1748-9326/8/3/035014

Garand, L., Trishchenko, A. P., Trichtchenko, L. D., & Nassar, R. (2014). The Polar Communications and Weather mission: Addressing remaining gaps in the Earth observing system. *Physics in Canada*, *70*, 247–254.

Garcia-Eidell, C., Comiso, J. C., Dinnat, E., & Brucker, L. (2017). Satellite observed salinity distributions at high latitudes in the Northern Hemisphere: A comparison of four products. *Journal of Geophysical Research: Oceans*, *122*, 7717–7736. https://doi.org/10.1002/2017JC013184

Gardner, A. S., Moholdt, G., Cogley, J. G., Wouters, B., Arendt, A. A., Wahr, J., et al. (2013). A Reconciled Estimate of Glacier Contributions to Sea Level Rise: 2003 to 2009. *Science*, *340*(6134), 852–857. https://doi.org/10.1126/science.1234532

Garrett, T. J., & Verzella, L. L. (2008). An evolving history of Arctic aerosols. *Bulletin of the American Meteorological Society*, *89*(3), 299–302. https://doi.org/10.1175/BAMS-89-3-299

Gauthier, S., Bernier, P., Kuuluvainen, T., Shvidenko, A. Z., & Schepaschenko, D. G. (2015). Boreal forest health and global change. *Science*, *349*(6250), 819–822. https://doi.org/10.1126/science.aaa9092

Generoso, S., Bey, I., Attie, J.-L., & Breon, F.-M. (2007). A satellite- and model-based assessment of the 2003 Russian fires: Impact on the Arctic region. *Journal of Geophysical Research*, *112*(D15), D15302. https://doi.org/10.1029/2006JD008344

Giglio, L., Csiszar, I., & Justice, C. O. (2006). Global distribution and seasonality of active fires as observed with the Terra and Aqua Moderate Resolution Imaging Spectroradiometer (MODIS) sensors. *Journal of Geophysical Research*, *111*(G2), G02016. https://doi.org/10.1029/2005JG000142

Giglio, L., Descloitres, J., Justice, C. O., & Kaufman, Y. J. (2003). An enhanced contextual fire detection algorithm for MODIS. *Remote Sensing of Environment*, *87*(3-Feb)(2-3), 273–282. https://doi.org/10.1016/S0034-4257(03)00184-6

Giglio, L., Loboda, T., Roy, D. P., Quayle, B., & Justice, C. O. (2009). An Active-Fire Based Burned Area Mapping Algorithm for the MODIS Sensor. *Remote Sensing of Environment*, *113*(2), 408–420. https://doi.org/10.1016/j.rse.2008.10.006

Giglio, L., van der Werf, G. R., Randerson, J. T., Collatz, G. J., & Kasibhatla, P. (2006). Global estimation of burned area using MODIS active fire observations. *Atmospheric Chemistry and Physics*, *6*(4), 957–974. https://doi.org/10.5194/acp-6-957-2006

Giles, K. A., Laxon, S. W., & Ridout, A. L. (2008). Circumpolar thinning of Arctic sea ice following the 2007 record ice extent minimum. *Geophysical Research Letters*, *35*, L22502. https://doi.org/10.1029/2008GL035710

Goetz, S. J., Bunn, A. G., Fiske, G. J., & Houghton, R. A. (2005). Satellite-observed photosynthetic trends across boreal North America associated with climate and fire disturbance. *Proceedings of the National Academy of Sciences of the United States of America*, *102*(38), 13521–13525. https://doi.org/10.1073/pnas.0506179102

Gogineni, S., Chuah, T., Allen, C., Jezek, K., & Moore, R. K. (1998). An improved coherent radar depth sounder. *Journal of Glaciology*, *44*(148), 659–669. https://doi.org/10.1017/S0022143000002161

Goldammer, J. G., Stocks, B. J., Furyaev, V. V., Valendik, E. N., Conard, S. G., Clark, J. S., et al. (1996). Fire in Ecosystems of Boreal Eurasia: The Bor Forest Island Fire Experiment Fire Research Campaign Asia-North (FIRESCAN). In J. S. Levine (Ed.), *Biomass Burning and Global Change* (Vol. 2, pp. 848–873). Cambridge, MA: MIT Press.

Gong, S. L., Zhao, T. L., Sharma, S., Toom-Sauntry, D., Lavoué, D., Zhang, X. B., et al. (2010). Identification of trends and interannual variability of sulfate and black carbon in the Canadian High Arctic: 1981–2007. *Journal of Geophysical Research*, *115*(D7), D07305. https://doi.org/10.1029/2009JD012943

Gong, W., Beagley, S. R., Cousineau, S., Sassi, M., Munoz-Alpizar, R., Ménard, S., et al. (2018). Assessing the impact of shipping emissions on air pollution in the Canadian Arctic and northern regions: Current and future modelled scenarios. *Atmospheric Chemistry and Physics*, *18*(22), 16653–16687. https://doi.org/10.5194/acp-18-16653-2018

Gonsamo, A., & Chen, J. M. (2016). Circumpolar vegetation dynamics product for global change study. *Remote Sensing of Environment*, *182*, 13–26. https://doi.org/10.1016/j.rse.2016.04.022

Gonsamo, A., Chen, J. M., & Ooi, Y. W. (2017). Peak season plant activity shift towards spring is reflected by increasing carbon uptake by extratropical ecosystems. *Global Change Biology*, *24*(5), 2117–2128. https://doi.org/10.1111/gcb.14001

Goodrich, L. E. (1982). The influence of snow cover on the ground thermal regime. *Canadian Geotechnical Journal*, *19*(4), 421–432. https://doi.org/10.1139/t82-047

Gould, J., Roemmich, D., Wijffels, S., Freeland, H., Ignaszewsky, M., Jianping, X., et al. (2004). Argo profiling floats bring new era of in situ ocean observations. *Eos Transactions AGU*, *85*(19), 185–191. https://doi.org/10.1029/2004EO190002

Grant, W. B. (Ed) (1989). *Ozone Measuring Instruments for the Stratosphere*. Washington, DC: Optical Society of America.

Groisman, P. Y., Karl, T. R., & Knight, R. W. (1994). Observed impact of snow cover on the heat balance and the rise of continental spring temperatures. *Science*, *263*(5144), 198–200. https://doi.org/10.1126/science.263.5144.198

Grosse, G., Goetz, S. J., McGuire, A. D., Romanovsky, V. E., & Schuur, E. A. G. (2016). Changing permafrost in a warming world and feedbacks to the Earth system. *Environmental Research Letters*, *11*(4), 040201. https://doi.org/10.1088/1748-9326/11/4/040201

Guan, H., Esswein, R., Lopez, J., Bergstrom, R., Warnock, A., Follette-Cook, M., et al. (2010). A multi-decadal history of biomass burning plume heights identified using aerosol index measurements. *Atmospheric Chemistry and Physics*, *10*(14), 6461–6469. https://doi.org/10.5194/acp-10-6461-2010

Guay, K. C., Beck, P. S., Berner, L. T., Goetz, S. J., Baccini, A., & Buermann, W. (2014). Vegetation productivity patterns at high northern latitudes: A multi-sensor satellite data assessment. *Global Change Biology*, *20*(10), 3147–3158. https://doi.org/10.1111/gcb.12647

Guo, D. L., & Wang, H. J. (2016). CMIP5 permafrost degradation projection: A comparison among different regions. *Journal of Geophysical Research: Atmospheres*, *121*, 4499–4517. https://doi.org/10.1002/2015JD024108

Guo, M., Li, J., Sheng, C., Xu, J., & Wu, L. (2017). A Review of Wetland Remote Sensing. *Sensors*, *17*(4), 777. https://doi.org/10.3390/s17040777

Hahn, C. J., & Warren, S. G. (2007). *A gridded climatology of clouds over land (1971–96) and ocean (1954–97) from surface observations worldwide, Numeric Data Package NDP-026E ORNL/CDIAC-153*. Oak Ridge, Tenn: CDIAC, Department of Energy.

Hall, D. K., Comiso, J. C., DiGirolamo, N. E., Shuman, C. A., Key, J. R., & Koenig, L. S. (2012). A Satellite-Derived Climate-Quality Data Record of the Clear-Sky Surface Temperature of the Greenland Ice Sheet. *Journal of Climate*, *25*(14), 4785–4798. http://doi.org/10.1175/JCLI-D-11-00365.1

Hall, D. K., Crawford, C. J., DiGirolamo, N. E., Riggs, G. A., & Foster, J. L. (2015). Detection of earlier snowmelt in the Wind River Range, Wyoming, using Landsat imagery, 1972 – 2013. *Remote Sensing of Environment*, *162*, 45–54. https://doi.org/10.1016/j.rse.2015.01.032

Hall, D. K., Cullather, R. I., DiGirolamo, N., Comiso, J. C., Medley, B. C., & Nowicki, S. M. (2018). A multilayer surface temperature, surface albedo, and water vapor product of Greenland from MODIS. *Remote Sensing*, *10*(4), 555. https://doi.org/10.3390/rs10040555

Hall, D. K., Riggs, G. A., & Salomonson, V. V. (1995). Development of methods for mapping global snow cover using Moderate Resolution Imaging Spectroradiometer data. *Remote Sensing of Environment*, *54*(2), 127–140. https://doi.org/10.1016/0034-4257(95)00137-P

Hall, D. K., Riggs, G. A., Salomonson, V. V., DiGirolamo, N. E., & Bayr, K. J. (2002). MODIS snow-cover products. *Remote Sensing of Environment*, *83*(1–2), 181–194. https://doi.org/10.1016/S0034-4257(02)00095-0

Hamlet, A. F., Mote, P. W., Clark, M. P., & Lettenmaier, D. P. (2005). Effects of temperature and precipitation variability on snowpack trends in the western United States. *Journal of Climate*, *18*(21), 4545–4561. https://doi.org/10.1175/JCLI3538.1

Hammerling, D. M., Kawa, S. R., Schaefer, K., Doney, S., & Michalak, A. M. (2015). Detectability of CO_2 flux signals by a space-based lidar mission. *Journal of Geophysical Research: Atmospheres*, *120*, 1794–1807. https://doi.org/10.1002/2014JD022483

Handorf, D., Jaiser, R., Dethloff, K., Rinke, A., & Cohen, J. (2015). Impacts of Arctic sea ice and continental snow cover changes on atmospheric winter teleconnections. *Geophysical Research Letters*, *42*, 2367–2377. https://doi.org/10.1002/2015GL063203

Hansen, M. C., Potapov, P. V., Moore, R., Hancher, M., Turubanova, S. A., Tyukavina, A., et al. (2013). High-Resolution Global Maps of 21st-Century Forest Cover Change. *Science*, *342*(6160), 850–853. https://doi.org/10.1126/science.1244693

Harding, D. J., & Carabajal, C. C. (2005). ICESat waveform measurements of within-footprint topographic relief and vegetation vertical structure. *Geophysical Research Letters*, *32*, L21S10. https://doi.org/10.1029/2005GL023471

Hare, F. K., & Ritchie, J. C. (1972). The boreal bioclimates. *Geographical Review*, *62*(3), 333–365. https://doi.org/10.2307/213287

Harris, N. R. P., Hassler, B., Tummon, F., Bodeker, G. E., Hubert, D., Petropavlovskikh, I., et al. (2015). Past changes in the vertical distribution of ozone – Part 3: Analysis and interpretation of trends. *Atmospheric Chemistry and Physics*, *15*(17), 9965–9982. https://doi.org/10.5194/acp-15-9965-2015

Hartley, I. P., Garnett, M. H., Sommerkorn, M., Hopkins, D. W., Fletcher, B. J., Sloan, V. L., et al. (2012). A potential loss of carbon associated with greater plant growth in the European Arctic. *Nature Climate Change*, *2*(12), 875–879. https://doi.org/10.1038/nclimate1575

Hartmann, D. L., Klein Tank, A. M. G., Rusticucci, M., Alexander, L. V., Bronnimann, S., Charabi, Y., ... Zhai, P. M. (2013). Observations: Atmosphere and Surface. In T. F. Stocker, D. Qin, G.-K. Plattner, M. Tignor, S. K. Allen, J. Boschung, ... P. M. Midgley (Eds.), *Climate Change 2013: The Physical Science Basis. Contribution of Working Group I to the Fifth Assessment Report of the Intergovernmental Panel on Climate Change* (pp. 159–254). Cambridge, UK and New York, NY, USA: Cambridge Universitty Press.

Hayes, D. J., McGuire, A. D., Kicklighter, D. W., Gurney, K. R., Burnside, T. J., & Melillo, J. M. (2011). Is the northern high-latitude land-based CO_2 sink weakening? *Global Biogeochemical Cycles*, *25*, GB3018. https://doi.org/10.1029/2010GB003813

Hegg, D. A., Warren, S. G., Grenfell, T. C., Doherty, S. J., & Clarke, A. D. (2010). Sources of light-absorbing aerosol in arctic snow and their seasonal variation. *Atmospheric Chemistry and Physics*, *10*(22), 10,923–10,938. https://doi.org/10.5194/acp-10-10923-2010

Helfrich, S. R., McNamara, D., Ramsay, B. H., Baldwin, T., & Kasheta, T. (2007). Enhancements to, and forthcoming developments in the Interactive Multisensor Snow and Ice Mapping System (IMS). *Hydrological Processes*, *21*(12), 1576–1586. https://doi.org/10.1002/hyp.6720

Helmig, D., Oltmans, S. J., Carlson, D., Lamarque, J.-F., Jones, A., Labuschagne, C., et al. (2007). A review of surface ozone in the polar regions. *Atmospheric Environment*, *41*(24), 5138–5161. https://doi.org/10.1016/j.atmosenv.2006.09.053

Hember, R. A., Kurz, W. A., & Coops, N. C. (2017). Relationships between individual-tree mortality and water-balance variables indicate positive trends in water stress-induced tree mortality across North America. *Global Change Biology*, *23*(4), 1691–1710. https://doi.org/10.1111/gcb.13428

Higgins, A. K. (1991). North Greenland Glacier Velocities and Calf Ice. *Polarforschung, Bremerhaven, Alfred Wegener Institute for Polar and Marine Research and German Society of Polar Research*, *60*(1), 1–23.

Hilker, T., Coops, N. C., Wulder, M. A., Black, T. A., & Guy, R. D. (2008). The use of remote sensing in light use efficiency based models of gross primary production: A review of current status and future requirements. *Science of the Total Environment*, *404*(2–3), 411–423. https://doi.org/10.1016/j.scitotenv.2007.11.007

Hill, S. L., Phillips, T., & Atkinson, A. (2013). Potential climate change effects on the habitat of Antarctic krill in the Weddell quadrant of the Southern Ocean. *PloS one*, *8*(8), e72246. https://doi.org/10.1371/journal.pone.0072246

Hinzman, L. D., Deal, C. J., McGuire, A. D., Mernild, S. H., Polyakov, I. V., & Walsh, J. E. (2013). Trajectory of the Arctic as an integrated system. *Ecological Applications*, *23*(8), 1837–1868. https://doi.org/10.1890/11-1498.1

Hirdman, D., Sodemann, H., Eckhardt, S., Burkhart, J. F., Jefferson, A., Mefford, T., et al. (2010). Source identification of short-lived air pollutants in the Arctic using statistical analysis of measurement data and particle dispersion model output. *Atmospheric Chemistry and Physics*, *10*(2), 669–693. https://doi.org/10.5194/acp-10-669-2010

Hoekstra, P., & Cappillino, P. (1971). Dielectric Properties of Sea and Sodium Chloride Ice at UHF and Microwave Frequencies. *Journal of Geophysical Research*, *76*(20), 4922–4931. https://doi.org/10.1029/JB076i020p04922

Hoffman, M. J., Catania, G., Neumann, T. A., Andrews, L., & Rumrill, J. (2011). Links between acceleration, melting, and supraglacial lake drainage of the western Greenland Ice Sheet. *Journal of Geophysical Research-Earth Surface*, *116*, F04035.

Holland, M. M., & Bitz, C. M. (2003). Polar amplification of climate change in coupled models. *Climate Dynamics*, *21*(3-4), 221–232. https://doi.org/10.1007/s00382-003-0332-6

Hollinger, D. Y., Goltz, S. M., Davidson, E. A., Lee, J. T., Tu, K., & Valentine, H. T. (1999). Seasonal patterns and environmental control of carbon dioxide and water vapour exchange in an ecotonal boreal forest. *Global Change Biology*, *5*(8), 891–902. https://doi.org/10.1046/j.1365-2486.1999.00281.x

Holmes, C. D., Prather, M. J., Sovde, O. A., & Myhre, G. (2013). Future methane, hydroxyl, and their uncertainties: Key climate and emission parameters for future predictions. *Atmospheric Chemistry and Physics*, *13*(1), 285–302. https://doi.org/10.5194/acp-13-285-2013

Holtmeier, F. K., & Broll, G. (2005). Sensitivity and response of northern hemisphere altitudinal and polar treelines to environmental change at landscape and local scales. *Global Ecology and Biogeography*, *14*(5), 395–410. https://doi.org/10.1111/j.1466-822X.2005.00168.x

Hope, C., & Schaefer, K. (2016). Economic impacts of carbon dioxide and methane released from thawing permafrost. *Nature Climate Change*, *6*(1), 56–59. https://doi.org/10.1038/nclimate2807

Houweling, S., Baker, D., Basu, S., Boesch, H., Butz, A., Chevallier, F., et al. (2015). An intercomparison of inverse models for estimating sources and sinks of CO_2 using GOSAT measurements. *Journal of Geophysical Research: Atmospheres*, *120*, 5253–5266. https://doi.org/10.1002/2014JD022962

Høyer, J. L., Karagali, I., Dybkjær, G., & Tonboe, R. (2012). Multi sensor validation and error characteristics of Arctic satellite sea surface temperature observations. *Remote Sensing of Environment*, *121*, 335–346. https://doi.org/10.1016/j.rse.2012.01.013

Hu, F. S., Higuera, P. E., Duffy, P., Chipman, M. L., Rocha, A. V., Young, A. M., et al. (2015). Arctic tundra fires: Natural variability and responses to climate change. *Frontiers in Ecology and the Environment*, *13*(7), 369–377. https://doi.org/10.1890/150063

Hu, H., Landgraf, J., Detmers, R., Borsdorff, T., Aan de Brugh, J., Aben, I., et al. (2018). Toward global mapping of methane with TROPOMI: First results and intersatellite comparison to GOSAT. *Geophysical Research Letters*, *45*(8), 3682–3689. https://doi.org/10.1002/2018GL077259

Hu, Y., Rodier, S., Xu, K. M., Sun, W., Huang, J., Lin, B., et al. (2010). Occurrence, liquid water content, and fraction of supercooled water clouds from combined CALIOP/IIR/MODIS measurements. *Journal of Geophysical Research*, *115*, D00H34. https://doi.org/10.1029/2009JD012384

Hugelius, G., Strauss, J., Zubrzycki, S., Harden, J. W., Schuur, E. A. G., Ping, C.-L., et al. (2014). Estimated stocks of circumpolar permafrost carbon with quantified uncertainty ranges and identified data gaps. *Biogeosciences*, *11*(23), 6573–6593. https://doi.org/10.5194/bg-11-6573-2014

HyspIRI (2018). HyspIRI Final Report. https://hyspiri.jpl.nasa.gov/downloads/reports_whitepapers/HyspIRI_FINAL_Report_1October2018_20181005a.pdf

Ialongo, I., Hakkarainen, J., Hyttinen, N., Jalkanen, J.-P., Johansson, L., Boersma, K. F., et al. (2014). Characterization of OMI tropospheric NO_2 over the Baltic Sea region. *Atmospheric Chemistry and Physics*, *14*(15), 7795–7805. https://doi.org/10.5194/acp-14-7795-2014

Ialongo, I., Hakkarainen, J., Kivi, R., Anttila, P., Krotkov, N. A., Yang, K., et al. (2015). Comparison of operational satellite SO_2 products with ground-based observations in northern Finland during the Icelandic Holuhraun fissure eruption. *Atmospheric Measurement Techniques*, *8*(6), 2279–2289. https://doi.org/10.5194/amt-8-2279-2015

Ichoku, C., & Ellison, L. (2014). Global top-down smoke-aerosol emissions estimation using satellite fire radiative power measurements. *Atmospheric Chemistry and Physics*, *14*(13), 6643–6667. https://doi.org/10.5194/acp-14-6643-2014

Ichoku, C., Martins, J. V., Kaufman, Y. J., Wooster, M. J., Freeborn, P. H., Hao, W. M., et al. (2008). Laboratory investigation of fire radiative energy and smoke aerosol emissions. *Journal of Geophysical Research*, *113*(D14), D14S09. https://doi.org/10.1029/2007JD009659

IDA Science and Technology Policy Institute and Sustaining Arctic Observing Networks (2017). International Arctic Observations Assessment Framework. IDA Science and Technology Policy Institute, Washington, DC, U.S.A., and Sustaining Arctic Observing Networks, Oslo, Norway, 73 pp. available from: https://www.arcticobserving.org/images/pdf/misc/STPI-SAON-International-Arctic-Observations-Framework-Report-2017.pdf.

Inoue, J., Yamazaki, A., Ono, J., Dethloff, K., Maturilli, M., Neuber, R., et al. (2015). Additional Arctic observations improve weather and sea-ice forecasts for the Northern Sea Route. *Scientific Reports*, *5*(1), 16868. https://doi.org/10.1038/srep16868

IOCCG (2015). *Ocean Colour Remote Sensing in Polar SeasRep*. Dartmouth, Canada: International Ocean Colour Coordinating Group.

Isachenko, A. G., Shlyapnikov, A. A., Robozertseva, O. D., & Filipetskaya, A. Z. (1988). *The landscape map of the USSR*. Moscow: General Ministry of Geodesy and Cartography of the USSR. [In Russian.]

Isaev, A. S. (Ed) (1990). *The forests of the USSR. The landscape map of the USSR*. Moscow: General Ministry of Geodesy and Cartography of the USSR. [In Russian.]

Jacob, D., Crawford, J., Maring, H., Clarke, A., Dibb, J., Emmons, L., et al. (2010). The Arctic Research of the Composition of the Troposphere from Aircraft and Satellites (ARCTAS) mission: Design, execution, and first results. *Atmospheric Chemistry and Physics*, *10*(11), 5191–5212. https://doi.org/10.5194/acp-10-5191-2010

Jacob, D. J., Turner, A. J., Maasakkers, J. D., Sheng, J., Sun, K., Liu, X., et al. (2016). Satellite observations of atmospheric methane and their value for quantifying methane emissions. *Atmospheric Physics and Chemistry*, *16*(22), 14,371–14,396. https://doi.org/10.5194/acp-16-14371-2016

Jagdhuber, T., Stockamp, J., Hajnsek, I., & Ludwig, R. (2014). Identification of Soil Freezing and Thawing States Using SAR Polarimetry at C-Band. *Remote Sensing*, *6*(3), 2008–2023. https://doi.org/10.3390/rs6032008

Jakobsson, M., Mayer, L., Coakley, B., Dowdeswell, J. A., Forbes, S., Fridman, B., et al. (2012). The International Bathymetric Chart of the Arctic Ocean (IBCAO) Version 3.0. *Geophysical Research Letters*, *39*, L12609. https://doi.org/:10.1029/2012GL052219

Jensen, K., & McDonald, K. (2019). Surface Water Microwave Product Series (SWAMPS) Version 3: A Near-Real Time and 25-year Historical Global Inundated Area Fraction Time Series from Active and Passive Microwave Remote Sensing. *IEEE Geoscience and Remote Sensing Letters.*, *16*(9), 1402–1406. https://doi.org/10.1109/LGRS.2019.2898779

Jiang, C., Youngryel, R., Fang, H., Myneni, R., Claverie, M., & Zhu, Z. (2017). Inconsistencies of interannual variability and trends inlong-term satellite leaf area index products. *Global Change Biology*, *23*(10), 4133–4146. https://doi.org/10.1111/gcb.13787

Johannessen, O. M., Miles, M., & Bjorgo, E. (1995). The Arctic's shrinking sea ice. *Nature*, *376*(6536), 126–127. https://doi.org/10.1038/376126a0

Johnston, R. N., & Sharpe, J. R. (1922). *Report of the James Bay Forest Survey, Moose River, Lower Basin*, (p. 16). Toronto, Ontario: Ontario Forestry Branch.

Johnstone, J. F., Hollingsworth, T. N., & Chapin, F. S. (2008). *A key for predicting postfire successional trajectories in black spruce stands of interior Alaska (No. General Technical Report PNW-GTR-767)*, (p. 37). Portland, OR: USDA Forest Service, Pacific Northwest Research Station.

Joiner, J., Yoshida, Y., Vasilkov, A. P., Yoshida, Y., Corp, L. A., & Middleton, E. M. (2011). First observations of global and seasonal terrestrial chlorophyll fluorescence from space. *Biogeosciences*, *8*(3), 637–651. https://doi.org/10.5194/bg-8-637-2011

Jones, M. O., Jones, L. A., Kimball, J. S., & McDonald, K. C. (2011). Satellite passive microwave remote sensing for monitoring global land surface phenology. *Remote Sensing of Environment*, *115*(4), 1102–1114. https://doi.org/10.1016/j.rse.2010.12.015

Jones, M. O., Kimball, J. S., & Jones, L. A. (2013). Satellite microwave detection of boreal forest recovery from the extreme 2004 wildfires in Alaska and Canada. *Global Change Biology*, *19*(10), 3111–3122. https://doi.org/10.1111/gcb.12288

Joughin, I., Smith, B., Howat, I. M., Scambos, T., & Moon, T. (2010). Greenland Flow Variability from Ice-Sheet-Wide Velocity Mapping. *Journal of Glaciology*, *56*(197), 415–430. https://doi.org/10.3189/002214310792447734

Ju, J., & Masek, J. G. (2016). The vegetation greenness trend in Canada and US Alaska from 1984-2012 Landsat data. *Remote Sensing of Environment*, *176*, 1–16. https://doi.org/10.1016/j.rse.2016.01.001

Justice, C. O., Román, M. O., Csiszar, I., Vermote, E. F., Wolfe, R. E., Hook, S. J., et al. (2013). Land and cryosphere products from Suomi NPP VIIRS: Overview and status. *Journal of Geophysical Research: Atmospheres*, *118*, 9753–9765. https://doi.org/10.1002/jgrd.50771

Kääb, A., Huggel, C., Fischer, L., Guex, S., Paul, F., Roer, I., et al. (2005). Remote sensing of glacier- and permafrost-related hazards in high mountains: An overview. *Natural Hazards and Earth System Sciences*, *5*(4), 527–554. https://doi.org/10.5194/nhess-5-527-2005

Kahn, R. A., Li, W.-H., Moroney, C., Diner, D. J., Martonchik, J. V., & Fishbein, E. (2007). Aerosol source plume physical characteristics from space-based multiangle imaging. *Journal of Geophysical Research*, *112*(D11), D11205. https://doi.org/10.1029/2006JD007647

Karhu, K., Auffret, M. D., Dungait, J. A. J., Hopkins, D. W., Prosser, J. I., Singh, B. K., et al. (2014). Temperature sensitivity of soil respiration rates enhanced by microbial community response. *Nature*, *513*(7516), 81–84. https://doi.org/10.1038/nature13604

Karion, A., Sweeney, C., Tans, P., & Newberger, T. (2010). AirCore An Innovative Atmospheric Sampling System. *Journal of Atmospheric and Oceanic Technology.*, *27*(11), 1839–1853. https://doi.org/10.1175/2010JTECHA1448.1

Karpechko, A. Y., Backman, L., Thölix, L., Ialongo, I., Andersson, M., Fioletov, V., et al. (2013). The link between springtime total ozone and summer UV radiation in Northern Hemisphere extratropics. *Journal of Geophysical Research: Atmospheres*, *118*, 8649–8661. https://doi.org/10.1002/jgrd.50601

Kashiwase, H., Ohshima, K. I., Nihashi, S., & Eicken, H. (2017). Evidence for ice-ocean albedo feedback in the Arctic Ocean shifting to a seasonal ice zone. *Scientific Reports*, *7*(1), 8170. https://doi.org/10.1038/s41598-017-08467-z

Kashkin, V. B., Zuev, D. V., Kurako, M. A., Romanov, A. A., Rubleva, T. V., & Simonov, K. V. (2018). Satellite monitoring of atmospheric sulphur dioxide pollution in polar latitudes. *IOP Conference Series: Earth and Environmental Science*, *193*, 012029. https://doi.org/10.1088/1755-1315/193/1/012029

Kasischke, E. S., Bourgeau-Chavez, L. L., & Johnstone, J. F. (2007). Assessing Spatial and Temporal Variations in Surface Soil Moisture in Fire-Disturbed Black Spruce Forests in Interior Alaska Using Spaceborne Synthetic Aperture Radar Imagery — Implications for Post-Fire Tree Recruitment. *Remote Sensing of Environment*. https://doi.org/10.1016/j.rse.2006.10.020

Kato, S., Loeb, N. G., Minnis, P., Francis, J. A., Charlock, T. P., Rutan, D. A., et al. (2006). Seasonal and interannual variations of top-of-atmosphere irradiance and cloud cover over polar regions derived from the CERES data set. *Geophysical Research Letters*, *33*, L19804. https://doi.org/10.1029/2006GL026685

Kato, S., Rose, F. G., Rutan, D. A., Thorsen, T. J., Loeb, N. G., Doelling, D. R., et al. (2018). Surface Irradiances of Edition 4.0 Clouds and the Earth's Radiant Energy System (CERES) Energy Balanced and Filled (EBAF) Data Product. *Journal of Climate*, *31*(11), 4501–4527. https://doi.org/10.1175/JCLI-D-17-0523.1

Kawa, S. R.; Abshire, J. B.; Baker, D. F.; Browell, E. V.; Crisp, D.; Crowell, S. M. R.; et al.; et al., 2018: Active Sensing of CO_2 Emissions over Nights, Days, and Seasons (ASCENDS): Final Report of the ASCENDS Ad Hoc Science Definition Team, Document ID: 20190000855, NASA/TP–2018-219034, GSFC-E-DAA-TN64573.

Kawa, S. R., Mao, J., Abshire, J. B., Collatz, G. J., Sun, X., & Weaver, C. J. (2010). Simulation studies for a space-based CO_2 lidar mission. *Tellus B*, *62*(5), 759–769. https://doi.org/10.1111/j.1600-0889.2010.00486.x

Kay, J. E., & Gettelman, A. (2009). Cloud influence on and response to seasonal Arctic sea ice loss. *Journal of Geophysical Research Atmospheres*, *114*, D18204. https://doi.org/10.1029/2009JD011773

Kay, J. E., & L'Ecuyer, T. (2013). Observational constraints on Arctic Ocean clouds and radiative fluxes during the early 21st century. *Journal of Geophysical Research: Atmospheres*, *118*, 7219–7236. https://doi.org/10.1002/jgrd.50489

Kay, J. E., L'Ecuyer, T., Chepfer, H., Loeb, N., Morrison, A., & Cesana, G. (2016). Recent advances in Arctic cloud and climate research. *Current Climate Change Reports*, *2*(4), 159–169. https://doi.org/10.1007/s40641-016-0051-9

Kayitakire, F., Hamel, C., & Defourny, P. (2006). Retrieving forest structure variables based on image texture analysis and IKONOS-2 imagery. *Remote Sensing of Environment*, *102*(3–4), 390–401. https://doi.org/10.1016/j.rse.2006.02.022

Kelly, R. E. J., Chang, A. T. C., Tsang, L., & Foster, J. L. (2003). A prototype AMSR-E global snow area and snow depth algorithm: Institute of Electrical and Electronic Engineers. *Transactions on Geoscience and Remote Sensing*, *41*(2), 230–242. https://doi.org/10.1109/TGRS.2003.809118

Kennedy, E., & Arthurs, D. (2018). Nordic and Arctic Imager Mission Requirements Consolidation, Study Report. Prepared by Polar View for the European Space Agency (version 1.0, November 2018).

Kennedy, R. E., Andrefouet, S., Cohen, W. B., Gomez, C., Griffiths, P., Hais, M., et al. (2014). Bringing an ecological view of change to Landsat-based remote sensing. *Frontiers in Ecology and the Environment*, *12*(6), 339–346. https://doi.org/10.1890/130066

Kerr, Y. H., Waldteufel, P., Wigneron, J.-P., Delwart, S., Cabot, F., Boutin, J., et al. (2010). The SMOS Mission: New Tool for Monitoring Key Elements of the Global Water Cycle. *Proc. IEEE*, *98*(5), 666–687. https://doi.org/10.1109/JPROC.2010.2043032

Key, J., & Haefliger, M. (1992). Arctic ice surface temperature retrieved from AVHRR thermal channels. *Journal of Geophysical Research*, *97*(D5), 5855–5893.

Kidder, S. Q., & Vonder Haar, T. H. (1990). On the use of satellites in Molniya orbits for meteorological observation of middle and high latitudes. *Journal of Atmospheric and Oceanic Technology*, *7*(3), 517–522. https://doi.org/10.1175/1520-0426(1990)007<0517:OTUOSI>2.0.CO;2

Kiemle, C., Kawa, S. R., Quatrevalet, M., & Browell, E. V. (2014). Performance simulations for a spaceborne methane lidar mission. *Journal of Geophysical Research: Atmospheres*, *119*, 4365–4379. https://doi.org/10.1002/2013JD021253

Kikuchi, T., Inoue, J., & Langevin, D. (2007). Argo-type profiling float observations under the Arctic multiyear ice. *Deep-Sea Research. Part I: Oceanographic Research Papers*, *54*(9), 1675–1686. https://doi.org/10.1016/j.dsr.2007.05.011

Kilpatrick, K. A., Podestá, G. P., & Evans, R. (2001). Overview of the NOAA/NASA advanced very high resolution radiometer Pathfinder algorithm for sea surface temperature and associated matchup database. *Journal of Geophysical Research*, *106*(C5), 9179–9197. https://doi.org/10.1029/1999JC000065

Kim, B.-M., Son, S.-W., Min, S.-K., Jeong, J.-H., Kim, S.-J., Zhang, X., et al. (2014). Weakening of the stratospheric polar vortex by Arctic sea-ice loss. *Nature Communications*, *5*(1), 4646. https://doi.org/10.1038/ncomms5646

Kim, Y., Kimball, J. S., Glassy, J., & Du, J. (2017). An extended global Earth system data record on daily landscape freeze–thaw status determined from satellite passive microwave remote sensing. *Earth System Science Data*, *9*(1), 133–147. https://doi.org/10.5194/essd-9-133-2017

Kim, Y., Kimball, J. S., Zhang, K., Didan, K., Velicogna, I., & McDonald, K. C. (2014). Attribution of divergent northern vegetation growth responses to lengthening non-frozen seasons using satellite optical-NIR and microwave remote sensing. *International Journal of Remote Sensing*, *35*(10), 3700–3721. https://doi.org/10.1080/01431161.2014.915595

Kim, Y., Kimball, J. S., Zhang, K., & McDonald, K. C. (2012). Satellite detection of increasing Northern Hemisphere non-frozen seasons from 1979 to 2008: Implications for regional vegetation growth. *Remote Sensing of Environment*, *121*, 472–487. https://doi.org/10.1016/j.rse.2012.02.014

Kirschke, S., Bousquet, P., Ciais, P., Saunois, M., Canadell, J. G., Dlugokencky, E. J., et al. (2013). Three decades of global methane sources and sinks. *Nature Geoscience*, *6*. https://doi.org/10.1038/NGEO1955

Kivinen, S., & Kumpula, T. (2014). Detecting Land Cover Disturbances in the Lappi Reindeer Herding District Using Multi Source Remote Sensing and GIS Data. *International Journal of Applied Earth Observation and Geoinformation*, *27*(A), 13–19. https://doi.org/10.1016/j.jag.2013.05.009

Klein, S. A., McCoy, R. B., Morrison, H., Ackerman, A. S., Avramov, A., Boer, G. d., et al. (2009). Intercomparison of model simulations of mixed-phase clouds observed during the ARM Mixed-Phase Arctic Cloud Experiment. *Part I: Single-layer cloud. Quarterly Journal of the Royal Meteorological Society*, *135*(641), 979–1002. https://doi.org/10.1002/qj.416

Klonecki, A., Hess, P., Emmons, L., Smith, L., Orlando, J., & Blake, D. (2003). Seasonal changes in the transport of pollutants into the Arctic troposphere-model study. *Journal of Geophysical Research*, *108*(D4), 8367. https://doi.org/10.1029/2002JD002199

Koenig, L., Martin, S., Studinger, M., & Sonntag, J. (2010). Polar Airborne Observations Fill Gap in Satellite Data. *Eos Transactions AGU*, *91*(38), 333–334. https://doi.org/10.1029/2010EO380002

Koenig, L. S., Miège, C., Forster, R. R., & Brucker, L. (2013). Initial in situ measurements of perennial meltwater storage in the Greenland firn aquifer. *Geophysical Research Letters*, *41*, 81–85. https://doi.org/10.1002/2013GL058083

Koenigk, T., Devasthale, A., & Karlsson, K.-G. (2014). Summer Arctic sea ice albedo in CMIP5 models. *Atmospheric Chemistry and Physics*, *14*(4), 1987–1998. https://doi.org/10.5194/acp-14-1987-2014

Korovin, G. N. (1996). Analysis of the distribution of forest fires in Russia. In J. G. Goldammer, & V. V. Furyaev (Eds.), *Fire in ecosys-tems of boreal Eurasia* (pp. 112–128). Netherlands: Kluwer Academic Publishers. https://doi.org/10.1007/978-94-015-8737-2_8

Korsgaard, N. J., Nuth, C., Khan, S. A., Kjeldsen, K. K., Bjørk, A. A., Schomacker, A., & Kjær, K. H. (2016). Digital elevation model and orthophotographs of Greenland based on aerial photographs from 1978–1987. *Scientific Data*, *3*(1), 160032. https://doi.org/10.1038/sdata.2016.32

Kort, E. A., Wofsy, S. C., Daube, B. C., Diao, M., Elkins, J. W., Gao, R. S., et al. (2012). Atmospheric observations of high latitude Arctic Ocean methane emissions up to 82°north. *Nature Geoscience*, *5*(5), 318–321. https://doi.org/10.1038/ngeo1452

Koven, C. D., Riley, W. J., & Stern, A. (2013). Analysis of permafrost thermal dynamics and response to climate change in the CMIP5 earth system models. *Journal of Climate*, *26*(6), 1877–1900. https://doi.org/10.1175/JCLI-D-12-00228.1

Krabill, W. B., Thomas, R. H., Martin, C. F., Swift, R. N., & Frederick, E. B. (1995). Accuracy of airborne laser altimetry over the Greenland ice sheet. *International Journal of Remote Sensing*, *16*, 7.

Krotkov, N. A., McLinden, C. A., Li, C., Lamsal, L. N., Celarier, E. A., Marchenko, S. V., et al. (2016). Aura OMI observations of regional SO2 and NO2 pollution changes from 2005 to 2014. *Atmospheric Chemistry and Physics*, *16*(7), 4605–4629. https://doi.org/10.5194/acp-2015-674

Kubryakov, A., Stanichny, S., & Zatsepin, A. (2014). River plume dynamics in the Kara and Black Sea from altimetry-based lagrangian model, satellite salinity and chlorophyll data. *Remote Sensing of Environment*, *176*, 177–187. https://doi.org/10.1016/j.rse.2016.01.020

Kujanpää, J., & Kalakoski, N. (2015). Operational surface UV radiation product from GOME-2 and AVHRR/3 data. *Atmospheric Measurement Techniques*, *8*(10), 4399–4414. https://doi.org/10.5194/amt-8-4399-2015

Kukla, G. (1981). *Climatic role of snow covers, in Allison, I., ed., Sea level, ice, and climate change: International Association of Hydrological Sciences*, IAHS Publication no. 131, Wallingford, Oxforshire OX10 8BB, England, U.K., p.79–107.

Kulawik, S. S., Jones, D. B. A., Nassar, R., Irion, F. W., Worden, J. R., Bowman, K. W., et al. (2010). Characterization of Tropospheric Emission Spectrometer (TES) CO2 for carbon cycle science. *Atmospheric Chemistry and Physics*, *11*(8), 3581–3593. https://doi.org/10.5194/acp-11-3581-2011

Kulmala, M., Lappalainen, H. K., Petäjä, T., Kurten, T., Kerminen, V.-M., Viisanen, Y., et al. (2015). Introduction: The Pan-Eurasian Experiment (PEEX) – multidisciplinary, multiscale and multicomponent research and capacity-building initiative. *Atmospheric Chemistry and Physics*, *15*(22), 13085–13096. https://doi.org/10.5194/acp-15-13085-2015

Kumpula, T. (2006). Very High Resolution Remote Sensing Data in Reindeer Pasture Inventory in Northern Fennoscandia. In: Forbes, B. C., Bölter, M., Müller-Wille, L., Hukkinen, J., Müller, F., Gunslay, N. & Y. Konstantinov (edit.): *Reindeer Management in northernmost Europe. Ecological studies* (Vol. 184). Berlin Heidelberg: Springer-Verlag 167-185, https://doi.org/10.1007/3-540-31392-3_9

Kumpula, T., Forbes, B. C., Stammler, F., & Meschtyb, N. (2012). Dynamics of a coupled system: Multi-resolution remote sensing in assessing social-ecological responses during 25 years of gas field development in Arctic Russia. *Remote Sensing*, *4*(4), 1046–1068. https://doi.org/10.3390/rs4041046

Kumpula, T., Pajunen, A., Forbes, B. C., & Stammler, F. (2011). Land use and cover change in arctic Russia: Ecological and social implications of industrial development. *Global Environmental Change*, *21*(2), 550–562. https://doi.org/10.1016/j.gloenvcha.2010.12.010

Kwok, R., Cunningham, G. F., Wensnahan, M., Rigor, I., Zwally, H. J., & Yi, D. (2009). Thinning and volume loss of the Arctic Ocean sea ice cover: 2003–2008. *Journal of Geophysical Research*, *114*(C7), C07005. https://doi.org/10.1029/2009JC005312

Kwok, R., Kurtz, N. T., Brucker, L., Ivanoff, A., Newman, T., Farrell, S. L., et al. (2017). Intercomparison of snow depth retrievals over Arctic sea ice from radar data acquired by Operation IceBridge. *The Cryosphere*, *11*(6), 2571–2593. https://doi.org/10.5194/tc-11-2571-2017

Kwok, R., & Markus, T. (2018). Potential basin-scale estimates of Arctic snow depth with sea ice freeboards from CryoSat-2 and ICESat-2: An exploratory analysis. *Advances in Space Research*, *62*(6), 1243–1250. https://doi.org/10.1016/j.asr.2017.09.007

Kwok, R., & Morison, J. (2016). Sea surface height and dynamic topography of the ice-covered oceans from CryoSat-2: 2011–2014. *Journal of Geophysical Research: Oceanography*, *120*(2), 1032–1047. https://doi.org/10.1002/2014JC010472

Kyrölä, E., Laine, M., Sofieva, V., Tamminen, J., Päivärinta, S.-M., Tukiainen, S., et al. (2013). Combined SAGE II-GOMOS ozone profile data set for 1984–2011 and trend analysis of the vertical distribution of ozone. *Atmospheric Chemistry and Physics*, *13*(21), 10645–10658. https://doi.org/10.5194/acp-13-10645-2013

Lachance, R. L., McConnell, J. C., McElroy, C. T., O'Neill, N., Nassar, R., Buijs, H., et al. (2012). PCW/PHEOS-WCA: quasi-geostationary Arctic measurements for weather, climate, and air quality from highly eccentric orbits. In *Proc. SPIE 8533, Sensors, Systems, and Next-Generation Satellites XVI, 85330O (19 November 2012)*. https://doi.org/10.1117/12.974795

Lagerloef, G., Colomb, F. R., Le Vine, D., Wentz, F., Yueh, S., Ruf, C., et al. (2008). The Aquarius/SAC-D Mission: Designed to Meet the Salinity Remote-Sensing Challenge. *Oceanography*, *21*(1), 68–81. https://doi.org/10.5670/oceanog.2008.68

Lagerloef, G., Kao, H.-Y., Meissner, T., & Vazquez, J. (2015). Aquarius Salinity Validation Analysis; Data Version 4.0. ftp://podaac.jpl.nasa.gov/allData/aquarius/docs/v4/AQ-014-PS-0016_AquariusSalinityDataValidationAnalysis_DatasetVersion4.0and3.0.pdf.

Langer, M., Westermann, S., Heikenfeld, M., Dorn, W., & Boike, J. (2013). Satellite-based modeling of permafrost temperatures in a tundra lowland landscape. *Remote Sensing of Environment*, *135*, 12–24. https://doi.org/10.1016/j.rse.2013.03.011

Langer, M., Westermann, S., Muster, S., Piel, K., & Boike, J. (2011). The surface energy balance of a polygonal tundra site in northern Siberia Part 2: Winter. *The Cryosphere*, *5*(2), 509–524. https://doi.org/10.5194/tc-5-509-2011

Lara, M. J., Nitze, I., Grosse, G., Martin, P., & McGuire, A. D. (2018). Reduced arctic tundra productivity linked with landform and climate change interactions. *Scientific Reports*, *8*, 2345. https://doi.org/10.1038/s41598-018-20692-8

Larsen, J.N., Anisimov, O.A., Constable, A., Hollowed, A.B., Maynard, N., Prestrud, P., et al., 2014: Polar regions. In: *Climate Change 2014: Impacts, Adaptation, and Vulnerability. Part B: Regional Aspects. Contribution of Working Group II to the Fifth Assessment Report of the Intergovernmental Panel on Climate Change* (Barros, V.R., C.B. Field, D.J. Dokken, M.D. Mastrandrea, K.J. Mach, T.E. Bilir, M. Chatterjee, K.L. Ebi, Y.O. Estrada, R.C. Genova, B. Girma, E.S. Kissel, A.N. Levy, S. MacCracken, P.R. Mastrandrea, & L.L. White (eds.)). Cambridge University Press, Cambridge, United Kingdom and New York, NY, USA, pp. 1567-1612.

Larson, K. M., & Small, E. E. (2014). Normalized microwave reflection index: A vegetation measurement derived from GPS networks. *IEEE Journal of Selected Topics in Applied Earth Observations and Remote Sensing*, *7*(5), 1501–1511. https://doi.org/10.1109/JSTARS.2014.2300116

Law, K. S., Roiger, A., Thomas, J. L., Marelle, L., Raut, J.-C., Dalsøren, S., et al. (2017). Local Arctic air pollution: Sources and impacts. *Ambio*, *46*(Suppl 3), 453–463. http://doi.org/10.1007/s13280-017-0962-2

Law, K. S., & Stohl, A. (2007). Arctic Air Pollution: Origins and Impacts. *Science*, *315*(5818), 1537–1540. https://doi.org/10.1126/science.1137695

Law, K. S., Stohl, A., Quinn, P. K., Brock, C. A., Burkhart, J. F., Paris, J., et al. (2014). Arctic Air Pollution: New Insights From POLARCAT-IPY. *Bulletin of the American Meteorogical Society*, *95*(12), 1873–1895. https://doi.org/10.1175/bams-d-13-00017.1

Lawrence, D. M., Koven, C. D., Swenson, S. C., Riley, W. J., & Slater, A. G. (2015). Permafrost thaw and resulting soil moisture changes regulate projected high-latitude CO_2 and CH_4 emissions. *Environmental Research Letters*, *10*(9), 094011. https://doi.org/10.1088/1748-9326/10/9/094011

Laxon, S. W., Giles, K. A., Ridout, A. L., Wingham, D. J., Willatt, R., Cullen, R., et al. (2013). CryoSat-2 estimates of Arctic sea ice thickness and volume. *Geophysical Research Letters*, *40*, 732–737. https://doi.org/10.1002/grl.50193

Le Toan, T., Quegan, S., Davidson, M. W. J., Balzter, H., Paillou, P., Papathanassiou, K., et al. (2011). The BIOMASS mission: Mapping global forest biomass to better understand the terrestrial carbon cycle. *Remote Sensing of Environment*, *115*(11), 2850–2860. https://doi.org/10.1016/j.rse.2011.03.020

Le Traon, P.-Y., Antoine, D., Bentamy, A., Bonekamp, H., Breivik, L. A., Chapron, B., et al. (2015). Use of satellite observations for operational oceanography: Recent achievements and future prospects. *Journal of Opererational Oceanography*, *8*(sup1), s12–s27. https://doi.org/10.1080/1755876X.2015.1022050

Le Vine, D. M., Dinnat, E. P., Meissner, T., Yueh, S. H., Wentz, F. J., Torrusio, S. E., & Lagerloef, G. (2015). Status of Aquarius/SAC-D and Aquarius Salinity Retrievals. *IEEE Journal of Selected Topics in Applied Earth Observations and Remote Sensing*, *8*(12), 5401–5415. https://doi.org/10.1109/JSTARS.2015.2427159

Le Vine, D. M., Lagerloef, G. S. E., & Torrusio, S. E. (2010). Aquarius and remote sensing of sea surface salinity from space. *Proceedings of the IEEE*, *98*(5), 688–703. https://doi.org/10.1109/JPROC.2010.2040550

Lee, S., Gong, T., Feldstein, S. B., Screen, J. A., & Simmonds, I. (2017). Revisiting the cause of the 1989-2009 Arctic surface warming using the surface energy budget: Downward infrared radiation dominates the surface fluxes. *Geophysical Research Letters*, *44*, 10,654–10,661. https://doi.org/10.1002/2017GL075375

Lee, Y. J., Matrai, P. A., Friedrichs, M. A., Saba, V. S., Antoine, D., Ardyna, M., et al. (2015). An assessment of phytoplankton primary productivity in the Arctic Ocean from satellite ocean color/in situ chlorophyll-a based models. *Journal of Geophysical Research: Oceans*, *120*, 6508–6541. https://doi.org/10.1002/2015JC011018

Lehner, B., & Doll, P. (2004). Development and validation of a global database of lakes, reservoirs and wetlands. *Journal of Hydrology*, *296*(1-4), 1–22. https://doi.org/10.1016/j.jhydrol.2004.03.028

Lettenmaier, D. P., Alsdorf, D., Dozier, J., Huffman, G. J., Pan, M., & Wood, E. F. (2015). Inroads of remote sensing into hydrologic science during the WRR era. *Water Resources Research*, *51*, 7309–7342. https://doi.org/10.1002/2015WR017616

Li, C., Hsu, N. C., Sayer, A. M., Krotkov, N. A., Fu, J., Lamsal, L. N., et al. (2016). Satellite observation of pollutant emissions from gas flaring activities near the Arctic. *Atmospheric Environment*, *133*, 1–11. https://doi.org/10.1016/j.atmosenv.2016.03.019

Liang, S., & Strahler, A. (1994). Retrieval of surface BRDF from multiangle remotely sensed data. *Remote Sensing of Environment*, *50*(1), 18–30. https://doi.org/10.1016/0034-4257(94)90091-4

Liebner, S., Ganzert, L., Kiss, A., Yang, S., Wagner, D., & Svenning, M. M. (2015). Shifts in methanogenic community composition and methane fluxes along the degradation of discontinuous permafrost. *Frontiers in Microbiology*, *6*. https://doi.org/10.3389/fmicb.2015.00356

Lind, S., Ingvaldsen, R. B., & Furevik, T. (2018). Arctic warming hotspot in the northern Barents Sea linked to declining sea-ice import. *Nature Climate Change*, *8*(7), 634–639. https://doi.org/10.1038/s41558-018-0205-y

Lindfors, A. V., Kujanpää, J., Kalakoski, N., Heikkilä, A., Lakkala, K., Mielonen, T., et al. (2018). The TROPOMI surface UV algorithm. *Atmospheric Measurement Techniques.*, *11*(2), 997–1008. https://doi.org/10.5194/amt-11-997-2018

Lindqvist, H., O'Dell, C. W., Basu, S., Boesch, H., Chevallier, F., Deutscher, N., et al. (2015). Does GOSAT capture the true seasonal cycle of carbon dioxide? *Atmospheric Chemistry and Physics*, *15*(22), 13,023–13,040. https://doi.org/10.5194/acp-15-13023-2015

Liston, G. E., & Hiemstra, C. A. (2011). The changing cryosphere: Pan-Arctic snow trends (1979–2009). *Journal of Climate*, *24*(21), 5691–5712. https://doi.org/10.1175/JCLI-D-11-00081.1

Liu, L., Jafarov, E. E., Schaefer, K. M., Jones, B. M., Zebker, H. A., Williams, C. A., et al. (2014). InSAR detects increase in surface subsidence caused by an Arctic tundra fire. *Geophysical Research Letters*, *41*, 3906–3913. https://doi.org/10.1002/2014GL060533

Liu, L., Zhang, T., & Wahr, J. (2010). InSAR measurements of surface deformation over permafrost on the North Slope of Alaska. *Journal of Geophysical Research*, *115*(F3), F03023. https://doi.org/10.1029/2009JF001547

Liu, Y., Ackerman, S. A., Maddux, B. C., Key, J. R., & Frey, R. A. (2010). Errors in cloud detection over the Arctic using a satellite imager and implications for observing feedback mechanisms. *Journal of Climate*, *23*(7), 1894–1907. https://doi.org/10.1175/2009JCLI3386.1

Liu, Y., Yang, D. X., & Cai, Z. N. (2013). A retrieval algorithm for TanSat XCO_2 observation: Retrieval experiments using GOSAT data. *Chinese Science Bulletin*, *58*(13), 1520–1523. https://doi.org/10.1007/s11434-013-5680-y

Loboda, T. V., Hoy, E. E., Giglio, L., & Kasischke, E. S. (2011). Mapping burned area in Alaska using MODIS data: A data limitations-driven modification to the regional burned area algorithm. *International Journal of Wildland Fire*, *20*(4), 487–496. https://doi.org/10.1071/WF10017

Loeb, N. G., Doelling, D. R., Wang, H., Su, W., Nguyen, C., Corbett, J. G., et al. (2018). Clouds and the Earth's Radiant Energy System (CERES) Energy Balanced and Filled (EBAF) Top-of-Atmosphere (TOA) Edition-4.0 Data Product. *Journal of Climate*, *31*(2), 895–918. https://doi.org/10.1175/JCLI-D-17-0208.1

Loeb, N. G., Wielicki, B. A., Doelling, D. R., Smith, G. L., Keyes, D. F., Kato, S., et al. (2009). Toward optimal closure of the Earth's top-of-atmosphere radiation budget. *Journal of Climate*, *22*(3), 748–766. http://doi.org/10.1175/2008JCLI2637.1

Loranty, M. M., Abbott, B. W., Blok, D., Douglas, T. A., Epstein, H. E., Forbes, B. C., et al. (2018). Reviews and syntheses: Changing ecosystem influences on soil thermal regimes in northern high-latitude permafrost regions. *Biogeosciences*, *15*(17), 5287–5313. https://doi.org/10.5194/bg-15-5287-2018

Loranty, M. M., Berner, L. T., Goetz, S. J., Jin, Y., & Randerson, J. T. (2014). Vegetation controls on northern high latitude snow-albedo feedback: Observations and CMIP5 model simulations. *Global Change Biology*, *20*(2), 594–606. https://doi.org/10.1111/gcb.12391

Losee, S. T. B. (1942). Air photographs and forest sites: I. mapping methods illustrated on an area of the petawawa forest experiment station. *The Forestry Chronicle*, *18*(3), 129–144. https://doi.org/10.5558/tfc18129-3

Lu, Z., & Sololik, I. N. (2013). The effect of smoke emission amount on changes in cloud properties and precipitation: a case study of Canadian boreal wildfires of 2007. *Journal of Geophysical Research*, *118*, 11,777–11,793. https://doi.org/10.1002/2013JD019860

Lucht, W., Schaaf, C., Strahler, A. H., & d'Entremont, R. (2000). Remote Sensing of Albedo Using the BRDF in Relation to Land Surface Properties. In *Observing Land from Space: Science, Customers and Technology*, (pp. 175–186). Dordrecht: Springer. https://doi.org/10.1007/0-306-48124-3_19

Lund-Hansen, L. C., Markager, S., Hancke, K., Stratmann, T., Rysgaard, S., Ramløv, H., & Sorrell, B. K. (2015). Effects of sea-ice light attenuation and CDOM absorption in the water below the Eurasian sector of central Arctic Ocean (> 88° N). *Polar Research*, *34*(1), 23978. https://doi.org/10.3402/polar.v34.23978

Lundquist, J. D., Dettinger, M. D., Stewart, I. T., & Cayan, D. R. (2009). Variability and trends in spring runoff in the western United States. In F. Wagner (Ed.), *Climate warming in western North America — Evidence and environmental effects* (Chap. 5, pp. 63–76). Salt Lake City, Utah: University of Utah Press.

Luo, H., Castelao, R. M., Rennermalm, A. K., Tedesco, M., Bracco, A., Yager, P. L., & Mote, T. L. (2016). Oceanic transport of surface meltwater from the southern Greenland ice sheet. *Nature Geoscience*, *9*(7), 528–532. https://doi.org/10.1038/ngeo2708

Lutz, D. A., Washington-Allen, R. A., & Shugart, H. H. (2008). Remote sensing of boreal forest biophysical and inventory parameters: A review. *Canadian Journal of Remote Sensing*, *34*(sup2), S286–S313. https://doi.org/10.5589/m08-057

Maaß, N., Kaleschke, L., Tian-Kunze, X., & Drusch, M. (2013). Snow thickness retrieval over thick Arctic sea ice using SMOS satellite data. *The Cryosphere*, *7*(6), 1971–1989. https://doi.org/10.5194/tc-7-1971-2013

Mace, G. G., & Zhang, Q. (2014). The CloudSat radar-lidar geometrical profile product (RL- GeoProf): Updates, improvements, and selected results. *Journal of Geophysical Research: Atmospheres*, *119*, 9441–9462. https://doi.org/10.1002/2013JD021374

Macias Fauria, M., Forbes, B. C., Zetterberg, P., & Kumpula, T. (2012). Eurasian Arctic greening reveals teleconnections and the potential for novel ecosystems. *Nature Climate Change*, *2*(8), 613–618. https://doi.org/10.1038/NCLIMATE1558

Mackie, A. R., Palmer, P. I., Barlow, J. M., Finch, D. P., Novelli, P., & Jaeglé, L. (2016). Reduced Arctic air pollution due to decreasing European and North American emissions. *Journal of Geophysical Research: Atmospheres*, *121*, 8692–8700. https://doi.org/10.1002/2016JD024923

Maghsoudi, Y., Collins, M., & Leckie, D. G. (2012). Polarimetric classification of Boreal forest using nonparametric feature selection and multiple classifiers. *International Journal of Applied Earth Observation and Geoinformation*, *19*, 139–150. https://doi.org/10.1016/j.jag.2012.04.015

Manney, G. L., Santee, M. L., Rex, M., Livesey, N. J., Pitts, M. C., Veefkind, P., et al. (2011). Unprecedented Arctic ozone loss in 2011. *Nature*, *478*(7370), 469–475. https://doi.org/10.1038/nature10556. https://doi.org/10.1038/nature10556

Mannino, A., Friedrichs, M., Hernes, P., Matrai, P., Salisbury, J., Tzortizou, M., & Del Castillo, C. (2018). "*NASA: Arctic-COLORS Scoping Study Report.*" NASA. NASA Ocean Biology and Biogeochemistry Program http://arctic-colors.gsfc.nasa.gov/

Mao, J., Ramanathan, A., Abshire, J. B., Kawa, S. R., Riris, H., Allan, G. R., et al. (2018). Measurement of Atmospheric CO_2 Column Concentrations to Cloud Tops with a Pulsed Multi-wavelength Airborne Lidar. *Atmospheric Measurement Techniques*, *11*(4), 2001–2025. https://doi.org/10.5194/amt-11-2001-2018

Mao, J., Ribes, A., Yan, B., Shi, X., Thornton, P. E., Séférian, R., et al. (2016). Human-induced greening of the northern extratropical land surface. *Nature Climate Change*, *6*(10), 959–963. https://doi.org/10.1038/nclimate3056

Marchenko, S., Hachem, S., Romanovsky, V., & Duguay, C. (2009). Permafrost and active layer modeling in the northern Eurasia using MODIS land surface temperature as an input data. *Geophysical Research Abstracts*, *11*, EGU2009–EGU11077.

Marelle, L., Raut, J.-C., Law, K. S., & Duclaux, O. (2018). Current and future Arctic aerosols and ozone from remote emissions and emerging local sources - modeled source contributions and radiative effects. *Journal of Geophysical Research: Atmospheres*, *123*(22), 123. https://doi.org/10.1029/2018JD028863

Markus, T., & Cavalieri, D. J. (1998). Snow depth distribution over sea ice in the Southern Ocean from satellite passive microwave data. In: *Antarctic Sea Ice: Physical Processes, Interactions and Variability* (ed. by M. O. Jeffries), American Geophysical Union, Washington, D.C., pp. 19-39.

Maslowski, W., Kinney, J. C., Higgins, M., & Roberts, A. (2012). The future of Arctic sea ice. *Annual Review of Earth and Planetary Sciences*, *40*(1), 625–654. https://doi.org/10.1146/annurev-earth-042711-105345

Massom, R., & Lubin, D. (2006). *Polar Remote Sensing, Volume II: Ice Sheets*. Berlin Heidelberg: Springer-Verlag. https://doi.org/10.1007/3-540-30565-3

Massom, R. A. (1991). *Satellite remote sensing of polar regions*. London: Belhaven Press. 307 pp

Masson-Delmotte, V., Schulz, M., Abe-Ouchi, A., Beer, J., Ganopolski, A., González Rouco, J.F., et al., 2013: Information from Paleoclimate Archives. In: Climate Change 2013: The Physical Science Basis. *Contribution of Working Group I to the Fifth Assessment Report of the Intergovernmental Panel on Climate Change* (Stocker, T.F., D. Qin, G.-K. Plattner, M. Tignor, S.K. Allen, J. Boschung, A. Nauels, Y. Xia, V. Bex & P.M. Midgley (eds.)). Cambridge University Press, Cambridge, United Kingdom and New York, NY, USA.

Mastepanov, M., Sigsgaard, C., Dlugokencky, E. J., Houweling, S., Ström, L., Tamstorf, M. P., & Christensen, T. R. (2008). Large tundra methane burst during onset of freezing. *Nature*, *456*(7222), 628–630. https://doi.org/10.1038/nature07464

Matrai, P. A., Olson, E., Suttles, S., Hill, V., Codispoti, L. A., Light, B., & Steele, M. (2013). Synthesis of primary production in the Arctic Ocean: I. Surface waters, 1954–2007. *Progress in Oceanography*, *110*, 93–106. https://doi.org/10.1016/j.pocean.2012.11.004

Matson, M., & Dozier, J. (1981). Identification of subresolution high temperature sources using a thermal IR sensor. *Photogramm. Engng. Remote Sensing*, *47*, 1311–1318.

Matson, M., Roeplewski, C. F., & Varnadore, M. S. (1986). *An atlas of satellite-derived Northern Hemisphere snow cover frequency*. Washington, D.C.: National Weather Service. 75 p

Matson, M., Schneider, S. R., Aldridge, B., & Satchwell, B. (1984). Fire detection using the NOAA-series satellites. In *NOAA-NESS Technical Report 7* (34 p.). Washington, D.C.: National Oceanic and Atmospheric Administration.

Matsuoka, A., Ortega-Retuerta, E., Bricaud, A., Arrigo, K. R., & Babin, M. (2015). Characteristics of colored dissolved organic matter (CDOM) in the Western Arctic Ocean: Relationships with microbial activities. *Deep-Sea Research Part II: Topical Studies in Oceanography*, *118*, 44–52. https://doi.org/10.1016/j.dsr2.2015.02.012

Matthews, E., & Fung, I. (1987). Methane emission from natural wetlands: Global distribution, area, and environmental characteristics of sources. *Global Biogeochemical Cycles*, *1*(1), 61–86. https://doi.org/10.1029/GB001i001p00061

McConnell, J.C., McElroy, C. T., Sioris, C., O'Neill, N., Nassar, R., Buijs, H., et al., & the PHEOS Science Team (2012). PCW/PHEOS-WCA: Quasi-geostationary viewing of the Arctic and environs for Weather, Climate and Air Quality, *Proceedings of the European Space Agency (ESA) Atmospheric Science Conference, Bruges, Belgium 2012*. European Space Agency. http://esamultimedia.esa.int/multimedia/publications/SP-708/SP-708_toc.pdf

McDonald, K. C., & Kimball, J. S. (2006). Estimation of surface freeze-thaw states using microwave sensors. *Encyclopedia of Hydrological Sciences*, *5*, 53.

McDonald, K. C., Kimball, J. S., Njoku, E., Zimmermann, R., & Zhao, M. (2004). Variability in Springtime Thaw in the Terrestrial High Latitudes: Monitoring a Major Control on the Biospheric Assimilation of Atmospheric CO_2 with Spaceborne Microwave Remote Sensing. *Earth Interactions*, *8*, 20.

McGuire, A. D., Anderson, L. G., Christensen, T. R., Dallimore, S., Guo, L., Hayes, D. J., et al. (2009). Sensitivity of the carbon cycle in the Arctic to climate change. *Ecological Monographs*, *79*(4), 523–555. https://doi.org/10.1890/08-2025.1

McGuire, A. D., Chapin, F. S. III, Walsh, J. E., & Wirth, C. (2006). Wirth Integrated Regional Changes in Arctic Climate Feedbacks: Implications for the Global Climate System. *Annual Review of Environment and Resources*, *31*(1), 61–91. https://doi.org/10.1146/annurev.energy.31.020105.100253

McGuire, A. D., Christensen, T. R., Hayes, D., Heroult, A., Euskirchen, E., Kimball, J. S., et al. (2012). An assessment of the carbon balance of Arctic tundra: Comparisons among observations, process models, and atmospheric inversions. *Biogeosciences*, *9*(8), 3185–3204. https://doi.org/10.5194/bg-9-3185-2012

McGuire, A. D., Koven, C., Lawrence, D. M., Clein, J. S., Xia, J., Beer, C., et al. (2016). Variability in the sensitivity among model simulations of permafrost and carbon dynamics in the permafrost region between 1960 and 2009. *Global Biogeochemical Cycles*, *30*, 1015–1037. https://doi.org/10.1002/2016GB005405

McGuire, A. D., Lawrence, D. M., Koven, C., Clein, J. S., Burke, E., Chen, G., Jafarov, E., et al. (2018). Dependence of the evolution of carbon dynamics in the northern permafrost region on the trajectory of climate change. *Proceedings of the National Academy of Sciences*, *115*(15), 3882–3887. https://doi.org/10.1073/pnas.1719903115

McKuin, B., & Campbell, J. E. (2016). Emissions and climate forcing from global and Arctic fishing vessels. *Journal of Geophysical Research*, *121*(4), 1844–1858. https://doi.org/10.1002/2015JD023747

McMillan, M., Leeson, A. A., Shepherd, A., Briggs, K., Armitage, T. W. K., Hogg, A., et al. (2016). A high-resolution record of Greenland mass balance. *Geophysical Research Letters*, *43*, 7002–7010. https://doi.org/10.1002/2016GL069666

MEA (2005). *Ecosystems and Human Well-Being: Wetlands and Water Synthesis*. Washington, DC: World Resources Institute.

Meier, W. N., & Markus, T. (2015). Remote sensing of sea ice. In M. Tedesco (Ed.), *Remote Sensing of the Cryosphere*, (pp. 248–272). Hoboken, New Jersey: John Wiley and Sons.

Melillo, J. M., Richmond, T. C., & Yohe, G. W. (2014). *Climate Change Impacts in the United States: The Third National Climate Assessment* (Vol. 841). Washington, DC: U.S. Global Change Research Program.

Melvin, A. M., Larsen, P., Boehlert, B., Neumann, J. E., Chinowsky, P., Espinet, X., et al. (2017). Climate change damages to Alaska public infrastructure and the economics of proactive adaptation. *Proceedings of the National Academy of Sciences*, *114*(2), E122–E131. https://doi.org/10.1073/pnas.1611056113

Ménard, C. B., Essery, R., & Pomeroy, J. (2014). Modelled sensitivity of the snow regime to topography, shrub fraction and shrub height. *Hydrology and Earth System Sciences*, *18*(6), 2375–2392. https://doi.org/10.5194/hess-18-2375-2014

Meng, L., Hess, P. G. M., Mahowald, N. M., Yavitt, J. B., Riley, W. J., Subin, Z. M., et al. (2012). Sensitivity of wetland methane emissions to model assumptions: Application and model testing against site observations. *Biogeosciences*, *9*(7), 2793–2819. https://doi.org/10.5194/bg-9-2793-2012

Messager, M. L., Lehner, B., Grill, G., Nedeva, I., & Schmitt, O. (2016). Estimating the volume and age of water stored in global lakes using a geo-statistical approach. *Nature Communications*, *7*(1), 13603 (2016). https://doi.org/10.1038/ncomms13603

Metcalfe, D. B., Hermans, T. D. G., Ahlstrand, J., Becker, M., Berggren, M., Björk, R. G., et al. (2018). Patchy field sampling biases understanding of climate change impacts across the Arctic. *Nature Ecology & Evolution*, *2*(9), 1443–1448. https://doi.org/10.1038/s41559-018-0612-5

Michaelides, R. J., Schaefer, K., Zebker, H. A., Parsekian, A., Liu, L., Chen, J., et al. (2019). Inference of the impact of wildfire on permafrost and active layer thickness in a discontinuous permafrost region using the remotely sensed active layer thickness (ReSALT) algorithm. *Environmental Research Letters*, *14*(3), 3. https://doi.org/10.1088/1748-9326/aaf932

Middleton, E. M., Ungar, S. G., Mandl, D. J., Ong, L., Frye, S. W., Campbell, P. E., et al. (2013). The Earth Observing One (EO-1) Satellite Mission: Over a Decade in Space. *IEEE Journal of Selected Topics in Applied Earth Observations and Remote Sensing*, *6*(2), 243–256. https://doi.org/10.1109/JSTARS.2013.2249496

Miège, C., Forster, R. R., Brucker, L., Koenig, L. S., Solomon, D. K., Paden, J. D., et al. (2016). Spatial extent and temporal variability of Greenland firn aquifers detected by ground and airborne radars. *Journal of Geophysical Research: Earth Surface*, *121*, 2381–2398. https://doi.org/10.1002/2016JF003869

Mielonen, T., Aaltonen, V., Lihavainen, H., Hyvärinen, A.-P., Arola, A., Komppula, M., & Kivi, R. (2013). Biomass Burning Aerosols Observed in Northern Finland during the 2010 Wildfires in Russia. *Atmosphere*, *4*(1), 17–34. https://doi.org/10.3390/atmos4010017

Mielonen, T., Portin, H., Komppula, M., Leskinen, A., Tamminen, J., Ialongo, I., et al. (2012). Biomass burning aerosols observed in Eastern Finland during the Russian wildfires in summer 2010—Part 2: Remote sensing. *Atmospheric Environment*, *47*, 279–287. https://doi.org/10.1016/j.atmosenv.2011.07.016

Miller, C. E., & Dinardo, S. J. (2012). *"CARVE: The Carbon in Arctic Reservoirs Vulnerability Experiment", IEEE Aerospace Conference 3-10 March 2012*, (pp. 1–17). MT: Big Sky. https://doi.org/10.1109/AERO.2012.6187026

Miller, C. E., Griffith, P. C., Goetz, S. J., Hoy, E. E., Pinto, N., McCubbin, I. B., et al. (2019). An overview of ABoVE airborne campaign data acquisitions and science opportunities. *Environmental Research Letters*, *14*(8), 080201. https://doi.org/10.1088/1748-9326/ab0d44

Miller, O. L., Solonon, D. K., Miège, C., Koenig, L. S., Forster, R. R., Montgomery, L. N., et al. (2017). Hydraulic conductivity of a firn aquifer system in southeast Greenland. *Frontiers in Earth Science - Cryospheric Sciences.*, *5*. https://doi.org/10.3389/feart.2017.00038

Miller, S. M., Miller, C. E., Commane, R., Chang, R. Y. W., Dinardo, S. J., Henderson, J. M., et al. (2016). A multiyear estimate of methane fluxes in Alaska from CARVE atmospheric observations. *Global Biogeochemical Cycles*, *30*, 1441–1453. https://doi.org/10.1002/2016GB005419

Minsley, B. J., Pastick, N. J., Wylie, B. K., Brown, D. R. N., & Kass, M. A. (2016). Evidence for nonuniform permafrost degradation after fire in boreal landscapes. *Journal of Geophysical Research: Earth Surface*, *121*, 320–335. https://doi.org/10.1002/2015JF003781

Monks, S. A., Arnold, S. R., Emmons, L. K., Law, K. S., Turquety, S., Duncan, B. N., et al. (2015). Multi-model study of chemical and physical controls on transport of anthropogenic and biomass burning pollution to the Arctic. *Atmospheric Chemistry and Physics*, *15*(6), 3575–3603. https://doi.org/10.5194/acp-15-3575-2015

Montesano, P., Neigh, C., Sexton, J., Feng, M., Channan, S., Ranson, K., & Townshend, J. (2016). Calibration and Validation of Landsat Tree Cover in the Taiga– Tundra Ecotone. *Remote Sensing*, *8*(7), 551. https://doi.org/10.3390/rs8070551

Montesano, P. M., Neigh, C., Sun, G., Duncanson, L., Van Den Hoek, J., & Ranson, K. J. (2017). The use of sun elevation angle for stereogrammetric boreal forest height in open canopies. *Remote Sensing of Environment*, *196*, 76–88. https://doi.org/10.1016/j.rse.2017.04.024

Montesano, P. M., Neigh, C. S. R., Wagner, W., Wooten, M., & Cook, B. D. (2019). Boreal canopy surfaces from spaceborne stereogrammetry. *Remote Sensing of Environment*, *225*, 148–159. https://doi.org/10.1016/j.rse.2019.02.012

Montesano, P. M., Nelson, R., Sun, G., Margolis, H., Kerber, A., & Ranson, K. J. (2009). MODIS tree cover validation for the circumpolar taiga-tundra transition zone. *Remote Sensing of Environment*, *113*(10), 2130–2141. https://doi.org/10.1016/j.rse.2009.05.021

Montesano, P. M., Sun, G., Dubayah, R. O., & Ranson, K. J. (2016). Spaceborne potential for examining taiga-tundra ecotone form and vulnerability. *Biogeosciences*, *13*(13), 3847–3861. https://doi.org/10.5194/bg-13-3847-2016

Moon, T., Ahlstrøm, A., Goelzer, H., Lipscomb, W., & Nowicki, S. (2018). Rising Oceans Guaranteed: Arctic Land Ice Loss and Sea Level Rise. *Current Climate Change Reports*, *4*(3), 211–222. https://doi.org/10.1007/s40641-018-0107-0

Moon, T. A., Overeem, I., Druckenmiller, M., Holland, M., Huntington, H., Kling, G., et al. (2019). The expanding footprint of rapid Arctic change. *Earth's Future*, *7*(3), 212–218. https://doi.org/10.1029/2018EF001088

Moore, B., Crowell, S. M. R., Rayner, P. J., Kumer, J., O'Dell, C. W., O'Brien, D., et al. (2018). The Potential of the Geostationary Carbon Cycle Observatory (GeoCarb) to Provide Multi-scale Constraints on the Carbon Cycle in the Americas. *Frontiers of Environmental Science*, *6*. https://doi.org/10.3389/fenvs.2018.00109

Mori, M., Watanabe, M., Shiogama, H., Inoue, J., & Kimoto, M. (2014). Robust Arctic sea-ice influence on the frequent Eurasian cold winters in past decades. *Nature Geoscience*, *7*(12), 869–873. https://doi.org/10.1038/NGEO2277

Morlighem, M., Rignot, E., Mouginot, J., Seroussi, H., & Larour, E. (2014). Deeply incised submarine glacial valleys beneath the Greenland Ice Sheet. *Nature Geoscience*, *7*(6), 418–422. https://doi.org/10.1038/ngeo2167

Morrison, H., de Boer, G., Feingold, G., Harrington, J., Shupe, M. D., & Sulia, K. (2012). Resilience of persistent Arctic mixed-phase clouds. *Nature Geoscience*, *5*(1), 11–17. https://doi.org/10.1038/NGEO1332

Morriss, B. F., Hawley, R. L., Chipman, J. W., Andrews, L. C., Catania, G. A., Hoffman, M. J., et al. (2013). A ten-year record of supraglacial lake evolution and rapid drainage in West Greenland using an automated processing algorithm for multispectral imagery. *The Cryosphere*, *7*(6), 1869–1877. https://doi.org/10.5194/tc-7-1869-2013

Mote, P. W., Hamlet, A. F., Clark, M. P., & Lettenmaier, D. P. (2005). Declining mountain snowpack in western North America. *Bulletin of the American Meteorological Society*, *86*(1), 39–50. https://doi.org/10.1175/BAMS-86-1-39

Mouginot, J., Rignot, E., Scheuchl, B., Fenty, I., Khazendar, A., Morlighem, M., et al. (2015). Fast retreat of Zachariæ Isstrøm, northeast Greenland. *Science*, *350*(6266), 1357–1361. https://doi.org/10.1126/science.aac7111

Mouginot, J., Rignot, E., Scheuchl, B., & Millan, R. (2017). Comprehensive Annual Ice Sheet Velocity Mapping Using Landsat-8, Sentinel-1, and RADARSAT-2 Data. *Remote Sensing*, *9*(4), 364. https://doi.org/10.3390/rs9040364

Muirhead, K., & Cracknell, A. P. (1984). Identification of gas flares in the North Sea using satellite data. *International Journal of Remote Sensing*, *5*(1), 199–212. https://doi.org/10.1080/01431168408948798

Muirhead, K., & Cracknell, A. P. (1985). Straw burning over Great Britain detected by AVHRR. *International Journal of Remote Sensing*, *6*(5), 827–833. https://doi.org/10.1080/01431168508948506

Muster, S., Roth, K., Langer, M., Lange, S., Cresto Aleina, F., Bartsch, A., et al. (2017). PeRL: A circum-Arctic Permafrost Region Pond and Lake database. *Earth System Science Data*, *9*(1), 317–348. https://doi.org/10.5194/essd-9-317-2017

Myers-Smith, I. H., Elmendorf, S. C., Beck, P. S. A., Wilmking, M., Hallinger, M., Blok, D., et al. (2015). Climate sensitivity of shrub expansion across the tundra biome. *Nature Climate Change*, *5*(9), 887–891. https://doi.org/10.1038/nclimate2697

Myers-Smith, I. H., Forbes, B. C., Wilmking, M., Hallinger, M., Lantz, T., Bok, D., et al. (2011). Shrub expansion in tundra ecosystems: Dynamics, impacts and research priorities. *Environmental Research Letters*, *6*(4), 045509. https://doi.org/10.1088/1748-9326/6/4/045509

Myhre, G., Shindell, D., Bréon, F.-M., Collins, W., Fuglestvedt, J., Huang, J., et al. (2013). Anthropogenic and Natural Radiative Forcing. In: *Climate Change 2013: The Physical Science Basis. Contribution of Working Group I to the Fifth Assessment Report of the Intergovernmental Panel on Climate Change*. Cambridge University Press, Cambridge, United Kingdom and New York, NY, USA.

Myneni, R., Knyazikhin, Y., & Park, T. (2015). MCD15A2H MODIS/Terra+Aqua Leaf Area Index/FPAR 8-day L4 Global 500m SIN Grid V006 [Data set]. *NASA EOSDIS Land Processes DAAC*. https://doi.org/10.5067/MODIS/MCD15A2H.006

Myneni, R. B., Keeling, C. D., Tucker, C. J., Asrar, G., & Nemani, R. R. (1997). Increased plant growth in the northern high latitudes from 1981 to 1991. *Nature*, *386*(6626), 698–702. https://doi.org/10.1038/386698a0

Naeimi, V., Paulik, C., Bartsch, A., Wagner, W., Kidd, R., Park, S. E., et al. (2012). ASCAT Surface State Flag (SSF): Extracting Information on Surface Freeze/Thaw Conditions From Backscatter Data Using an Empirical Threshold-Analysis Algorithm. *IEEE Transactions on Geoscience and Remote Sensing*, *50*(7), 2566–2582. https://doi.org/10.1109/TGRS.2011.2177667

Nakamura, T., Yamazaki, K., Iwamoto, K., Honda, M., Miyoshi, Y., Ogawa, Y., et al. (2016). The stratospheric pathway for Arctic impacts on midlatitude climate. *Geophysical Research Letters*, *43*, 3494–3501. https://doi.org/10.1002/2016GL068330

Nassar, R., McLinden, C., Sioris, C. E., McElroy, C. T., Mendonca, J., Tamminen, J., et al. (2019). The Atmospheric Imaging Mission for Northern Regions: AIM-North. *Canadian Journal of Remote Sensing*, *45*(3-4), 423–442. https://doi.org/10.1080/07038992.2019.1643707

Nassar, R., Sioris, C. E., Jones, D. B. A., & McConnell, J. C. (2014). Satellite observations of CO_2 from a highly elliptical orbit for studies of the Arctic and boreal carbon cycle. *Journal of Geophysical Research: Atmospheres*, *119*, 2654–2673. https://doi.org/10.1002/2013JD020337

National Academies of Sciences, Engineering, and Medicine (2018). *Thriving on Our Changing Planet: A Decadal Strategy for Earth Observation from Space*. Washington, DC: The National Academies Press. https://doi.org/10.17226/24938

National Research Council (2003). *Satellite Observations of the Earth's Environment: Accelerating the Transition of Research to Operations*. Washington, D.C.: The National Academies Press.

National Research Council (2007). *Earth Science and Applications from Space: National Imperatives for the Next Decade and Beyond*. Washington, DC: The National Academies Press. https://doi.org/10.17226/11820

National Research Council (2013). *Abrupt Impacts of Climate Change: Anticipating Surprises*. Washington, D.C.: The National Academies Press.

National Research Council (2014a). *The Arctic in the Anthropocene: Emerging Research Questions*. Washington, DC: The National Academies Press. https://doi.org/10.17226/18726, http://www.nap.edu/openbook.php?record_id=18726
National Research Council (2014b). *Opportunities to Use Remote Sensing in Understanding Permafrost and Related Ecological Characteristics*. Washington, DC: The National Academies Press. http://www.nap.edu/openbook.php?record_id=18711
Neigh, C. S. R., Nelson, R. F., Ranson, K. J., Margolis, H. A., Montesano, P. M., Sun, G., et al. (2013). Taking stock of circumboreal forest carbon with ground measurements, airborne and spaceborne LiDAR. *Remote Sensing of Environment*, *137*, 274–287. https://doi.org/10.1016/j.rse.2013.06.019
Nghiem, S. V., Rigor, I. G., Perovich, D. K., Clemente-Colon, P., Weatherly, J. W., & Neumann, G. (2007). Rapid reduction of Arctic perennial sea ice. *Geophysical Research Letters*, *34*, L19504. https://doi.org/10.1029/2007GL031138
Nghiem, S. V., & Tsai, W.-Y. (2001). Global snow cover monitoring with spaceborne K-band scatterometer, Institute of Electrical and Electronic Engineers. *Transactions on Geoscience and Remote Sensing*, *39*(10), 2118–2134. https://doi.org/10.1109/36.957275
Novelli, P. C., Masarie, K. A., & Lang, P. M. (1998). Distributions and recent changes of carbon monoxide in the lower troposphere. *Journal of Geophysical Research*, *103*(D15), 19015–19033. https://doi.org/10.1029/98JD01366
Oechel, W. C., Laskowski, C. A., Burba, G., Gioli, B., & Kalhori, A. A. M. (2014). Annual patterns and budget of CO_2 flux in an Arctic tussock tundra ecosystem. *Journal of Geophysical Research: Biogeosciences*, *119*, 323–339. https://doi.org/10.1002/2013JG002431
Olefeldt, D., Goswami, S., Grosse, G., Hayes, D., Hugelius, G., Kuhry, P., et al. (2016). Circumpolar distribution and carbon storage of thermokarst landscapes. *Nature Communications*, *7*(1), 13043. https://doi.org/10.1038/ncomms13043.
Omar, A. H., Winker, D. M., Vaughan, M. A., Hu, Y., Trepte, C. R., Ferrare, R. A., et al. (2009). The CALIPSO Automated Aerosol Classification and Lidar Ratio Selection Algorithm. *Journal of Atmospheric and Oceanic Technology*, *26*(10), 1994–2014. https://doi.org/10.1175/2009JTECHA1231.1
Osborne, E., Richter-Menge, J., & Jeffries, M. (Eds) (2018). *Arctic Report Card*, 2018. https://www.arctic.noaa.gov/Report-Card
Osterkamp, T. E. (2007). Characteristics of the recent warming of permafrost in Alaska. *Journal of Geophysical Research Atmospheres*, *112*(F2), 10. https://doi.org/10.1029/2006JF000578
Osterkamp, T. E., & Romanovsky, V. E. (1996). Characteristics of changing permafrost temperatures in the Alaskan Arctic, USA. *Arctic and Alpine Research*, *28*(3), 267–273. https://doi.org/10.2307/1552105
Overland, J. E., Hanna, E., Hanssen-Bauer, I., Kim, S. J., Walsh, J. E., Wang, M., et al. (2018). Surface Air Temperature. *Arctic Report Card*, *2018*. https://www.arctic.noaa.gov/Report-Card
Overland, J. E., & Wang, M. (2018). Resolving future Arctic/Midlatitude weather connections. *Earth's Future*, *6*(8), 1146–1152. https://doi.org/10.1029/2018EF000901
Oyle, J. W., Mildrexler, D. J. & Comiso, J. C., (2019, in press). Surface temperature inter-relationships, in "*Taking the Temperature of the Earth*," Chapter 6, Springer.
Palm, S. P., Kayetha, V., Yang, Y., & Pauly, R. (2017). Blowing Snow Sublimation and Transport over Antarctica from 11 Years of CALIPSO Observations. *The Cryosphere*, *11*(6), 2555–2569. https://doi.org/10.5194/tc-11-2555-2017
Palm, S. P., Yang, Y. K., Spinhirne, J. D., & Marshak, A. (2011). Satellite remote sensing of blowing snow properties over Antarctica. *Journal of Geophysical Research Atmospheres*, *116*, 116. https://doi.org/10.1029/2011jd015828
Pantze, A., Santoro, M., & Fransson, J. E. S. (2014). Change detection of boreal forest using bi-temporal ALOS PALSAR backscatter data. *Remote Sensing of Environment*, *155*, 120–128. https://doi.org/10.1016/j.rse.2013.08.050
Parazoo, N. C., Koven, C. D., Lawrence, D. M., Romanovsky, V., & Miller, C. E. (2018). Detecting the permafrost carbon feedback: Talik formation and increased cold-season respiration as precursors to sink-to-source transitions. *The Cryosphere*, *12*(1), 123–144. https://doi.org/10.5194/tc-12-123-2018
Parida, B. R., & Buermann, W. (2014). Increasing summer drying in North American ecosystems in response to longer nonfrozen periods. *Geophysical Research Letters*, *41*, 5476–5483. https://doi.org/10.1002/2014GL060495
Park, H., Fedorov, A. N., Zheleznyak, M. N., Konstantinov, P. Y., & Walsh, J. E. (2015). Effect of snow cover on pan-Arctic permafrost thermal regimes. *Climate Dynamics*, *44*(9-10), 2873–2895. https://doi.org/10.1007/s00382-014-2356-5
Parkinson, C. L. (2014). Spatially mapped reductions in the length of the Arctic sea ice season. *Geophysical Research Letters*, *41*, 4316–4322. https://doi:10.1002/2014GL060434
Parkinson, C. L., & Cavalieri, D. J. (2012). Floating ice: Sea ice. In R. S. Williams, Jr., & J. G. Ferrigno (Eds.), *Satellite Image Atlas of Glaciers of the World: State of the Earth's Cryosphere at the Beginning of the 21st Century: Glaciers, Global Snow Cover, Floating Ice, Permafrost and Periglacial Environments* (pp. A345-A380 – A415-A424). Washington, DC: U.S. Geological Survey.
Parkinson, C. L., Cavalieri, D. J., Gloersen, P., Zwally, H. J., & Comiso, J. C. (1999). Arctic sea ice extents, areas, and trends, 1978-1996. *Journal of Geophysical Research*, *104*(C9), 20837–20856. https://doi.org/10.1029/1999JC900082
Parmentier, F.-J. W., Christensen, T. R., Sørensen, L. L., Rysgaard, S., McGuire, A. D., Miller, P. A., & Walker, D. A. (2013). The impact of lower sea-ice extent on Arctic greenhouse-gas exchange. *Nature Climate Change*, *3*(3), 195–202. https://doi.org/10.1038/nclimate1784
Parmentier, F. J. W., Christensen, T. R., Rysgaard, S., Bendtsen, J., Glud, R. N., Else, B., et al. (2017a). A synthesis of the arctic terrestrial and marine carbon cycles under pressure from a dwindling cryosphere. *Ambio*, *46*(Suppl 1), 53–69. https://doi.org/10.1007/s13280-016-0872-8
Parmentier, F.-J. W., Christensen, T. R., Rysgaard, S., Bendtsen, J., Glud, R. N., Else, B., et al. (2017b). A synthesis of the arctic terrestrial and marine carbon cycles under pressure from a dwindling cryosphere. *Ambio*, *46*(Suppl 1), 53–69. http://doi.org/10.1007/s13280-016-0872-8
Parmentier, F.-J. W., Zhang, W., Mi, Y., Zhu, X., van Huissteden, J., Hayes, D. J., et al. (2015). Rising methane emissions from northern wetlands associated with sea ice decline. *Geophysical Research Letters*, *42*, 7214–7222. https://doi.org/10.1002/2015GL065013
Pastick, N.J., Duffy, P., Genet, H., Rupp, T. S., Wylie, B. K., Johnson, K. D., et al. (2017). Historical and projected trends in landscape drivers affecting carbon dynamics in Alaska. *Ecological Applications*, *27*(5), 2017, pp. 1383–1402. https://doi.org/10.1002/eap.1538.
Payne, V. H., Shephard, M. W., Clough, S. A., Logan, J. A., & Nassar, R. (2009). Information-centered representation of retrievals with limited degrees of freedom for signal: Application to methane from the Tropospheric Emission Spectrometer. *Journal of Geophysical Research*, *114*(D10), D10307. https://doi.org/1029/2008JD101055
Pearson, R. G., Phillips, S. J., Loranty, M. M., Beck, P. S. A., Damoulas, T., Knight, S. J., & Goetz, S. J. (2013). Shifts in Arctic vegetation and associated feedbacks under climate change. *Nature Climate Change*, *3*(7), 673–677. https://doi.org/10.1038/NCLIMATE1858
Pekel, J. F., Cottam, A., Gorelick, N., & Belward, A. S. (2016). High-resolution mapping of global surface water and its long-term changes. *Nature*, *540*(7633), 418–422. https://doi.org/10.1038/nature20584

Peng, C., Ma, Z., Lei, X., Zhu, Q., Chen, H., Wang, W., et al. (2011). A drought-induced pervasive increase in tree mortality across Canada's boreal forests. *Nature Climate Change*, *1*(9), 467–471. https://doi.org/10.1038/NCLIMATE1293

Perovich, D. K., Grenfell, T. C., Righter-Menge, J. A., Light, B., Tucker, W. B. III, & Eicken, H. (2003). Thin and thinner: Sea ice mass balance measurements during SHEBA. *Journal of Geophysical Research*, *108*(C3), 8050. https://doi.org/10.1029/2001JC001079

Perovich, D. K., Light, B., Eicken, H., Jones, K. F., Runciman, K., & Nghiem, S. V. (2007). Increasing solar heating of the Arctic Ocean and adjacent seas, 2979-2005: Attribution and role in the ice-albedo feedback. *Geophysical Research Letters*, *34*, L19505. https://doi.org/10.1029/2007GL031480

Persson, P. O. G., Fairall, C. W., Andreas, E. L., Guest, P. S., & Perovich, D. K. (2002). Measurements near the Atmospheric Surface Flux Group tower at SHEBA: Near-surface conditions and surface energy budget. *Journal of Geophysical Research*, *107*(C10), 8045. https://doi.org/10.1029/2000JC000705

Peters, G. P., Nilssen, T. B., Lindholt, L., Eide, M. S., Glomsrød, S., Eide, L. I., & Fuglestvedt, J. S. (2011). Future emissions from petroleum and shipping activities in the Arctic. *Atmospheric Chemistry and Physics*, *11*(11), 5305–5320. https://doi.org/10.5194/acp-11-5305-2011

Peterson, C. A., Chen, X., Yue, Q., & Huang, X. (2019). The spectral dimension of Arctic outgoing longwave radiation and greenhouse efficiency trends from 2003 to 2016. *Journal of Geophysical Research: Atmospheres*, *124*, 8467, 2019JD030428–8480. https://doi.org/10.1029/2019JD030428

Peterson, D. A., Campbell, J. R., Hyer, E. J., Fromm, M. D., Kablick, G. P., Cossuth, J. H., & DeLand, M. T. (2018). Wildfire-driven thunderstorms cause a volcano-like stratospheric injection of smoke. *Nature Partner Journals Climate and Atmospheric Science*, *1*(1), 30. https://doi.org/10.1038/s41612-018-0039-3

PGC (2017). In U.O.M.S.P.M. Polar Geospatial Center (Ed.), *Arctic DEM*. St. Paul, Miennesota, USA: Polar Geospatial Center, University of Minnesota St. Paul Minnesota.

Phoenix, G. K., & Bjerke, J. W. (2016). Arctic browning: Extreme events and trends reversing arctic greening. *Global Change Biology*, *22*(9), 2960–2962. https://doi.org/10.1111/gcb.13261

Piao, S., Ciais, P., Friedlingstein, P., Peylin, P., Reichstein, M., Luyssaert, S., et al. (2008). Net carbon dioxide losses of northern ecosystems in response to autumn warming. *Nature*, *451*(7174), 49–52. https://doi.org/10.1038/nature06444

Piao, S., Friedlingstein, P., Ciais, P., Viovy, N., & Demarty, J. (2007). Growing season extension and its impact on terrestrial carbon cycle in the Northern Hemisphere over the past 2 decades. *Global Biogeochemical Cycles*, *21*, GB3018. https://doi.org/10.1029/2006GB002888

Pistone, K., Eisenman, I., & Ramanathan, V. (2014). Observational determination of albedo decrease caused by vanishing Arctic sea ice. *Proceedings of the National Academy of Sciences*, *111*(9), 3322–3326. https://doi.org/10.1073/pnas.1318201111

Pithan, F., & Mauritsen, T. (2014). Arctic amplification dominated by temperature feedbacks in contemporary climate models. *Nature Geoscience*, *7*(3), 181–184. https://doi.org/10.1038/ngeo2071

Platnick, S., King, M. D., Ackerman, S. A., Menzel, W. P., Baum, B. A., Riedi, J. C., & Frey, R. A. (2003). The MODIS cloud products: Algorithms and examples from Terra. *IEEE Trans. Geosci. Remote Sens.*, *41*(2), 459–473. https://doi.org/10.1109/TGRS.2002.808301

Podest, E., McDonald, K. C., & Kimball, J. S. (2014). Multisensor Microwave Sensitivity to Freeze/Thaw Dynamics Across a Complex Boreal Landscape. *IEEE Transactions on Geoscience and Remote Sensing*, *52*(11), 6818–6828. https://doi.org/10.1109/TGRS.2014.2303635

Poinar, K., Joughin, I., Lilien, D., Brucker, L., Kehrl, L., & Nowicki, S. (2017). Drainage of Southeast Greenland firn aquifer water through crevasses to the bed. *Frontiers in Earth Science - Cryospheric Sciences*, *5*. https://doi.org/10.3389/feart.2017.00005

Polar Space Task Group - SAR Coordination Working Group (2016). *Data Compendium - Summary Documentation of SAR Satellite Data Collections*. Saint Hubert, QC, Canada: Plans and Activities. 44 p

Pommier, M., Law, K. S., Clerbaux, C., Turquety, S., Hurtmans, D., Hadji-Lazaro, J., et al. (2010). IASI carbon monoxide validation over the Arctic during POLARCAT spring and summer campaigns. *Atmospheric Chemistry and Physics*, *10*(21), 10655–10678. https://doi.org/10.5194/acp-10-10655-2010

Ponomarev, E., Kharuk, V., & Ranson, K. (2016). Wildfires Dynamics in Siberian Larch Forests. *Forests*, *7*(12), 125. https://doi.org/10.3390/f7060125

Poulter, B., Bousquet, P., Canadell, J. G., Ciais, P., Peregon, A., Saunois, M., et al. (2017). Global wetland contribution to 2000-2012 atmospheric methane growth rate dynamics. *Environmental Research Letters*, *12*(9), 094013. https://doi.org/10.1088/1748-9326/aa8391

Price, C., & Rind, D. (1994). Possible implications of global climate change on global lightning distributions and frequencies. *Journal of Geophysical Research*, *99*(D5), 10823–10831. https://doi.org/10.1029/94JD00019

Prigent, C., Lettenmaier, D. P., Aires, F., & Papa, F. (2016). Towards a high-resolution monitoring of continental surface water extent and dynamics, at global scale: From GIEMS (Global Inundation Extent from Multi-Satellites) to SWOT (Surface Water Ocean Topography). *Surveys in Geophysics*, *37*(2), 339–355. https://doi.org/10.1007/s10712-015-9339-x

Prigent, C., Matthews, E., Aires, F., & Rossow, W. B. (2001). Remote sensing of global wetland dynamics with multiple satellite data sets. *Geophysical Research Letters*, *28*(24), 4631–4634. https://doi.org/10.1029/2001GL013263

Prigent, C., Papa, F., Aires, F., Jimenez, C., Rossow, W. B., & Matthews, E. (2012). Changes in land surface water dynamics since the 1990s and relation to population pressure. *Geophysical Research Letters*, *39*, L08403. https://doi.org/10.1029/2012GL051276

Proshutinsky, A., Ashik, I. M., Dvorkin, E. N., Häkkinen, S., Krishfield, R. A., & Peltier, W. R. (2004). Secular sea level change in the Russian sector of the Arctic Ocean. *Journal of Geophysical Research*, *109*(C3), C03042. https://doi.org/10.1029/2003JC002007

Pulliainen, J., Aurela, M., Laurila, T., Aalto, T., Takala, M., Salminen, M., et al. (2017). Early snowmelt significantly enhances boreal springtime carbon uptake. *Proceedings of the National Academy of Sciences*, *114*(42), 11081–11086. www.pnas.org/cgi/, https://doi.org/10.1073/pnas.1707889114

Qian, Y., Yasunari, T. J., Doherty, S. J., Flanner, M. G., Lau, W. K. M., Ming, J., et al. (2015). Light-absorbing particles in snow and ice: Measurement and modeling of climatic and hydrological impact. *Advances in Atmospheric Sciences*, *32*(1), 64–91. https://doi.org/10.1007/s00376-014-0010-0

Quinn, P. K., Bates, T. S., Baum, E., Doubleday, N., Fiore, A. M., Flanner, M., et al. (2008). Short-lived pollutants in the Arctic: Their climate impact and possible mitigation strategies. *Atmospheric Chemistry and Physics*, *8*(6), 1723–1735. https://doi.org/10.5194/acp-8-1723-2008

Quinn, P. K., Shaw, G., Andrews, E., Dutton, E. G., Ruoho-Airola, T., & Gong, S. L. (2007). Arctic haze: Current trends and knowledge gaps. *Tellus*, *59*(1), 115–129. https://doi.org/10.1111/j.1600-0889.2006.00238.x

Ramsay, B. H. (1998). The interactive multisensor snow and ice mapping system. *Hydrological Processes*, *12*(10–11), 1537–1546. https://doi.org/10.1002/(SICI)1099-1085(199808/09)12:10/11<1537::AID-HYP679>3.0.CO;2-A

Rango, A., Salomonson, V. V., & Foster, J. L. (1977). Seasonal streamflow estimation in the Himalayan region employing meteorological satellite snow cover observations. *Water Resources Research*, *13*(1), 109–112. https://doi.org/10.1029/WR013i001p00109

Ranson, K. J., Montesano, P. M., & Nelson, R. (2011). Object-based mapping of the circumpolar taiga-tundra ecotone with MODIS tree cover. *Remote Sensing of Environment*, *115*(12), 3670–3680. https://doi.org/10.1016/j.rse.2011.09.006

Rappold, A. G., Stone, S. L., Cascio, W. E., Neas, L. M., Kilaru, V. J., Carraway, M. S., et al. (2011). Peat Bog Wildfire Smoke Exposure in Rural North Carolina Is Associated with Cardiopulmonary Emergency Department Visits Assessed through Syndromic Surveillance. *Environmental Health Perspectives*, *119*(10), 1415–1420. https://doi.org/10.1289/ehp.1003206

Rautiainen, K., Parkkinen, T., Lemmetyinen, J., Schwank, M., Wiesmann, A., Ikonen, J., et al. (2016). SMOS prototype algorithm for detecting autumn soil freezing. *Remote Sensing of Environment*, *180*, 346–360. https://doi.org/10.1016/j.rse.2016.01.012

Rawlins, M. A., Fahnestock, M., Frolking, S., & Vorosmarty, C. J. (2007). On the evaluation of snow water equivalent estimates over the terrestrial Arctic drainage basin. *Hydrological Processes*, *21*(12), 1616–1623. https://doi.org/10.1002/hyp.6724

Rawlins, M. A., McGuire, A. D., Kimball, J. S., Dass, P., Lawrence, D., Burke, E., et al. (2015). Assessment of model estimates of land-atmosphere CO_2 exchange across Northern Eurasia. *Biogeosciences*, *12*(14), 4385–4405. https://doi.org/10.5194/bg-12-4385-2015

Rawlins, M. A., Steele, M., Holland, M. M., Adam, J. C., Cherry, J. E., Francis, J. A., et al. (2010). Analysis of the Arctic System for Freshwater Cycle Intensification: Observations and Expectations. *Journal of Climate*, *23*(21), 5715–5737. https://doi.org/10.1175/2010JCLI3421.1

Raynolds, M., Comiso, J., Walker, D., & Verbyla, D. (2008). Relationship between satellite-derived land and surface temperatures, arctic vegetation types, and NDVI. *Remote Sensing of Environment*, *112*(4), 1884–1894. https://doi.org/10.1016/j.rse.2007.09.008

Razavi, A., Clerbaux, C., Wespes, C., Clarisse, L., Hurtmans, D., Payan, S., et al. (2009). Characterization of methane retrievals from the IASI space-borne sounder. *Atmospheric Chemistry and Physics*, *9*(20), 7889–7899. https://doi.org/10.5194/acp-9-7889-2009

Reshetnikov, A. I., Paramonova, N. N., & Shashkov, A. A. (2000). An evaluation of historical methane emissions from the Soviet gas industry. *Journal of Geophysical Research*, *105*(D3), 3517–3529. https://doi.org/10.1029/1999JD900761

Reverdin, G., Durand, F., Mortensen, J., Schott, F., Valdimarsson, H., & Zenk, W. (2002). Recent changes in the surface salinity of the North Atlantic subpolar gyre. *Journal of Geophysical Research Oceanography*, *107*(C12), SFR 11-1–SFR 11-13. https://doi.org/10.1029/2001JC001010

Ricker, R., Hendricks, S., Girard-Ardhuin, F., Kaleschke, L., Lique, C., Tian-Kunze, X., et al. (2017). Satellite-observed drop of Arctic sea-ice growth in winter 2015-2016. *Geophysical Research Letters*, *44*, 3236–3245. https://doi.org/10.1002/2016GL072244

Riggs, G.A., Hall, D.K. & Román, M.O. (2015). *MODIS snow products user guide for Collection 6 (C6)*. NASA.

Riggs, G.A., Hall, D.K. & Román, M.O. (2016). *NASA VIIRS snow products algorithm theoretical basis document (ATBD)*. Greenbelt, MD: NASA

Riggs, G. A., Hall, D. K., & Román, M. O. (2017). Overview of NASA's MODIS and visible infrared imaging radiometer suite (VIIRS) snow-cover earth system Data Records. *Earth System Science Data*, *9*(2), 765–777. https://doi.org/10.5194/essd-9-765-2017

Rignot, E., Box, J. E., Burgess, E., & Hanna, E. (2008). Mass balance of the Greenland ice sheet from 1958 to 2007. *Geophysical Research Letters*, *35*, L20502. https://doi.org/10.1029/2008GL035417

Rigor, I. G., Colony, R. L., & Martin, S. (2000). Variations in surface air temperatures over the Arctic Ocean from 1979-1997. *Journal of Climate*, *13*(5), 896–914. https://doi.org/10.1175/1520-0442(2000)013<0896:VISATO>2.0.CO:2

Rigor, I. G., Wallace, J. M., & Colony, R. L. (2002). Response of sea ice to the Arctic Oscillation. *Journal of Climate*, *15*(18), 2648–2663. https://doi.org/10.1175/1520-0442(2002)015%3C2648:ROSITT%3E2.0.CO;2

Rind, D., Healy, R., Parkinson, C., & Martinson, D. (1995). The role of sea ice in 2 x CO_2 climate model sensitivity. Part 1: The total influence of sea ice thickness and extent. *Journal of Climate*, *8*(3), 449–463. https://doi.org/10.1175/1520-0442(1995)008<0449:TROSII>2.0.CO;2

Robinson, D. A. (1993). Hemispheric snow cover from satellites. *Annals of Glaciology*, *17*, 367–371. https://doi.org/10.1017/S0260305500013112

Robinson, D.A. (2013). *Climate Data Record Program (CDRP): Climate Algorithm Theoretical Basis Document (C-ATBD) Northern Hemisphere Snow Cover Extent, CDRP-ATBD-0156, Asheville, North Carolina, USA* (28 pp.). National Oceanic and Atmospheric Administration (NOAA).

Rocha, A. V., Blakely, B., Jiang, Y., Wright, K. S., & Curasi, S. R. (2018). Is arctic greening consistent with the ecology of tundra? Lessons from an ecologically informed mass balance model. *Environmental Research Letters*, *13*, 125007. https://doi.org/10.1088/1748-9326/aaeb50

Roemmich, D., Johnson, G., Riser, S., Davis, R., Gilson, J., Owens, W. B., et al. (2009). The Argo Program: Observing the Global Oceans with Profiling Floats. *Oceanography*, *22*(2), 34–43. https://doi.org/10.5670/oceanog.2009.36

Rogers, B. M., Soja, A. J., Goulden, M. L., & Randerson, J. T. (2015). Influence of tree species on continental differences in boreal fires and climate feedbacks. *Nature Geoscience*, *8*(3), 228–234. https://doi.org/10.1038/ngeo2352

Roiger, A., Thomas, J. L., Schlager, H., Law, K. S., Kim, J., Schafler, A., et al. (2015). Quantifying Emerging Local Anthropogenic Emissions in the Arctic Region: The ACCESS Aircraft Campaign Experiment. *Bulletin of the American Meteorological Society, American Meteorological Society*, *96*(3), 441–460. https://doi.org/10.1175/BAMS-D-13-00169.1

Romanovsky, V. E., Drozdov, D. S., Oberman, N. G., Malkova, G. V., Kholodov, A. L., Marchenko, S. S., et al. (2010). Thermal state of permafrost in Russia. *Permafrost and Periglacial Processes*, *21*(2), 136–155. https://doi.org/10.1002/ppp.683

Rossow, W. B., & Garder, L. C. (1993). Cloud detection using satellite measurements of infrared and visible radiances for ISCCP. *Journal of Climate*, *6*(12), 2341–2369. https://doi.org/10.1175/1520-0442(1993)006<2341:CDUSMO>2.0.CO;2

Rossow, W. B., & Zhang, Y.-C. (1995). Calculation of surface and top of atmosphere radiative fluxes from physical quantities based on ISCCP data sets: 2. Validation and first results. *Journal of Geophysical Research*, *100*(D1), 1167–1197. https://doi.org/10.1029/94JD02746

Rostosky, P., Spreen, G., Farrell, S. L., Frost, T., Heygster, G., & Melsheimer, C. (2018). Snow depth retrieval on Arctic sea ice from passive microwave radiometers – Improvements and extensions to multiyear ice using lower frequencies. *Journal of Geophysical Research: Oceans*, *123*(10), 7120–7138. https://doi.org/10.1029/2018JC014028

Rothrock, D. A., Yu, Y., & Maykut, G. A. (1999). Thinning of the Arctic sea-ice cover. *Geophysical Research Letters*, *26*(23), 3469–3472. https://doi.org/10.1029/1999GL010863

Rouyet, L., Lauknes, T. R., Christiansen, H. H., Strand, S. M., & Larsen, Y. (2019). Seasonal dynamics of a permafrost landscape, Adventdalen, Svalbard, investigated by InSAR. *Remote Sensing of Environment*, *231*, 111236. https://doi.org/10.1016/j.rse.2019.111236

Roy, A., Royer, A., Derksen, C., Brucker, L., Langlois, A., Mialon, A., & Kerr, Y. H. (2015). Evaluation of Spaceborne L-Band Radiometer Measurements for Terrestrial Freeze/Thaw Retrievals. *Canada IEEE Journal of Selected Topics in Applied Earth Observations and Remote Sensing*, *8*(9), 4442–4459. https://doi.org/10.1109/JSTARS.2015.2476358

Roy, D. P., Boschetti, L., Justice, C. O., & Ju, J. (2008). The collection 5 MODIS burned area product — Global evaluation by comparison with the MODIS active fire product. *Remote Sensing of Environment*, *112*(9), 3690–3707. https://doi.org/10.1016/j.rse.2008.05.013

Roy, D. P., Jin, Y., Lewis, P. E., & Justice, C. O. (2005). Prototyping a global algorithm for systematic fire affected area mapping using MODIS time series data. *Remote Sensing of Environment*, *97*(2), 137–162. https://doi.org/10.1016/j.rse.2005.04.007

Rudolf, A., & Walther, T. (2014). Laboratory demonstration of a Brillouin lidar to remotely measure temperature profiles of the ocean. *Optical Engineering*, *53*(5), 051407. https://doi.org/10.1117/1.OE.53.5.051407

Rupp, D., Zipf, A., Godinovic, N., Lux, K., Walther, T., & Trees, C. (2017). A Brillouin lidar for remote sensing of the temperature profile in the ocean—Towards a simultaneous measurement of temperature and salinity. OCEANS 2017-Anchorage: 1-7.

Ruppel, C. D., & Kessler, J. D. (2017). The interaction of climate change and methane hydrates. *Reviews of Geophysics*, *55*, 126–168. https://doi.org/10.1002/2016RG000534

Ryan, J. C., Hubbard, A., Irvine-Fynn, T. D., Doyle, S. H., Cook, J. M., Stibal, M., & Box, J. E. (2017). How robust are in situ observations for validating satellite derived albedo over the dark zone of the Greenland Ice Sheet? *Geophysical Research Letters*, *44*, 6218–6225. https://doi.org/10.1002/2017GL073661

Saunois, M., Bousquet, P., Poulter, B., Peregon, A., Ciais, P., Canadell, J. G., et al. (2016). The global methane budget 2000-2012. *Earth System Science Data*, *8*(2), 697–751. https://doi.org/10.5194/essd-8-697-2016

Saunois, M., Bousquet, P., Poulter, B., Peregon, A., Ciais, P., Canadell, J. G., et al. (2017). Variability and quasi-decadal changes in the methane budget over the period 2000–2012. *Atmospheric Chemistry and Physics*, *17*(18), 11,135–11,161. https://doi.org/10.5194/acp-17-11135-2017

Schaefer, K., Lantuit, H., Romanovsky, V. E., Schuur, E. A. G., & Witt, R. (2014). The impact of the permafrost carbon feedback on global climate. *Environmental Research Letters*, *9*(8), 085003. https://doi.org/10.1088/1748-9326/9/8/085003

Scharlemann, J. P. W., Tanner, E. V. J., Hiederer, R., & Kapos, V. (2014). Global soil carbon: Understanding and managing the largest terrestrial carbon pool. *Carbon Management*, *5*(1), 81–91. https://doi.org/10.4155/cmt.13.77

Schepers, D., Guerlet, S., Butz, A., Landgraf, J., Frankenberg, C., Hasekamp, O., et al. (2012). Methane retrievals from Greenhouse Gases Observing Satellite (GOSAT) shortwave infrared measurements: Performance comparison of proxy and physics retrieval algorithms. *Journal of Geophysical Research*, *117*(D10), D10307. https://doi.org/10.1029/2012JD017549

Schimel, D., Pavlick, R., Fisher, J. B., Asner, G. P., Saatchi, S., Townsend, P., et al. (2015). Observing terrestrial ecosystems and the carbon cycle from space. *Global Change Biology*, *21*(5), 1762–1776. https://doi.org/10.1111/gcb.12822

Schmale, J., Arnold, S. R., Law, K. S., Thorp, T., Anenberg, S., Simpson, W. R., et al. (2018). Local Arctic air pollution: A neglected but serious problem. *Earth's Future*, *6*(10), 1385–1412. https://doi.org/10.1029/2018EF000952

Schmidt, A., Leadbetter, S., Theys, N., Carboni, E., Witham, C. S., Stevenson, J. A., et al. (2015). Satellite detection, long-range transport, and air quality impacts of volcanic sulfur dioxide from the 2014–2015 flood lava eruption at Bárðarbunga (Iceland). *Journal of Geophysical Research: Atmospheres*, *120*, 9739–9757. https://doi.org/10.1002/2015JD023638

Schneider, J., Jungkunst, H. F., Wolf, U., Schreiber, P., Gazovic, M., Miglovets, M., et al. (2016). Russian boreal peatlands dominate the natural European methane budget. *Environmental Research Letters*, *11*(1), 014004. https://doi.org/10.1088/1748-9326/11/1/014004

Schneising, O., Bergamaschi, P., Bovensmann, H., Buchwitz, M., Burrows, J. P., Deutscher, N. M., et al. (2012). Atmospheric greenhouse gases retrieved from SCIAMACHY: Comparison to ground-based FTS measurements and model results. *Atmospheric Chemistry and Physics*, *12*(3), 1527–1540. https://doi.org/10.5194/acp-12-1527-2012

Schneising, O., Buchwitz, M., Reuter, M., Heymann, J., Bovensmann, H., & Burrows, J. P. (2011). Long-term analysis of carbon dioxide and methane column-averaged mole fractions retrieved from SCIAMACHY. *Atmospheric Chemistry and Physics*, *11*(6), 2863–2880. https://doi.org/10.5194/acp-11-2863-2011

Schroeder, R., McDonald, K., Chapman, B. D., Jensen, K., Podest, E., Tessler, Z., et al. (2015). Development and Evaluation of a Multi-Year Fractional Surface Water Data Set Derived from Active/Passive Microwave Remote Sensing Data. *Remote Sensing*, *7*(12), 16688–16732. https://doi.org/10.3390/rs71215843

Schroeder, W., Oliva, P., Giglio, L., & Csiszar, I. A. (2014). The New VIIRS 375m active fire detection data product: Algorithm description and initial assessment. *Remote Sensing of Environment*, *143*, 85–96. https://doi.org/10.1016/j.rse.2013.12.008

Schroeder, W., Oliva, P., Giglio, L., Quayle, B., Lorenz, E., & Morelli, F. (2016). Active fire detection using Landsat-8/OLI data. *Remote Sensing of Environment*, *185*, 210–220. https://doi.org/10.1016/j.rse.2015.08.032

Schuur, E. A. G., McGuire, A. D., Schädel, C., Grosse, G., Harden, J. W., Hayes, D. J., et al. (2015). Climate change and the permafrost carbon feedback. *Nature*, *520*(7546), 171–179. https://doi.org/10.1038/nature14338

Schuur, E. A. G., McGuire, A. D., Romanovsky, V., Schädel, C., & Mack, M. (2018). In N. Cavallaro, G. Shrestha, R. Birdsey, M. A. Mayes, R. G. Najjar, S. C. Reed, P. Romero-Lankao, & Z. Zhu (Eds.), *Chapter 11: Arctic and boreal carbon. In Second State of the Carbon Cycle Report (SOCCR2): A Sustained Assessment Report*, (pp. 428–468). Washington, DC, USA: U.S. Global Change Research Program. https://doi.org/10.7930/SOCCR2.2018.Ch11

Screen, J. A., & Simmonds, I. (2010). The central role of diminishing sea ice in recent Arctic temperature amplification. *Nature*, *464*(7293), 1334–1337. https://doi.org/10.1038/nature09051

Sellers, P. J., Hall, F. G., Kelly, R. D., Black, A., Baldocchi, D., Berry, J., et al. (1997). BOREAS in 1997: Experiment overview, scientific results, and future directions. *Journal of Geophysical Research-Atmospheres*, *102*(D24), 28731–28769. https://doi.org/10.1029/97JD03300

Sellers, P. J., Schimel, D. S., Moore, B., Liu, J., & Eldering, A. (2018). Observing carbon cycle–climate feedbacks from space. *Proceedings of the National Academy of Sciences*, *115*(31), 7860–7868. https://doi.org/10.1073/pnas.1716613115

Serreze, M. C., Barrett, A. P., Slater, A. G., Woodgate, R. A., Aagaard, K., Lammers, R. B., et al. (2006). The large-scale freshwater cycle of the Arctic. *Journal of Geophysical Research-Oceans*, *111*(C11), C11010. https://doi.org/10.1029/2005JC003424

Serreze, M. C., Barrett, A. P., & Stroeve, J. (2012). Recent changes in tropospheric water vapor over the Arctic as assessed from radiosondes and atmospheric reanalyses. *Journal of Geophysical Research Atmospheres*, *117*(D10), D10104. https://doi.org/10.1029/2011JD017421

Serreze, M. C., & Barry, R. G. (2005). *The Arctic Climate System*. Cambridge: Cambridge University Press. ISBN: 978051153 5888.

Serreze, M. C., & Barry, R. G. (2011). Processes and impacts of Arctic amplification: A research synthesis. *Global Planetary Change*, *77*(1-2), 85–96. https://doi.org/10.1016/j.gloplacha.2011.03.004

Serreze, M. C., & Barry, R. G. (2014). In A. J. Dessler, J. T. Houghton, & M. J. Rycroft (Eds.), *The Arctic Climate System*. New York, NY: Cambridge University Press. ISBN: 978-1-107-03717-5.

Seviour, W. J. M. (2017). Weak- ening and shift of the Arctic stratospheric polar vortex: Internal variability or forced response? *Geophysical Research Letters*, *44*, 3365–3373. https://doi.org/10.1002/2017GL073071

Sexton, J. O., Song, X.-P., Feng, M., Noojipady, P., Anand, A., Huang, C., et al. (2013). Global, 30-m resolution continuous fields of tree cover: Landsat-based rescaling of MODIS vegetation continuous fields with lidar-based estimates of error. *International Journal of Digital Earth*, *6*(5), 427–448. https://doi.org/10.1080/17538947.2013.786146

Sharma, S., Andrews, E., Barrie, L. A., Ogren, J. A., & Lavoué, D. (2006). Variations and sources of the equivalent black carbon in the high Arctic revealed by long-term observations at Alert and Barrow: 1989–2003. *Journal of Geophysical Research*, *111*(D14), D14208. https://doi.org/10.1029/2005JD006581

Sharma, S., Ishizawa, M., Chan, D., Lavoué, D., Andrews, E., Eleftheriadis, K., & Maksyutov, S. (2013). 16-year simulation of Arctic black carbon: Transport, source contribution, and sensitivity analysis on deposition. *Journal of Geophysical Research: Atmospheres*, *118*, 943–964. https://doi.org/10.1029/2012JD017774

Sharma, S., Lavoué, D., Cachier, H., Barrie, L. A., & Gong, S. L. (2004). Long-term trends of the black carbon concentrations in the Canadian Arctic. *Journal of Geophysical Research*, *109*(D15), D15203. https://doi.org/10.1029/2003JD004331

Shaver, G. R., Rastetter, E. B., Salmon, V., Street, L. E., van de Weg, M. J., Rocha, A., et al. (2013). Pan-arctic modelling of net ecosystem exchange of CO_2. *Philosophical Transactions of the Royal Society B*, *368*(1624), 20120485. https://doi.org/10.1098/rstb.2012.0485

Shaw, G. E. (1995). The Arctic Haze Phenomenon. *Bulletin of the American Meteorological Society*, *76*(12), 2401–2413.

Shepherd, A., Ivins, E. R., G., A., Barletta, V. R., Bentley, M. J., Bettadpur, S., et al., et al. (2012). A reconciled estimate of ice-sheet mass balance. *Science*, *338*(6111), 1183–1189. https://doi.org/10.1126/science.1228102

Shibata, A. (2013). Description of GCOM-W1 AMSR2 Sea Surface Temperature Algorithm, in *Descriptions of GCOM-W1 AMSR2 Level 1R and Level 2 Algorithms*. Japan Aerospace Exploration Agency Earth Observation Research Center: Ibaraki, Japan, p. 119.

Shibata, A., Murakami, H., & Comiso, J. (2010). Anomalous Warming in the Arctic Ocean in the Summer of 2007. *Journal of Remote Sensing Society of Japan*, *30*(2), 105–113.

Short, N., Brisco, B., Couture, N., Pollard, W., Murnaghan, K., & Budkewitsch, P. (2011). A comparison of TerraSAR-X, RADARSAT-2 and ALOS-PALSAR interferometry for monitoring permafrost environments, case study from Herschel Island, Canada. *Remote Sensing of Environment*, *115*(12), 3491–3506. https://doi.org/10.1016/j.rse.2011.08.012

Shugart, H. H., Leemans, R., & Bonan, G. B. (1991). *A Systems Analysis of the Global Boreal Forest*. New York: Cambridge University Press.

Shvidenko, A. Z. & Nilsson, S. (2000). Extent, distribution, and ecological role of fire in Russian forests. In *Fire, Climate Change, and Carbon Cycling in the Boreal Forest*, edited by E. S. Kasischke & B. J. Stocks, (New York: Springer-Verlag), 132-150, DOI: https://doi.org/10.1007/978-0-387-21629-4_8.

Simmons, A., Fellous, J.-L., Ramaswamy, V., Trenberth, K., Asrar, G., Balmaseda, M., et al. (2016). Observation and integrated Earth-system science: A roadmap for 2016–2025. *Advances in Space Research*, *57*(10), 2037–2103. https://doi.org/10.1016/j.asr.2016.03.008

Simpson, J. J., & Yhann, S. R. (1994). Reduction of noise in AVHRR channel 3 data with minimum distortion. *IEEE Transactions on Geoscience and Remote Sensing*, *32*(2), 315–328. https://doi.org/10.1109/36.295047

Singh, O. N., & Fabian, P. (Eds) (2003). *Atmospheric Ozone: A Millennium Issue, Copernicus Publications*. Germany: Katlenburg - Lindau.

Sitch, S., McGuire, A. D., Kimball, J., Gedney, N., Gamon, J., Engstrom, R., et al. (2007). Assessing the carbon balance of circumpolar Arctic tundra using remote sensing and process modeling. *Ecological Applications*, *17*(1), 213–234. https://doi.org/10.1890/1051-0761(2007)017[0213:ATCBOC]2.0.CO;2

Skogland, T., Lomeland, S., & Goksoyr, J. (1988). Respiratory burst after freezing and thawing of soil: Experiments with soil bacteria. *Soil Biology and Biochemistry*, *20*(6), 851–856. https://doi.org/10.1016/0038-0717(88)90092-2

Slater, A. G., & Lawrence, D. M. (2013). Diagnosing present and future permafrost from climate models. *Journal of Climate*, *26*(15), 5608–5623. https://doi.org/10.1175/JCLI-D-12-00341.1

Smith, L. C., Chu, V. W., Yang, K., Gleason, C. J., Pitcher, L. H., Rennermalm, A. K., et al. (2015). Efficient meltwater drainage through supraglacial streams and rivers on the southwest Greenland ice sheet. *Proceedings of the National Academy of Sciences*, *112*(4), 1001–1006. https://doi.org/10.1073/pnas.1413024112

Smith, L. C., & Stephenson, S. R. (2013). New trans-Arctic shipping routes navigable by midcentury. *Proceedings of the National Academy of Sciences*, *110*(13), E1191–E1195. https://doi.org/10.1073/pnas.1214212110

Smith, S., & Brown, J. (2009). Permafrost and seasonally frozen ground. Assessment of the status of the development of standards for the terrestrial essential climate variables. *Global Terrestrial Observing System*. 22 pp., version 13, 8 May 2009, Rome, 2009

Smith, S. L., Romanovsky, V. E., Lewkowicz, A. G., Burn, C. R., Allard, M., Clow, G. D., et al. (2010). Thermal state of permafrost in North America: A contribution to the International Polar Year. *Permafrost and Periglacial Processes*, *21*(2), 117–135. https://doi.org/10.1002/ppp.690

Smith, W. L., Hansen, C., Bucholtz, A., Anderson, B. E., Beckley, M., Corbett, J. G., et al. (2017). Arctic Radiation-IceBridge Sea and Ice Experiment: The Arctic Radiant Energy System during the Critical Seasonal Ice Transition. *Bulletin of the American Meteorological Society*, *98*(7), 1399–1426. https://doi.org/10.1175/BAMS-D-14-00277.1

Smith, W. L. & Rao, P. K. (1971). The determination of surface temperature from satellite "window" radiation measurements. *Fifth Symposium on Temperature*, Washington, D.C., (Instrument Society of America), 2251-2257.

Sofieva, V. F., Kyrölä, E., Laine, M., Tamminen, J., Degenstein, D., Bourassa, A., et al. (2017). Merged SAGE II, Ozone_cci and OMPS ozone profile dataset and evaluation of ozone trends in the stratosphere. *Atmospheric Chemistry and Physics*, *17*, 12533–12552. https://doi.org/10.5194/acp-17-12533-2017

Sofronov, M. A., Volokitina, A. V., & Schvidenko, A. Z. (1998). Wildland fires in the north of Central Siberia. *Commonwealth Forestry Review*, *77*, 124–127.

Soja, A., Fairlie, D., Westberg, D., Pouliot, G., & Szykman, J. (2012). Biomass Burning Plume Injection Height Estimates using CALIOP, MODIS and the NASA Langley Trajectory Model. In *Environmental Protectin Agency (EPA) International Emission Inventory Conference (EIC) Emission Inventories - Meeting the Challenges Posed by Emerging Global* (pp. 1–17). National, Regional and Local Air Quality Issues: Tampa Fl. https://www3.epa.gov/ttn/chief/conference/ei20/session7/asoja.pdf

Soja, A., & Groisman, P. (2018). Earth science and the integral climatic and socio-economic drivers of change across northern Eurasia: The NEESPI legacy and future direction. *Environmental Research Letters*, *13*(4), 040401. https://doi.org/10.1088/1748-9326/aab834

Soja, A. J., Cofer, W. R. III, Shugart, H. H., Sukhinin, A. I., Stackhouse, P. W. Jr., McRae, D. J., & Conard, S. G. (2004). Estimating fire emissions and disparities in boreal Siberia (1998 through 2002). *Journal of Geophysical Research*, *109*(D14), D14S06. https://doi.org/10.1029/2004JD004570

Soja, A. J., Shugart, H. H., Sukhinin, A., Conard, S., & Stackhouse, P. W. (2006). Satellite-derived mean fire return intervals as indicators of change in Siberia (1995-2002). *Mitigation and Adaptation Strategies for Global Change*, *11*(1), 75–96. https://doi.org/10.1007/s11027-006-1009-3

Soja, A. J., Tchebakova, N. M., French, N. H. F., Flannigan, M. D., Shugart, H. H., Stocks, B. J., et al. (2007). Climate-induced boreal forest change: Predictions versus current observations. *Global and Planetary Change, Special NEESPI Issue*, *56*(3-4), 274–296. https://doi.org/10.1016/j.gloplacha.2006.07.028

SPARC, 2017. The SPARC Data Initiative: Assessment of stratospheric trace gas and aerosol climatologies from satellite limb sounders. By M. I. Hegglin & S. Tegtmeier (eds.), *SPARC Report No. 8, WCRP-5/2017*. Zurich, Switzerland: World Climate Research Programme (WCRP). available at www.sparc-climate.org/publications/sparc-reports/

Spielhagen, R. F., Werner, K., Sørensen, S. A., Zamelczyk, K., Kandiano, E., Budeus, G., et al. (2011). Enhanced Modern Heat Transfer to the Arctic by Warm Atlantic Water. *Science*, *331*(6016), 450–453. https://doi.org/10.1126/science.1197397

Stark, S., & Ylänne, H. (2015). Grazing in Arctic peatlands – an unknown agent in the global carbon budget. *Environmental Research Letters*, *10*(5), 051002. https://doi.org/10.1088/1748-9326/10/5/051002

Steele, M., Ermold, W., & Zhang, J. (2008). Arctic Ocean surface warming trends over the past 100 years. *Geophysical Research Letters*, *35*, L02614. https://doi.org/10.1029/2007GL031651

Steffen, C., Box, J., & Abdalati, W., (1996). Greenland Climate Network: GC-Net, in US Army Cold Regions Reattach and Engineering (CRREL). *CRREL Special Report 96-27* (pp. 98–103). US Army Corps of Engineers.

Steffen, K., Cavalieri, D. J., Comiso, J., Germain, K.S., Gloersen, P., Key, J., & Rubinstein, I. (1992). "The estimation of geophysical parameters using Passive Microwave Algorithms," Chapter 10, *Microwave Remote Sensing of Sea Ice,* (ed. by Frank Carsey), American Geophysical Union, Washington, D.C., 201-231, https://doi.org/10.1029/GM068p0201

Stephenson, S. R., & Smith, L. C. (2015). Influence of climate model variability on projected Arctic shipping futures. *Earth's Future*, *3*(11), 331–343. https://doi.org/10.1002/2015EF000317

Stettner, S., Beamish, A., Bartsch, A., Heim, B., Grosse, G., Roth, A., & Lantuit, H. (2017). Monitoring inter-and intra-seasonal dynamics of rapidly degrading ice-rich permafrost riverbanks in the Lena Delta with TerraSAR-X time series. *Remote Sensing*, *10*(2), 51. https://doi.org/10.3390/rs10010051

Stewart, I. T., Cayan, D. R., & Dettinger, M. D. (2005). Changes toward earlier streamflow timing across western North America. *Journal of Climate*, *18*(8), 1136–1155. https://doi.org/10.1175/JCLI3321.1

Stieglitz, M., Déry, S. J., Romanovsky, V. E., & Osterkamp, T. E. (2003). The role of snow cover in the warming of Arctic permafrost. *Geophysical Research Letters*, *30*(13), 1721. https://doi.org/10.1029/2003GL017337

Stieglitz, M., Giblin, A., Hobbie, J., Williams, M., & Kling, G. (2000). Simulating the effects of climate change and climate variability on carbon dynamics in Arctic tundra. *Global Biogeochemical Cycles*, *14*(4), 1123–1136. https://doi.org/10.1029/1999GB001214

Stocks, B. J., Alexander, M. E., & Lanoville, R. A. (2004). Overview of the International Crown Fire Modelling Experiment (ICFME). *Canadian Journal of Forest Research*, *34*(8), 1543–1547. https://doi.org/10.1139/x04-906

Stocks, B. J., Fosberg, M. A., Lynham, T. J., Mearns, L., Wotton, B. M., Yang, Q., et al. (1998). Climate change and forest fire potential in Russian and Canadian boreal forests. *Climatic Change*, *38*(1), 1–13. https://doi.org/10.1023/A:1005306001055

Stohl, A. (2006). Characteristics of atmospheric transport into the Arctic troposphere. *Journal of Geophysical Research*, *111*(D11), D11306. https://doi.org/10.1029/2005JD006888

Stone, R. S., Dutton, E. G., Harris, J. M., & Longenecker, D. (2002). Earlier spring snowmelt in northern Alaska as an indicator of climate change. *Journal of Geophysical Research*, *107*(D10), 4,089. https://doi.org/10/1029/2000JD00286

Stone, R. S., Sharma, S., Herber, A., Eleftheriadis, K., & Nelson, D. W. (2014). A characterization of Artic aerosols on the basis of aerosol optical depth and black carbon measurements. *Elementa: Science of the Anthropocene*, *2*. https://doi.org/10.12952/journal.elementa.0000027

Stroeve, J. C., Serreze, M. C., Holland, M. M., Kay, J. E., Malanik, J., & Barrett, A. P. (2011). The Arctic's rapidly shrinking sea ice cover: A research synthesis. *Climatic Change*, *110*(3-4), 1005–1027. https://doi.org/10.1007/s10584-011-0101-1

Stroeve, J. C., Serreze, M. C., Holland, M. M., Kay, J. E., Maslanik, J., & Barrett, A. P. (2012). The Arctic's rapidly shrinking sea ice cover: A research synthesis. *Climatic Change*, *110*(3-4), 1005–1027. https://doi.org/10.1007/s10584-011-0101-1

Stroh, J. N., Panteleev, G., Kirillov, S., Makhotin, M., & Shakhova, N. (2015). Sea-surface temperature and salinity product comparison against external in situ data in the Arctic Ocean. *Journal of Geophysical Research: Oceans*, *120*, 7223–7236. https://doi.org/10.1002/2015JC011005

Strozzi, T., Antonova, S., Günther, F., Mätzler, E., Vieira, G., Wegmüller, U., et al. (2018). Sentinel-1 SAR Interferometry for Surface Deformation Monitoring in Low-Land Permafrost Areas. *Remote Sensing*, *10*(9), 1360. https://doi.org/10.3390/rs10091360

Stubenrauch, C. J., Rossow, W. B., Kinne, S., Ackerman, S., Cesana, G., Chepfer, H., et al. (2013). Assessment of Global Cloud Datasets from Satellites: Project and Database Initiated by the GEWEX Radiation Panel. *Bulletin of the American Meteorological Society*, *94*(7), 1031–1049. https://doi.org/10.1175.BAMS-D-12-00117.1

Stuecker, M. F., Bitz, C. M., Armour, K. C., Proistosescu, C., Kang, S. M., Xie, S.-P., et al. (2018). Polar amplification dominated by local forcing and feedbacks. *Nature Climate Change*, *8*(12), 1076–1081. https://doi.org/10.1038/s41558-018-0339-y

Sturm, M., Durand, M., Robinson, D. & Serreze, M. (undated). Got Snow?, publication produced at the National Snow and Ice Data Center for NASA, http://neptune.gsfc.nasa.gov/uploads/images_db/Got_SnowSM.pdf.

Sturm, M., Goldstein, M. A., & Parr, C. (2017). Water and life from snow: A trillion dollar science question. *Water Resources Research*, *53*, 3534–3544. https://doi.org/10.1002/2017WR020840

Sukhinin, A. I., French, N. H. F., Kasischke, E. S., Hewson, J. H., Soja, A. J., Csiszar, I. A., et al. (2004). AVHRR-based mapping of fires in Russia: New products for fire management and carbon cycle studies. *Remote Sensing of Environment*, *93*(4), 546–564. https://doi.org/10.1016/j.rse.2004.08.011

Sun, L., Deser, C., & Tomas, R. A. (2015). Mechanisms of stratospheric and tropospheric circulation response to projected Arctic sea ice loss. *Journal of Climate*, *28*(19), 7824–7845. https://doi.org/10.1175/JCLI-D-15-0169.1

Sutherland, D. A., & Pickart, R. S. (2008). The East Greenland Coastal Current: Structure, variability, and forcing. *Progress in Oceanography*, *78*(1), 58–77. https://doi.org/10.1016/j.pocean.2007.09.006

Sweeney, C., Dlugokencky, E., Miller, C. E., Wofsy, S., Karion, A., Dinardo, S., et al. (2016). No significant increase in long-term CH_4 emissions on North Slope of Alaska despite significant increase in air temperature. *Geophysical Research Letters*, *43*, 6604–6611. https://doi.org/10.1002/2016GL069292

Takala, M., Luojus, K., Pulliainen, J., Derksen, C., Lemmetyinen, J., Karna, J.-P., et al. (2011). Estimating northern hemisphere snow water equivalent for climate research through assimilation of space-borne radiometer data and ground-based measurements. *Remote Sensing of Environment*, *115*(12), 3517–3529. https://doi.org/10.1016/j.rse.2011.08.014

Tan, Z., & Zhuang, Q. (2015). Methane emissions from pan-Arctic lakes during the 21st century: An analysis with process-based models of lake evolution and biogeochemistry. *Journal of Geophysical Research: Biogeosciences*, *120*, 2641–2653. https://doi.org/10.1002/2015JG003184

Tanskanen, A., Krotkov, N. A., Herman, J. R., & Arola, A. (2006). Surface Ultraviolet Irradiance from OMI. *IEEE Transactions on Geoscience and Remote Sensing Aura Special Issue*, *44*(5), 1267–1271. https://doi.org/10.1109/TGRS.2005.862203

Tarnocai, C., Canadell, J. G., Schuur, E. A. G., Kuhry, P., Mazhitova, G., & Zimov, S. (2009). Soil organic carbon pools in the northern circumpolar permafrost region. *Global Biogeochemical Cycles*, *23*, GB2023. https://doi.org/10.1029/2008GB003327

Taylor, P., Hegyi, B., Boeke, R., & Boisvert, L. (2018). On the increasing importance of air-sea exchange in a thawing Arctic: A review. *Atmosphere*, *9*(2), 41. https://doi.org/10.3390/atmos9020041

te Beest, M., Sitters, J., Ménard, C. B., & Olofsson, J. (2016). Reindeer grazing increases summer albedo by reducing shrub abundance in Arctic tundra. *Environmental Research Letters*, *11*(12), 125013. https://doi.org/10.1088/1748-9326/aa5128

Tedesco, M. (Ed.) (2015). "*Remote Sensing of the Cryosphere*", *Wiley-Blackwell Cryosphere Science Series*. John Wiley & Sons, Ltd. https://doi.org/10.1002/9781118368909

Thackeray, C. W., Fletcher, C. G., & Derksen, C. (2014). The influence of canopy snow parameterizations on snow albedo feedback in boreal forest regions: Boreal forest snow albedo feedback. *Journal of Geophysical Research: Atmospheres*, *119*, 9810–9821. https://doi.org/10.1002/2014JD021858

Thelen, B., French, N. H. F., Koziol, B. W., Billmire, M., Owen, R. C., Johnson, J., et al. (2013). Modeling acute respiratory illness during the 2007 San Diego wildland fires using a coupled emissions-transport system and generalized additive modeling. *Environmental Health*, *12*(1), 94–94. https://doi.org/10.1186/1476-069X-12-94

Theys, N., De Smedt, I., van Gent, J., Danckaert, T., Wang, T., Hendrick, F., et al. (2015). Sulfur dioxide vertical column DOAS retrievals from the Ozone Monitoring Instrument: Global observations and comparison to ground-based and satellite data. *Journal of Geophysical Research: Atmospheric*, *120*(6), 2470–2491. https://doi.org/10.1002/2014JD022657

Thomas, J. L., Polashenski, C. M., Soja, A. J., Marelle, L., Casey, K. A., Choi, H. D., et al. (2017). Quantifying black carbon deposition over the Greenland ice sheet from forest fires in Canada. *Geophysical Research Letters*, *44*, 7965–7974. https://doi.org/10.1002/2017GL073701

Thornton, B. F., Wik, M., & Crill, P. M. (2016). Double-counting challenges the accuracy of high-latitude methane inventories. *Geophysical Research Letters*, *43*, 12,569–12,577. https://doi.org/10.1002/2016GL071772

Tian-Kunze, X., Kaleschke, L., Maaß, N., Mäkynen, M., Serra, N., Drusch, M., & Krumpen, T. (2014). SMOS-derived thin sea ice thickness: Algorithm baseline, product specifications and initial verification. *The Cryosphere*, *8*(3), 997–1018. https://doi.org/10.5194/tc-8-997-2014

Tjernström, M., Leck, C., Birch, C. E., Bottenheim, J. W., Brooks, B. J., Brooks, I. M., et al. (2014). The Arctic Summer Cloud Ocean Study (ASCOS): Overview and experimental design. *Atmospheric Chemistry and Physics*, *14*(6), 2823–2869. https://doi.org/10.5194/acp-14-2823-2014

Tømmervik, H., Bjerke, J. W., Gaare, E., Johansen, B., & Thannheiser, D. (2012). Rapid recovery of recently overexploited winter grazing pastures for reindeer in northern Norway. *Fungal Ecology*, *5*(1), 3–15. https://doi.org/10.1016/j.funeco.2011.08.002

Tømmervik, H., Johansen, B., Riseth, J. Å., Karlsen, S. R., Solberg, B., & Hogda, K. A. (2009). Above ground biomass changes in the mountain birch forests and mountain heaths of Finnmarksvidda, Northern Norway, in the period 1957-2006. *Forest Ecology and Management*, *257*(1), 244–257. https://doi.org/j.foreco.2008.08.038

Toole, J. M., Krishfield, R. A., Timmermans, M.-L., & Proshutinsky, A. (2011). The ice-tethered profiler: Argo of the Arctic. *Oceanography*, *24*(3), 136–145. https://doi.org/10.5670/oceanog.2011.65

Treat, C. C., Bloom, A. A., & Marushchak, M. E. (2018). Nongrowing season methane emissions–a significant component of annual emissions across northern ecosystems. *Global Change Biology*, *24*(8), 3331–3343. https://doi.org/10.1111/gcb.14137

Treat, C. C., & Frolking, S. (2013). A permafrost carbon bomb? The fate of permafrost soil carbon following thaw depends on hydrology. *Nature Climate Change*, *3*(10), 865–867. https://doi.org/10.1038/nclimate2010

Treffeisen, R. E., Thomason, L. W., Strom, J., Herber, A. B., Burton, S. P., & Yamanouchi, T. (2006). Stratospheric Aerosol and Gas Experiment (SAGE) II and III aerosol extinction measurements in the Arctic middle and upper troposphere. *Journal of Geophysical Research*, *111*(D17), D17203. https://doi.org/10.1029/2005JD006271

Treharne, R., Bjerke, J. W., Tømmervik, H., Stendardi, L., & Phoenix, G. K. (2018). Arctic browning: Impacts of extreme climatic events on heathland ecosystem CO_2 fluxes. *Global Change Biology*, *25*(2), 489–503. https://doi.org/10.1111/gcb.14500

Trishchenko, A. P., Garand, L., & Trichtchenko, L. D. (2011). Three-Apogee 16-h Highly Elliptical Orbit as Optimal Choice for Continuous Meteorological Imaging of Polar Regions. *Journal of Atmospheric and Oceanic Technology*, *28*(11), 1407–1422. https://doi.org/10.1175/JTECH-D-11-00048.1

Tritchtchenko, L. D., Nikitina, L. V., Trishchenko, A. P., & Garand, L. (2014). Highly Elliptical Orbits for Arctic observations: Assessment of ionizing radiation. *Advances in Space Research*, *54*(11), 2398–2414. https://doi.org/10.1016/j.asr.2014.09.012

Turetsky, M.R., Abbott, B.W., Jones, M.C., Anthony, K.W., Olefeldt, D., Schuur, E.A.G., et al. (2019). Permafrost collapse is accelerating carbon release. *Nature, 569*, 32-34 (2019). https://doi.org/10.1038/d41586-019-01313-4, 7754.

Turner, A. J., Jacob, D. J., Wecht, K. J., Maasakkers, J. D., Lundgren, E., Andrews, A. E., et al. (2015). Estimating global and North American methane emissions with high spatial resolution using GOSAT satellite data. *Atmospheric Chemistry and Physics*, *15*(12), 7049–7069. https://doi.org/10.5194/acp-15-7049-2015

Turquety, S., Hadji-Lazaro, J., Clerbaux, C., Hauglustaine, D. A., Clough, S. A., Cassé, V., et al. (2004). Operational trace gas retrieval algorithm for the Infrared Atmospheric Sounding Interferometer. *Journal of Geophysical Research*, *109*(D21), D21301. https://doi.org/10.1029/2004JD004821

Tzortziou M., Mannino, A., Friedrichs, M., Hernes, P., Matrai, P., Salisbury, J., & Del Castillo, C. (2019). The Arctic Coastal Land Ocean Interactions Field Campaign Program, Ocean Carbon & Biogeochemistry (OCB) Summer Workshop. https://web.whoi.edu/ocb-workshop/wp-content/uploads/sites/59/2019/07/18-Arctic_COLORS_OCB_2019_062319.pdf.

USGCRP (2018). In D. R. Reidmiller, C. W. Avery, D. R. Easterling, K. E. Kunkel, K. L. M. Lewis, T. K. Maycock, & B. C. Stewart (Eds.), *Impacts, Risks, and Adaptation in the United States: Fourth National Climate Assessment, Volume II*. Washington, DC, USA: U.S. Global Change Research Program. https://doi.org/10.7930/NCA4.2018

Uttal, T., Curry, J. A., McPhee, M. G., Perovich, D. K., Moritz, R. E., Maslanik, J. A., et al. (2002). Surface heat budget of the Arctic Ocean. *Bulletin of the American Meteorological Society*, *83*(2), 255–275. https://doi.org/10.1175/1520-0477(2002)083<0255:SHBOTA>2.3.CO;2

Uttal, T., Starkweather, S., Drummond, J. R., Vihma, T., Makshtas, A. P., Darby, L. S., et al. (2016). International arctic systems for observing the atmosphere: An International Polar Year Legacy Consortium. *Bulletin of the American Meteorological Society*, *97*(6), 1033–1056. https://doi.org/10.1175/BAMS-D-14-00145.1

Uvarova, N. E., Ishkov, A. G., Akopova, G. S., Ginzburg, V. A., Romanov, K. V., Kruglova, N. Y., & Gytarsky, M. L. (2014). The update of methane emission parameters for natural gas operations in Russia. *Carbon Management*, *5*(5-6), 573–577. https://doi.org/10.1080/17583004.2015.1049105

Väisänen, M., Ylänne, H., Kaarlejärvi, E., Sjogersten, S., Olofsson, J., Crout, N., & Stark, S. (2014). Consequences of warming on tundra carbon balance determined by reindeer grazing history. *Nature Climate Change*, *4*(5), 384–388. https://doi.org/10.1038/nclimate2147

Val Martin, M., Logan, J. A., Kahn, R. A., Leung, F.-Y., Nelson, D. L., & Diner, D. J. (2010). Smoke injection heights from fires in North America: Analysis of 5 years of satellite observations. *Atmospheric Chemistry and Physics*, *10*(4), 1491–1510. https://doi.org/10.5194/acp-10-1491-2010

van As, D., & Fausto, R. S. (2011). The PROMICE project team Programme for Monitoring of the Greenland Ice Sheet (PROMICE): First temperature and ablation records. *Geological Survey of Denmark and Greenland Bulletin*, *23*, 73–76.

van den Broeke, M., Bamber, J., Ettema, J., Rignot, E., Schrama, E., van de Berg, W. J., et al. (2009). Partitioning Recent Greenland Mass Loss. *Science*, *326*(5955), 984–986. https://doi.org/10.1126/science.1178176

van den Broeke, M. R., Enderlin, E. M., Howat, I. M., Kuipers Munneke, P., Noël, B. P. Y., van de Berg, W. J., et al. (2016). On the recent contribution of the Greenland ice sheet to sea level change. *The Cryosphere*, *10*(5), 1933–1946. https://doi.org/10.5194/tc-10-1933-2016

van Everdingen, R. (Ed) (1998). *Multi-Language Glossary of Permafrost and Related Ground-Ice Terms, revised May 2005*. Boulder, CO: National Snow and Ice Data Center/World Data Center for Glaciology. http://nsidc.org/fgdc/glossary/

Vaughan, D.G., Comiso, J.C., Allison, I., Carrasco, J., Kaser, G., Kwok, R., et al. (2013). Observations: Cryosphere. In: *Climate Change 2013: The Physical Science Basis. Contribution of Working Group I to the Fifth Assessment Report of the Intergovernmental Panel on Climate Change* (Stocker, T.F., D. Qin, G.-K. Plattner, M. Tignor, S.K. Allen, J. Boschung, A. Nauels, Y. Xia, V. Bex & P.M. Midgley (eds.)). Cambridge University Press, Cambridge, United Kingdom and New York, NY, USA.

Vaughan, M. A., Powell, K. A., Winker, D. M., Hostetler, C. A., Kuehn, R. E., Hunt, W. H., et al. (2009). Fully Automated Detection of Cloud and Aerosol Layers in the CALIPSO Lidar Measurements. *Journal of Atmospheric and Oceanic Technology*, *26*(10), 2034–2050. https://doi.org/10.1175/2009JTECHA1228.1

Vavrus, S., Waliser, D., Schweiger, A., & Francis, J. (2009). Simulations of 20th and 21st century Arctic cloud amount in the global climate models assessed in the IPCC AR4. *Climate Dynamics*, *33*(7-8), 1099–1115. https://doi.org/10.1007/s00382-008-0475-6

Velicogna, I., Sutterley, T. C., & van den Broeke, M. R. (2014). Regional acceleration in ice mass loss from Greenland and Antarctica using GRACE time-variable gravity data. *Journal of Geophysical Research: Space Physics*, *41*, 8130–8137. https://doi.org/10.1002/2014GL061052

Veraverbeke, S., Rogers, B. M., Goulden, M. L., Jandt, R. R., Miller, C. E., Wiggins, E. B., & Randerson, J. T. (2017). Lightning as a major driver of recent large fire years in North American boreal, forests. *Nature Climate Change*, *7*(7), 529–534. https://doi.org/0.1038/NCLIMATE3329

Verbyla, D. (2008). The greening and browning of Alaska based on 1982–2003 satellite data. *Global Ecology and Biogeography*, *17*(4), 547–555. https://doi.org/10.1111/j.1466-8238.2008.00396.x

Verlinde, J., Harrington, J. Y., McFarquhar, G. M., Yannuzzi, V. T., Avramov, A., Greenberg, S., et al. (2007). The Mixed-Phase Arctic Cloud Experiment (M-PACE). *Bulletin of the American Meteorolgical Society*, *88*(2), 205–222. https://doi.org/10.1175/BAMS-88-2-205

Verpoorter, C., Kutser, T., Seekell, D. A., & Tranvik, L. J. (2014). A global inventory of lakes based on high-resolution satellite imagery. *Geophysical Research Letters*, *41*, 6396–6402. https://doi.org/10.1002/2014GL060641

Virtanen, R., Oksanen, L., Oksanen, T., Cohen, J., Forbes, B. C., Johansen, B., et al. (2016). Where do the treeless tundra areas of northern highlands fit in the global biome system: Toward an ecologically natural subdivision of the tundra biome. *Ecology and Evolution*, *6*(1), 143–158. https://doi.org/10.1002/ece3.1837

Virtanen, T., & Ek, M. (2014). The fragmented nature of tundra landscape. *International Journal of Applied Earth Observation and Geoinformation*, *27*(Part A), 4–12. https://doi.org/10.1016/j.jag.2013.05.010

Vizcaino, M. (2014). Ice sheets as interactive components of Earth system models: Progress and challenges. *WIREs Climate Change*, *5*(4), 557–568. https://doi.org/10.1002/wcc.285

Volkov, D. L., & Pujol, M. I. (2012). Quality assessment of a satellite altimetry data product in the Nordic, Barents, and Kara seas. *Journal of Geophysical Research*, *117*(C3), C03025. https://doi.org/10.1029/2011JC007557

Walker, D. A., Epstein, H. E., Jia, G. J., Balser, A., Copass, C., Edwards, E. J., et al. (2003). Phytomass, LAI, and NDVI in northern Alaska: Relationships to summer warmth, soil pH, plant functional types, and extrapolation to the circumpolar Arctic. *Journal of Geophysical Research Atmospheres*, *108*(D2), 8169. https://doi.org/10.1029/2001JD000986

Walker, D. A., Leibman, M. O., Epstein, H. E., Forbes, B. C., Bhatt, U. S., Raynolds, M. K., et al. (2009). Spatial and temporal patterns of greenness on the Yamal Peninsula, Russia: Interactions of ecological and social factors affecting the Arctic normalized difference vegetation index. *Environmental Research Letters*, *4*(4), 045004. https://doi.org/10.1088/1748-9326/4/4/045004

Walker, D. A., Raynolds, M. K., Daniëls, F. J. A., Einarsson, E., Elvebakk, A., Gould, W. A., et al. (2005). The circumpolar Arctic vegetation map. *Journal of Vegetation Science*, *16*, 267–282. https://doi.org/10.1111/j.1654-1103.2005.tb02365.x

Walker, X. J., Baltzer, J. L., Cumming, S. G., Day, N. J., Ebert, C., Goetz, S., et al. (2019). Increasing wildfires threaten historic carbon sink of boreal forest soils. *Nature*, *572*(7770), 520–523. https://doi.org/10.1038/s41586-019-1474-y

Walker, X. J., Rogers, B. M., Baltzer, J. L., Cumming, S. G., Day, N. J., Goetz, S. J., et al. (2018). Cross-scale controls on carbon emissions from boreal forest mega-fires. *Global Change Biology*, *24*(9), 4251–4265. https://doi.org/10.1111/gcb.14287

Walsh, J. E. (2013). Melting ice: What is happening to Arctic sea ice, and what does it mean for us? *Oceanography*, *26*(2), 171–181. https://doi.org/10.5670/oceanog.2013.19

Walter, H. (1979). *Vegetation of the Earth and Ecological Systems of the Geo-biosphere*, (Vol. 274). New York: Springer-Verlag. https://doi.org/10.1007/978-1-4684-0468-5

Wang, J. S., Kawa, S. R., Collatz, G. J., Sasakawa, M., Gatti, L. V., Machida, T., et al. (2018). A global synthesis inversion analysis of recent variability in CO_2 fluxes using GOSAT and in situ observations. *Atmospheric Chemistry and Physics*, *18*(15), 11097–11124. https://doi.org/10.5194/acp-18-11097-2018

Wang, X., & Key, J. R. (2003). Recent trends in Arctic surface, cloud, and radiation properties from space. *Science*, *299*(5613), 1725–1728, 2003. https://doi.org/10.1126/science.1078065

Warren, S. G. (2013). Can black carbon in snow be detected by remote sensing? *Journal of Geophysical Research: Atmosphere*, *118*(2), 779–786. https://doi.org/10.1029/2012JD018476

Warren, S. G. (2019). Optical properties of ice and snow. *Philosophical Transactions of the Royal Society A*, *377*(2146), 20180161. https://doi.org/10.1098/rsta.2018.0161

Warren, S. G., & Wiscombe, W. J. (1980). A Model for the Spectral Albedo of Snow. II: Snow Containing Atmospheric Aerosols. *Journal Atmospheric Sciences*, *37*(12), 2734–2745. https://doi.org/10.1175/1520-0469(1980)037<2734:AMFTSA>2.0.CO;2

Wassmann, P., Duarte, C. M., Agusti, S., & Sejr, M. K. (2011). Footprints of climate change in the Arctic marine ecosystem. *Global Change Biology*, *17*(2), 1235–1249. https://doi.org/10.1111/j.1365-2486.2010.02311.x

Watanabe, S., Sudo, K., Nagashima, T., Takemura, T., Kawase, H., & Nozawa, T. (2011). Future projections of surface UV-B in a changing climate. *Journal of Geophysical Research*, *116*(D16), D16118. https://doi.org/10.1029/2011JD015749

Watts, J. D., Kimball, J. S., Bartsch, A., & McDonald, K. C. (2014). Surface water inundation in the boreal-Arctic: Potential impacts on regional methane emissions. *Environmental Research Letters*, *9*(7), 075001. https://doi.org/10.1088/1748-9326/9/7/075001

Watts, J. D., Kimball, J. S., Jones, L. A., Schroeder, R., & McDonald, K. C. (2012). Satellite Microwave remote sensing of contrasting surface water inundation changes within the Arctic–Boreal Region. *Remote Sensing of Environment*, *127*, 223–236. https://doi.org/10.1016/j.rse.2012.09.003

Webster, M. A., Rigor, I. G., Nghiem, S. V., Kurtz, N. T., Farrell, S. L., Perovich, D. K., & Sturm, M. (2014). Interdecadal changes in snow depth on Arctic sea ice. *Journal of Geophysical Research: Oceans*, *119*, 5395–5406. https://doi.org/10.1002/2014JC009985

Westermann, S., Duguay, C.R., Grosse, G., & Kääb, A. (2015). "Remote sensing of permafrost and frozen ground," in *Remote Sensing of the Cryosphere*, First Edition, Edited by M. Tedesco, John Wiley and Sons, Ltd., https://doi.org/10.1002/9781118368909.ch13

Whitcomb, J., Moghaddam, M., McDonald, K. C., Kellndorfer, J., & Podest, E. (2009). Wetlands map of Alaska using L-band radar satellite imagery. *Canadian Journal of Remote Sensing*, *35*(1), 1–20.

White, D., Hinzman, L., Alessa, L., Cassano, J., Chambers, M., Falkner, K., et al. (2007). The arctic freshwater system: Changes and impacts. *Journal of Geophysical Research-Biogeosciences*, *112*(G4), n/a. https://doi.org/10.1029/2006JG000353

White, J. C., Wulder, M. A., Hermosilla, T., Coops, N. C., & Hobart, G. W. (2017). A nationwide annual characterization of 25 years of forest disturbance and recovery for Canada using Landsat time series. *Remote Sensing of Environment*, *194*, 303–321. https://doi.org/10.1016/j.rse.2017.03.035

Willis, J. K., & Church, J. A. (2012). Regional sea-level projection. *Science*, *336*(6081), 550–551. https://doi.org/10.1126/science.1220366

Willis, M. D., Bozem, H., Kunkel, D., Lee, A. K. Y., Schulz, H., Burkart, J., et al. (2019). Aircraft-based measurements of High Arctic springtime aerosol show evidence for vertically varying sources, transport and composition. *Atmospheric Chemistry and Physics*, *19*(1), 57–76. https://doi.org/10.5194/acp-19-57-2019

WMO (2009). *Vision for the Global Observing System (GOS) in 2025. WMO Recommendation 6.1/1 (CBS-XIV)* (7 pp.). Geneva, Switzerland: World Meteorological Organization. (Available online at http://www.wmo.int/pages/prog/www/OSY/WorkingStructure/documents/CBS-2009_Vision-GOS-2025.pdf.)

Wolfe, R.E. & Ramapriyan, H.K. (2010). Scaling the pipe: NASA EOS Terra data systems at 10, *Proceedings of the Geoscience and Remote Sensing Symposium (IGARSS), 2010, Honolulu, HI, 25 – 30 July, 2010* (pp. 1300 – 1303). IEEE, Institute of Electrical and Electronics Engineers, Inc.

Wood, E. M., Pidgeon, A. M., Radeloff, V. C., & Keuler, N. S. (2012). Image texture as a remotely sensed measure of vegetation structure. *Remote Sensing of Environment*, *121*, 516–526. https://doi.org/10.1016/j.rse.2012.01.003

Woodhouse, I. H. (2006). *Introduction to Microwave Remote Sensing* (382 p.). Boca Raton, FL: CRC Press.

Woodruff, S. D., Worley, S. J., Lubker, S. J., Ji, Z., Eric Freeman, J., Berry, D. I., et al. (2011). ICOADS Release 2.5: Extensions and enhancements to the surface marine meteorological archive. *International Journal of Climatology*, *31*(7), 951–967. https://doi.org/10.1002/joc.2103

Wooster, M. J., Roberts, G., Perry, G. L. W., & Kaufman, Y. J. (2005). Retrieval of biomass combustion rates and totals from fire radiative power observations: FRP derivation and calibration relationships between biomass consumption and fire radiative energy release. *Journal of Geophysical Research*, *110*(D24), D24311. https://doi.org/10.1029/2005JD006318

Worthy, D. E. J., Chan, E., Ishizawa, M., Chan, D., Poss, C., Dlugokencky, E. J., et al. (2009). Decreasing anthropogenic methane emissions in Europe and Siberia inferred from continuous carbon dioxide and methane observations at Alert, Canada. *Journal of Geophysical Research*, *114*(D10), D10301. https://doi.org/10.1029/2008JD011239

Wotton, B. M., Nock, C. A., & Flannigan, M. D. (2010). Forest fire occurrence and climate change in Canada. *International Journal of Wildland Fire*, *19*(3), 253–271. https://doi.org/10.1071/WF09002

Wu, D. L., Ackerman, S. A., Davies, R., Diner, D. J., Garay, M. J., Kahn, B. H., et al. (2009). Vertical distributions and relationships of cloud occurrence frequency as observed by MISR, AIRS, MODIS, OMI, CALIPSO, and CloudSat. *Geophysical Research Letters*, *36*, L09821. https://doi.org/10.1029/2009GL037464

Wu, D. L., & Lee, J. N. (2012). Arctic low cloud changes as observed by MISR and CALIOP: Implication for the enhanced autumnal warming and sea ice loss. *Journal of Geophysical Research Atmospheres*, *117*, D07107. https://doi.org/10.1029/2011JD017050

Wulder, M., Niemann, K. O., & Goodenough, D. G. (2000). Local maximum filtering for the extraction of tree locations and basal area from high spatial resolution imagery. *Remote Sensing of Environment*, *73*(1), 103–114. https://doi.org/10.1016/S0034-4257(00)00101-2

Wulder, M. A., Masek, J. G., Cohen, W. B., Loveland, T. R., & Woodcock, C. E. (2012). Opening the archive: How free data has enabled the science and monitoring promise of Landsat. *Remote Sensing of Environment*, *122*, 2–10. https://doi.org/10.1016/j.rse.2012.01.010

Wulder, M. A., Ortlepp, S. M., White, J. C., & Coops, N. C. (2008). Impact of sun-surface-sensor geometry upon multitemporal high spatial resolution satellite imagery. *Canadian Journal of Remote Sensing*, *34*(5), 455–461. https://doi.org/10.5589/m08-062

Wulder, M. A., White, J. C., Bater, C. W., Coops, N. C., Hopkinson, C., & Chen, G. (2012). Lidar plots—A new large-area data collection option: Context, concepts, and case study. *Canadian Journal of Remote Sensing*, *38*(5), 600–618. https://doi.org/10.5589/m12-049

Wulder, M. A., White, J. C., Loveland, T. R., Woodcock, C. E., Belward, A. S., Cohen, W. B., et al. (2016). The global Landsat archive: Status, consolidation, and direction. *Remote Sensing of Environment*, *185*, 271–283. https://doi.org/10.1016/j.rse.2015.11.032

Wunch, D., Toon, G. C., Blavier, J.-F. L., Washenfelder, R. A., Notholt, J., Connor, B. J., et al. (2011). The Total Carbon Column Observing Network. *Philosophical Transactions of the Royal Society A*, *369*(1943), 2087–2112. https://doi.org/10.1098/rsta.2010.0240

Wunch, D., Wennberg, P. O., Osterman, G., Fisher, B., Naylor, B., Roehl, C. M., et al. (2017). Comparisons of the Orbiting Carbon Observatory-2 (OCO-2) X_{CO2} measurements with TCCON. *Atmospheric Measurement Techniques*, *10*(6), 2209–2238. https://doi.org/10.5194/amt-10-2209-2017

Xia, J., McGuire, A. D., Lawrence, D., Burke, E., Chen, G., Chen, X., et al. (2017). Terrestrial ecosystem model performance in simulating productivity and its vulnerability to climate change in the northern permafrost region. *Journal of Geophysical Research: Biogeosciences*, *122*(2), 430–446. https://doi.org/10.1002/2016JG003384

Xiong, X., Barnet, C., Maddy, E., Sweeney, C., Liu, X., Zhou, L., & Goldberg, M. (2008). Characterization and validation of methane products from the Atmospheric Infrared Sounder (AIRS). *Journal of Geophysical Research*, *113*(null), G00A01. https://doi.org/10.1029/2007JG000500

Xu, X. L., Derksen, C., Yueh, S. H., Dunbar, R. S., & Colliander, A. (2016). Freeze/Thaw Detection and Validation Using Aquarius' L-Band Backscattering Data. *IEEE Journal of Selected Topics in Applied Earth Observations and Remote Sensing*, *9*(4), 1370–1381. https://doi.org/10.1109/JSTARS.2016.2519347

Yamazaki, D., O'Loughlin, F., Trigg, M. A., Miller, Z. F., Pavelsky, T. M., & Bates, P. D. (2014). Development of the Global Width Database for Large Rivers. *Water Resources Research*, *50*, 3467–3480. https://doi.org/10.1002/2013WR014664

Yamazaki, D., Trigg, M. A., & Ikeshima, D. (2015). Development of a global ~90 m water body map using multi-temporal Landsat images. *Remote Sensing of Environment*, *171*, 337–351. https://doi.org/10.1016/j.rse.2015.10.014

Yang, Q., Dixon, T. H., Myers, P. G., Bonin, J., Chambers, D., & van den Broeke, M. R. (2016). Recent increases in Arctic freshwater flux affects Labrador Sea convection and Atlantic overturning circulation. *Nature Communications*, *7*(1), 10525. https://doi.org/10.1038/ncomms10525

Ylänne, H., Stark, S., & Tolvanen, A. (2015). Vegetation shift from deciduous to evergreen dwarf shrubs in response to selective herbivory offsets carbon losses: Evidence from 19 years of warming and simulated herbivory in the sub-arctic tundra. *Global Change Biology*, *21*(10), 3696–3711. https://doi.org/10.1111/gcb.12964

Yokota, T., Yoshida, Y., Eguchi, N., Ota, Y., Tanaka, T., Watanabe, H., & Maksyutov, S. (2009). Global concentrations of CO_2 and CH_4 retrieved from GOSAT: First Preliminary Results. *Sola*, *5*, 160–163. https://doi.org/10.2151/sola.2009-041

Yu, L., & Weller, R. A. (2007). Objectively analyzed air–sea heat fluxes for the global ice-free oceans (1981–2005). *Bulletin of the American Meteorolgical Society*, *88*(4), 527–540. https://doi.org/10.1175/BAMS-88-4-527

Yu, Y., Maykut, G. A., & Rothrock, D. A. (2004). Changes in the thickness distribution of Arctic sea ice between 1958–1970 and 1993–1997. *Journal of Geophysical Research*, *109*(C8), C08004. https://doi.org/10.1029/2003JC001982

Zamora, L. M., Kahn, R. A., Cubison, M. J., Diskin, G. S., Jimenez, J. L., Kondo, Y., et al. (2016). Aircraft-measured indirect cloud effects from biomass burning smoke in the Arctic and subarctic. *Atmospheric Chemistry and Physics*, *16*(2), 715–738. https://doi.org/10.5194/acp-16-715-2016

Zamora, L. M., Kahn, R. A., Eckhardt, S., McComiskey, A., Sawamura, P., Moore, R., & Stohl, A. (2017). Aerosol indirect effects on the nighttime Arctic Ocean surface from thin, predominantly liquid clouds. *Atmospheric Chemistry and Physics*, *17*(12), 7311–7332. https://doi.org/10.5194/acp-17-7311-2017

Zamora, L. M., Kahn, R. A., Stohl, A., Huebert, K. B., & Eckhardt, S. (2018). A satellite-based estimate of combustion aerosol cloud microphysical effects over the Arctic Ocean. *Atmospheric Chemistry and Physics*, *18*(20), 14,949–14,964. https://doi.org/10.5194/acp-18-14949-2018

Zhang, B., Tian, H., Lu, C., Chen, G., Pan, S., Anderson, C., & Poulter, B. (2017). Methane emissions from global wetlands: An assessment of the uncertainty associated with various wetland extent data sets. *Atmospheric Environment*, *165*, 310–321. https://doi.org/10.1016/j.atmosenv.2017.07.001

Zhang, T., Barry, R. G., Knowles, K., Ling, F., & Armstrong, R. L. (2003). Distribution of seasonally and perennially frozen ground in the Northern Hemisphere. In M. Phillips, S. M. Springman, & L. U. Arenson (Eds.), *Proceedings of the 8th International Conference on Permafrost, 21-25. Zurich, Switzerland* (pp. 1289–1294). Lisse, The Netherlands: A.A. Balkema.

Zhang, T., Osterkamp, T. E., & Stamnes, K. (1996). Some characteristics of the climate in northern Alaska, USA. *Arctic and Alpine Research*, *28*(4), 509–518. https://doi.org/10.2307/1551862

Zhang, X., Jiang, H., Lu, X., Cheng, M., Zhang, X., Li, X., & Zhang, L. (2013). Estimate of methane release from temperate natural wetlands using Envisat/SCIAMACHY data in China. *Atmospheric Environment*, *69*, 191–197. https://doi.org/10.1016/j.atmosenv.2012.12.023

Zhang, Y., Wolfe, S. A., Morse, P. D., Olthof, I., & Fraser, R. H. (2015). Spatiotemporal impacts of wildfire and climate warming on permafrost across a subarctic region. *Canada. Journal of Geophysical Research: Earth Surface*, *120*(11), 2338–2356. https://doi.org/10.1002/2015JF003679

Zhang, Y.-C., Rossow, W. B., & Lacis, A. A. (1995). Calculation of surface and top of atmosphere radiative fluxes from physical quantities based on ISCCP data sets: 1. Method and sensitivity to input data uncertainties. *Journal of Geophysical Research*, *100*(D1), 1149–1165. https://doi.org/10.1029/94JD02747

Zhang, Y.-C., Rossow, W. B., Lacis, A. A., Oinas, V., & Mishchenko, M. I. (2004). Calculation of radiative fluxes from the surface to top of atmosphere based on ISCCP and other global data sets: Refinements of the radiative transfer model and the input data. *Journal of Geophysical Research*, *109*(D19), D19105. https://doi.org/10.1029/2003JD004457

Zhao, C., & Garrett, T. J. (2015). Effects of Arctic haze on surface cloud radiative forcing. *Geophysical Research Letters*, *42*, 557–564. https://doi.org/10.1002/2014GL062015

Zhou, Y., Guo, D., Qiu, G., Cheng, G., & Li, S. (2000). *Frozen Ground in China*. 450 pp. Beijing: Science Press.

Zhu, X., Zhuang, Q., Gao, X., Sokolov, A., & Schlosser, C. A. (2013). Pan-Arctic land–atmospheric fluxes of methane and carbon dioxide in response to climate change over the 21st century. *Environmental Research Letters*, *8*(4), 045003. https://doi.org/10.1088/1748-9326/8/4/045003

Zhu, Z., Bi, J., Pan, Y., Ganguly, S., Anav, A., Xu, L., et al. (2013). Global Data Sets of Vegetation Leaf Area Index (LAI)3g and Fraction of Photosynthetically Active Radiation (FPAR)3g Derived from Global Inventory Modeling and Mapping Studies (GIMMS) Normalized Difference Vegetation Index (NDVI3g) for the Period 1981 to 2011. *Remote Sensing*, *5*(2), 927–948. https://doi.org/10.3390/rs5020927

Zhu, Z., Piao, S., Myneni, R. B., Huang, M., Zeng, Z., Canadell, J. G., et al. (2016). Greening of the Earth and its drivers. *Nature Climate Change*, *6*(8), 791–795. https://doi.org/10.1038/NCLIMATE3004

Zoltai, S. C. & Martikainen, P. J. (1996). The role of forested peatlands in the global carbon cycle. *In Forest Ecosystems, Forest Management and the Global Carbon Cycle*, edited by M. J. Apps & D. T. Price, (Heidelberg: Springer-Verlag), 47-58, https://doi.org/10.1007/978-3-642-61111-7_5.

Zona, D., Gioli, B., Commane, R., Lindaas, J., Wofsy, S. C., Miller, C. E., et al. (2016). Cold season emissions dominate the Arctic tundra methane budget. *Proceedings of the National Academy of Sciences*, *113*(1), 40–45. https://doi.org/10.1073/pnas.1516017113

Zwally, H. J., Li, J., Brenner, A. C., Beckley, M., Cornejo, H. G., DiMarzio, J., et al. (2011). Greenland ice sheet mass balance: Distribution of increased mass loss with climate warming 2003-2007 versus 1992-2002. *Journal of Glaciology*, *57*, 201.